PCM BASED THERMAL STORAGE SYSTEM/PLANT MODELS FOR BUILDING ENERGY SYSTEM ANALYSIS

Thesis submitted for the award of Doctor of Philosophy Degree

By

Agbanigo, Andrew Olubunmi

JUNE 1, 2021

MECHANICAL AND AEROSPACE ENGINEERING DEPARTMENT

University of Strathclyde, Glasgow

To God who made me an object of His mercy

Abstract

Energy storage is an important measure in efforts to improve buildings' energy efficiency and reduce CO_2 emissions from the building sector. Affording opportunities for better utilisation and management of building's energy and reducing wastages, it can serve as a vital mitigant to the negative impact of electrification of energy systems, which the UK government has chosen as means of achieving its goal of reducing CO_2 emissions by 80% by the year 2050. Energy storage with phase change materials, though capable of improving energy systems' performance and reducing building energy demand, present challenges that necessitates pre-analysis and study for which virtualisation and simulation with numerical models is the most cost effective and risk-averse method. This requires use/application of whole building modelling applications like ESP-r that have capabilities to model PCMs. Existing PCM models in the software lack ability to represent current available physical PCM based thermal energy storage systems. These form the basis for the work reported herein, which discusses solution methods and their implementations.

Models of two PCM thermal stores were developed using the enthalpy formulation method, which is more reliable and devoid of many of the problems associated with the heat capacity method. The thermal stores were modelled as shell and tube heat exchangers where the PCM, contained in the shell, was treated as one of the heat transfer fluids with the main heat transfer fluid flowing through the tube/pipes. Energy conservation equations for the PCM were formulated in terms of the heat balance over a volume of material and time interval leading to development of representative equations for heat exchange between PCM and heat transfer fluid, and temperature and phase changes experienced by the phase change material. An

algorithm was developed employing iterative schemes to solve the discretised energy equations.

The source code and algorithms were verified using structured walk throughs, debugging and consistency tests, and sanity test from ESP-r simulation of building model containing the plant models. They were also validated by comparing results from running simulation of the models with results reported for models of similar phase change thermal storage systems by Hosseini et al. (2012), Hosseini, Rahimi, & Bahrampoury, (2014) and Seddegh et al (2016). Results from the verification tests show that the models were accurate to within expected range and for the intended purpose while results from validation show close agreement with reference materials.

The models were also subjected to sensitivity analysis aimed at assessing impact of grid sizes and convergence criteria on models' performance. These parameters, unlike other variable parameters of the model source codes, are determined internally within the codes while the others are determined by ESP-r. Results show that the models' outputs, HTF and PCM, are unaffected by changes in both the grid size and convergence criteria. The models' sensitivity to the convergence criteria is in regard to the code processing time. Additional sensitivity analysis was done for the fabric integrated thermal store to assess the source code's sensitivity to type of materials with which PCM cells at extreme ends of the PCM block interacted. Results show that outputs are unaffected by type of materials with which PCM cells at extreme ends of the PCM block interacted.

Installation/implementation of the models' source codes in ESP-r was afterwards done by writing algorithms for each plant model in line with source codes source formatting and description in ESP-r incorporating the software's common variables and parameters, building

up plant database entries and editing necessary code compilation and execution codes and programs within the software's database and archives.

Demonstration of the models were accomplished by deploying the plants in the heating system plant network of a 2-storey semi-detached building model, for which simulations were run over a winter week for analysis of impact of deploying PCM based thermal storage plant system on heating system's energy consumption, energy cost and CO2 emission. Comparative analyses were also conducted between heating systems with employing latent heat thermal storage systems (PCM) for thermal storage and those employing sensible heat thermal storage systems. While results from the demonstration tests show improvement in performance of the test building energy system and the clear advantage of latent heat thermal storage systems over sensible heat thermal storage systems, in agreement with established findings and conclusions from similar systems, this was not its objective of the demonstration tests. Rather it was to lend credence to validation of the thermal storage models with regards to correctness and accuracy of the computer/numerical codes, and to show that they are comparable to similar systems in terms of application and usage. It was also a means of demonstrating usefulness of the plant systems for building energy simulation systems such as ESP-r.

Acknowledgement

All my gratitude is to God.

I acknowledge and appreciate my wife and children for their support, financially and emotionally. I appreciate the management of the Federal Polytechnic, Ado Ekiti and Mechanical Engineering Department.

I acknowledge my supervisor, Dr. Nick Kelly for his support and guidance. Thank you. I also acknowledge the support and assistance of the admin staff and support team of Mechanical and Aerospace Engineering department. I am grateful to the assessment and viva team.

Table of Content

List of Tables

List of Figures

Nomenclature

Letters

A	heat flow cross-sectional area (m^2), matrix coefficients of future time step
a	axial spatial distance/thickness (m).
B	matrix coefficients of present time step
b	breadth (m).
c	specific heat capacity (J/kgK),
C	thermal conductance (W/K), matrix coefficients of known terms and boundary conditions
D	diameter (m)
d	thickness of cells/nodes (m)
e	specific enthalpy (J/kg)
E	enthalpy density, volumetric enthalpy, energy per unit volume (J/m3),
H	enthalpy (J/kg),
h	heat transfer coefficient (W/m^2K)
k	thermal conductivity (W/mK)
l	length (of exchanger) (m).
L	specific latent heat (J/kg)
m	mass (kg)
n	number of cells/nodes
q	heat/energy flow rate (W), heat flux (W/m^2)
r	radius (of radial cells/nodes) (m)
R	thermal resistance (m^2K/W)
S	thermal conductance (W/K)
t	thickness, time/elapsed time (s)
T	temperature (K, ^oC)
u	matrix, Kirchhoff temperature (K)
x	spatial dimension (m)
y	spatial dimension (m)
Z	present time step matrix
z	spatial dimension (m)

Subscripts

a	axial dimension/plane
atm	atmosphere
hw	PCM and surrounding wall interface
i	inlet, reference dimensional control volume/cell/node
j	reference dimensional control volume
k	reference dimensional control volume
l	liquid
L	maximum exchanger length (m)
m	melt/melting/phase change
M	cell/node at max length
N	maximum exchanger breadth (m)
n	cell/node number
o	out
p	phase change material, constant pressure
P	cell/node at max exchanger breadth
ph	HTF and PCM interface
Q	maximum exchanger depth (m)
R	cell/node at max depth
r	radial dimension/plane
s	solid, shell
t	tube, time interval (s)
w	heat transfer fluid (water)
x	spatial interval (m), reference dimensional control volume - x- axis
y	reference dimensional control volume - y-axis
z	reference dimensional control volume - z-axis

Superscripts

l	liquid
s	solid
t	specific time (s)
p	iteration number

Greek letters

$\mathbf{v}$	enthalpy (J/kg) given effective specific heat capacity
∂	differential
$\boldsymbol{\theta}$	implicit-explicit weighing factor
∞	system/component surrounding/environment.
$\boldsymbol{\rho}$	density (kg/m^3)
δ	change in/difference
γ	liquid fraction
$\boldsymbol{\Delta}$	interval

Special characters

C_i'	specific heat capacities (J/kgK)
$\dot{\boldsymbol{m}}$	mass flow rate (kg/s)
$\boldsymbol{X}$	partial differential over space with respect to time
$\boldsymbol{X'}$	double partial differential over space with respect to time
$\boldsymbol{\nabla}$	partial differential over space

Chapter 1

INTRODUCTION AND RESEARCH BACKGROUND

1.0 Introduction

Since 1987, after publication of the Brundland report, Our Common Future, the issues of sustainability and development has taken centre stage both economically and politically. The report defined sustainable development as "development that meets needs of the present without compromising the ability of future generations to meet their own needs" (Brundtland Commission, 1987). Basic human needs (present), according to the report, are employment, food, energy, housing, water supply, sanitation, and health care. The report's basic argument is that "sustainable development requires the conservation of plant and animal species" (Brundtland Commission, 1987), contending that ability of future generation to meet their needs rests upon availability of the earth's resources (Holden, Linnerud, & Banister, 2014). Therefore, meeting basic human needs sustainably must involve preservation of the Earth's natural base.

1.1 Energy Consumption

One of the seven basic human needs, according to the report is energy. This has the potential to aid production and/supply of the other six. The supply and availability of energy affords opportunities for improving and increasing provision of comfort (housing), water supply and transportation, production of food and material goods, health care (including sanitation) and

employment. Energy is so vital to human development that its consumption is an indication of a country's level of development, the per capital energy consumption. Demand for, or use/consumption of, energy has been on an upward trajectory over the years (figure 1.1), with figures for 2019 put at 5.492 x 10^9 GWh globally, an increase from 4.127 x 10^9 GWh in 2005 (Energy Information Administration, 2019). It is projected to reach 7.978 x 10^9 GWh by 2050 if annual rate of increase continues at the current relatively steady average of 1.48% per annum (Energy Information Administration, 2019).

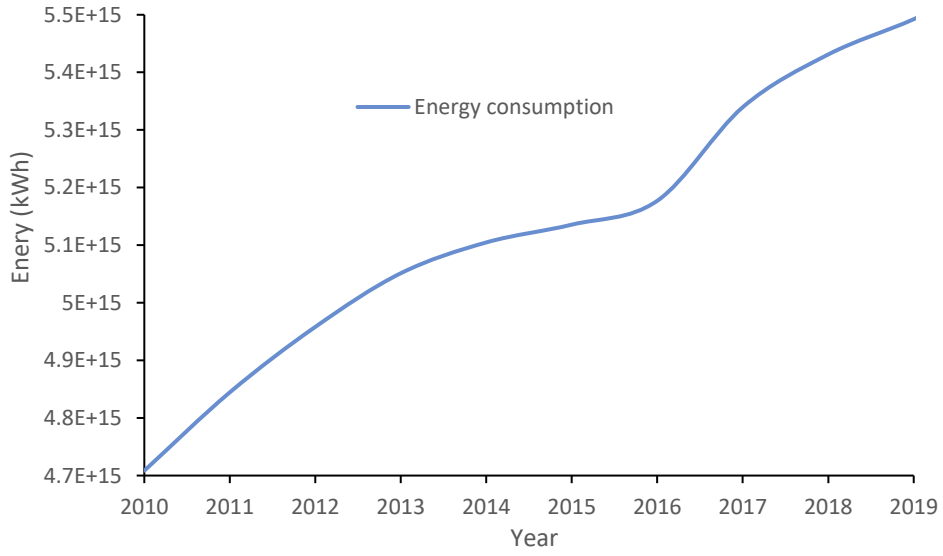

Figure 1.1: Global energy consumption (2010 -2019) (Energy Information Administration, 2019)

Demand for energy, for many nations, often outweighs ability of local available resources to cope. Meeting, or satisfying, the demand is also one of the most significant factors responsible for the non-sustainability of present development, and of the environment. This is due, majorly, to the fact that for years supply has been the main approach to solving, and/or satisfying, energy demand problems.

Understanding that human development tends to damage ecosystems, sourcing and consumption of energy has had one of the greatest damaging effects on the planet. The ever-

increasing demand for energy has been, for the most part of human existence, with little or no regard for its impact on, or implication for, the environment. Devastation of arctic ecosystems and pollution of air and water resources by petroleum exploration processes are clear examples. Given that not every energy conversion process or device is 100% efficient (Narisada & Schreuder, 2004), it is not surprising that the supply driven approach has given way to a more environment friendly one, where emphasis is on reducing and utilising waste energy.

According to European Commission (2020), final energy consumed in the EU in 2017 was about 50.4% of total energy input. This implies ample opportunities for energy savings in areas like generation and transmission (Luburić et al., 2018) and production processes (Onget al., 2017), as well as at the final end consumption (Chinese, Santin, & Saro (2017); Gai et al. (2019); Pablo-Romeroa, Pozo-Barajas, & Yñiguez (2017) as most of the waste energy is released as low-grade heat to the surroundings.

1.2 Energy Consumption[1] in Buildings

Human dependence on energy stems, so it seems, from the desire to satisfy most, if not all, of the basic needs outlined in the Brundtland report within the confines of a limited space and with little physical effort. Humans require an environment that is self-contained and tightly controlled, one wherein a wide variety of services can be accessed in comfort and (sometimes) effortlessly. Buildings provide warmth, place to prepare and preserve food, carry

[1] Energy consumption in buildings refers to total energy taken up by buildings from primary energy sources and not energy consumed within them to power appliances and maintain indoor environment conditions. It is sometimes interchanged with energy demand by buildings, referring to energy draw by buildings from the grid or other energy sources.

out industrial and commercial activities, entertainment and recreation. These are energy intensive activities.

The building and construction sector accounts for over one third of total global energy consumption (International Energy Agency, 2020(a)) while residential buildings alone accounted for 26.1% of the global total in 2018 (Eurostat, 2020), with urban residential buildings taking up between 20%–40% of this over the past decades (Li, Koua, & Wang, 2019). Estimates for the UK domestic sector was approximately 482645 GWh, that is 28.9% of total energy, in 2018 (Department for Business, Energy and Industrial Strategy, 2019), with more than 80% of this employed for space and water heating (Watson, Lomas, & Buswell, 2019). Globally, about half of energy consumption in buildings is taken up by heating, ventilating, and air-conditioning (HVAC) systems (Young et al., 2018) in Faraj et al., 2020). According to Odyssee-Mure (2020), over 66% of households' energy consumption in the EU in 2017 was used for space heating purposes and 13.2% for domestic hot water.

Appreciation of the fact that the building sector is the third largest global energy consumer after industry and transportation (Nejat et al., 2015; Dong et al., 2018; Pannier, Schalbart, & Peuportier, 2018), and that it accounts for about 28% of energy related global CO_2 emissions in 2019 (International Energy Agency, 2020(b)) (15.3% of the UK's total (Department for Business, Energy and Industrial Strategy, UK, 2020)) some, like Nejat et al (2015), conclude that residential energy consumptions have "direct, significant effects on the world environment", one of the factors responsible for its return, as noted by Li et al (2019), "to the top of the agenda in academia, business and policy". The residential sector is indeed "an obvious target for energy conservation policies" (Aydin & Brounen, 2019) as there are huge potentials for energy reduction in urban centres through building energy efficiency measures (Commission to the European Parliament and The Council, 2014).

1.3 Building Energy Conservation and Demand Reduction

A primary goal of recent research efforts, according to Liu et al (2019), has been the reduction of percentage of total energy (global/national/local) consumed/demand by buildings while creating "a comfortable thermal environment for humans". This is because, Souayfane et al (2016) posits, energy consumption in the building sector, whose annual increase is estimated at 1.5% (Verbeke & Audenaert, 2018), could reach 150% of present levels by 2050 if buildings are not made more energy efficient.

To this end, several measures have been suggested (even implemented) with the aim of reducing energy demand by buildings. According to Chwieduk (2017), the importance of energy conservation in buildings can be seen at the national energy policy level … in many countries. Prominent example is the EU's 20–20–20 goals, which proposed a 20% increase in energy efficiency, 20% reduction in carbon dioxide emissions and 20% utilisation of renewable energy systems and sources for buildings by 2020 (European Commission, 2020(a)), for which the zero energy buildings concept was adopted as a strategy.

The zero-energy buildings concept implies reducing energy demand of buildings through various energy-saving measures, namely, energy storage, implementation of energy efficient technologies and utilisation of renewable energy systems and sources, to the point where zero amount of conventional energy is utilised (Li et al, 2013). It is sometimes referred to as Nearly Zero Energy Building concept (European Commission, 2020). This approach, Qian et al (2019) contends, is effective, and a practical one, capable of reducing overall energy consumption in the building sector. According to (Pacheco-Torgal, 2017) implementation of the EU's directive on building energy performance, the European Energy Performance of Buildings Directive 2010/31/EU (European Parliament and the Council of the European Union (EUROPA), 2010), which proposes that all new constructions must be net zero-energy

building standards from 31st of December 2020 is implemented energy savings of up to 755.95 MWh of energy can be achieved.

Energy saving measures include heat/energy storage and heat loss prevention measures and systems while energy efficient technologies entail building energy systems, such as heating, cooling and ventilation (HVAC), lighting and controls, that are optimised for low energy demand and efficient energy utilisation. And, as the name implies, use of renewable energy systems entails sourcing some (or all) of the energy requirement for the building from renewable sources.

An example of energy efficiency technology is the Passive House concept, or standard. The concept, established by the Passivhaus Institute in Darmstadt, Germany in 1996 (Passive House Institute (a), 2015), is a standard for energy efficiency in buildings focused on taking advantage of the "passive" influences of sunshine, shading and ventilation on a building. It is based on five basic principles of airtightness, continuous thermal insulation that eliminates thermal bridging, superior quality and performance windows, ventilation heat and moisture recovery, and minimal space conditioning system. Buildings designed to this standard require very small energy input to satisfy requirements for space heating and/or cooling (Passive House Institute (b), 2015).

1.4 Energy Storage in Buildings

Energy storage in buildings contribute to increasing buildings' share of renewable energy utilisation and to reducing its energy demand (Heier, Bales, & Martin, 2015). They function to reduce energy demand by harnessing/capturing free and/or waste heat/energy from atmosphere, the building and/or its systems (Liu, Li, Chen, Luo, & Zhang, 2019) and using, or reusing to offset some of the building's energy demand.

Energy storage affords opportunities for better utilisation and management of building's energy. It reduces wastages because energy systems would not necessarily have to be designed for maximum load but for an optimum that is some mid-way between highest and lowest demand. Excesses during periods of low utilisation, or high resource availability from natural, renewable sources, can be stored away and utilised to meet up supply during periods of high energy demand, or little or no resource availability. This way energy demand and supply profile can be levelled. For natural, renewable energy resources, it provides opportunity for extending supply and making it appear continuous.

While there are enormous potentials for energy savings with storage there are shortcomings which include requirements and cost of additional components and space, and of retrofits and upgrades of existing systems to accommodate storage system. Also, the energy storage system/material/substance amounts to additional load on the building's energy source, which could lead to occasional increase in energy demand when storage in being charged. Nevertheless, it is an important measure in efforts towards improving buildings' energy efficiency and reducing CO_2 emissions from the sector.

1.4.1 Energy Storage in Building envelopes

One of the ways of employing energy storage to reduce building energy demand is by taking advantage of the energy storage capabilities of its envelope, made up of the walls, floors, doors, windows and roof. According to Meng et al. (2015), between 60–80% of the heating and cooling load is due to heat loss and gain through these building components while the walls alone, Abanda & Byers (2016) posit, can capture between 25–30% of thermal energy that would otherwise have been lost from buildings.

Thermal performance improvement of building envelopes is achievable by applying thermal insulation to it. Materials employed for thermal insulation of buildings are of two types: (1),

materials that reduce rate of heat flow in or out of the building and (2), materials that capture and store heat flowing in or out which can later be used for heating the building. The former are materials with low thermal conductivities or high thermal resistance used for thermal insulation while the latter constitute substances/materials with energy/heat storing capabilities and include high thermal mass materials like concrete or bricks or phase change materials installed as panels or integrated into building envelope's construction materials.

Potentials for reducing CO_2 and SO_2 emissions by up to 50% and 54%, respectively have been reported by (Özkan & Onan, 2011) when insulation is added to building's envelope and varying the thickness of glazing while Kuczyński & Staszczuk (2020) reported a reduction of between 67% and 75% in cooling energy demand with application of high thermal mass masonry construction as opposed to lightweight skeletal construction for residential buildings in temperate climate regions. These are indications of opportunities for energy and greenhouse gas emission reductions through building fabrics.

1.4.1.1 Passive Building Envelope Thermal Storage Systems

Energy systems/materials employed for capturing and storing heat flowing in or out of buildings are of two types, active and passive. A passive system is defined as one that takes advantage of available (free) energy like energy (heat or cold) from heating systems and appliances or (and) natural/renewable energy sources, like the sun (on hot sunny days), or cold energy from cold night air, without requiring a dedicated specific energy input or carrier/transport medium. The system employs high density construction materials that also have relatively high specific heat capacities, like concrete, rock and stones, or materials that store large amount of heat when they change from one phase to another (phase change materials), for capturing heat, or cold. Energy stored is re-used in the building later either as main energy input or to augment the building's energy supply.

These types of system work by absorbing heat transmitted through, say, the glazing and/or opaque enclosures during the day, thereby stabilizing indoor temperatures, and releasing the stored heat during the night when the indoor temperatures drop. In so doing they prevent the space temperatures from getting too low and indoor environment from becoming excessively cold at night (Peippo, Kauranen, & Lund, 1991; Mehling & Cabeza, 2008). No heat transfer medium is employed for removing stored heat from the storage material, rather the heat is removed by natural air flow within the building/space as it makes contact with the heat storage material/system.

They are often referred to as thermal mass and find use and application in passive houses for heat recovery and reuse, being fundamental with regards to the Passive House concepts of ventilation heat recovery and requirement for minimal space conditioning system. They are effective in capturing heat and helping to stabilise indoor temperatures, as well as reduce overall energy consumption of buildings since they consume virtually no energy. However, their effectiveness could be compromised in the event of little or no availability of energy from the energy sources, for example on cloudy days.

A review of PCM applications in building envelopes passive systems was reported by Faraj et al. (2020) and Zhou, et al. (2020) while an analysis and comparison of the different types of thermal mass employed for building envelopes passive thermal energy storage system were reported by (Kensby, Trüschel, & Dalenbäck, 2015; Reynders, Nuytten, & Saelens, 2013; Hurtado et al., 2017).

1.4.1.2 Active Building Envelope Thermal Storage Systems

Active thermal energy storage systems utilise, or require, dedicated heat input and output, and/or employ a heat transfer medium/system to transfer heat/energy to and from the storage material and to and from the building. The dedicated system is a separate system whose

function is to supply and/or distribute heat to and within the storage material. Heat release to the building's interior is accomplished by either direct flow of the heat transport medium through the storage material into the building/space, or through a heat exchanger to a secondary heat transport medium (usually building's internal air) flowing into the building/space. The system could be composed of any of the thermal storage materials employed in passive systems but would be in combination with a dedicated heating system and/or mechanical driven heat transport medium, which forces or distributes heat through them. The thermal storage materials still store heat as they would when used in passive systems, but heat delivery and removal of the stored heat is accomplished by the dedicated heat transfer medium. A well-known example is underfloor heating. Their potential use as demand side energy and load management tool was reported by Russell & Surendran (2001), Ellerbrok (2014) and Dréau & Heiselberg (2016). Faraj et al. (2020) and Zhou, et al. (2020) also did comprehensive reviews of active building PCM integrated energy systems.

1.4.2 Energy Storage in HVAC Systems

HVAC systems are mechanical systems employed for providing heating and cooling to a building with the aim of regulating the atmosphere within its interior for thermal comfort of its occupants. They are active building energy systems and function by moving heat from either the interior to the exterior of a building or vice versa using a heat transfer fluid mechanically driven into and out of it. They extract heat from one source and deliver heat to a sink, either of which can be located in the building's interior or exterior. When coupled with thermal storage systems, they become a type of active thermal energy storage systems. They help utilise energy storage to manage building energy demand by storing away energy/heat from building energy systems, or from natural, renewable sources like solar, wind, wave and tidal energy, for use (later) to offset some (or all) of its energy needs.

They employ high density, large mass, materials like concrete or bricks for thermal mass heat storage in systems like underfloor heating system (Maivel et al, 2018), electrical space heating systems, water or water- based systems with hot water storage tanks, boilers and heat pumps, or phase change materials in combination with other heat storage or transport materials (Qiu et al., 2017; Frazzica, et al., 2016; Kumar, et al., 2016). The storage material may be alone or used as suplement to the primary heat store in active water and space heating or cooling systems (Labat et al., 2014; Mankibi et al., 2015; Navarro, et al., 2016).

Using thermal storage with HVAC systems, especially when the energy source is a clean renewable source like wind, solar and geothermal, is a means by which overall building energy demand and CO_2 emissions can be reduced. It is particularly beneficial and effective when phase change thermal materials are employed for heat storage (De-Gracia, et al., 2013; Real, et al., 2014).

1.5 Utilisation of PCMs for Thermal Energy Storage in Buildings

Applications of PCMs for thermal energy storage in building dates back to the mid-1940s (Kośny, 2015) and has grown considerably ever since. These materials store heat as latent heat during phase change, allowing storage of more heat/energy per unit mass and volume. Subsequently, storage systems are smaller, lighter and more compact, which results in reduced heat loss, heat loss being proportional to surface area.

Change of phase, from solid to liquid or liquid to gas and back, occurs at relatively constant temperatures, implying that difference between heat storage and heat delivery temperatures need not be large. This implies heat supply and delivery at relatively constant temperatures,

which would reduce or limit heat loss or wastage from the system (Farid et al., 2004). This method is effective for smoothening out fluctuations in supply (Münster & Lund, 2007; David, Kuznik, & Roux, 2011).

PCM energy storage systems offer huge benefits and opportunities for reducing energy and CO_2 emissions from buildings (Tian & Zhao, 2013) and for enhancing buildings' ability to stabilize and maintain steady internal temperature conditions (Singh, Muetze, & Eames, 2010; Hong et al,, 2012; Halford & Boehm, 2007). According to Arteconi, Hewitt, & Polonara (2012), phase change energy storage can ensure energy security, efficiency and environmental quality.

Ability and potential of phase change thermal energy storage materials to improve heating and cooling systems' performance and reduce energy consumption in buildings have been well established, being primary motivations for many research works. However, utilisation of PCMs for heat storage is not without shortcomings, relating mostly to their properties and applicability. There are also associated (additional) energy cost (Kośny, 2015). This is discussed in more details in section 1.7.

1.5.1 PCM in Building fabric and construction – Passive Systems

PCMs are employed in building fabrics to capture and save heat either flowing from the external or the internal of buildings through windows, roofs and walls. This is subsequently utilised to either provide heating directly for the building or supplement heating provided by the heating system. PCMs can be employed in either for passive building fabric heat storage or for active building fabric heat storage.

Passive PCM based heating (or cooling) systems are systems employed for improving energy systems' efficiency without consuming any power or energy. They work to either transfer

heat to or from a natural heat sink or source from or to a living space, or by preventing heat from entering or leaving a living space from or to external heat sources or sinks.

Passive PCM based heat storage systems have found applications in building structures like boards/panels and claddings for walls (Wijesuriya et al., 2018) and floors (Entrop et al., 2016), roof/ceilings (Hasan, Basher, & Shdhan, 2018), and in building components like window shades and glass panels (Silva, et al., 2016); and in construction materials like concrete (Pomianowski et al., 2014) and bricks and blocks (Kant, Shukla, & Sharma, 2017).

Impact of PCMs in external building walls on heating energy demand, energy consumption and thermal comfort have been reported by Sajjadian, Lewis, & Sharples (2015), Gassenfeit & Brüggemann (2014), Guarino, et al. (2015), and a host of others. Its applications in demand side management (Qureshi, Nair, & Farid, 2011), energy and load shifting (Muruganantham et al., 2010) and for analysing energy cost and implication to stake holders (Entrop et al., 2016) is also well reported.

Application of these type of systems suffer from one significant flaw. They do not perform effectively during cold seasons and may often require assistance from an active system (Kusama & Ishidoya, 2017) because the PCMs are unable to complete full thermal cycles. This can be addressed by adding a dedicated heating system, in which case, they become active.

1.5.2 PCM in Building fabric and construction – Active Systems

Active heat storage systems are systems that require dedicated continuous, or regular, input of energy (or power) to extract, store and release heat. They could be constituted by passive building structure/materials, or any type of thermal storage material/device, to which a dedicated heat energy supply and retrieval system, often assisted with mechanical equipment, has been added. The stored energy may be from direct or indirect energy/power consumption

and/or input of heat to the storage material. They have applications in space heating systems like underfloor heating (Lu et al., 2017; Barzin et al., 2015; Devaux & Farid, 2017) and ceiling plenums (Morovat, Athienitis, Candanedoa, & Dermardiros, 2019).

Application of active PCM heat storage systems in building walls is, however, relatively new with very little reported research on the subject. A notable recent attempt was reported by (Kong, Wang, Li, Yuan, & Yao, 2020) who combined a passive PCM wallboard and active solar water heating system. Their system consists of thin pipes carrying hot water from a solar water heater embedded into PCM wallboards which they installed on the internal surfaces of walls and ceilings of a test building. This is one of the motivations for this research, a proposal to develop an active PCM based fabric integrated heat storage system using PCM as storage material.

The addition of mechanical heat delivery and transport system to PCM based building fabric integrated heat storage system leads to improved performance during periods when effectiveness of passive systems would have become compromised due to little or no availability of energy from the energy sources.

1.5.3 PCM in HVAC and Water Heating systems

Use of PCMs in energy saving measures in buildings include application with mechanical air and water heating (HVAC) systems as well as in space cooling HVAC systems (Zeinelabdein, Omer, & Gana, 2018). Residual or waste heat from the heating systems, or cold energy from the ambient at night, is stored in the PCM. They may be employed as primary store/source wherein heat, or cold, supply to building is obtained directly from the PCM (Mankibi et al., 2015) or as secondary heat store/source wherein they augment the primary heat store/source. (Badescu, 2003; Talmatsky & Kribus, 2008; Canbazoğlu et al., 2005)

Applications as secondary heat store with domestic water and space heating systems have been examined for assessment and/or determination of effectiveness (Frazzica et al., 2016; Cabeza et al., 2006; Kumar et al,, 2016); for quantity of PCM required (Chaabane et al., 2014; Nkwetta et al., 2014), for impact on energy consumption and cost (Najafian et al., 2015; De Gracia et al., 2011), load shifting capability (Moreno et al., 2014) and for environmental impact of buildings' heating/cooling systems (De-Gracia et al., 2014) with encouraging results.

1.6 Challenge of PCM Deployment in Building Systems

There are challenges with use and application of PCMs in buildings for thermal storage and energy efficiency, which relates mostly with the negative and counter-productive properties of the material (Zhou, et al., 2020). Finding ways to overcome and/or compensate for these property flaws has presented researchers, building and energy managers with numerous opportunities for research and development in an ever-increasing area of selection, design, application and implementation methods.

Virtually every PCM has at least one undesirable property, or as Cui, et al. (2015) puts it "there are scarcely any PCM that can meet all desirable criteria". Highest thermal conductivity of organic PCMs is around 0.2 W/m^2K (Fang, et al., 2014), which, according to Şahan, Fois, & Paksoy (2015), does not promote rapid thermal response and leads to some loss in energy recovery (Farid, et al., 2004). There are also problems of high volume variation and liquid seepage during phase change (Mehrali, et al., 2014; Schossig, et al., 2005), which could lead to undesirable wetness of structures and components (Almeida, et al., 2010). This is a particularly limiting factor for application of organic PCMs (Khadiran et al., 2015) as it can compromise the structural integrity of structural/construction materials, with negative

consequences on their strength, durability and safety. Liquid seepage is of great concern particularly for paraffin based PCMs, most of which are highly flammable.

Inorganic PCMs, on the other hand, have high corrosive tendencies, incongruent melting and propensity for phase segregation upon melting (Akeiber, et al., 2016). Incongruent melting results from salts dissolving out of their water of hydration upon solidification and not becoming rehydrated after temperature rises above melting point while phase segregation is when the different components of the PCM change phase individually and at different temperatures resulting in macroscopic separation of phases with different composition after many cycles. The outcome is a thermal storage system containing two (or more) separate substances with different properties, leading to reduced overall heat storage capacity because the initial system composition optimised for design storage capacity will have been altered. These class of PCMs also have a problem of subcooling (or supercooling), a phenomenon whereby a PCM remains in the liquid phase at temperatures below its phase change temperature. Subcooling tends to reduce solidification rate and PCM is unable to release heat at the required temperature, resulting in overall reduction in energy storage capacity.

Hysteresis is another phenomenon that presents uncertainties with PCM applications. Hysteresis is experienced by all PCMs and occurs when there is incomplete transition from one phase to the other due to either of the heat supply temperature being lower than the maximum melting temperature or the or withdrawal temperature being higher than the minimum melting temperature of the PCM before cycle reversal. This results in large amounts of heat that is neither stored nor released (Zastawna-Rumin, Kisilewicz, & Berardi, 2020) leading to reduced effectiveness of the thermal storage system.

Application of PCMs in buildings also presents uncertainties about reliability, cost, economic feasibility and safety, as well as design configuration and integration with other sustainable energy technologies (AL-Saadi & Zhai, 2013). So, deployment of the material into buildings

and systems require pre-analysis and study. This presents a challenge, as conducting experiments on buildings with uncertainties relating to properties like flammability, corrosiveness and chemical reactivity is risky and dangerous. Also, experimentation with buildings is generally costly, and sometimes require elaborate retrofitting and modifications to an existing structure, which may not be practicable or cost effective. An alternative to experimentation is employing numerical models which enables a building to be analysed without high cost of materials and the risk of damage to structure and/or rendering it unsafe.

1.6.1 Building and Building System Modelling

Numerical modelling refers to theoretical research methods that employs mathematical equations as representation of the studied system, or conditions within, to develop a numerical model/representation of the system. It entails development of an algorithm that enables the model to mimic behaviour of actual system and its response to changes in input parameters. This method is quick and less expensive.

Mathematical models make it possible to analyse hypothetical systems which can easily be adapted and examined over wide range of scenarios (Crawley, et al., 2008). Also, there are vast advantages in terms of speed, cost (Pomianowski, Heiselberg, Jensen, Cheng, & Zhang, 2014) and accuracy, and it is the cheapest way to conduct different analysis of designs and material innovations (Marin, et al., 2016), with combinations of all possible conditions, scenarios and control strategies required for effective optimisation of the final product.

Numerical analysis of buildings with PCM installed in various parts, components and systems are reported by several authors like Sajjadian, et al. (2015), (Izquierdo-Barrientos, et al. (2012), Gassenfeit & Brüggemann (2014), De-Gracia et al. (2014) and a host of others.

1.7 Modelling and Simulation of Buildings with PCMs

1.7.1 Building Energy Modelling and Simulation Tools

Performance analysis and evaluation of buildings that have PCM deployed often requires use of whole-building simulation platforms. These tools have capabilities for analysing a building, its components and system's dynamic thermal behaviour numerically. A list of various whole building modelling software packages, comparative assessments of their functionalities and reviews are reported by Saffari, et al. (2017), Madad, et al. (2018), Kylili & Fokaides (2017) and Crawley, et al. (2008).

While there exists many programs and software with capabilities for conducting whole-building simulations, very few have capacities to simulate buildings with PCMs (or PCMs in buildings). These are Trnsys, EnergPlus and ESP-r. Of them. Only EnergPlus and ESP-r are available as free, open-source software. These two will be examined in more details.

EnergyPlus is based on some popular features of BLAST (Building Loads Analysis and System Thermodynamics) and DOE-2.1E (Corrado & Fabrizio, 2019); (Castell & Solé, 2015), both of which were developed in the 1970s and 80s (Crawley, Hand, Kummert, & Griffith, 2008), and predicated on the integrated interactive simulation of zone and the air conditioning systems, while ESP-r (Environmental Systems Performance – r for the European Reference Program) is a general purpose, multi-domain building energy simulation program based on the mathematical model proposed by Clarke (2001).

EnergyPlus works as a modular system integrated with a heat balance-based zone simulation using equations sets that define energy consumption of the building Torres-Rivas et al., 2018). It employs a predictor–corrector scheme to estimate zone thermal loads in a heat balance engine, which passes its results onto the building systems simulation module. Input and output are via text files (ASCII texts), it is a stand-alone with no 'user-friendly' graphic

interface and is available via free downloads. There are, however, graphic user interfaces developed by private software developers for the tool, like Design Builder (DesignBuilder Software Ltd, 2021), Simergy (Energy Technologies Area, 2013) and a host of others. These are not part of EnergyPlus nor are necessary to run it but they make it easier to use. Some are available for free while others require purchase. ESP-r, on the other hand, models energy and fluid flows within a combined building and plant systems using advanced numerical methods to integrate the various equation types representative of the heat and mass balances within the building along with real time series climate data and control, and occupancy-related boundary conditions.

1.7.2 PCM Simulation in EnegyPlus and ESP-r

PCM modelling in building energy simulation packages have, for the most part, been focused, primarily on building structures like walls, ceilings and floors. This is because employing PCMs for energy conservation in buildings emanated from use of thermal mass storage systems, which generally involves these building structures. So PCMs are simply added or integrated into the structures and their models are representation of both the structures and the PCM. This is generally the case with PCM models in ESP-r. A building structure, or a plant, is modelled with provision for incorporating PCMs. Example of PCM incorporated into building structure was reported by Heim & Clarke (2004) using a special material modelling concept described by Kelly (1998).

In the special material modelling concept, a mathematical function is employed to represent changes in thermophysical properties (like phase) of a material upon influence or excitation by an external source (like heat). This can then be applied to nodes within a building component or node of an entire component.

ESP-r also employs a method whereby the PCM is modelled separately for integration into a plant component. A link is provided for calling up the subroutine containing numerical codes of the PCM model whose results are added to those of the plant component/system if it is specified as having PCMs in its configuration. This has been reported by (Padovan, Analysis and Optimization of PCM Enhanced Storage Tanks for Solar Domestic Hot Water Systems, 2014).

In EnergyPlus, PCM is modelled in a similar fashion to the treatment for plant component/system incorporation/integration in ESP-r, as a separate component which can be called up when required for both structures and components.

1.7.3 PCM Modelling in ESP-r

Modelling generally entails developing and solving mathematical equations representative of the energy transformation and change experienced by a substance. With problems involving phase change, solutions are quite complicated because there are two phases involved, whose equations must be solved simultaneously. Also, the phase change interface is not stationary, and latent heat absorption and/or released occur at the interface. It would require writing separate energy equations for all the phases involved and coupling their temperatures at the interphase. This is problematic, as it requires determining the interphase location, which is not easy if the problem is to be solved by finite difference methods (Ozdenefe & Dewsbury, 2012).

In ESP-r, modelling of PCM in the (passive) building structure, is accomplished by employing the apparent heat capacity method with explicit scheme where the nonlinear behaviour of the phase change is captured in definition of the apparent heat capacity term. Determination of this term is done either by experimentation or approximation, analytically/empirically (Fang & Medina, 2009; Faghri & Zhang, 2006) or numerically

(Comini, Del-Giudice, & Saro, 1990). There are problems with this determination, occasioned by the non-isothermal behaviour of PCMs during phase change (Mehling & Cabeza, 2008), which increases complexities even with the introduction of fictitious melting temperature range (Madad, Mouhib, & Mouhsen, 2018; Al-Saadi & Zhai, 2013). Also, there is the possibility of there being a 'skipping' of the latent heat contribution during phase change. One of the methods proposed for dealing with the skip is to apply a 'post iterative" correction which is expected to ensure all latent heat contributions are accounted for (Voller, 1996). Additionally, the effective heat capacity method is based on variations of heat capacity with temperature during phase change.

This is non-linear and requires the explicit numerical scheme for the determination. The variations of heat capacity with temperature during phase transition is equally changing, very rapidly over a very short temperature interval, introducing errors into the results (Sadasivam et al., 2011), a phenomenon that is even more pronounced for substances whose phase changes occur over a single, or fixed, temperature.

Figure 1.2a and b are heat capacity-temperature curves showing variation of effective heat capacity with temperature, from which enthalpy change is determined, represented by the shaded area. Figure 1.2a shows the change in enthalpy over elapsed time, Δt, that would be obtained from application of the effective heat capacity method, equation 2.14, whereas the actual enthalpy change is somewhat different, represented by shaded area under figure 1.2b.

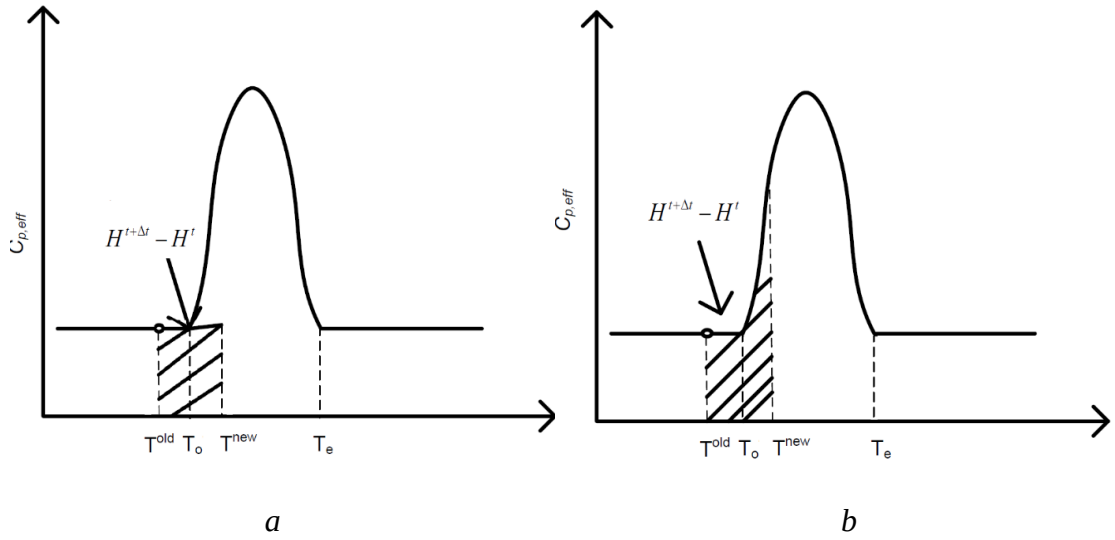

a *b*

Figure 1.2: $C_{p,eff}$–T curve, (a) erroneous calculation based on equation 2.13 & 2.14, (b) actual enthalpy change. (Sadasivam et al., 2011)

Solution adopted to overcome, (or eliminate) the error is to assume or suggest a phase change (or melting) temperature range regardless of material's actual characteristics. Since this is a guess, it cannot be standardised and there is no way to ascertain correctness, therefore it has the potential to introduce errors that result in underestimation of calculated properties of PCMs whose phase change temperature range is large and overestimation of calculated properties of PCMs with fixed, single phase change temperatures (Obitayo, 2011).

1.7.4 PCM Modelling in EnergyPlus

In EnergyPlus specific heat capacity of the PCM is determined from enthalpy of the substance, which is a measure of its energy level (or content), from which temperature is determined. Advantages of the enthalpy method is that by adopting enthalpy form of the energy equation, which is applicable to all phases, only one energy equation need be written for both (or all) phases. Subsequently, accurate temperatures and specific heat capacity can be determined from the enthalpy, which is easily obtainable even during phase change, at successive time intervals.

The method for determining the temperature and enthalpy values in the PCM code employed in EnergyPlus is somewhat complicated as it requires that the values (enthalpy and corresponding temperatures) be successively inputted into the program during execution. This could be done manually by user through an enthalpy-temperature curve of the PCM (Ozdenefe & Dewsbury, 2012) introduced before programme execution, or by coupling the program to an enthalpy-temperature function that reads enthalpy values at different temperatures (Crawley, et al., 2004; Zastawna-Rumin, Kisilewicz, & Berardi, 2020). Accuracy of the method/procedure depends largely on provision of these values for the system to model the PCM.

1.8 Rational and Justification for Research

1.8.1 Modelling Method/Approach

The challenges with physical deployment of PCM in building or systems for analysis necessitates use of whole building modelling applications like EnergyPlus and ESP-r. The methods and/approaches to PCM modelling in these applications presents some challenges. In EnergyPlus for instance, enthalpy-temperature values for PCM, which are not readily available for most substances, must be loaded/inputted into the program manually or in the form of a chart. This is challenging prospect because while enthalpy values and corresponding temperatures are available for many liquids and gases, one would need to experimentally determine them for most solid substances. The fact that manufacturers of PCMs do not normally provide elaborate or detailed data about their products compounds the situation. Despite the various modifications and upgrades the software has undergone to improve PCM modelling, like introduction of CondFD algorithm and the finite differencing schemes, the user is still required to input enthalpy-temperature data (sample shown in

appendix D) that is expected to 'cover the entire temperature range that will be seen by the material in the simulation' (University of Illinois, 2021). In the most recent version of the sofware this data is read using an enthalpy-temperature function, which is unique to different materials. Subsequently, using the software (EnergyPlus) is a little technical and limits choice of PCM.

The apparent heat capacity method adopted in ESP-r relies on variations of specific heat capacity with temperature, which is non-linear and not easy to determine during phase change, especially for substances whose phase change occur over a single, or fixed, temperature. One solution for this is to introduce a fictitious melting temperature range for the PCM (AL-Saadi & Zhai, 2013). The method presupposes that heat capacities of the solid phase is different to that of the liquid phase of the material. This is not always the case, particularly with the paraffins that have the same specific heat capacities for both solid and liquid phases. This implies that enthalpy change during phase change may not be adequately captured for some (or many) substances even with the introduction of a fictitious melting temperature range (Al-Saadi & Zhai, 2013).

The requirements for inputting an h-T curve or data in the more accurate enthalpy method employed in EnergyPlus can be eliminated by utilising property values of the PCM at each of the phases it is expected to undergo during the process, as well as the phase change energy (or enthalpy). Subsequently, values of the specific heat capacity and thermal conductivity of the solid, liquid and gaseous phases of the PCM, the phase change enthalpy and phase change temperatures, are all that will be required to model the PCM as its temperature rises (or drops) to phase change temperature, its phase change process, and subsequent temperature rise (or fall) thereon.

The method had been proposed by Sadasivam et al. (2011) as a replacement for the apparent heat capacity method employed for modelling PCMs embedded in building structures (fabric

integrated) in ESP-r but has not been implemented. It was employed for the stand alone PCM plant model whose subroutine is called up when required for integrated specifically into hot water storage tanks plant components models in ESP-r by Padovan (2014). This is primarily an ad on for existing models of hot water storage tanks in the system, with the aim of enhancing the tanks heat storage capability. The PCM code is a subroutine that is called if the hot water tank plant is configured to have PCM models.

1.8.2 Benefit of Improved PCM modelling and Models

ESP-r does not have a dedicated PCM thermal energy storage plant, one that has capabilities for substituting conventional hot water storage tank systems. This type of system is germane to efforts and research into ways of reducing energy demand and consumption, as well as CO_2 emissions, from buildings and have been advertised by several manufactures and developers, the likes of Sunamp (Sunamp technology, 2020), CrodaTherm (Croda International Plc, 2020), Heatventors (HeatVentors Kft, 2020), etc., as available for deployment for both domestic and industrial applications. ESP-r would benefit a great deal and would be improved as a building energy assessment platform from having such systems in its arsenal of tools.

Existing building fabric integrated PCM model in ESP-r is the passive type, which does not require a dedicated heat input or extraction mechanism. The concept of active fabric integrated PCM heat storage system, like that reported by (Kong, Wang, Li, Yuan, & Yao, 2020), though relatively new, is gradually gaining attraction. This type of system has applications in both direct and indirect space heating as well as in water heating. It has not been implemented in ESP-r, nor any building energy analysis software package.

The proposed models, with regards to modelling method and approach, are improvements over the cumbersome modelling method employed in EnergyPlus (Ozdenefe & Dewsbury,

2012; University of Illinois, 2021). The proposed modelling method seeks to eliminate the requirements for inputting an enthalpy-temperature (h-T) curve/chart or data before or during the simulation.

1.9 Research Aim and Objectives

1.9.1 Aim

Aim of the research is the development of models of active PCM based heat/thermal energy storage plant system for integration/incorporation into ESP-r building energy modelling system.

1.9.2 Objectives

Employing the more accurate enthalpy method but eliminating the need for enthalpy-temperature data input into the system as required in EnergyPlus, the research proposes to:

1. To develop numerical model of a heat/thermal storage battery for implementation in ESP-r using PCM as heat storage medium.
2. To develop numerical model of an active building fabric integrated heat/thermal store also for implementation in ESP-r
3. To integrate/implement models in(to) the ESP-r building energy simulation software's plant system/database.
4. To demonstrate models with case studies, assessing for possible areas of application, effectiveness in building energy management with regard to cost and CO_2 emission reduction and comparing with similar conventional sensible heat thermal energy storage systems.

Chapter 2

MODELLING AND PCM REPRESENTATION IN ESP-r

2.0. Introduction

Using PCMs in buildings has challenges and uncertainties mostly relating to their properties. There are also uncertainties about their reliability, cost, economic feasibility and safety, as well as design configuration and integration with other sustainable energy technologies (Al-Saadi & Zhai, 2013). Conducting experiments on buildings with uncertainties relating to PCM properties like flammability, corrosiveness and chemical reactivity is risky and dangerous. Also, experimentation with buildings is generally costly, and sometimes require elaborate retrofitting and modifications to an existing structure which may not be practicable or cost effective. By employing numerical models, a building can be analysed without the risk of damage to its structure or rendering it unsafe.

Mathematical models make it possible to analyse hypothetical systems which can easily be adapted and examined over wide range of scenarios (Crawley, Hand, Kummert, & Griffith, 2008). Also, there are vast advantages in terms of speed, cost (Pomianowski, Heiselberg, Jensen, Cheng, & Zhang, 2014) and accuracy, and it is the cheapest way to conduct different analysis of designs and material innovations (Marin, et al., 2016) with combinations of all possible conditions, scenarios and control strategies required for effective optimisation of the final product.

The chapter discusses modelling and representation of phase change materials in ESP-r building energy modelling/simulation system, being one of the few programs and software

with capabilities for conducting whole-building simulation of buildings with PCMs (or PCMs in buildings).

2.1. The ESP-r Building Energy Simulation System

The Environmental Systems Performance, research version (ESP-r), is an open source building energy simulation program developed by the University of Strathclyde in the 1970s. The program is still undergoing development and improvements and was based on a set of mathematical models described by (Clarke, 2001). While it has gone through series of developments, improvements and augmentations, its core purpose and principle remain the same, the simulation of building energy performance in a manner that is both realistic and very close in resemblance to actual systems (Aasem, 1993; Heim & Clarke, 2004; Hensen 1991).

The objective is achieved by employing advanced numerical methods to simultaneously integrate several mathematical equations employed for representing energy, heat and mass balances, CFD and electrical domain of a building at successive time-steps in response to influences by climate, occupants and control systems. This way, an in-depth appraisal of factors that influence the building's thermal performance is conducted while estimating the heat and moisture exchanges, and its thermal and electrical energy demand.

Designed primarily as a research tool, ESP-r affords opportunities for exploring inter-relationships between the geometry, construction, occupancy and air flow and distribution of a building, as well as interactions with plant systems, employing integral plant and zone control strategies. Its intention is 'to allow users conduct a high integrity, first principle appraisal of buildings whilst modelling all aspects of the energy subsystem simultaneously' (Jensen, 1993). It can be employed for simulating the thermal, optical and acoustic performance of a building, its associated energy use and gaseous emissions.

It has capabilities for assessing effects of weather, external shading, occupancy and various plant systems on building performance. It can address diverse problem types and configurations, which may range from a one zone enclosure with no plant to a full-scale building with many zones and comprising many plants.

According to Hensen (1991) and Al-Mosawi (2011), some of ESP-r's attributes include:

- An objective to simulate real world as rigorously as possible to a level dictated by international research efforts and results.
- Ability to assess building performance in terms of thermal comfort and gaseous emissions by taking all building and plant energy flows, and their interconnections into full account.
- A modular structure that makes source codes available and accessible.
- A robust repository of programs and codes (mathematical equations) and database representing every possible system and component that would compose a building, from construction materials that make up its walls, doors, windows, floors, ceiling and roofs to the types of boilers and heat radiators, and the pipes connecting them.

2.1.1. Problem Definition in ESP-r - Control Volumes

ESP-r uses control volume scheme to discretize problems into small discrete control volumes. Each represents a region of space (or, sometimes, a solid object or a plant, or part of a plant) wherein ‘‘local equilibrium’’ is (assumed to be) achieved at a time scale comparatively shorter than computational time step. It is denoted by a node and the value of a field quantity at its centre is assumed to be representative of the average over the entire volume. A typical ESP-r building model will consist of thousands of control volumes.

For each node, between one (1) and three (3) conservation equations are developed for heat, mass and momentum flow depending on whether the node represents a solid structure/object,

water or air. One (1) equation – heat only – if volume refers to a solid object, two (2) – heat and mass flow – if water, and three (3) equations if air – one (1) for heat and two (2) for mass flow equations, one for dry air and one for water vapour.

CFD domains are modelled separately as it allows more accurate representation of the air flow and temperature distribution withing zones. This is done by subdividing the zones into smaller control volumes and solving the associated conservation of mass momentum, energy and concentration equations. A similar approach is adopted for the electrical network/domain. The methods and solvers employed for solving the heat, momentum and mass equations for zones, mass and heat flow, CFD and electrical domain is discussed further in subsequent sections.

As well as the variability of their nature, i.e., what they represent, control volumes also possess a flexibility that makes them applicable for modelling any of the various parts of the building and a variety of physical processes. Solutions to the representative equations of the control volumes ultimately lead to solution of the part of the building they represent, be it zones, plants or part of a plant, and, in turn, the entire building.

A control volume would have as its boundaries other control volumes, which could represent solid constructions or fluid and would exchange heat (energy) or fluid (or both) with them. It would also experience exchanges and interactions with the exterior (fluid flow), occupants (heat and vapour gains) and plants. Sample interaction between control volumes is depicted in figure 2.1.

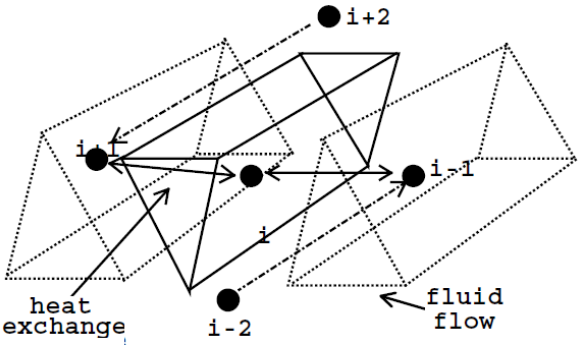

Figure 2.1: Control volume interaction in ESP-r (Kelly, 1998)

Nodes ***i, i+1, i-1, i+2 and i-2*** represent control volumes ***i, i+1 and i-1,*** exchanging energy, and possibly, mass flow with the surrounding, ***i+2 and i-2***.

$$\boldsymbol{m_i c_{p,i} \frac{\partial T_{ave,i}}{\partial t_i} = q_i + q_{i-1} + q_{i+1} + q_{i-2} + q_{i+2}} \qquad 2.1.$$

The conservation equation for a control volume depicted by ***i*** takes the form (eq. 2.1).

2.1.2. ESP-r Problem Processing - Matrix Equation Processor

The core of ESP-r's numerical engine is its customised matrix equation processor. This has the capacity to handle variations in time steps and can process mathematically 'stiff' systems for which time variations is in large order of magnitudes. It is also able to handle complex distributed controls. It employs a special numerical technique that ensures simultaneous evolution of all flow-paths during simulation. This guarantees preservation of important spatial and temporal relationships that exists between components and systems.

The general expression of the matrix equation is given in equation 2.1.

$$\boldsymbol{AT^{t+\delta t} = Z} \qquad 2.2.$$

If,

$$\boldsymbol{Z = BT^{t} + C} \qquad 2.3.$$

$$\boldsymbol{AT^{t+\delta t} = BT^{t} + C} \qquad 2.4.$$

A represents matrix coefficients of future time step,

$\boldsymbol{B}$ is the matrix coefficient of present time step coefficients and

$\boldsymbol{C}$ is the matrix coefficients of known terms and boundary conditions,

$\boldsymbol{T}$ and $\boldsymbol{t}$ represent the column matrices of nodal temperatures and time, respectively.

General form of the energy conservation equation derived for system shown in fig 2.1, with heat and mass flow between nodes *(i-1), i,* and *(i+1)* given in equation 2.4.

$$\begin{aligned} \boldsymbol{C_i}\left(\boldsymbol{T_i^{t+\Delta t}} - \boldsymbol{T_i^t}\right) \\ = \boldsymbol{C_i'}\left(\boldsymbol{T_{i-1}^{t+\Delta t}} - \boldsymbol{T_i^t}\right) + \boldsymbol{S_{i+1}}\left(\boldsymbol{T_{i+1}^{t+\theta}} - \boldsymbol{T_i^{t+\theta}}\right) + \boldsymbol{S_{i-1}}\left(\boldsymbol{T_{i-1}^{t+\theta}} - \boldsymbol{T_i^{t+\theta}}\right) \\ + \boldsymbol{S_\infty}\left(\boldsymbol{T_\infty^{t+\theta}} - \boldsymbol{T_i^{t+\theta}}\right) \end{aligned} \qquad 2.5.$$

Where $\boldsymbol{C_i}$ (W/K, or J/sK) represents specific thermal conductance. This is a combination of mass and specific heat capacities per unit time.

$\boldsymbol{C_i'}$ (W/K) represents specific thermal conductance and is a combination of mass flow rate and specific heat capacity.

$\boldsymbol{S_{i+1}}$, $\boldsymbol{S_{i-1}}$ are the thermal conductance (W/K) between node $\boldsymbol{i}$ and the neighbouring fluid and air volumes, $\boldsymbol{S_\infty}$ is the thermal conductance (W/K) between system/component and the environment external to it. These combine heat transfer coefficient/thermal conductivities and heat transfer surface area.

$\boldsymbol{C_i}$,, $\boldsymbol{S_{i-1}}$, $\boldsymbol{S_i}$, $\boldsymbol{S_{i+1}}$ and $\boldsymbol{S_\infty}$ are naturally composed of thermo-physical properties, heat transfer coefficients and mass flow properties of working fluids. Re-writing in explicit and implicit forms, gives

$$\begin{aligned} [\boldsymbol{C_i} + \boldsymbol{\theta}(\boldsymbol{C_i'} + \boldsymbol{S_{i+1}} + \boldsymbol{S_{i-1}} + \boldsymbol{S_\infty})]\boldsymbol{T_i^{t+1}} \\ - \boldsymbol{\theta}\left(\boldsymbol{C_i'}\boldsymbol{T_{i-1}^{t+1}} + \boldsymbol{S_{i+1}}\boldsymbol{T_{i+1}^{t+1}} + \boldsymbol{S_{i-1}}\boldsymbol{T_{i-1}^{t+1}} + \boldsymbol{S_\infty}\boldsymbol{T_\infty^{t+1}}\right) \\ = \boldsymbol{C_i}\boldsymbol{T_i^t} \\ + (\boldsymbol{1} - \boldsymbol{\theta})[\boldsymbol{C_i'}(\boldsymbol{T_{i-1}^t} - \boldsymbol{T_i^t}) + \boldsymbol{S_{i+1}}(\boldsymbol{T_{i+1}^t} - \boldsymbol{T_i^t}) \\ + \boldsymbol{S_{i-1}}(\boldsymbol{T_{i-1}^t} - \boldsymbol{T_i^t}) + \boldsymbol{S_\infty}(\boldsymbol{T_\infty^t} - \boldsymbol{T_i^t})] \end{aligned} \qquad 2.6.$$

$$
\begin{aligned}
&[\boldsymbol{C_i} + \boldsymbol{\theta}(\boldsymbol{C_i'} + \boldsymbol{S_{i+1}} + \boldsymbol{S_{i-1}} + \boldsymbol{S_\infty})]\boldsymbol{T_i^{t+1}} - \boldsymbol{\theta C_i' T_{i-1}^{t+1}} \\
&\qquad = \boldsymbol{C_i T_i^t} \\
&\qquad + (\mathbf{1} - \boldsymbol{\theta})[\boldsymbol{C_i'}(\boldsymbol{T_{i-1}^t} - \boldsymbol{T_i^t}) + \boldsymbol{S_{i+1}}(\boldsymbol{T_{i+1}^t} - \boldsymbol{T_i^t}) \\
&\qquad + \boldsymbol{S_{i-1}}(\boldsymbol{T_{i-1}^t} - \boldsymbol{T_i^t}) + \boldsymbol{S_\infty}(\boldsymbol{T_\infty^t} - \boldsymbol{T_i^t})] \\
&\qquad + \boldsymbol{\theta}\left(\boldsymbol{S_{i-1}T_{i-1}^{t+1}} + \boldsymbol{S_{i+1}T_{i+1}^{t+1}} + \boldsymbol{S_\infty T_\infty^{t+1}}\right)
\end{aligned}
\qquad 2.7.
$$

Matrix coefficient can be extracted thus,

$$\boldsymbol{C_i} + \boldsymbol{\theta}(\boldsymbol{C_i'} + \boldsymbol{S_{i+1}} + \boldsymbol{S_{i-1}} + \boldsymbol{S_\infty}) = \boldsymbol{A} \qquad 2.8.$$

$$
\begin{aligned}
&\boldsymbol{C_i T_i^t} + (\mathbf{1} - \boldsymbol{\theta})[\boldsymbol{C_i'}(\boldsymbol{T_{i-1}^t} - \boldsymbol{T_i^t}) + \boldsymbol{S_{i+1}}(\boldsymbol{T_{i+1}^t} - \boldsymbol{T_i^t}) + \boldsymbol{S_{i-1}}(\boldsymbol{T_{i-1}^t} - \boldsymbol{T_i^t}) \\
&\qquad + \boldsymbol{S_\infty}(\boldsymbol{T_\infty^t} - \boldsymbol{T_i^t})] + \boldsymbol{\theta}\left(\boldsymbol{S_{i+1}T_{i+1}^{t+1}} + \boldsymbol{S_\infty T_\infty^{t+1}}\right) = \boldsymbol{B}
\end{aligned}
\qquad 2.9.
$$

$$-\boldsymbol{\theta}(\boldsymbol{S_{i-1}} + \boldsymbol{C_i'}) = \boldsymbol{C} \qquad 2.10.$$

The state equations contain a self-coupling and cross coupling coefficients (represented by **A**, future time step matrix coefficient), previously calculated and known values (represented by ***B***, present time step matrix coefficients), and ***C***, known terms and boundary conditions matrix, (or ***Z***, solved present time step combined matrix). $\boldsymbol{T^{t+1}}$ and $\boldsymbol{T^t}$ are nodal temperatures column matrices for future and present time steps, respectively.

For every building model, all the conservation equations representing the various nodes (be it zone or plant) are combined into a multi-layered matrix equation set. The future time step coefficient matrix, **A**, usually contains thousands of entries (most being equal to zero), which would consume large amount of processing power and time to invert at every time step. Therefore ESP-r brakes up the whole building matrix equation into smaller equation sets derived for zones: one each for every multi-layered construction and fluid volume enclosed within, and for plants. These are later grouped in a much smaller matrix equation and all the equations are solved by the matrix equation processor (Clarke, 2001; Hensen, 1991; Kelly, 1998).

Fluid volume enclosed within a zone is transient, as there is constant and continual movement/flow of air (or fluid) in and out of zones. ESP-r uses a mass balance/flow network approach to model, or account for the fluid flow (Hensen, 1991). The method assumes that the zone/building (or plant) is composed of several zones (or nodes) that are connected through openings (doorways, cracks, ducts, pipes, etc.), for which relationship between flow and pressure differentials is nonlinear. The mass flow conservation equations is processed with aid of a dedicated standalone module/processor called ***mfs***. Description of this and other ESP-r modules/processors are described in appendix A while description of fluid flow problems in terms of a mass flow network, as well as method by which the module/processor is incorporated into other ESP-r modules, is described by Hensen (1991) and Clarke (2001).

2.1.3. Building/zone-Plant Integration

While solutions of representative energy balance equations and processing of matrix equations for zones and plants are done separately, ESP-r also accounts for and processes interactions between them (such as an air conditioning system delivering or extracting heat from a zone), which is necessary for accurate simulation of the entire system. This interaction is accounted for by utilising one or more node(s) to represent the interaction point(s). The node could be located at an air point in the zone/building to indicate addition or removal of energy to or from the zone air (convective heating or cooling flux), at an intra-construction to indicate injection or extraction to or from some intra-material node or storage regions such as underfloor heating systems or electrical storage units. Addition coefficients, derived from energy balance equation for the interaction node are added to the zone's nodal matrix equation to represent the additional zonal content. Further explanation of zone/plant interaction and formation of consequent zonal matrix can be found in Clarke (2001) and Aasem (1993).

2.1.4. ESP-r Modules

To simulate the whole building, the entire model – building, zones and components, and its interaction with other systems like weather and HVAC systems – needs to be solved simultaneously. ESP-r does this by applying a unified solution technique that incorporates solvers for every subsystem and equation sets (Aasem, 1993; Hensen, 1991). This is a bottom-up approach whereby solutions of energy and mass balance equations for systems and components are solved first at individual level, grouped according to subsystems and solved at this level separately, and then integrated into a single solution afterwards. Solutions at the subsystem levels are handled by solvers/modules, some of which are simple supporting codes, applications and/or interfaces.

The method integrates all the energy and mass conservation equations that represent the building (fabric and zones) and components, and associated plants, with inputs from real climate data and boundaries imposed/defined by user via control strategies Almeida et al., 2010; Kelly, 1998). The energy and mass flow equations are contained in source codes, which contain algorithms for numerical models of various components and plants saved as subroutines, program files, in the software's database.

These modules are twenty-one (21) executable files (supporting code or/and interfaces) that make up ESP-r's solution and simulation package. Each is designed to perform specific functions. A brief description of the solvers is attempted below.

These modules can be viewed as individual organs in the body, each performing different functions, with their combination, or linking together, resulting in mobility or activity of the body. Similarly, the combination of modules produces a unified solution process for the entire model. As with the body, not all modules are always engaged or utilised for every building model. The way the modules are combined is variable. The number and type of modules used, called up or invoked at any one time, and for any building model, is

determined by the make up or characteristics of the model, its components and associated plants, flow and CFD. This ensures that solution of the model's energy subsystems is done using the most appropriate and efficient means. Compartmentalisation of the codes or solvers into technical domains, or modules, makes this possible, so that only required solvers, and codes, are accessed for any model and simulation. This is referred to as a modular solution method (Al-Mosawi, 2011). It allows flexibility of the simulation process.

Advantage of the modular solution method is that it allows each equation set to be solved, not just separately but independently, at different and varying time steps, which enables effective capture of the system's thermal dynamics by overall solution without constraining all solvers to a common time step or frequency. Combination of the solvers is controlled by the simulation controller, which provides the governing control algorithm. This forms ESP-r's 'numerical engine' (Kelly, 1998). Additionally, it gives the modeller opportunity to decide number and combination of subsystems to use for his/her model, as well as option to focus attention on any one subsystem for more detailed modelling.

2.2. PCM Modelling Approach/Method in ESP-r

Solution to problems involving phase change requires simultaneously solving two distinct problems, one involving pure heat conduction until the substance reaches melting temperature at a given time, *t*, and another involving two-phase Stefan problem after this time. The Stefan problem is given by the expression,

$$\boldsymbol{\rho \frac{\partial H}{\partial t} = k \nabla^2 T} \qquad 2.11.$$

where $\boldsymbol{\rho}$ (kg/m^3) is density, $\boldsymbol{H}$ (J/kg) enthalpy, $\boldsymbol{t}$ (s) is time, $\boldsymbol{k}$ (W/mK) thermal conductivity and $\boldsymbol{T}$ (K) is temperature.

This is complicated by the fact that the phase change front is not stationary. It changes with time and its location needs to be determined at every time step (Ozdenefe & Dewsbury, 2012). This is attributable to the geometric nonlinearity of the problem. Also, the phase change front may not be sharp but an extended mushy region.

Two numerical approaches are employed to solve the moving boundary problem. They are the front-tracking and fixed-domain methods. Front-tracking methods, as the name implies, tracks the phase change interface while fixed-domain methods regard all the phases, solid, liquid and/or gaseous, as one continuous medium. Here the interface condition is determined from equations defining the enthalpy, effective heat capacity or heat-generation term. Fixed-domain methods have an advantage, in that they can handle phase change problems with a finite phase change temperature range (Lewis & Ravindran, 2000). The most common fixed domain methods employed for PCM modelling are the effective heat capacity method and the enthalpy method.

In the effective capacity method, the effective heat capacity is defined as the slope of the enthalpy–temperature curve. Energy/heat absorbed or released during phase change is simply regarded as heat capacity. Whereas in the enthalpy method, a continuous and reversible function is defined for a given volume of the material. This function then returns temperature values based on values obtained for the enthalpy. Both methods have been employed for modelling PCM in ESP-r, see Clarke (2001), Al-Mosawi (2011) and Padovan (2014).

2.2.1. Effective heat capacity method

The effective heat capacity method is based on the relationship between enthalpy and temperature according to equation 2.8.

$$\frac{\partial H}{\partial t} = \frac{\partial H}{\partial T}\frac{\partial T}{\partial t} \qquad 2.12.$$

Here,

$$\frac{\partial H}{\partial T} = c_{p,eff}(T) \tag{2.13.}$$

So that the heat conduction expression becomes

$$\rho \frac{\partial H}{\partial t} = \rho c_{p,eff}(T) \frac{\partial T}{\partial t} \tag{2.14.}$$

where $c_{p,eff}$ (J/kgK) is effective heat capacity.

This is a non-linear function of the phase change energy (latent heat of fusion). the temperature dependence of effective heat capacity can be removed by applying the Goodman transformation (Samarskij & Vabiščevič, 1995) to define a new dependent variable, thus:

$$v = \int_{c_{p,s}}^{c_{p,l}} c_{p,eff}(T)\, dT \tag{2.15.}$$

A possible solution to equation 2.12 is equation 2.13 (Šavija & Schlangen, 2016),

$$c_{p,eff}(T) = \begin{cases} c_{p,s} & if \quad \ldots\ldots\ T < T_m - \Delta T\ (solid) \\ \dfrac{c_{p,s} + c_{p,l}}{2} + \dfrac{L}{2\Delta T} & if \quad \ldots\ T_m - \Delta T \le T \le T_m + \Delta T\ (interphase) \\ c_{p,l} & if \quad \ldots\ T > T_m + \Delta T\ (liquid) \end{cases} \tag{2.16.}$$

There are many other variations of the solution of equation 2.12 for effective heat capacity during phase change, a detailed compilation of which is done by Caggiano, Mankel, & Koenders (2019). These equations are solved using the explicit numerical scheme.

This method was employed for modelling PCM-gypsum composite wallboard employed for internal and external walls of buildings by Heim & Clarke (2004).

There are challenges with the method, such as approximated solutions which suffers from a singularity problem for both the specific heat capacity and the thermal conductivity when phase change occurs at a fixed temperature (Hashemi & Sliepcevich, 1967; Lerner et al, 2007). This refers to points at which the terms are not defined or cease to be well-behaved

and not differentiable. One of the ways to circumvent this is by assuming the phase change occurs over a small temperature range (Civan & Sliepcevich, 1984), regardless of the actual PCM characteristics. The size of the assumed phase change or melting temperature range, however, requires some expertise and precision, as a wrong selection could produce indeterminate results. This temperature range is also expected to be maintained for the duration of phase change for the effective heat capacity to be directly applicable. These requirements have the potential to result in underestimation for PCMs whose phase change temperature range is large and overestimation for PCMs with fixed, single phase change temperatures (Obitayo, 2011). Besides, heat capacity during phase change can only be approximated either analytically/empirically (Fang & Medina, 2009; Faghri & Zhang, 2006) or numerically, which increases complexities with using the method for modelling of the phase change process, even with the introduction of fictitious melting temperature range (Madad, Mouhib, & Mouhsen, 2018; Al-Saadi & Zhai, 2013).

2.2.2. The Enthalpy method

As discussed in section 2.2, solution to phase change problems is complicated due to moving phase change and its width. However, by reformulating the Stefan problem in terms of enthalpy, it is possible to bypasses tracking the interface explicitly (equation 2.14). The enthalpy method utilises a continuous and reversible function to describe heat transfer/exchange process in the material.

General heat conduction equation 2.7 can be written in simple form as,

$$\boldsymbol{E_t = q_x} \qquad 2.17.$$

with $\boldsymbol{E}$ being thermal energy density per unit volume,

$$\boldsymbol{E = \int_{T_{ref}}^{T} \rho c_{p,}(T)\, dT} \qquad 2.18.$$

and $\boldsymbol{q}$ being heat flux,

$$\boldsymbol{q = -kT_x} \qquad 2.19.$$

The method applies enthalpy form of the energy equation, which can deal with both mushy and isothermal phase change problems (Kuravi et al., 2010), latent heat flow, and is applicable to both phases, accommodating sensible heat flows as well. Therefore, the phase change problem becomes much simpler, thus the need for separate equations for the phases is eliminated and the finite difference solution methods can be applied.

It has been successfully applied and confirmed by numerous authors (Dutil et al., 2011). It was proposed for implementation in ESP-r by Sadasivam, Zhang, & Fung (2011) as an alternative to its effective heat capacity PCM modelling method but has not been implemented. It was implemented to model PCM as add on to an existing ESP-r plant model of a domestic hot water tank by Padovan (2014). It will be discussed in more details subsequently.

2.3 ESP-r PCM Models

The two existing PCM models in ESP-r are discussed within the context of active and passive systems. As discussed in chapter 1, passive heating/cooling systems do not consume power nor require dedicated heat/energy supply, They are energy-efficient and eco-friendly techniques used to improve the thermal comfort (Samuel, Nagendra, & Maiya, 2013) and for demand side management energy management of buildings (Rahimpour et al., 2017) while active heating/cooling systems require dedicated continuous heat/energy input.

2.3.1 Passive System PCM Models – Building Fabric/Envelope integrated

Building fabric or envelope here refers to all building structures except the floor, i.e. the walls, windows, doors and roof. This characterisation is necessary to establish distinction from the well-established underfloor heating systems applied to floors.

The existing ESP-r passive PCM model is PCM impregnated into the porous structure of gypsum and employed to make a PCM-gypsum composite wallboard. The PCM is introduced into gypsum (composite wallboard of building models) during model configuration/description by adding it as active (special) materials. The system allows user to indicate target layer within surface and within zone. There are other components for which there are provision in ESP-r to be added as special materials – wind turbines, thermo-chromic glazing and evaporating surface.

The modelling approach treats the system (or component) to which the special material (PCM) is added along with the PCM as a single system/component having uniform equivalent thermo-physical properties, density, specific heat, thermal conductivity and latent heat. Adopting the control volume approach, physical elements of the PCM-component composite can be described using zones and networks elements as special material. Mathematical function representing changes in thermophysical properties, like phase, of the material upon influence or excitation by an external energy source is subsequently added to the energy balance equation via material property substitution. This is referred to as ‘special materials’ concept (Kelly, 1998; Heim & Clarke, 2004). The special material function is applicable to nodes within a multi-layered construction and any such node becomes subject to variations in its thermo-physical properties over time.

The model has provision for defining thermo-physical properties of the PCM, but no indication of what percentage of PCM is present in the composite. This limits ability to judge or ascertain optimum proportion of PCM required to achieve desired goal.

2.3.2 Active System PCM Models – Space and Water Heating

PCM is also modelled in ESP-r as an active system which is continually supplied with heat/energy from heating systems via a heat transfer medium. Employed as add on or supplemental heat storage system for existing models of a water storage tank, it takes the form of cylindrical modules which are immersed into the water storage tanks (Padovan, 2014). Heat supply to the tank is obtained from either immersed heating coils in the tank or water heating system external to it such as a solar water heater or heat pump. Heat is delivered to the PCM from the tank water during charging when its temperature (water) is higher than that of the PCM and withdrawn from them by same when their temperature (water) drops below the PCM's. The PCM model subroutine can be called up during simulation if tank is specified in the configuration as having PCM by user during plant description.

The modelling approach employs the enthalpy formulation to describe transformations of the PCM. It calculates temperature values for the PCM modules using data from layers of water around them, as well as heat exchanged between them and water in the tank.

The PCM model is included in the plant description for hot water tank with PCM and permits designation of number, size, length and positioning of the PCM modules from top and bottom of the tank. The last two parameters are necessitated by the stratified nature of the hot water tank. The model also has provision for user to define thermo-physical properties of the PCM.

2.4 Research gap with respect to the ESP-r Building Energy Simulation System

2.4.1 Shortcomings of modelling approach/method

Modelling of heat flow involving PCM often requires that values of heat capacity or enthalpy at any given time be determined using discretisation equations that are based on values of temperatures at a previous time. With the effective heat capacity method dependence of heat capacity on temperature during phase change, which is non-linear, entails employing the explicit numerical scheme for the determination. Because heat capacity change with temperature during phase transition is very rapid, changing multiple times over a short temperature interval, this introduces errors into the results (Sadasivam, Zhang, & Fung, 2011). This is even more pronounced for substances whose phase changes occur over a single, or fixed, temperature.

The solution adopted for overcoming, this error is itself problematic and likely to introduce more errors for materials that change phase over large temperature intervals. Likewise, the requirement for precision in suggestion of a phase change (or melting) temperature range, which must not be too small or too large, implies high probability for indeterminate results. Besides, heat capacity during phase change can only be approximated either analytically/empirically (Fang & Medina, 2009; Faghri & Zhang, 2006) or numerically, which increases complexities even with the introduction of fictitious melting temperature range (Madad, Mouhib, & Mouhsen, 2018; Al-Saadi & Zhai, 2013).

Another shortcoming of the apparent heat capacity method is that it relies on the assumption (or expectation) that the substance has different specific heat capacities for each of its phases (liquid, solid, etc). This is not always the case, practically, with organic PCMs, especially the paraffins. Most have the same specific heat capacity for both liquid and solid phases.

Therefore, attempting to differentiate between phases using the property for these types of PCM might be met with some difficulties, and limit application of the method to only PCMs whose thermal conductivities differ from one phase to the other.

2.4.2 Novel Building Envelope Integrated PCM Thermal Storage/Heating System

The ESP-r PCM model for which the apparent heat capacity method is employed is a passive building fabric integrated PCM heat storage system. When employed for heating purposes, the phase change materials suffer from not being able to complete full thermal cycles because they often do not absorb enough heat to reach or complete melting. As discussed in chapter 1, this can be addressed by actively supplying heat to the PCM.

Active building envelope thermal storage systems are not new. Active underfloor heating systems have been well established. A detailed review of building envelope thermal energy storage systems, types and application, can be found in Verbeke & Audenaert (2018). The concept of actively supplying heat to phase change materials applied to building walls (internal or external) for building heating applications is, however, relatively new. The only available literature on the subject is that reported by Kong et al., (2020) of an experimental analysis of a PCM composite made from expanded perlite and paraffin and employed for wallboard which they installed on the internal surfaces of walls and ceilings of a test building. Heat was supplied via thin pipes carrying hot water from a solar water heating system embedded into the wallboards. Development of a numerical model of this type of system, an active building envelope PCM heat storage system, which does not yet exist in ESP-r, is one of the proposed outcomes/objectives of this work.

2.4.3 New ESP-r PCM Heat Storage Plants

The existing ESP-r PCM based system discussed above is a building component while the proposed active fabric integrated model/system is a plant. As stated, there are no active fabric

integrated heat/thermal energy storage systems in ESP-r, it however has a number active non-fabric integrated heat/thermal storage systems/plants, the simplest of which is the domestic hot water storage tank. These plant systems store heat indirectly by storing large volumes of heat transfer fluids, water.

Padovan (2014) described a modification of the codes of some the domestic hot water tank to enable it call up a subroutine containing codes of a phase change material encased in cylindrical modules which they developed to augment the tank's thermal storage capacity. The PCM modules serve as secondary, or auxiliary heat storage for the heating system. They employed the enthalpy method to model the PCM, which determines temperature changes in the PCM based on energy inputs from the surrounding tank water. The model is, however, not a stand-alone ESP-r plant model but a tool employed by the hot water tank model, which is an ESP-r plant, for determining temperature of the PCM for use when required during the tank's code processing. Since it does not stand alone, nor is it an ESP-r plant, the potential for employing it, combined with the hot water tank model that utilises it, for comparison and/or as possible replacement for conventional hot water storage tanks.

A second iteration of the proposed systems is a stand-alone non-fabric integrated ESP-r heat/thermal energy storage plant. This is a dedicated PCM thermal energy storage plant system that stores heat using the phase change materials contained within. It has potentials and capabilities for comparison and substitution of conventional hot water storage tank systems. Systems of this nature has attracted attention with some manufacturers advertising units for installation and deployment (Croda International Plc, 2020; HeatVentors Kft, 2020). The benefit of having such a system in ESP-r system includes ability to employ the software for building assessments and analysis of under scenarios that have similar systems deployed.

2.5 Summary

An appraisal has been done of the ESP-r building energy modelling system, examining its functionality regarding problem definition, processing, analysis and solution. The methods and approaches by which phase change materials are modelled for thermal/heat energy storage in it were also appraised. This was done based on categorisation of the PCM systems into active and passive systems, or/and building fabric integrated and non-fabric integrated systems (plants). ESP-r has a building fabric integrated PCM heat storage system that is passive and a non-fabric integrated but active (plant) system. It was noted that both the apparent heat capacity was employed for modelling PCM in the building fabric integrated passive system while the enthalpy methods was employed in the active (plant) system.

The existing PCM models were also critically assessed to identify inadequacies and shortcomings. The apparent heat capacity method employed for modelling the passive fabric integrated PCM system is problematic due to the non-linear nature of heat capacity during phase change, whose value changes very rapidly, multiple times over a short temperature interval, and the requirements for adopted method for solving the errors due to the phenomenon have the potential to produce more errors. The apparent heat capacity method is also reliant on the assumption (or expectation) that PCMs have different specific heat capacities for each of their phases (liquid, solid, etc), which is not always the case with many organic PCMs whose specific heat capacity is the same for both liquid and solid phases.

The active PCM (plant) system model in the software is not a stand-alone ESP-r plant model but a tool employed by models of hot water tanks present in the machine (an ESP-r plant) for determining temperature of the PCM when required during processing of the tank's code. Because it does not stand alone, nor is it an ESP-r plant, it lacks the the potential for use as a comparative analysis tool, and/or as possible replacement for conventional hot water storage

tanks which limits the machine's ability to be employed for building assessments and analysis of under scenarios that include deployment of PCM based heat stores.

In the preceding chapter the development of the PCM thermal/heat storage systems models, the design and formulation of the heat and energy and flow equations will be explained. The chapter will also attempt brief discussions and explanation of the underlying theories for developing the mathematical equations, and the numerical analysis and iterative scheme employed for the modelling.

Chapter 3

PCM THERMAL STORAGE SYSTEM MODELLING

3.0 Introduction

In this chapter the modelling of two (2) PCM thermal stores are discussed and explained. The processes involved in heat Conduction through substances and the formulation of the enthalpy formula for modelling of changes on state and phase experienced by phase change materials due to heat absorption and release were explained and described. The chapter also contains detailed description of each physical model and determination of the energy balance equations and expressions representing and describing the energy change and transformation, state and phase change processes, experienced by both heat transfer fluid and PCM, as well as details of the iterative process employed for the modelling.

3.1 Modelling Approach/Method

3.1.1 Heat Conduction and Total Energy

Heat absorbed or released by pure substances at constant pressure is the sum of its energy content, the specific enthalpy, energy content per unit mass. It is related to temperature change accordingly:

$$\boldsymbol{\delta e = c_p \delta T} \qquad 3.1.$$

$\boldsymbol{e}$ (J/kg) being energy per unit mass, $\boldsymbol{c_p}$ (J/kgK) is specific heat capacity of substance at constant pressure and $\boldsymbol{T}$ (K) is its temperature.

If the substance has a temperature that's below or above its phase change temperature, $\boldsymbol{T_p}$, equation 3.1 equates to sensible heat.

The energy content of any substance in the liquid phase is higher than energy content when it is solid, the difference being the latent heat absorbed (or released) during transformation. For substances with constant specific heat capacities, the following holds.

$$\boldsymbol{e} = \begin{cases} \boldsymbol{e^l(T) = L + c_l(T - T_p)} & \boldsymbol{T \geq T_p} \\ \boldsymbol{e^s(T) = \quad c_s(T - T_p)} & \boldsymbol{T \leq T_p} \end{cases} \qquad 3.2.$$

Where $\boldsymbol{L}$ (J/kg) is the latent heat, $\boldsymbol{c_l}$ and $\boldsymbol{c_s}$ (J/kgK) are specific heat capacities the liquid and solid phases of substance, respectively, and $\boldsymbol{e^l}$ and $\boldsymbol{e^s}$ are enthalpy of liquid and solid phases.

Energy, or heat, flowing through cross-section of the material (assumed solid) over a specific time, $\boldsymbol{t}$, is related to its thermal conductivity by the heat conduction equation:

$$\boldsymbol{\rho c_p T_t = \nabla(k \nabla T)} \qquad 3.3.$$

$\boldsymbol{k}$ (W/mK) is thermal conductivity of substance.

Equation 3.3 can then be re-written as equation 3.4, the conservation of energy equation.

$$\boldsymbol{(\rho e)_t = \nabla \vec{q}} \qquad 3.4.$$

Where,

$$\boldsymbol{\vec{q} = k \nabla T} \qquad 3.5.$$

and

$$\boldsymbol{(\rho e)_t = \rho c_p T_t} \qquad 3.6.$$

For a substance undergoing phase change, the latent heat absorbed (or released) is determined accordingly,

$$\boldsymbol{\rho L X' = -k_l T_x(X(t)^-, t) + k_s T_x(X(t)^+, t)} \qquad 3.7.$$

Equation 3.7 is referred to as the two-phase Stefan equation (condition). It stipulates that rate of change of latent heat is equal to the amount of energy that crosses the interface between solid and liquid phases.

Solution to problems involving phase change processes requires simultaneously solving equations/problems involving pure heat conduction (equation 3.2) until the substance reaches phase change temperature at a given time, ***t***, and the two-phase Stefan problem (condition) after this time. The latter involves a moving boundary problem; the phase change front is not stationary, changing with time requiring continuous determination of its location at every time step (Ozdenefe & Dewsbury, 2012).

3.1.2 Enthalpy Formulation

Determination of the progression and movement of the phase change process (or front) requires knowledge of its location within a volume of material at any given time, or identification of a small volume of the material wherein the phase change is occurring. If the energy conservation equation is reformulated in terms of the simple integral heat balance over arbitrary volume and time interval, ***Δt***, we have an expression that is valid for the two (2) phases of the substance, solid and liquid (equation 3.8).

$$\int_{t}^{t+\Delta t} \frac{d}{dt}\left(\int_{x}^{x+\Delta x} E(x,t)dx\right)dt = -\int_{t}^{t+\Delta t} A\int_{x}^{x+\Delta x} q_x(x,t)\,dxdt \qquad 3.8.$$

$$E = \rho e \qquad 3.9.$$

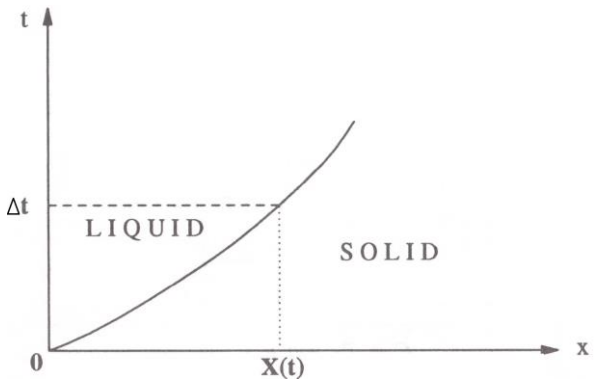

Figure 3.1: Space-time diagram for 2 phase Stefan problem (Alexiades & Solomon, 1993)

Therefore, the heat conduction equation 3.2, can be re-written as

$$\boldsymbol{E}(\boldsymbol{x}.\boldsymbol{t}) = \begin{cases} \int_{T_p}^{T(x,t)} \boldsymbol{\rho c_l}(\boldsymbol{T})\boldsymbol{\partial T} + \boldsymbol{\rho L} & T(x,t) > T_p \\ \int_{T_p}^{T(x,t)} \boldsymbol{c_s}(\boldsymbol{T})\boldsymbol{\partial T} & T(x,t) < T_p \end{cases} \quad 3.10.$$

If specific heat capacities, $\boldsymbol{c_l}$ and $\boldsymbol{c_s}$, are constant, then,

$$\boldsymbol{E} = \begin{cases} \boldsymbol{\rho c_l}(\boldsymbol{T} - \boldsymbol{T_p}) + \boldsymbol{\rho_l L} & \ldots \quad T > T_p\ (liquid) \\ \boldsymbol{\rho c_s}(\boldsymbol{T} - \boldsymbol{T_p}) & \ldots \quad T < T_p\ (solid) \end{cases} \quad 3.11.$$

And,

$$\boldsymbol{T} = \begin{cases} \boldsymbol{T_p} + \dfrac{\boldsymbol{E}}{\boldsymbol{\rho c_s}} & \ldots \quad E^t \leq 0\ (solid) \\ \boldsymbol{T_p} & \ldots \quad 0 < E^t < \rho L\ (mushy) \\ \boldsymbol{T_p} + \dfrac{\boldsymbol{E} - \boldsymbol{\rho L}}{\boldsymbol{\rho c_l}} & \ldots \quad E^t \geq \rho_l L\ (liquid) \end{cases} \quad 3.12.$$

The method makes it possible to bypass tracking the phase change interface explicitly and accounts for whatever jump may be experienced by $\boldsymbol{E}$ and $\boldsymbol{q}$. Thus, the Stefan condition is simply automatically obeyed as a ‘‘natural boundary condition’’ (Alexiades & Solomon, 1993) and interface conditions are automatically achieved, creating a mushy zone between the phases that avoid sharp discontinuities which could otherwise have led to numerical instabilities (Dutil et al., 2011). This is the basis behind the enthalpy solution method.

It applies enthalpy form of the energy conservation equation, which has capacity to deal with both mushy and isothermal phase change problems (Kuravi et al., 2010) and is applicable to both phases. Subsequently, the phase change problem becomes much simpler and the need for separate equations for the phases is eliminated.

3.2 Enthalpy Formulation applied to Phase Change Model

Since latent heat of a material represents the difference in thermal energy (or enthalpy) levels between its different states or phases any heat absorbed or rereleased at constant pressure adds to or subtracts from its total energy, or enthalpy. So that, its thermal state at any time is completely determined by its enthalpy (equations 3.13 – 3.16). Thus, for a phase-change process (melting or solidification), energy conservation can be expressed in terms of total volumetric enthalpy or enthalpy per unit volume and temperature.

$$\frac{\boldsymbol{dE}}{\boldsymbol{dt}} = \boldsymbol{\nabla \cdot (k \nabla T)} \tag{3.13.}$$

where $\boldsymbol{E}$ (J/m3) is the total volumetric enthalpy and is the sum of both latent and sensible enthalpies, $\boldsymbol{t}$ (s) is the time, $\boldsymbol{k}$ (W/mK) is thermal conductivity and $\boldsymbol{T}$ (K) is temperature.

Integrating equation 3.32 yields,

$$\frac{\boldsymbol{d}}{\boldsymbol{dT}} \int_{\boldsymbol{V}} \boldsymbol{E \cdot dV} = \int_{\boldsymbol{A}} \boldsymbol{\nabla \cdot (k \nabla T)\, dA} \tag{3.14.}$$

$\boldsymbol{A}$ (m^2) is heat flow cross-sectional area.

Enthalpy of PCM at a given time, $\boldsymbol{t}$, during melting/solidification is given by:

$$\boldsymbol{E^t} = \begin{cases} \boldsymbol{\rho C_{p,s}(T^t - T_s)} & \ldots \quad T^t < T_s \ (solid) \\ \boldsymbol{\rho L} & \ldots \quad T_s < u^t < T_l \ (mushy) \\ \boldsymbol{\rho C_{p,l}(T^t - T_l) + \rho_l L} & \ldots \quad T^t > T_l \ (liquid) \end{cases} \tag{3.15.}$$

Temperature,

$$\boldsymbol{T^t} = \begin{cases} \boldsymbol{T_s + \dfrac{E^t}{\rho_s C_{p,s}}} & if \quad \ldots\ldots \ E^t \leq 0 \ (solid) \\ \boldsymbol{\dfrac{E^t}{\rho_l L}(T_l - T_s) + T_s} & if \quad \ldots \quad 0 < E^t < \rho_l L \ (mushy) \\ \boldsymbol{T_l + \dfrac{E^t - \rho_l L}{\rho_l C_{p,l}}} & if \quad \ldots \quad E^t \geq \rho_l L \ (liquid) \end{cases} \tag{3.16.}$$

Liquid fraction,

$$\boldsymbol{\gamma^t} = \begin{cases} \mathbf{0} & if \quad \ldots\ldots \; E^t \leq 0 \; (solid) \\ \dfrac{\boldsymbol{E^t}}{\boldsymbol{\rho_l L}} & if \quad \ldots \; 0 < E^t < \rho_{p,l} L \; (mushy) \\ \mathbf{1} & if \quad \ldots \; E^t \geq \rho_{p.l} L \; (liquid) \end{cases} \qquad 3.17.$$

The method determines PCM phases by its enthalpy, with no regards to interface location(s), thereby tracking "volume'' rather than ''phase front''. Thus, enthalpy is determined from heat flow employing thermal conductivities (or resistance) rather than from specific heat capacity.

3.3 PCM Thermal Storage Battery Model

Heat energy storage using phase change material has gained momentum over the years, not surprisingly, as response to CO_2 and energy reduction efforts. Several manufactures and developers, the likes of Sunamp (Sunamp technology, 2020), CrodaTherm (Croda International Plc, 2020), Heatventors (HeatVentors Kft, 2020), etc., have developed a range of PCM thermal storage systems and devices for both domestic and industrial applications. However, implementation and modelling of thermal energy systems containing PCMs in a whole-building simulation environment is scarce (Belmonte et al., 2016), as is the ability to model them properly in building energy simulation tools.

Model proposed and discussed below is an attempt at proffering solution to this and providing a tool that can be employed for assistance in the decision-making process about building energy systems.

3.3.1 Physical Model

To model the PCM heat store a shell-and-tube heat exchanger with a cylindrical shell and circular tubes/pipes running the length from one end to the other was assumed. Heat transfer fluid flows through the tubes/pipes while the PCM is contained in the shell. The number of

tubes can vary from one to any number, limited only by diameters of both tube and shell, and spacing or arrangement while the PCM is contained in the shell. Basically, so long as number of tubes can be contained in the shell with adequate spaces between them. The tubes'/pipes' arrangement follows one of four patterns depending on how many there are. A simple in-line arrangement if maximum number is 2, triangular if 3, square arrangement if 4 and hexagonal arrangement if number of tubes is greater than 4. The hexagonal arrangement has one central tube/pipe around which a series of rings is formed by remaining tubes/pipes in a 6, 12, 18 … series pattern (see Figure 3.2). Each of these patterns allow for closeness and even spacing of the tubes/pipes.

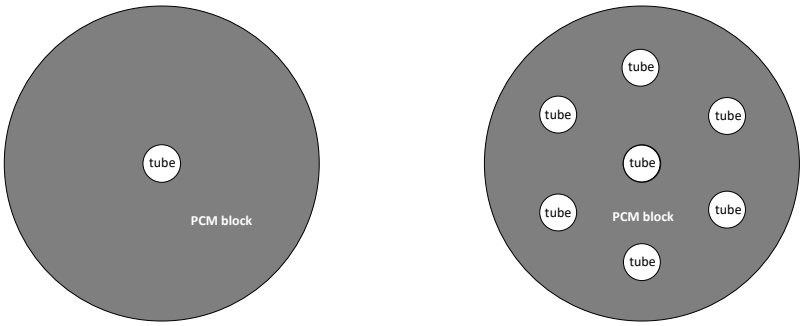

a: Single tube b: multi-tubes

Figure 3.2: Cross-sectional view of thermal store showing relationship between PCM and HTF tubes

The heat exchanger is assumed adequately insulated but able to exchange heat with its surrounding through the insulation material. By factoring effects of energy exchange with environmental into the numerical models, the coding can account for and incorporates interaction between the thermal store and its environment, or space it is located.

3.3.2 Heat Exchanger Modelling

The PCM storage system is represented with mathematical expressions and equations which capture both its physical characteristics and energy transfer and transformations of the PCM and heat transfer fluid (HTF). Figure 3.3 shows an annular tube of two (2) concentric pipes, representing a shell and one (1) tube configuration.

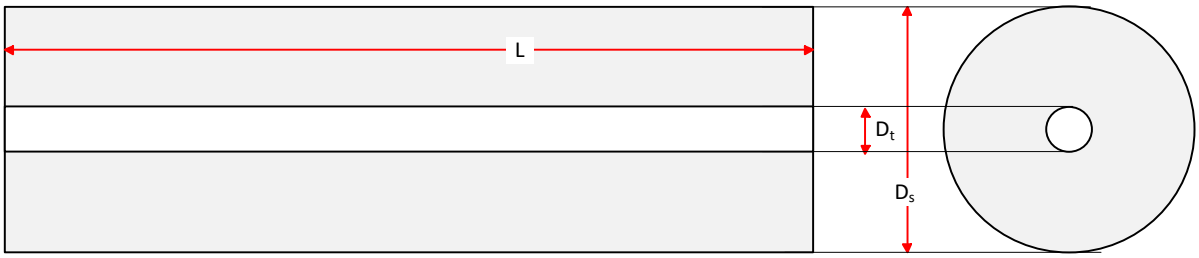

Figure 3.3: Shell and tube heat store configuration of PCM thermal store

3.3.2.1 Heat Transfer Surface Area

Figure 3.2 is cross-sectional view of half of the thermal store showing relationship between tubes and PCM.

Diameter of heat transfer fluid column is equal to the inner diameter of tube/pipe while innermost diameter of PCM layer is the outer diameter of tube/pipe, and the inner diameter of shell equals outermost diameter of PCM layer.

That is,

$$\boldsymbol{D_0 = D_w} \quad 3.18.$$

$$\boldsymbol{D_t = D_{pcm}} \quad 3.19.$$

$$\boldsymbol{D_s = D_n} \quad 3.20.$$

Heat transfer surface area of between HTF and exchanger inner surface is given by,

$$\boldsymbol{A_w = \pi D_0 l} \quad 3.21.$$

While heat transfer surface area between exchanger outer surface and PCM is given by,

$$\boldsymbol{A_t = \pi D_t l} \quad 3.22.$$

3.3.2.2 Heat Exchanger Discretisation (Shell) – Cell Dimensions

Discretization is achieved by subdividing spatial regions of the shell and tube into ‘‘small’’ sub-regions (control volumes) by a grid, to which the energy equation is applied.

The model assumes that temperature of heat transfer fluid varies with time only along the radial axis but vary with both time and space along the length, axial axis. Therefore, no discretisation was done for the heat transfer fluid along the radial axis.

Taking the PCM block as a hollow cylinder, it was divided into discrete segments along its length and, radially, along its radius to develop a two (2) dimensional grid (Fig 3.3). This is accomplished by simply dividing length of cylinder by total number of regions/sections or grid factors for axial division while radial division is achieved by dividing radius of cylinder by total number of radial sections. The heat transfer fluid was similarly sub-divide along the heat exchanger length.

The discretisation approach was adopted to capture the two (2) planar heat flow direction (pattern) from the heat transfer fluid flowing in the inner tube. The heat flow is radial through the circumference of the tube and along its length, axially, following flow direction of heat transfer fluid from entry to exit.

Cell Diameter/Radius thickness and Depth

As mentioned above, radial discretisation was done for only the PCM block contained in the shell. This produces a series of cylindrical rings with increasing inner and outer radii, whose depth is equal to $\boldsymbol{d_a}$ with a uniform thickness of $\boldsymbol{d_r}$ (figure 3.4a and 3.4b).

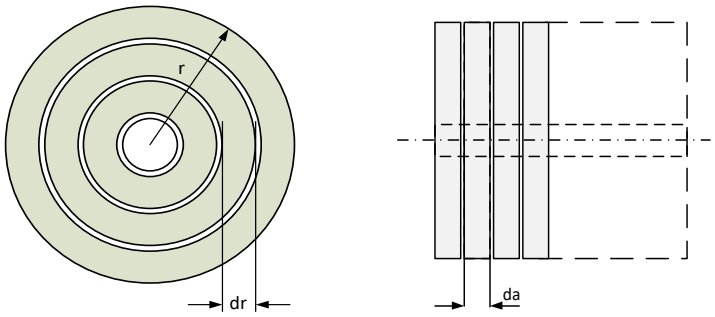

a: Radial discretisation b: Axial discretisation

Figure 3.4: Cross-sectional and lateral views of heat exchanger showing radial and axial discretisation.

The inner and outer radii of nth cell division are obtained from equations 3.23 and 3.24

$$r_n = r_t + (n-1)d_r \quad 3.23.$$

$$r_{n+1} = r_t + nd_r \quad 3.24.$$

Cell heat exchange surface Area

Although, as mentioned above, temperature of heat transfer fluid is assumed to vary with both time and space along the length, axial axis, discretised mass and heat flow of heat transfer fluid along the heat exchanger length (axial axis) does not include surface area, as energy change is determined on mass flow basis.

Figures 3.5 a and b are 3 dimensional representations of the PCM rings. They have equal thickness axially and heat exchange surface areas are equal on either of the opposing sides along the same axial axis.

$$A_{axial} = \frac{\pi\left(r_{n+1}^2 - r_n^2\right)}{4} \quad 3.25.$$

The PCM heat exchange surface areas, however, differ from inner to outer surface along the radial axis.

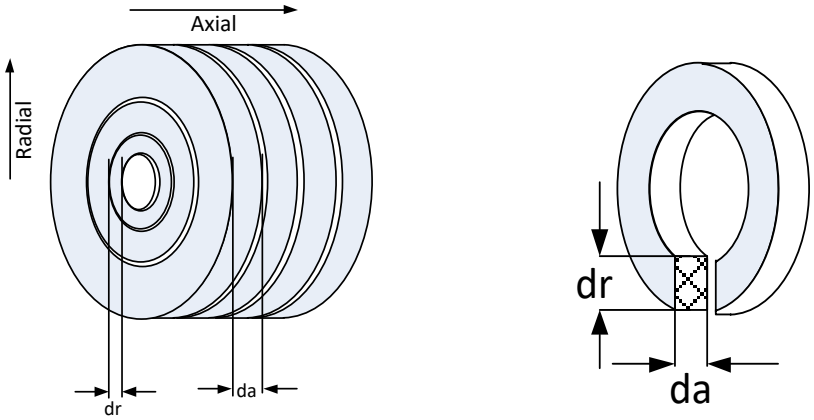

a: Radial division *b: Axial division*

Figure 3.5: 3-dimensional representations of the PCM rings

Adopting the solution for heat flow through pipe of thickness d_r, internal and outer radii r_{n-1} and r_n, length d_a and thermal conductivity, k,

$$q = -kA_r \frac{dT}{dr} \quad 3.26.$$

$$q = 2\pi d_a r_n k \frac{dT}{dr} \quad 3.27.$$

$$q r_n ln\left(\frac{r_{n+1}}{r_n}\right) = 2\pi d_a r_n k(T_{n+1} - T_n) \quad 3.28.$$

Equation 3.10 gives expression for inner heat exchange surface area

$$A_r = 2\pi d_a r_n \quad 3.29.$$

3.3.2.3 Heat and Energy Flow Equation

For the heat flow energy balance equation, the PCM was treated as second heat transfer material, and phase change and heat exchange between it and the heat transfer fluid, through the heat exchanger material is represented by an effective heat flux term. Heat flow from heat transfer fluid flowing in the inner tube of a simple double pipe heat exchanger, shown in figure 3.3, was adopted for developing the energy equation. The following is assumptions were made in formulating the energy equation:

1. potential and kinetic energy changes of heat transfer fluid is neglected. Since in domestic applications, mass flow rates of heat transfer fluids are small in comparison to industrial applications, implying relatively low flow velocities and small changes in kinetic energy which can be considered negligible. Also, differences in elevation between fluid inlet and outlet are equally small. Therefore, change in potential energy is small and assumed negligible.
2. specific heat at constant pressure is assumed constant for both heat transfer fluid and PCM. This is because both are incompressible.
3. For the same reason of incompressibility of both PCM and heat transfer fluid pressure drop inside shell and tubes are neglected
4. Temperatures are uniform over every flow cross section. The assumption is base on relatively low mass flow rate and flow velocity which is laminar with no turbulence.

The energy balance equation for the heat exchanger is given in equation 3.30. It represents the energy change experienced by the heat transfer fluid contained within the exchanger over an elapsed time (***δt***) as a result of mass and heat flow in and out (HTF) and heat exchange with PCM (and to the surroundings through the insulation).

$$\boldsymbol{m_w C_{p,w} \frac{\Delta T_w}{\Delta t} = \dot{m}_w C_{p,w} \Delta T_w - \Delta q_{pcm}} \quad 3.30.$$

Expansion of equation 3.30 yields equation 3.31.

$$\boldsymbol{m_w C_{p,w} \frac{T_w^{n+1} - T_w^n}{\Delta t} = \dot{m}_w C_{p,w} \left(T_{w,i}^{n+\theta} - T_{w,o}^{n+\theta}\right) - \Delta q_{pcm}^{n+\theta}} \quad 3.31.$$

Effective heat flow through PCM, $\boldsymbol{\delta q_{pcm}}$, is obtained in equation 3.32,

$$\boldsymbol{\Delta q_{pcm} = \frac{A_t \left(T_w - T_p\right)}{R_P}} \quad 3.32.$$

The mass and mass flow rate of the HTF can be represented in terms of density, $\boldsymbol{\rho}$, (kg/m^3), cross sectional area of flow region, $\boldsymbol{A_w}$, (m^2), length of exchanger, $\boldsymbol{L}$, (m) and elapsed time, $\boldsymbol{t}$, (s), with equations 3.33 to 3.35.

$$\boldsymbol{m_w = \rho A_w L} \quad 3.33.$$

$$\boldsymbol{\dot{m}_w = \frac{\rho A_w L}{t}} \quad 3.34.$$

$$\boldsymbol{A_w = \pi r_0^2} \quad 3.35.$$

The combined thermal resistance of PCM, fluid stream and heat loss to the surrounding through insulation is a combination of the thermal conductivity of PCM, the heat transfer coefficient of heat transfer fluid stream and the thermal transmittance, ***UA*** (W/K), representing heat loss to the surrounding. Both thermal conductivity of PCM and heat transfer coefficient of the heat transfer fluid stream change and vary as PCM exchanges heat with the heat transfer fluid. This is represented by equations 3.36 and 37.

$$\boldsymbol{R_P = r_0 \left[\frac{1}{r_0 h_w} + \frac{1}{R_t} + \frac{1}{R_{pcm}} + \frac{1}{r_s UA}\right]} \quad 3.36.$$

UA is chosen based on the type and thickness of insulation material employed for model simulation, and exposed surface area.

Thermal resistance of exchanger material is given by,

$$\boldsymbol{R_t = \frac{k_t}{ln\left(\frac{r_t}{r_0}\right)}} \qquad 3.37.$$

3.3.3 PCM Modelling – Discrete Model Energy Balance Equation

The energy equation is applied to discrete cells to obtain the discrete heat/energy balance for developing and solving the numerical algorithms.

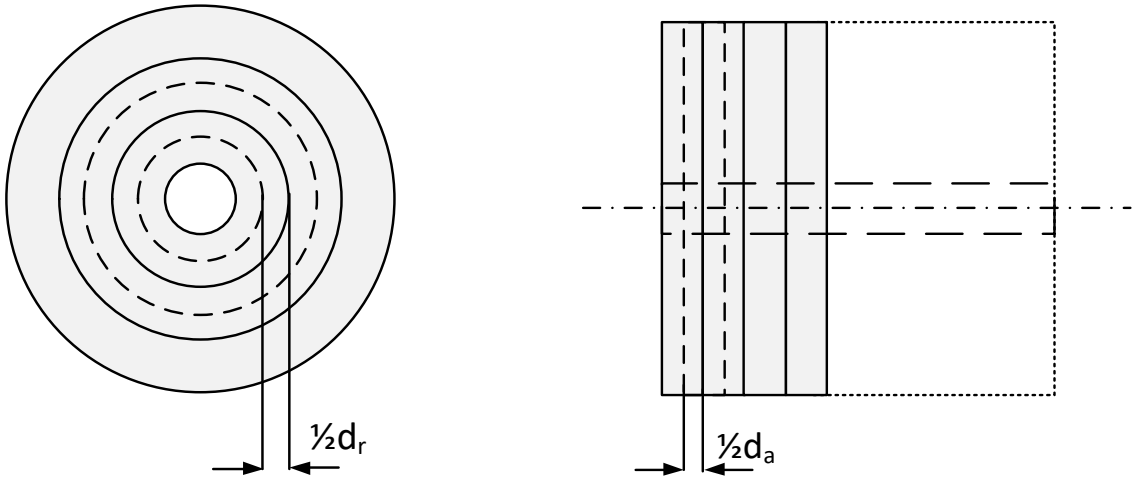

a, Radial *b, Axial*

Figure 3.6: Spatial grid half section

Each control volume represents regions wherein ‘‘local equilibrium’’ is achieved at a time scale considerably shorter than the computational time step. Thus, properties and conditions of a nodal point at centre of a control volume may be considered as representing the averages over the control volume. Simulation of heat flow for the chosen and ‘‘appropriate’’ spatial grid, cell or node, is undertaken by using conservation laws for updating its states through discrete time increments. The enthalpy formula was employed for developing the energy balance equation.

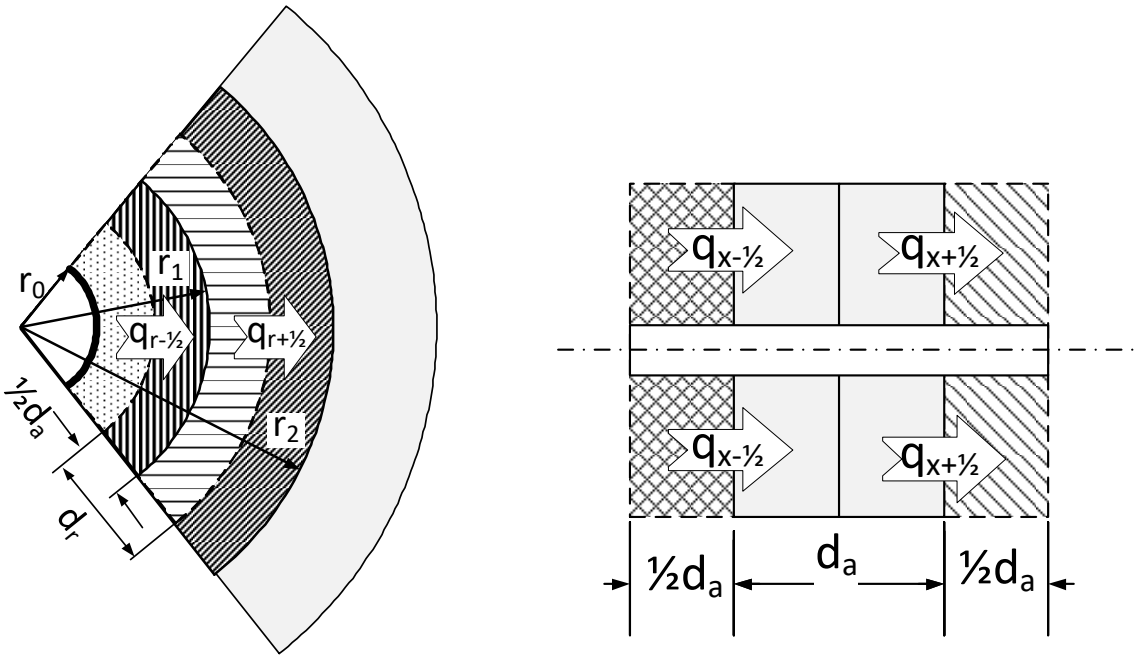

a, Radial b, Axial

Figure 3.7: Cross boundary fluxes

Change in enthalpy over time due to heat flow across the PCM control volumes is formulated based on the following assumptions:

1. The PCM has radial and axial symmetry with equal and uniform thermo-physical properties.
2. Thermo-physical properties are independent of temperature but are distinct for the different phases.
3. It is homogenous and isotropic.
4. Sub-units or sections are unique and different to each other with regards to property and state.
5. The initial phase is solid.
6. The influence of buoyancy and energy/heat exchange via liquid PCM flow has been ignored (this assumption is valid for narrow channels according to Shatikian, Ziskind, & Letan (2005), applicable to PCM in tubes).
7. Hysteresis and its effect have been ignored because the phenomenon is not fully understood with regards to necessary refinement for numerical models to account for

it (Zastawna-Rumin, Kisilewicz, & Berardi, 2020) and, according to Hu et al (2020), its influence on building thermal and energy performance have not been fully understood.

Equation 3.14 can be re-written in its simple form as

$$\partial E_t + \partial q_r + \partial q_a = 0 \tag{3.38.}$$

$$\frac{\Delta E}{\Delta t} + \frac{\Delta q_r}{\Delta r} + \frac{\Delta q_a}{\Delta a} = 0 \tag{3.39.}$$

Designating discrete cells along the radial axis by i, and cells along the axial axis by j, for cell (i, j),

$$\frac{\Delta E_{i,j}}{\Delta t} + \frac{\Delta q_{r,i}}{\Delta r} + \frac{\Delta q_{a,j}}{\Delta a} = 0 \tag{3.40.}$$

$$E_{i,j}^{t+1} - E_{i,j}^{t} = q_{r,i}\frac{\Delta t}{\Delta r} + q_{a,j}\frac{\Delta t}{\Delta a} = 0 \tag{3.41.}$$

The heat flux, q_r can be re-written in terms of two (2) fluxes, $q_{n\text{-}½}$ and $q_{n+½}$, (fig 3.7a and equations 3.42 and 3.43) crossing the inner and outer boundaries of the cell radially.

$$q_{r,i}^{t} = q_{i-½,j}^{t} - q_{i+½,j}^{t} \tag{3.42.}$$

Similarly, q_a can also be re-written in terms of two (2) fluxes, $q_{i,j\text{-}½}$ and $q_{i,j+½}$, (figure 3.4b and equations 3.32 and 3.33) crossing inner and outer boundaries axially.

$$q_{a,j}^{t} = q_{i,j-½}^{t} - q_{i,j+½}^{t} \tag{3.43.}$$

Therefore, heat balance equation 3.41, transforms to equation 3.44 upon substitution of equations 3.42 and 3.43,

$$E_{i,j}^{t+1} - E_{i,j}^{t} = \frac{\Delta t}{\Delta r}\left[q_{i-½,j}^{n+\theta} - q_{i+½,j}^{n+\theta}\right] + \frac{\Delta t}{\Delta a}\left[q_{i,j-½}^{n+\theta} - q_{i,j+½}^{n+\theta}\right] \tag{3.44.}$$

Also,

$$q_{i-½,j}^{t} = -\frac{T_{i,j}^{t} - T_{i-1,j}^{t}}{R_{i-½,j}^{t}} \tag{3.45.}$$

$$q^t_{i+½,j} = -\frac{T^t_{i+1,j} - T^t_{i,j}}{R^t_{i+½,j}} \quad 3.46.$$

And,

$$q^t_{i,j-½} = -\frac{T^t_{i,j} - T^t_{i,j-1}}{R^t_{i,j-½}} \quad 3.47.$$

$$q^t_{i,j+½} = -\frac{T^t_{i,j+1} - T^t_{i,j}}{R^t_{i,j+½}} \quad 3.48.$$

$R_{i±½}$, $R_{i±½}$, $R_{i±½}$ and $R_{i±½}$ (m^2K/W) are cell thermal resistances, which are combinations of thermal resistances of the current cell (i, j), and the two adjacent half cells, on either side (left and right) (fig 3.7), as follows.

Radial resistances

$$R_{i-½,j} = \left[\frac{r_{i-1} ln \frac{r_{i-1} + ½d_r}{r_{i-1}}}{K_{i-1,j}} + \frac{r_{x,j} ln \frac{r_i + ½d_r}{r_i}}{k_{i,j,}}\right] \quad 3.49.$$

$$R_{i+½,j} = \left[\frac{r_i ln \frac{r_i + ½d_r}{r_i}}{K_{i,j}} + \frac{r_{i+1} ln \frac{r_{i+1} + ½d_r}{r_{i+1}}}{k_{i+1,j}}\right] \quad 3.50.$$

$$A_{i+1,j} \neq A_{i,j} \neq A_{i-1,j} \neq 0$$

Axial resistances

$$R_{i,j-½} = \frac{d_a}{2}\left[\frac{1}{K_{i,j-1}} + \frac{1}{k_{i,j}}\right] \quad 3.51.$$

$$R_{i,j+½} = \frac{d_a}{2}\left[\frac{1}{K_{i,j}} + \frac{1}{k_{i,j+1}}\right] \quad 3.52.$$

$$A_{i,j+1} = A_{i,j} = A_{i,j-1}$$

For both radial and axial resistances,

$K_{i-1,j} \neq K_{i,j} \neq K_{i+1,j} \neq 0$ and $K_{i,j-1} \neq K_{i,j} \neq K_{i,j+1} \neq 0$

Equations 3.49 and 3.50 takes into account the non-uniform heat flow cross-sectional area on either side of the cells along the radial direction.

Varying thermal conductivity of cell (***i***, ***j)*** at time, ***t***, can be obtained from the state (or phase) of the PCM, equation 3.53.

$$\boldsymbol{k_{i,j}^{t}} = \left[\frac{\boldsymbol{\gamma_{i,j}^{t}}}{\boldsymbol{k_l}} + \frac{\mathbf{1} - \boldsymbol{\gamma_{i,j}^{t}}}{\boldsymbol{k_s}}\right]^{-\mathbf{1}} \qquad 3.53.$$

The following conditions apply for the model:

Initial conditions

$\boldsymbol{t} = 0$,

$\boldsymbol{T_{i,j}^{0}} = \boldsymbol{T_{w,i}^{0}} = \boldsymbol{T_{w,o}^{t}} =$ initial temperature

$$\boldsymbol{E_{i,j}} = \boldsymbol{\rho c_{p,s}}\left(\boldsymbol{T_{w,o}} - \boldsymbol{T_p}\right) \qquad 3.54.$$

Boundary conditions, radial

At $\boldsymbol{r} = \boldsymbol{r_t}$, $\boldsymbol{i} = 1$

$$\boldsymbol{q_0^t} = \boldsymbol{q_{½}^t} = -\frac{\boldsymbol{T_1^t} - \boldsymbol{T_w^t}}{\boldsymbol{R_{½}^t}} \qquad 3.55.$$

$$\boldsymbol{R_{½}} = \left[\frac{\mathbf{1}}{\boldsymbol{h_w}} + \frac{\boldsymbol{r_0 ln}\dfrac{\boldsymbol{r_{0,}} + ½\boldsymbol{d_r}}{\boldsymbol{r_0}}}{\boldsymbol{k_{1,1}}}\right] \qquad 3.56.$$

At $\boldsymbol{r} = \boldsymbol{r_N}$, $\boldsymbol{i}$ = N (for single tube/pipe)

$$\boldsymbol{q_{N+½}^t} = -\frac{\boldsymbol{T_{N-1}^t} - \boldsymbol{T_{N+1}^t}}{\boldsymbol{R_{atm}^t}} \qquad 3.57.$$

$\boldsymbol{R_{atm}}$ represents total combined thermal conductance of ***N***th PCM section and ***AU***, combined thermal conductance (W/K) of shell material, insulation material and the exchanger's immediate environment, while $\boldsymbol{T_{N+1}}$ represents the surrounding temperature.

At $\boldsymbol{r = r_N}$, $\boldsymbol{i}$ = N (for multiple tubes/pipes)[2]

$$\boldsymbol{q^t_{N+½} = q^t_N = -\frac{T^t_{N-1} - T^t_{N+1}}{R^t_n}} \quad 3.58.$$

$\boldsymbol{N+1}$ represents the $\boldsymbol{n}$th cell of neighbouring tube/PCM. The diameter at $\boldsymbol{N}$, $2\boldsymbol{r_N}$ is equal to the tubes' pitch (dependent on tube arrangement). $\boldsymbol{R_n}$ and $\boldsymbol{T_{N+1}}$ represent thermal resistance and temperature of $\boldsymbol{N}$th PCM section, respectively.

Boundary conditions, axial

At $a = a_j$, j = 1

$$\boldsymbol{q^t_0 = q^t_{½} = -\frac{T^t_1 - T^t_{atm}}{R^t_{½}}} \quad 3.59.$$

$$\boldsymbol{R_{½} = \left[\frac{1}{h_{atm}} + \frac{d_a}{2k_{1,1}}\right]} \quad 3.60.$$

At $a = a_M$, j = M

$$\boldsymbol{q^t_M = q^t_{M+½} = -\frac{T^t_{M-1} - T^t_{M+1}}{R^t_{atm}}} \quad 3.61.$$

$\boldsymbol{N}$ and $\boldsymbol{M}$ represent the maximum number of PCM cell divisions along the radial and axial axes, respectively.

For system with multiple tubes, heat conductance to the surrounding is accounted for by employing $\boldsymbol{AU}$ for determining heat flow in the heat exchanger model.

3.4 Active Fabric-integrated PCM Thermal Store

Application of PCMs into building fabrics has, for the most part, been limited to passive systems. Active fabric integrated PCM thermal energy storage systems are available but majorly in underfloor heating systems (Verbeke & Audenaert, 2018). Development of active

[2] The tube arrangement method assumes a hexagonal arrangement, which is ensures tight closeness. Nevertheless, a tiny portion of PCM is not captured by the modelling method. This proportion is reduced with large quantity of tubes with small diameters

systems for walls is rare and relatively new (Kong et al., 2020) but, nonetheless, gaining grounds. Also, there is little in the way of modelling such systems using building simulation, whether it be underfloor systems or wall integrated systems.

The model proposed and described here is the model of a PCM slab that can be integrated into building fabrics for modelling and performance assessment.

3.4.1 Physical Model of Fabric integrated Thermal Store

The fabric integrated PCM wall store was represented by a rectangular block/slab heat store/exchanger, like the PCM heat store developed by Shatikian, Ziskind, & Letan (2005). Their system is a rectangular block containing PCM between columns of metal plates which they referred to as internal fins. The fins in this case serve as tubes for heat transf flow and the entire system sealed in a thin sheet of metal.

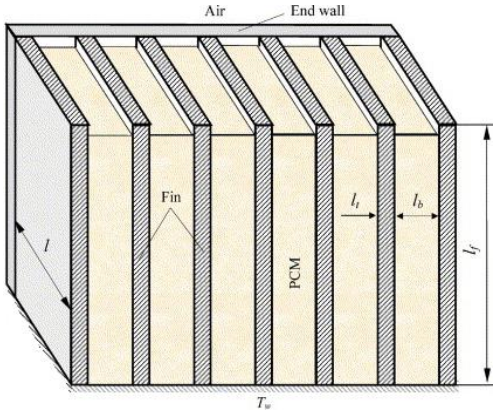

Figure 3.8: PCM heat storage unit described in Shatikian, Ziskind, & Letan (2005)

The rectangular HTF tubes divide the PCM block into small rectangular columns along its breadth, forming a series of PCM-tube-PCM sandwiches (Figure 3.9). There are no fins, and it is assumed to be adequately insulated from the surrounding.

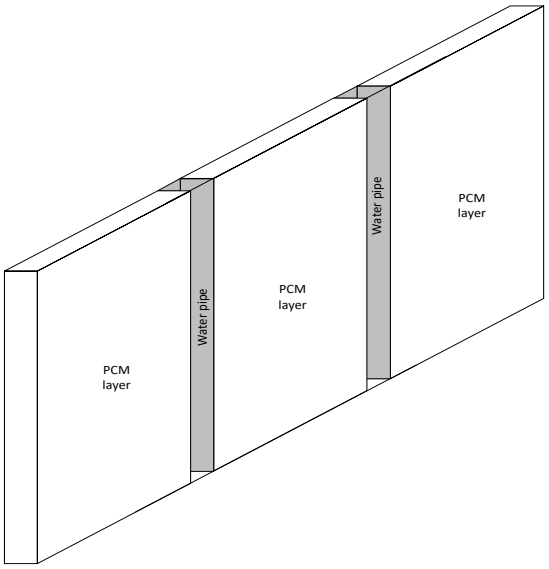

Figure 3.9: PCM wall slab

3.4.2 Heat Exchanger Modelling of Fabric Integrated Thermal Store

The fabric integrated PCM thermal storage system was similarly represented with mathematical expressions and equations which capture both its physical characteristics, energy transfer and transformations of the PCM and heat transfer fluid (HTF).

3.4.2.1 Heat Transfer Surface Area

As stated in section 3.4.1, the PCM slab comprises series of PCM-tube-PCM sandwiches. One such sandwich is simulated and scaled up to entire slab by multiplying by number of tubes, N.

Heat flow from (or to) the HTF follows two (2) paths, as shown in Figure 3.10. The heat exchange surface areas are determined from tube breadth, b_{tube} (m), length, L_{tube} (m), and thickness of the PCM wall slab, t_{slab}, (equations 3.62 and 3.63). Length of tube is also taken to be equal to height of PCM wall slab.

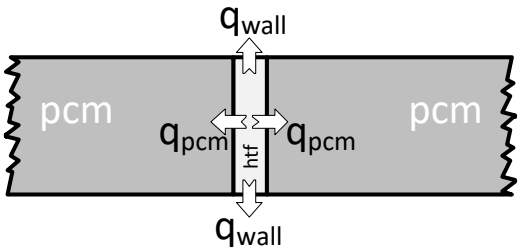

Figure 3.10: PCM-tube-PCM sandwich showing heat flow paths.

HTF-to-tube (PCM sides),

$$\boldsymbol{A_{hp} = l_{tube} \times t_{slab}} \qquad 3.62.$$

HTF-to-tube (containment wall sides),

$$\boldsymbol{A_{hw} = l_{tube} \times b_{tube}} \qquad 3.63.$$

$\boldsymbol{A_{hp}}$ and $\boldsymbol{A_{hw}}$, (m^2) are heat exchange surface areas between HTF and tube on both PCM and containment wall sides, respectively, as well as from tube to PCM and tube to containment wall, also respectively.

3.4.2.2 Heat Exchanger Discretisation

3-dimensional discretization was carried out for the PCM wall slab. This was achieved by subdividing spatial regions by number of cell divisions along the x-, y- and z- axes (figure 3.11).

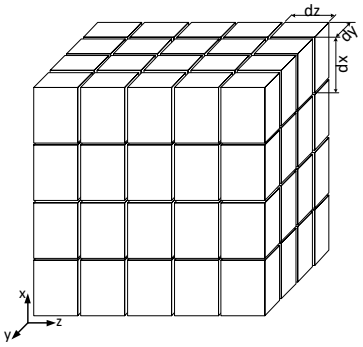

Figure 3.11: Discretisation of PCM wall slab

Cell Dimensions

Discretisation produced a series of cuboids of dimensions $\boldsymbol{d_x}$, $\boldsymbol{d_y}$ and $\boldsymbol{d_z}$ (m) (figure 3.12).

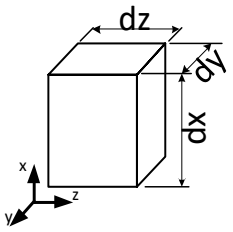

Figure 3.12: Discrete cell (PCM wall slab)

Cell heat exchange surface Area

Each discrete cell has three (3) heat exchange surface areas. From Figure 3.12,

$$\boldsymbol{A_x = d_y \times d_z} \quad 3.64.$$

$$\boldsymbol{A_y = d_x \times d_z} \quad 3.65.$$

$$\boldsymbol{A_z = d_x \times d_y} \quad 3.66.$$

3.4.2.3 Heat and Energy Flow Equation

Like with the shell-and-tube heat exchanger, PCM is treated as second heat transfer fluid in the heat flow energy balance equation. Heat energy exchange between PCM and HTF is represented by an effective heat flux term.

Assumptions made in formulating the energy equation are the same as those for the shell-and-tube PCM heat exchanger. They are:

1. potential and kinetic energy changes of heat transfer fluid is neglected,
2. specific heat at constant pressure is constant for both heat transfer fluid and PCM,
3. pressure drop inside shell and tubes are neglected,
4. temperatures are uniform over every flow cross section,

Change in energy of HTF as it flows through the tubes and exchange heat with PCM over elapsed time (***Δt***) is represented in equation 3.67 and 3.68.

The HTF exchanges heat with PCM and containment wall as depicted in figures 3.10 and 3.13.

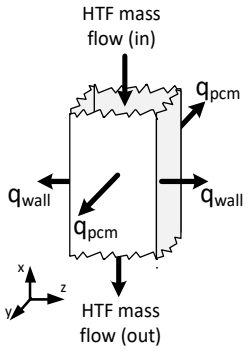

Figure 3.13: HTF tube showing mass and heat flow paths/directions.

$$\boldsymbol{m_w C_{p,w} \frac{\Delta T_w}{\Delta t} = \dot{m}_w C_{p,w} \Delta T_w - 2\left(\Delta q_{pcm} - \Delta q_{wall}\right)} \quad 3.67.$$

$$\boldsymbol{m_w C_{p,w} \frac{T_w^{n+1} - T_w^n}{\Delta t} = \dot{m}_w C_{p,w}\left(T_{w,i}^{n+\theta} - T_{w,o}^{n+\theta}\right) - 2\left(\Delta q_{pcm}^{n+\theta} - \Delta q_{wall}^{n+\theta}\right)} \quad 3.68.$$

$\boldsymbol{\Delta q_{pcm}}$ (W) is change in heat flow rate (term) for PCM, exchanger material and heat transfer fluid combined and $\boldsymbol{\Delta q_{wall}}$ (W) is change in heat flow rate between HTF, exchanger material and containment wall

Effective heat flow through PCM and exchanger material, $\boldsymbol{\Delta q_{pcm}}$, and containment wall and exchanger material, $\boldsymbol{\Delta q_{wall}}$, from HTF are obtained in equations 3.69 and 3.70.

$$\boldsymbol{\Delta q_{pcm} = \frac{A_{ph}\left(T_w - T_p\right)}{R_p}} \quad 3.69.$$

$$\boldsymbol{\Delta q_{wall} = \frac{A_{hw}(T_w - T_{wall})}{R_{wall}}} \quad 3.70.$$

$\boldsymbol{R_p}$ represents combined thermal resistance of fluid stream, exchanger material and PCM while $\boldsymbol{R_{wall}}$ represents thermal resistance of fluid stream, exchanger material and the containment wall.

Also, mass and mass flow rate of HTF can be represented in terms of density, $\boldsymbol{\rho}$, (kg/m^3), cross sectional area of flow region, $\boldsymbol{A_{tube}}$, (m^2), length of exchanger, $\boldsymbol{l_{tube}}$, (m) and elapsed time, $\boldsymbol{t}$, (s), with equations 3.71 and 3.72.

$$\boldsymbol{m_w = \rho A_{tube} l_{tube}} \quad 3.71.$$

$$\dot{m}_w = \frac{\rho A_{tube} l_{tube}}{t} \quad 3.72.$$

Combined thermal resistance of PCM and fluid stream is a combination of thermal conductivity of PCM and heat transfer coefficient of heat transfer fluid stream. Both change and vary as PCM exchanges heat with heat transfer fluid. They are represented by equations 3.73 and 3.74.

$$R_P = \left[\frac{1}{h_w} + \frac{1}{2R_{pcm}} + \frac{1}{2k_t}\right] \quad 3.73.$$

$$R_{wall} = \frac{1}{h_w} + \frac{t_{wall}}{2k_{wall}} + \frac{1}{2k_t} \quad 3.74.$$

h_w, (W/m^{2}K) heat transfer coefficient for HTF stream, is a function of the fluid volume flow rate, its Nusselt and Reynolds numbers, thermal conductivity, viscosity and temperature. R_{pcm} is equivalent heat transfer coefficient for PCM cells. This is similarly determined from modelling of the phase change process.

3.4.3 PCM – Discrete Model Energy Equation

The 3-dimensional cuboid shown in Figure 3.9 represents regions wherein local equilibrium is achieved at a shorter time scale compared to the computational time step. Properties and conditions at centre of this control volume is representative of average over the control volume whose heat flow is simulated by applying conservation laws and updating states over discrete time increments.

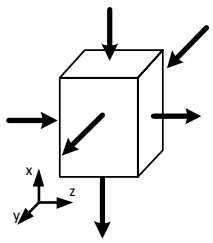

Figure 3.14: Discrete PCM control volume showing heat flow pattern.

Same assumptions as with the shell-and-tube heat exchanger (save for the radial symmetry) were made in formulating the heat/energy flow equating used for determining changes in enthalpy over time due to heat flow across the control volume.

Employing the heat flow energy equations 3.38 and 3.39, and extending to 3-D yields,

$$\boldsymbol{\partial E_t + \partial q_x + \partial q_y + \partial q_z = 0} \tag{3.75.}$$

$$\boldsymbol{\frac{\Delta E}{\Delta t} + \frac{\Delta q_x}{\Delta x} + \frac{\Delta q_y}{\Delta y} + \frac{\Delta q_z}{\Delta z} = 0} \tag{3.76.}$$

Designating discrete cells along the x- axis by ***i,*** y- axis by ***j*** and along the z- axis by ***k***, for cell (***i***, ***j***, *k)*,

$$\boldsymbol{\frac{\Delta E_{i,j,k}}{\Delta t} + \frac{\Delta q_{x,i}}{\Delta x} + \frac{\Delta q_{y,j}}{\Delta y} + \frac{\Delta q_{z,k}}{\Delta z} = 0} \tag{3.77.}$$

$$\boldsymbol{E_{i,j,k}^{t+1} - E_{i,j,k}^{t} = q_{x,i}\frac{\Delta t}{\Delta x} + q_{y,j}\frac{\Delta t}{\Delta y} + q_{z,k}\frac{\Delta t}{\Delta z} = 0} \tag{3.78.}$$

Integrating 3.78 and rewriting heat flux, $\boldsymbol{q_{x,i}}$, $\boldsymbol{q_{y,j}}$ and $\boldsymbol{q_{z,k}}$ in terms of two (2) fluxes, $\boldsymbol{q_{i-½,j,k}}$ and $\boldsymbol{q_{i+½,j,k}}$; $\boldsymbol{q_{i,j-½,k}}$ and $\boldsymbol{q_{i,j+½,k}}$; and $\boldsymbol{q_{i,j,k-½}}$ and $\boldsymbol{q_{i,j,k+½}}$ (respectively) (fig 3.12), that is,

$$\boldsymbol{q_{x,i}^{t} = q_{i-½,j,k}^{t} - q_{i+½,j,k}^{t}} \tag{3.79.}$$

$$\boldsymbol{q_{y,j}^{t} = q_{i,j-½,k}^{t} - q_{i,j+½,k}^{t}} \tag{3.80.}$$

$$\boldsymbol{q_{z,k}^{t} = q_{i,j,k-½}^{t} - q_{i,j,k+½}^{t}} \tag{3.81.}$$

Gives,

$$\boldsymbol{E_{i,j,k}^{t+1} - E_{i,j,k}^{t} = \frac{\Delta t}{\Delta x}\left[q_{i-½,j,k}^{n+\theta} - q_{i+½,j,k}^{n+\theta}\right] + \frac{\Delta t}{\Delta y}\left[q_{i,j-½,k}^{n+\theta} - q_{i,j+½,k}^{n+\theta}\right] + \frac{\Delta t}{\Delta z}\left[q_{i,j,k-½}^{n+\theta} - q_{i,j,k+½}^{n+\theta}\right]} \tag{3.82.}$$

Heat flux across discrete node boundaries, $\boldsymbol{q_{i-½,j,k}}$ and $\boldsymbol{q_{i+½,j,k}}$, $\boldsymbol{q_{i,j-½,k}}$ and $\boldsymbol{q_{i.j+½}}$, and $\boldsymbol{q_{i,j,k-½}}$ and $\boldsymbol{q_{i,j,k+½}}$ (Figure 3.12) are obtained from equation 3.83 to 3.88.

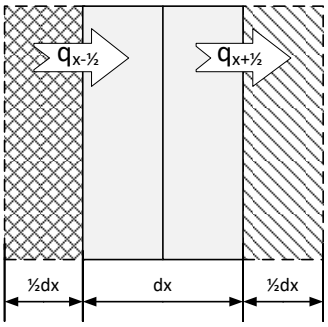

Figure 3.15: Discrete PCM control volume showing heat flow pattern for x- axis

$$q^t_{x-½,j,k} = -\frac{T^t_{i,j,k} - T^t_{i-1,j,k}}{R^t_{i-½,j,k}} \quad 3.83.$$

$$q^t_{x+½,j,k} = -\frac{T^t_{i+1,j,k} - T^t_{i,j,k}}{R^t_{i+½,j,k}} \quad 3.84.$$

$$q^t_{i,j-½,k} = -\frac{T^t_{i,j,k} - T^t_{i,j-1,k}}{R^t_{i,j-½,k}} \quad 3.85.$$

$$q^t_{i,j+½,k} = -\frac{T^t_{i,,j+1,k} - T^t_{i,j,k}}{R^t_{i,j+½,k}} \quad 3.86.$$

$$q^t_{i,j,k-½} = -\frac{T^t_{i.j.k} - T^t_{i,j,k-1}}{R^t_{i,j,k-½}} \quad 3.87.$$

$$q^t_{i,j,k+½} = -\frac{T^t_{i,j,k+1} - T^t_{i,j,k}}{R^t_{i,j,k+½}} \quad 3.88.$$

Also, thermal resistances for each cell consists of thermal resistances of the current cell (or node) and the two adjacent half cells.

$$R_{i-½,j,k} = \frac{d_x}{2}\left[\frac{1}{K_{i-1,j,k}} + \frac{1}{k_{i,j,k}}\right] \quad 3.89.$$

$$R_{i+½,j,k} = \frac{d_x}{2}\left[\frac{1}{K_{i,j,k}} + \frac{1}{k_{i+1,j,k}}\right] \quad 3.90.$$

$$R_{i,j-½,k} = \frac{d_y}{2}\left[\frac{1}{k_{i,j-1,k}} + \frac{1}{k_{j,j,k}}\right] \quad 3.91.$$

$$\boldsymbol{R_{i,j+½,k}} = \frac{\boldsymbol{d_y}}{\boldsymbol{2}}\left[\frac{\boldsymbol{1}}{\boldsymbol{K_{i,j,k}}} + \frac{\boldsymbol{1}}{\boldsymbol{k_{i,j+1,k}}}\right] \quad 3.92.$$

$$\boldsymbol{R_{i,j,k-½}} = \frac{\boldsymbol{d_z}}{\boldsymbol{2}}\left[\frac{\boldsymbol{1}}{\boldsymbol{K_{i,j,k-1}}} + \frac{\boldsymbol{1}}{\boldsymbol{k_{i,j,k}}}\right] \quad 3.93.$$

$$\boldsymbol{R_{i,j,k+½}} = \frac{\boldsymbol{d_z}}{\boldsymbol{2}}\left[\frac{\boldsymbol{1}}{\boldsymbol{K_{i,j,k}}} + \frac{\boldsymbol{1}}{\boldsymbol{k_{i,j,k+1}}}\right] \quad 3.94.$$

For each cell,

$$\boldsymbol{A_{i+1,j,k}} = \boldsymbol{A_{i,j,k}} = \boldsymbol{A_{i-1,j,k}}$$

$$\boldsymbol{A_{i,j+1,k}} = \boldsymbol{A_{i,j,k}} = \boldsymbol{A_{i,j-1,k}}$$

$$\boldsymbol{A_{i,j,k+1}} = \boldsymbol{A_{i,j,k}} = \boldsymbol{A_{i,j,k-1}}$$

and,

$$\boldsymbol{k_{i-1,j,k}} = \boldsymbol{k_{i,j,k}} = \boldsymbol{k_{i+1,j,k}}$$

$$\boldsymbol{k_{i,j-1,k}} = \boldsymbol{k_{i,j,k}} = \boldsymbol{k_{i,j+1,k}}$$

$$\boldsymbol{k_{i,j,k-1}} = \boldsymbol{k_{i,j,k}} = \boldsymbol{k_{i,j,k+1}}$$

Varying thermal conductivity of cell (***i, j, k***) at time, ***t***, can be obtained from the state (or phase) of the PCM, equations 3.95.

$$\boldsymbol{k^t_{i,j,k}} = \left[\frac{\boldsymbol{\gamma^t_{i,j,k}}}{\boldsymbol{k_l}} + \frac{\boldsymbol{1 - \gamma^t_{i,j,k}}}{\boldsymbol{k_s}}\right]^{\boldsymbol{-1}} \quad 3.95.$$

Similarly, the following conditions apply:

Initial conditions

$\boldsymbol{t} = 0$,

$\boldsymbol{T^0_{i,j,k}} = \boldsymbol{T^0_{w,i}} = \boldsymbol{T^t_{w,o}}$ = initial temperature

$$\boldsymbol{E_{i,j,k}} = \boldsymbol{\rho c_{p,s}}\left(\boldsymbol{T_{w,o} - T_p}\right) \quad 3.96.$$

Boundary conditions,

At $\boldsymbol{x} = 0$, $\boldsymbol{i} = 1$

$$q_0^t = q_{½}^t = -\frac{T_1^t - T_{wall}^t}{R_{½}^t} \quad 3.97.$$

$$R_{½} = \left[\frac{d_x}{2k_{wall}} + \frac{d_x}{2k_1}\right] \quad 3.98.$$

At x = **L**, i = **M**

$$q_M^t = q_{M+½}^t = -\frac{T_{M-1}^t - T_{wall}^t}{R_{i+½}^t} \quad 3.99.$$

$$R_{M+½} = \left[\frac{d_x}{2k_M} + \frac{d_x}{2k_{wall}}\right] \quad 3.10($$

At y = 0, j = 1

$$q_0^t = q_{½}^t = -\frac{T_1^t - T_w^t}{R_{½}^t} \quad 3.101$$

$$R_{½} = \left[\frac{1}{h_w} + \frac{d_y}{2k_1}\right] \quad 3.102.$$

At y = **N**, j = **P**

$$q_P^t = q_{P+½}^t = -\frac{T_{P-1}^t - T_{wall}^t}{R_{j+½}^t} \quad 3.103.$$

$$R_{P+½} = \left[\frac{d_y}{2k_P} + \frac{d_y}{2k_{wall}}\right] \quad 3.104.$$

At z = 0, k = 1

$$q_0^t = q_{½}^t = -\frac{T_1^t - T_{wall}^t}{R_{½}^t} \quad 3.105.$$

$$R_{½} = \left[\frac{d_z}{2k_{wall}} + \frac{d_z}{2k_1}\right] \quad 3.106.$$

At z = **Q**, k = **R**

$$q_R^t = q_{R+½}^t = -\frac{T_{R-1}^t - T_{wall}^t}{R_{k+½}^t} \quad 3.107.$$

$$R_{R+½} = \left[\frac{d_z}{2k_R} + \frac{d_z}{2k_{wall}}\right] \quad 3.108.$$

L, ***N*** and ***Q*** represent maximum length, breadth and depth of slab and M, P and R represent cells at maximum length, breadth and depth of slab respectively.

3.5 Iterative Solution – Implicit/Explicit Scheme

The energy equation for the discretised cell (node) was solved with a numerical algorithm using finite difference method with a mixture of explicit and implicit schemes. Mixing both implicit and explicit forms of the energy balance equation ensures that the algorithm is numerically stable (Mitchell, 1969). This explicit/implicit combination is the method adopted in ESP-r and is done here by multiplying both energy equation (for heat exchanger and PCM models) with weighing fractions and summing them up. The future time components, variables in future time ***(t+1)***, are multiplied by the weighing factor, ***μ***, and the present time component, variables in present time ***(t)***, are multiplied by the weighing factor, ***(1- μ)***. The sum of both equates to a weighing factor of 1 for entire equation. Depending on the value of ***θ***, the equation set could transform into either an explicit scheme, fully implicit scheme or a fraction in between. Properties at future times are computed based on properties at present time and over all discrete cells of the component.

3.5.1 Solution of the Shell-and-tube PCM Thermal Store

3.5.1.1 Heat exchanger Model

Iteration for the thermal store is accomplished with the ESP-r engine. However, the model is required to generate the self- and cross- coupling coefficients and present time step coefficients for the matrix equation processor.

Subsequently, rewriting equations 3.31 in the explicit-implicit iterative form, wherein the weighing factor is between zero and one (1) ***(0 < μ < 1)***,

$$m_w C_{p,w} \frac{T_w^{t+1}}{\Delta t} - \mu\left[\dot{m}_w C_{p,w}\left(T_{w,i}^{t+1} - T_{w,o}^{t+1}\right) - q_{pcm}^{t+1}\right] = m_w C_{p,w} \frac{T_w^{t}}{\Delta t} + (1-\mu)\left[\dot{m}_w C_{p,w}\left(T_{w,i}^{t} - T_{w,o}^{t}\right) - q_{pcm}^{t}\right] \quad 3.109.$$

Substituting q_{pcm} with equation 3.32,

$$m_w C_{p,w} \frac{T_w^{t+1}}{\Delta t} - \mu\left[\dot{m}_w C_{p,w}\left(T_{w,i}^{t+1} - T_{w,o}^{t+1}\right) - \frac{A_t}{R_p^{t+1}}\left(T_w^{t+1} - T_p^{t+1}\right)\right] = m_w C_{p,w} \frac{T_w^{t}}{\Delta t} + (1-\mu)\left[\dot{m}_w C_{p,w}\left(T_{w,i}^{t} - T_{w,o}^{t}\right) - \frac{A_t}{R_p^{t}}\left(T_w^{t} - T_p^{t}\right)\right] \quad 3.110.$$

Rearranging in the general ESP-r matrix equation format, equation 2.4,

$$\left(\frac{m_w C_{p,w}}{\Delta t} + \mu\left[\dot{m}_w C_{p,w} + \frac{A_t}{R_p^{t+1}}\right]\right) T_w^{t+1} = \left(\frac{m_w C_{p,w}}{\Delta t} - (1-\mu)\left[\dot{m}_w C_{p,w} + \frac{A_t}{R_p^{t+1}}\right]\right) T_w^{t} + \mu\left(\dot{m}_w C_{p,w} T_{w,i}^{t+1} + \frac{A_t}{R_p^{t+1}} T_p^{t+1}\right) + (1-\mu)\left(\dot{m}_w C_{p,w} T_{w,i}^{t} + \frac{A_t}{R_p^{t}} T_p^{t}\right) \quad 3.111.$$

That is,

$$AT_w^t = BT_w^t + C \quad 3.112.$$

Note – Exit temperature of HTF, $T_{w,o}$, is made equal to stream temperature, T_w.

3.5.1.2 PCM Model

Iteration of the PCM model is done with the aid of the Gauss-Seidel iterative method. Here, future equation for determining future property values of a given cell (or node) is solved using present/latest known property values for all other cells (or nodes).

Energy (enthalpy) change/transformation of the phase change material is given in equation 3.44. Choosing μ, $(0 < \mu < 1)$ it becomes,

$$E_{i,j}^{t+1} - \mu\left(\frac{\Delta t}{\Delta r}\left[q_{i-½,j}^{t+1} - q_{i+½,j}^{t+1}\right] + \frac{\Delta t}{\Delta a}\left[q_{i,j-½}^{t+1} - q_{i,j+½}^{t+1}\right]\right) = E_{i,j}^{t} + (1-\mu)\left(\frac{\Delta t}{\Delta r}\left[q_{i-½,j}^{t} - q_{i+½,j}^{t}\right] + \frac{\Delta t}{\Delta a}\left[q_{i,j-½}^{t} - q_{i,j+½}^{t}\right]\right) \quad 3.113.$$

Substituting for q_{i+1}, q_{i-1}, q_{j+1} and q_{j-1} with equations 3.45 To 3.48

$$E_{i,j}^{t+1} - \mu\left(\frac{\Delta t}{\Delta r}\left[\frac{T_{i-1,j}^{t+1} - T_{i,j}^{t+1}}{R_{i-½,j}^{t+1}} + \frac{T_{i,j}^{t+1} - T_{i+1,j}^{t+1}}{R_{i+½,j}^{t+1}}\right] + \frac{\Delta t}{\Delta a}\left[\frac{T_{i,j-1}^{t+1} - T_{i,j}^{t+1}}{R_{i,j-½}^{t+1}} + \frac{T_{i,j}^{t+1} - T_{i,j+1}^{t+1}}{R_{i,j+½}^{t+1}}\right]\right) \quad 3.114.$$

$$= \boldsymbol{E}_{i,j}^{t} + (\mathbf{1} - \boldsymbol{\mu})\left(\frac{\Delta t}{\Delta r}\left[\frac{T_{i-1,j}^{t} - T_{i,j}^{t}}{R_{i-½,j}^{t}} + \frac{T_{i,j}^{t} - T_{i+1,j}^{t}}{R_{i+½,j}^{t}}\right] + \frac{\Delta t}{\Delta a}\left[\frac{T_{i,j-1}^{t} - T_{i,j}^{t}}{R_{i,j-½}^{t}} + \frac{T_{i,j}^{t} - T_{i,j+1}^{t}}{R_{i,j+½}^{t}}\right]\right)$$

Introducing the term

$$\boldsymbol{\tau} = \boldsymbol{T} - \boldsymbol{T_m} \tag{3.115.}$$

And taking $\boldsymbol{T_l}$ and $\boldsymbol{T_s}$ to be equal to $\boldsymbol{T_m}$, the fluxes can be rewriting in terms of $\boldsymbol{\tau}$, which is the Kirchhoff's temperature, thus,

$$\begin{aligned}\boldsymbol{E}_{i,j}^{t+1} - \boldsymbol{\mu}\left(\frac{\Delta t}{\Delta r}\left[\frac{1}{R_{i-½,j}^{t+1}}\boldsymbol{\tau}_{i-1,j}^{t+1} - \left(\frac{1}{R_{i+½,j}^{t+1}} + \frac{1}{R_{i-½,j}^{t+1}}\right)\boldsymbol{\tau}_{i,j}^{t+1} + \frac{1}{R_{i+½,j}^{t+1}}\boldsymbol{\tau}_{i+1,j}^{t+1}\right] + \right.\\ \left.\frac{\Delta t}{\Delta a}\left[\frac{1}{R_{i,j-½}^{t+1}}\boldsymbol{\tau}_{i,j-1}^{t+1} - \left(\frac{1}{R_{i,j+½}^{t+1}} + \frac{1}{R_{i,j-½}^{t+1}}\right)\boldsymbol{\tau}_{i,j}^{t+1} + \frac{1}{R_{i,j+½}^{t+1}}\boldsymbol{\tau}_{i,j+1}^{t+1}\right]\right)\\ = \boldsymbol{E}_{i,j}^{t} + (\mathbf{1} - \boldsymbol{\mu})\left(\frac{\Delta t}{\Delta r}\left[\frac{1}{R_{i-½,j}^{t}}\boldsymbol{\tau}_{i-1,j}^{t} - \left(\frac{1}{R_{i+½,j}^{t}} + \frac{1}{R_{i-½,j}^{t}}\right)\boldsymbol{\tau}_{i,j}^{t} + \frac{1}{R_{i+½,j}^{t}}\boldsymbol{\tau}_{i+1,j}^{t}\right] + \right.\\ \left.\frac{\Delta t}{\Delta a}\left[\frac{1}{R_{i,j-½}^{t}}\boldsymbol{\tau}_{i,j-1}^{t} - \left(\frac{1}{R_{i,j+½}^{t}} + \frac{1}{R_{i,j-½}^{t}}\right)\boldsymbol{\tau}_{i,j}^{t} + \frac{1}{R_{i,j+½}^{t}}\boldsymbol{\tau}_{i,j+1}^{t}\right]\right)\end{aligned} \tag{3.116.}$$

From this, the enthalpy per unit volume and temperature of cell/node at given time can be determined.

$$\boldsymbol{E^t} = \begin{cases} \boldsymbol{\rho C_{p,s}\tau^t} & \ldots \quad \tau^t < T_s\ (solid) \\ \boldsymbol{\rho L} & \ldots \quad T_s < \tau^t < T_l\ (mushy) \\ \boldsymbol{\rho C_{p,l}\tau^t + \rho_l L} & \ldots \quad \tau^t > T_l\ (liquid) \end{cases} \tag{3.117.}$$

Temperature,

$$\boldsymbol{\tau^t} = \begin{cases} \dfrac{\boldsymbol{E^t}}{\boldsymbol{\rho_s C_{p,s}}} & if \quad \ldots\ldots \quad E^t \le 0\ (solid) \\ \mathbf{0} & if \quad \ldots \quad 0 < E^t < \rho_l L\ (mushy) \\ \dfrac{\boldsymbol{E^t - \rho_l L}}{\boldsymbol{\rho_l C_{p,l}}} & if \quad \ldots \quad E^t \ge \rho_l L\ (liquid) \end{cases} \tag{3.118.}$$

If the right-hand side of equation 3.116 is made equal to $\boldsymbol{g}$, that is,

$$\begin{aligned}\boldsymbol{E}_{i,j}^{t} + (\mathbf{1} - \boldsymbol{\mu})\left(\frac{\Delta t}{\Delta r}\left[\frac{1}{R_{i-½,j}^{t}}\boldsymbol{\tau}_{i-1}^{t} - \left(\frac{1}{R_{i+½,j}^{t}} + \frac{1}{R_{i-½,j}^{t}}\right)\boldsymbol{\tau}_{i}^{t} + \frac{1}{R_{i+½,j}^{t}}\boldsymbol{\tau}_{i+1}^{t}\right] + \right.\\ \left.\frac{\Delta t}{\Delta a}\left[\frac{1}{R_{i,j-½}^{t}}\boldsymbol{\tau}_{i,j-1}^{t} - \left(\frac{1}{R_{i,j+½}^{t}} + \frac{1}{R_{i,j-½}^{t}}\right)\boldsymbol{\tau}_{i,j}^{t} + \frac{1}{R_{i,j+½}^{t}}\boldsymbol{\tau}_{i,j+1}^{t}\right]\right) = \boldsymbol{g}_{i,j}^{t}\end{aligned} \tag{3.119.}$$

Then we can re-write it as,

$$\boldsymbol{E_{i,j}^{t+1} - \mu\left(\frac{\Delta t}{\Delta r}\left[\frac{1}{R_{i-½,j}^{t+1}}\tau_{i-1,j}^{t+1} - \left(\frac{1}{R_{i+½,j}^{t+1}} + \frac{1}{R_{i-½,j}^{t+1}}\right)\tau_{i,j}^{t+1} + \frac{1}{R_{i+½,j}^{t+1}}\tau_{i+1,j}^{t+1}\right] + \frac{\Delta t}{\Delta a}\left[\frac{1}{R_{i,j-½}^{t+1}}\tau_{i,j-1}^{t+1} - \left(\frac{1}{R_{i,j+½}^{t+1}} + \frac{1}{R_{i,j-½}^{t+1}}\right)\tau_{i,j}^{t+1} + \frac{1}{R_{i,j+½}^{t+1}}\tau_{i,j+1}^{t+1}\right]\right) = g_{i,j}^{t}} \quad 3.120.$$

Equation 3.120 can be solved by making an initial guess for $\vec{\tau}^{0}$, adopting superscript, $\boldsymbol{p}$, for $\boldsymbol{p}$th iteration and re-writing as equation 3.121.

$$\boldsymbol{E_{i,j}^{p+1} + \mu\left[\frac{\Delta t}{\Delta r}\left(\frac{1}{R_{i+½,j}^{p}} + \frac{1}{R_{i-½,j}^{p}}\right) + \frac{\Delta t}{\Delta a}\left(\frac{1}{R_{i,j+½}^{p}} + \frac{1}{R_{i,j-½}^{p}}\right)\right]\tau_{i,j}^{p+1} = g_{i,j}^{t} + \mu\left[\frac{\Delta t}{\Delta r}\left(\frac{1}{R_{i-½,j}^{p}}\tau_{i-1,j}^{p} + \frac{1}{R_{i+½,j}^{p}}\tau_{i+1,j}^{p}\right) + \frac{\Delta t}{\Delta a}\left(\frac{1}{R_{i,j-½}^{p}}\tau_{i,j-1}^{p} + \frac{1}{R_{i,j+½}^{p}}\tau_{i,j+1}^{p}\right)\right]} \quad 3.121.$$

This will need to be solved/iterated repeatedly for $\boldsymbol{\tau_{i,j}^{p+1}}$ until maximum absolute value of $\left(\boldsymbol{\tau_{i,j}^{p+1} - \tau_{i,j}^{p}}\right)$ is less than a tolerance.

Equation 3.121 can therefore be re-written as,

$$\boldsymbol{E_{i,j}^{p+1} + F_{i,j}^{p}\tau_{i,j}^{p+1} = Q_{i,j}^{p}} \quad 3.122.$$

From which temperature and phase of PCM can be determined accordingly.

$$\boldsymbol{u_{i,j}^{p+1}} = \begin{cases} \dfrac{\boldsymbol{Q_{i,j}^{p}}}{\boldsymbol{\rho_s c_{p,s} + F_{i,j}^{p}}} & if \quad \ldots\ldots \; Q_{i,j}^{p+1} \leq 0 \; (solid) \\ \boldsymbol{0} & if \quad \ldots \; 0 < Q_{i,j}^{p+1} < \rho_l L \; (mushy) \\ \dfrac{\boldsymbol{Q_{i,j}^{p} - \rho_l L}}{\boldsymbol{\rho_l c_{p,l} + F_{i,j}^{p}}} & if \quad \ldots \; Q_{i,j}^{p+1} \geq \rho_l L \; (liquid) \end{cases} \quad 3.123.$$

After convergence,

$$\boldsymbol{\tau_{i,j}^{t+1} = \tau_{i,j}^{p+1}} \quad 3.124.$$

and

$$\boldsymbol{E_{i,j}^{t+1} = Q_{i,j}^{t} - F_{i,j}^{t}\tau_{i,j}^{t+1}} \quad 3.125.$$

Where,

$$F_{i,j}^{t} = \mu\left[\frac{\Delta t}{\Delta r}\left(\frac{1}{R_{i+½,j}^{t}} + \frac{1}{R_{i-½,j}^{t}}\right) + \frac{\Delta t}{\Delta a}\left(\frac{1}{R_{i,j+½}^{t}} + \frac{1}{R_{i,j-½}^{t}}\right)\right] \quad 3.126.$$

And,

$$Q_{i,j}^{t} = g_{i,j}^{t} + \mu\left[\frac{\Delta t}{\Delta r}\left(\frac{1}{R_{i-½,j}^{t}}\tau_{i-1,j}^{t} + \frac{1}{R_{i+½,j}^{t}}\tau_{i+1,j}^{t}\right) + \frac{\Delta t}{\Delta a}\left(\frac{1}{R_{i,j-½}^{t}}\tau_{i,j-1}^{p} + \frac{1}{R_{i,j+½}^{t}}\tau_{i,j+1}^{p}\right)\right] \quad 3.127.$$

3.5.2 Solution of the Active Fabric-integrated PCM Thermal Store

3.5.2.1 Heat Exchanger Model

As with the shell-and-tube heat PCM heat exchanger, iteration of the PCM wall slab is also done within ESP-r. So, the is written to generate the self- and cross- coupling coefficients and present time step coefficients for the matrix equation processor.

Equations 3.31 written explicit-implicit iterative form wherein ***(0 < μ < 1),*** becomes,

$$m_w C_{p,w}\frac{T_w^{t+1}}{\Delta t} - \mu\left[\dot{m}_w C_{p,w}\left(T_{w,i}^{t+1} - T_{w,o}^{t+1}\right) - 2\left(q_{pcm}^{t+1} + q_{wall}^{t+1}\right)\right] = m_w - C_{p,w}\frac{T_w^{t}}{\Delta t} + (1-\mu)\left[\dot{m}_w C_{p,w}\left(T_{w,i}^{t} - T_{w,o}^{t}\right) - 2\left(q_{pcm}^{t} + q_{wall}^{t}\right)\right] \quad 3.128.$$

Substituting q_{pcm} and q_{wall} with equations 3.69 and 3.70,

$$m_w C_{p,w}\frac{T_w^{t+1}}{\Delta t} - \mu\left[\dot{m}_w C_{p,w}\left(T_{w,i}^{t+1} - T_{w,o}^{t+1}\right) - 2\left(\frac{A_{ph}\left(T_w^{t+1} - T_p^{t+1}\right)}{R_{pcm}^{t+1}} + \frac{A_{hw}\left(T_w^{t+1} - T_{wall}^{t+1}\right)}{R_{wall}^{t+1}}\right)\right] = m_w C_{p,w}\frac{T_w^{t}}{\Delta t} + (1-\mu)\left[\dot{m}_w C_{p,w}\left(T_{w,i}^{t} - T_{w,o}^{t}\right) - 2\left(\frac{A_{ph}\left(T_w^{t} - T_p^{t}\right)}{R_{pcm}^{t}} + \frac{A_{hw}\left(T_w^{t} - T_{wall}^{t}\right)}{R_{wall}^{t}}\right)\right] \quad 3.129.$$

Rearranging in the general ESP-r matrix equation format, equation 2.4 with $T_{w,o}$, equal to T_w,

$$\left(\frac{m_w C_{p,w}}{\Delta t} + \mu\left[\dot{m}_w C_{p,w} + 2\left(\frac{A_{ph}}{R_p^{t+1}} + \frac{A_{hw}}{R_{wall}^{t+1}}\right)\right]\right) T_w^{t+1}$$

$$= \left(\frac{m_w C_{p,w}}{\Delta t} - (1-\mu)\left[\dot{m}_w C_{p,w} + 2\left(\frac{A_{ph}}{R_p^{t}} + \frac{A_{hw}}{R_{wall}^{t}}\right)\right]\right) T_w^{t}$$

$$+ \mu\left(\dot{m}_w C_{p,w} T_{w,i}^{t+1} + 2\left[\frac{A_{ph}}{R_p^{t+1}} T_p^{t+1} + \frac{A_{hw}}{R_{wall}^{t+1}} T_{wall}^{t+1}\right]\right) \quad 3.130.$$

$$+ (1-\mu)\left(\dot{m}_w C_{p,w} T_{w,i}^{t} + 2\left[\frac{A_{ph}}{R_p^{t}} T_p^{t} + \frac{A_{hw}}{R_{wall}^{t}} T_{wall}^{t}\right]\right)$$

That is,

$$A T_w^t = B T_w^t + C \quad 3.131.$$

3.5.2.2 PCM Model

Similarly, the iterative method was adopted for determining cell/node temperature at future timestep using present/latest known property values of other cells (or nodes).

Again, choosing ***(0 < μ < 1)*** equation 3.82 becomes,

$$E_{i,j,k}^{t+1} - \mu\left(\frac{\Delta t}{\Delta x}\left[q_{i-½,j,k}^{t+1} - q_{i+½,j.k}^{t+1}\right] + \frac{\Delta t}{\Delta y}\left[q_{i,j-½.k}^{t+1} - q_{i,j+½.k}^{t+1}\right]\right.$$

$$\left. + + \frac{\Delta t}{\Delta z}\left[q_{i,j-½}^{t+1} - q_{i,j,k+½}^{t+1}\right]\right) \quad 3.132.$$

$$= E_{i,j}^{t} + (1-\mu)\left(\frac{\Delta t}{\Delta x}\left[q_{i-½,j,k}^{t} - q_{i+½,j,k}^{t}\right] + \frac{\Delta t}{\Delta y}\left[q_{i,j-½,k}^{t} - q_{i,j+½,k}^{t}\right]\right.$$

$$\left. + \frac{\Delta t}{\Delta z}\left[q_{i,j,k-½}^{t} - q_{i,j,k+½}^{t}\right]\right)$$

Substituting for q_{i+1}, q_{i-1}, q_{j+1} and q_{j-1} with equations 3.83 To 3.88

$$E_{i,j,k}^{t+1} - \mu\left(\frac{\Delta t}{\Delta x}\left[\frac{T_{i-1,j,k}^{t+1} - T_{i,j,k}^{t+1}}{R_{i-½,j,k}^{t+1}} + \frac{T_{i,j,k}^{t+1} - T_{i+1,j,k}^{t+1}}{R_{i+½,j,k}^{t+1}}\right] + \frac{\Delta t}{\Delta y}\left[\frac{T_{i,j-1,k}^{t+1} - T_{i,j,k}^{t+1}}{R_{i,j-½,k}^{t+1}} + \frac{T_{i,j,k}^{t+1} - T_{i,j+1,k}^{t+1}}{R_{i,j+½,k}^{t+1}}\right] + \right. \quad 3.133.$$

$$\left. \frac{\Delta t}{\Delta z}\left[\frac{T_{i,j,k-1}^{t+1} - T_{i,j,k}^{t+1}}{R_{i,j,k-½}^{t+1}} + \frac{T_{i,j,k}^{t+1} - T_{i,j,k+1}^{t+1}}{R_{i,j,k+½}^{t+1}}\right]\right)$$

$$= \boldsymbol{E}_{i,j,k}^{t} + (\mathbf{1} - \boldsymbol{\mu})\left(\frac{\Delta t}{\Delta x}\left[\frac{T_{i-1,j,k}^{t} - T_{i,j,k}^{t}}{R_{i-½,j,k}^{t}} + \frac{T_{i,j,k}^{t} - T_{i+1,j,k}^{t}}{R_{i+½,j,k}^{t}}\right] + \frac{\Delta t}{\Delta y}\left[\frac{T_{i,j-1,k}^{t} - T_{i,j,k}^{t}}{R_{i,j-½,k}^{t}} + \right.\right.$$

$$\left.\left.\frac{T_{i,j,k}^{t} - T_{i,j+1,k}^{t}}{R_{i,j+½,k}^{t}}\right] + \frac{\Delta t}{\Delta z}\left[\frac{T_{i,j,k-1}^{t} - T_{i,j,k}^{t}}{R_{i,j,k-½}^{t}} + \frac{T_{i,j}^{t} - T_{i,j,k+1}^{t}}{R_{i,j,k+½}^{t}}\right]\right)$$

Taking $\boldsymbol{T_l}$ and $\boldsymbol{T_s}$ to be equal to $\boldsymbol{T_m}$ and substituting for $(\boldsymbol{\tau = T - T_m})$, the Kirchhoff's temperature, equation 3.133 can be rewritten in terms of $\boldsymbol{\tau}$,

$$\boldsymbol{E}_{i,j,k}^{t+1} - \boldsymbol{\mu}\left(\frac{\Delta t}{\Delta x}\left[\frac{1}{R_{i-½,j,k}^{t+1}}\boldsymbol{\tau}_{i-1,j,k}^{t+1} - \left(\frac{1}{R_{i+½,j,k}^{t+1}} + \frac{1}{R_{i-½,j,k}^{t+1}}\right)\boldsymbol{\tau}_{i,j,k}^{t+1} + \right.\right.$$

$$\frac{1}{R_{i+½,j,k}^{t+1}}\boldsymbol{\tau}_{i+1,j,k}^{t+1}\Big] + \frac{\Delta t}{\Delta y}\left[\frac{1}{R_{i,j-½,k}^{t+1}}\boldsymbol{\tau}_{i,j-1,k}^{t+1} - \left(\frac{1}{R_{i,j+½,k}^{t+1}} + \frac{1}{R_{i,j-½,k}^{t+1}}\right)\boldsymbol{\tau}_{i,j,k}^{t+1} + \right.$$

$$\frac{1}{R_{i,j+½,k}^{t+1}}\boldsymbol{\tau}_{i,j+1,k}^{t+1}\Big] + \frac{\Delta t}{\Delta z}\left[\frac{1}{R_{i,j,k-½}^{t+1}}\boldsymbol{\tau}_{i,j-1,k}^{t+1} - \left(\frac{1}{R_{i,j,k+½}^{t+1}} + \frac{1}{R_{i,j,k-½}^{t+1}}\right)\boldsymbol{\tau}_{i,j,k}^{t+1} + \right.$$

$$\left.\left.\frac{1}{R_{i,j,k+½}^{t+1}}\boldsymbol{\tau}_{i,j,k+1}^{t+1}\right]\right) \qquad 3.134.$$

$$= \boldsymbol{E}_{i,j,k}^{t} + (\mathbf{1} - \boldsymbol{\mu})\left(\frac{\Delta t}{\Delta x}\left[\frac{1}{R_{i-½,j,k}^{t}}\boldsymbol{\tau}_{i-1,j,k}^{t} - \left(\frac{1}{R_{i+½,j,k}^{t}} + \frac{1}{R_{i-½,j,k}^{t}}\right)\boldsymbol{\tau}_{i,j,k}^{t} + \right.\right.$$

$$\frac{1}{R_{i+½,j,k}^{t}}\boldsymbol{\tau}_{i+1,j,k}^{t}\Big] + \frac{\Delta t}{\Delta y}\left[\frac{1}{R_{i,j-½,k}^{t}}\boldsymbol{\tau}_{i,j-1,k}^{t} - \left(\frac{1}{R_{i,j+½,k}^{t}} + \frac{1}{R_{i,j-½,k}^{t}}\right)\boldsymbol{\tau}_{i,j,k}^{t} + \right.$$

$$\frac{1}{R_{i,j+½,k}^{t}}\boldsymbol{\tau}_{i,j+1,k}^{t}\Big] + \frac{\Delta t}{\Delta z}\left[\frac{1}{R_{i,j,k-½}^{t}}\boldsymbol{\tau}_{i,j,k-1}^{t} - \left(\frac{1}{R_{i,j,k+½}^{t}} + \frac{1}{R_{i,j,k-½}^{t}}\right)\boldsymbol{\tau}_{i,j,k}^{t} + \right.$$

$$\left.\left.\frac{1}{R_{i,j,k+½}^{t}}\boldsymbol{\tau}_{i,j,k+1}^{t}\right]\right)$$

Similarly, enthalpy per unit volume and temperature of cell at given time can be determined from equations 3.135 and 3.136.

$$\boldsymbol{E^t} = \begin{cases} \boldsymbol{\rho C_{p,s}\tau^t} & \ldots \quad \tau^t < T_s\ (solid) \\ \boldsymbol{\rho L} & \ldots \quad T_s < \tau^t < T_l\ (mushy) \\ \boldsymbol{\rho C_{p,l}\tau^t + \rho_l L} & \ldots \quad \tau^t > T_l\ (liquid) \end{cases} \qquad 3.135.$$

Temperature,

$$\boldsymbol{\tau^t} = \begin{cases} \dfrac{\boldsymbol{E^t}}{\boldsymbol{\rho_s C_{p,s}}} & if \quad \ldots\ldots \; E^t \leq 0 \; (solid) \\ \boldsymbol{0} & if \quad \ldots \; 0 < E^t < \rho_l L \; (mushy) \\ \dfrac{\boldsymbol{E^t - \rho_l L}}{\boldsymbol{\rho_l C_{p,l}}} & if \quad \ldots \; E^t \geq \rho_l L \; (liquid) \end{cases} \qquad 3.136.$$

Making the right-hand side of equation 3.134 equal to $\boldsymbol{g}$, that is,

$$\boldsymbol{E^t_{i,j,k}} + (\boldsymbol{1-\mu})\left(\frac{\boldsymbol{\Delta t}}{\boldsymbol{\Delta x}}\left[\frac{\boldsymbol{1}}{\boldsymbol{R^t_{i-½,j,k}}}\boldsymbol{\tau^t_{i-1,j,k}} - \left(\frac{\boldsymbol{1}}{\boldsymbol{R^t_{i+½,j,k}}} + \frac{\boldsymbol{1}}{\boldsymbol{R^t_{i-½,j,k}}}\right)\boldsymbol{\tau^t_{i,j,k}} + \frac{\boldsymbol{1}}{\boldsymbol{R^t_{i+½,j,k}}}\boldsymbol{\tau^t_{i+1,j,k}}\right] + \frac{\boldsymbol{\Delta t}}{\boldsymbol{\Delta y}}\left[\frac{\boldsymbol{1}}{\boldsymbol{R^t_{i,j-½,k}}}\boldsymbol{\tau^t_{i,j-1,k}} - \left(\frac{\boldsymbol{1}}{\boldsymbol{R^t_{i,j+½,k}}} + \frac{\boldsymbol{1}}{\boldsymbol{R^t_{i,j-½,k}}}\right)\boldsymbol{\tau^t_{j,j,k}} + \frac{\boldsymbol{1}}{\boldsymbol{R^t_{i,j+½,k}}}\boldsymbol{\tau^t_{i,j+1,k}}\right] + \frac{\boldsymbol{\Delta t}}{\boldsymbol{\Delta z}}\left[\frac{\boldsymbol{1}}{\boldsymbol{R^t_{i,j,k-½}}}\boldsymbol{\tau^t_{i,j,k-1}} - \left(\frac{\boldsymbol{1}}{\boldsymbol{R^t_{i,j,k+½}}} + \frac{\boldsymbol{1}}{\boldsymbol{R^t_{i,j,k-½}}}\right)\boldsymbol{\tau^t_{i,j,k}} + \frac{\boldsymbol{1}}{\boldsymbol{R^t_{i,j,k+½}}}\boldsymbol{\tau^t_{i,j,k+1}}\right]\right) = \boldsymbol{g^t_{i,j,k}} \qquad 3.137.$$

Then we can re-write it as,

$$\boldsymbol{E^{t+1}_{i,j,k}} - \boldsymbol{\mu}\left(\frac{\boldsymbol{\Delta t}}{\boldsymbol{\Delta x}}\left[\frac{\boldsymbol{1}}{\boldsymbol{R^{t+1}_{i-½,j,k}}}\boldsymbol{\tau^{t+1}_{i-1,j,k}} - \left(\frac{\boldsymbol{1}}{\boldsymbol{R^{t+1}_{i+½,j,k}}} + \frac{\boldsymbol{1}}{\boldsymbol{R^{t+1}_{i-½.j.k}}}\right)\boldsymbol{\tau^{t+1}_{i,j,k}} + \frac{\boldsymbol{1}}{\boldsymbol{R^{t+1}_{i+½,j,k}}}\boldsymbol{\tau^{t+1}_{i+1,j,k}}\right] + \frac{\boldsymbol{\Delta t}}{\boldsymbol{\Delta y}}\left[\frac{\boldsymbol{1}}{\boldsymbol{R^{t+1}_{i,j-½,k}}}\boldsymbol{\tau^{t+1}_{i,j-1,k}} - \left(\frac{\boldsymbol{1}}{\boldsymbol{R^{t+1}_{i,j+½,k}}} + \frac{\boldsymbol{1}}{\boldsymbol{R^{t+1}_{i,j-½,k}}}\right)\boldsymbol{\tau^{t+1}_{i,j,k}} + \frac{\boldsymbol{1}}{\boldsymbol{R^{t+1}_{i,j+½,k}}}\boldsymbol{\tau^{t+1}_{i,j+1,k}}\right] + \frac{\boldsymbol{\Delta t}}{\boldsymbol{\Delta z}}\left[\frac{\boldsymbol{1}}{\boldsymbol{R^{t+1}_{i,j,k-½}}}\boldsymbol{\tau^{t+1}_{i,j,k-1}} - \left(\frac{\boldsymbol{1}}{\boldsymbol{R^{t+1}_{i,j,k+½}}} + \frac{\boldsymbol{1}}{\boldsymbol{R^{t+1}_{i,j,k-½}}}\right)\boldsymbol{\tau^{t+1}_{i,j,k}} + \frac{\boldsymbol{1}}{\boldsymbol{R^{t+1}_{i,j,k+½}}}\boldsymbol{\tau^{t+1}_{i,j,k+1}}\right]\right) = \boldsymbol{g^t_{i,j,k}} \qquad 3.138.$$

Also beginning with an initial guess for $\vec{\boldsymbol{\tau}}^0$ and adopting superscript, $\boldsymbol{p}$, for $\boldsymbol{p}$th iteration, equation 3.138 can be re-written as equation 3.139 and iterated/solved repeatedly for $\boldsymbol{\tau^{p+1}_{i,j}}$until there is convergence.

$$\boldsymbol{E^{p+1}_{i,j,k}} + \boldsymbol{\mu}\left[\frac{\boldsymbol{\Delta t}}{\boldsymbol{\Delta x}}\left(\frac{\boldsymbol{1}}{\boldsymbol{R^p_{i+½,j,k}}} + \frac{\boldsymbol{1}}{\boldsymbol{R^p_{i-½,j,k}}}\right) + \frac{\boldsymbol{\Delta t}}{\boldsymbol{\Delta y}}\left(\frac{\boldsymbol{1}}{\boldsymbol{R^p_{i,j+½,k}}} + \frac{\boldsymbol{1}}{\boldsymbol{R^p_{i,j-½,k}}}\right) + \frac{\boldsymbol{\Delta t}}{\boldsymbol{\Delta z}}\left(\frac{\boldsymbol{1}}{\boldsymbol{R^p_{i,j,k+½}}} + \frac{\boldsymbol{1}}{\boldsymbol{R^p_{i,j,k-½}}}\right)\right]\boldsymbol{\tau^{p+1}_{i,j,k}} \qquad 3.139.$$

$$= \boldsymbol{g}^{t}_{i,j,k} + \boldsymbol{\mu}\left[\frac{\Delta t}{\Delta x}\left(\frac{1}{R^{p}_{i-½,j,k}}\boldsymbol{\tau}^{p}_{i-1,j,k} + \frac{1}{R^{p}_{i+½,j,k}}\boldsymbol{\tau}^{p}_{i+1,j,k}\right) + \frac{\Delta t}{\Delta y}\left(\frac{1}{R^{p}_{i,j-½,k}}\boldsymbol{\tau}^{p}_{i,j-1,k} + \frac{1}{R^{p}_{i,j+½,k}}\boldsymbol{\tau}^{p}_{i,j+1,k}\right) + \frac{\Delta t}{\Delta z}\left(\frac{1}{R^{p}_{i,j,k-½}}\boldsymbol{\tau}^{p}_{i,j,k-1} + \frac{1}{R^{p}_{i,j,k+½}}\boldsymbol{\tau}^{p}_{i,j,k+1}\right)\right]$$

That is,

$$\boldsymbol{E}^{p+1}_{i,j,k} + \boldsymbol{F}^{p}_{i,j,k}\boldsymbol{\tau}^{p+1}_{i,j,k} = \boldsymbol{Q}^{p}_{i,j,k} \qquad 3.140.$$

Also, temperature and phase of PCM can be determined from equation 3.141.

$$\boldsymbol{\tau}^{p+1}_{i,j,k} = \begin{cases} \dfrac{\boldsymbol{Q}^{p}_{i,j,k}}{\boldsymbol{\rho_s c_{p,s}} + \boldsymbol{F}^{p}_{i,j,k}} & if \quad \ldots\ldots\ Q^{p+1}_{i,j,k} \le 0\ (solid) \\ \boldsymbol{0} & if \quad \ldots\ 0 < Q^{p+1}_{i,j,k} < \rho_l L\ (mushy) \\ \dfrac{\boldsymbol{Q}^{p}_{i,j,k} - \boldsymbol{\rho_l L}}{\boldsymbol{\rho_l c_{p,l}} + \boldsymbol{F}^{p}_{i,j,k}} & if \quad \ldots\ Q^{p+1}_{i,j,k} \ge \rho_l L\ (liquid) \end{cases} \qquad 3.141.$$

After convergence,

$$\boldsymbol{\tau}^{t+1}_{i,j,k} = \boldsymbol{\tau}^{p+1}_{i,j,k} \qquad 3.142.$$

and

$$\boldsymbol{E}^{t+1}_{i,j,k} = \boldsymbol{Q}^{t}_{i,j,k} - \boldsymbol{F}^{t}_{i,j,k}\boldsymbol{\tau}^{t+1}_{i,j,k} \qquad 3.143.$$

Where,

$$\boldsymbol{F}^{t}_{i,j,k} = \boldsymbol{\mu}\left[\frac{\Delta t}{\Delta x}\left(\frac{1}{R^{t}_{i+½,j,k}} + \frac{1}{R^{t}_{i-½,j,k}}\right) + \frac{\Delta t}{\Delta y}\left(\frac{1}{R^{t}_{i,j+½,k}} + \frac{1}{R^{t}_{i,j-½,k}}\right) + \frac{\Delta t}{\Delta z}\left(\frac{1}{R^{t}_{i,j,k+½}} + \frac{1}{R^{t}_{i,j,k-½}}\right)\right] \qquad 3.144.$$

And,

$$Q^{t}_{i,j,k} = g^{t}_{i,j,k} + \mu\left[\frac{\Delta t}{\Delta x}\left(\frac{1}{R^{t}_{i-½,j,k}}\tau^{t}_{i-1,j,k} + \frac{1}{R^{t}_{i+½,j,k}}\tau^{t}_{i+1,j,k}\right)\right.$$
$$+\frac{\Delta t}{\Delta y}\left(\frac{1}{R^{t}_{i,j-½,k}}\tau^{p}_{i,j-1,k} + \frac{1}{R^{t}_{i,j+½,k}}\tau^{p}_{i,j+1,k}\right) \qquad 3.145.$$
$$\left.+\frac{\Delta t}{\Delta z}\left(\frac{1}{R^{p}_{i,j,k-½}}\tau^{p}_{i,j,k-1} + \frac{1}{R^{p}_{i,j,k+½}}\tau^{p}_{i,j,k+1}\right)\right]$$

3.6 Stability

Stability of an iterative method or scheme refers to the sensitivity of computed values at each timestep to input and round-off errors. It also refers to their being affected by the size of timesteps as well as the grid size. Adoption of a mixed implicit-explicit scheme, as is done in ESP-r, ensures stability of the scheme (Kelly, Towards a Design Environment for Building Integrated Energy Systems: The Integration Of Electrical Power Flow Modelling with Building Simulation, 1998). The software also employs a method for determining the weighing factor that is three-fold, 1) fully implicit (weighing factor equals 1), 2) user-specified and 3) calculated based on the relative r (Kelly, Towards a Design Environment for Building Integrated Energy Systems: The Integration Of Electrical Power Flow Modelling with Building Simulation, 1998) elationship between the source code's time step and the internal ESP-r time step. All these are written into the source codes and the source codes' time steps are determined withing them. This iterative scheme is unaffected by size of timesteps, it is unconditionally stable.

3.7 Summary

The model development and formulation of energy balance equations for the thermal stores have been discussed. Starting with the heat conduction problem, the energy conservation equation was formulated in terms of heat balance over a volume of material and time interval to develop an expression that is valid for both the liquid and solid phases of the material. Development of equations for heat exchange and temperature and phase changes experienced by the phase change material was also enumerated, as well as the method for discretising the model and the iterative scheme for solving the discretised energy equations.

The proceeding chapter will focus on processes and procedures for deploying the models into ESP-r and description of how each integrates and interacts within the system and in the following chapter the process and results of validation and verification analysis for the models shall be discussed.

Chapter 4

MODEL DEPLOYMENT AND INTEGRATION INTO ESP-r

4.0 Introduction

The chapter describes deployment and integration of the thermal store models into the ESP-r building energy simulation program. A brief description of ESP-r's plant matrix solver and methods employed (within the software) for establishing sub-matrices and main matrix equation sets leading to solution of its overall plant network matrix equations is presented. Explanation of the processes involved in discretising the plant network into control volumes and determination of characteristic equation set for individual components (plants) as well as the formulation of integrated solution for the overall plant matrix for the programme is also attempted as prelude to description of the model's source codes.

Explanation and walkthrough of the PCM thermal stores' source codes execution, solution and result generation processes is given, as well as explanation of how heat absorption and release by the PCMs to the representative water nodes is simulated. The chapter concludes with details of the differences in structure and application of the two thermal store models in ESP-r as well as their interaction and communication with the ESP-r plant matrix sub-system, with regards the input and output information and data into the program for processing.

4.1 ESP-r Plant Matrix Equation Solver/Processor

As discussed in chapter 2, ESP-r employs an integrated solution technique whereby sub-systems (mass and heat flow, electrical, CFD, etc.) are solved separately and later integrated into a single unified solution (Al-Mosawi, 2011). Solution of the energy and mass balance equations describing plant sub-systems (or components of a plant system) is carried out by the plant system matrix processor. This processor is also responsible for coordinating the assembling of energy and mass flow equations representing all the components in the plant network (system) into a single matrix which is employed for solving the set of equations simultaneously to obtain time-variate mass flow rates and temperatures.

A plant network is, at a minimum, composed of two plant components linked together in a manner that allows exchanges of mass and heat between them. Each plant is represented by, at least, one node for which a field quantity at its centres is assumed to be representative of the average over the entire volume. That is, a node represents the plant, its energy level/content, temperature, mass, etc. The nodes are the points of connection for the plants within networks and represent channels/conduits through which they interact and exchange energy and mass. Further explanation of nodes is given under control volumes in section 2.1.1 of chapter 2.

The processing of plant networks is accomplished in three (3) stages or via three (3) procedures/processes. These are (1) discretisation – subdivision of the plant/system into numerous uniform elemental finite/discrete regions; (2) determination of characteristic equation set; and (3) formulation and solution of the plat equation matrix – this entails building (or forming) the matrix and solving all equation sets for each state variable simultaneously. These processes are explained in more details below.

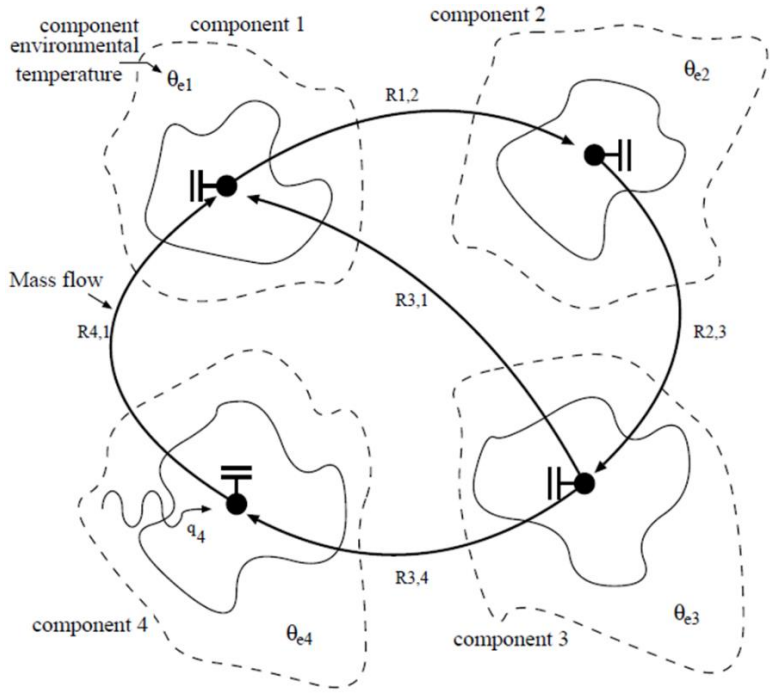

Figure 4.1: Arbitrary plant network - (Aasem, 1993)

4.1.1 Component Discretisation - State/Nodal Parameters and Control Volumes

As discussed in chapter 2, by virtue of its control volume approach/method, ESP-r employs discrete nodal schemes for modelling plant and systems (Kelly, 1998; Clarke, 2001). Modelling of the plant network/system begins with the solver subdividing the system (network) into several elemental uniform finite regions (discretisation), control volumes, and represented each control volume by a node (Figure 4.1).

The process entails representing all derivations of the energy and mass flow equations describing plants (whole or sub- systems) and inter-nodal exchanges (mass and heat) over time and space by a small number of nodes (usually one, two (2) or three at the most per component). Properties at theses nodes represent state variable/properties of the component and are determined by employing a set of "state" equations. These are derived by applying the concepts of conservation of energy and mass to control volumes.

State variables refer to one of four different quantities that are determined (calculated) during simulation, which are energy, mass flow (first and second phase) and hydrogen flow. They are determined from the state equations employed for representing nodal state properties of the plant component. The state equations are energy balance equations for energy state variable, mass flow balance equations for mass flow and hydrogen flow equations for hydrogen flow. Hydrogen flow state variable is often omitted in model source codes except for fuel cell or Hydrogen powered energy systems. Example of fuel cell model developed for/in ESP-r was reported by Beausoleil-Morrison, et al. (2007)

Mass flows, which are of two types, refer to the phase or state of air and water that is exchanged between systems and nodes. First phase refers to water in liquid form and second phase to water in gaseous form, vapour, and air.

The number of these state variables/parameters calculated in one plant system is dependent on its nature. For a thermal storage plant system, the important properties/parameters for modelling are enthalpy and the flow properties of heat transfer fluid. Therefore, the nodal state variable determined are energy and first phase mass flow and the parameters chosen for determining them are temperature and mass flow rate of heat transfer fluid, water.

4.1.2 Characteristic Equation Set – Plant Sub-Matrix

The discretisation process is followed by derivation/establishment of characteristic equations for each of the nodes and state variables in the plant network. During the process, equations describing the important and necessary state parameters/variables are derived and arranged for solution with tri-diagonal matrices. The number of matrices, and number of equation sets, per component, is based on the number of nodes used to model the plant component and the number of state parameters (Aasem, 1993). Figures 4.2a and 4.2b are representations of a typical energy equations and mass flow matrices for the plant network of figure 4.1.

$$\begin{bmatrix} A_{11} & & A_{13} & A_{14} \\ A_{21} & A_{22} & & \\ & A_{32} & A_{33} & \\ & & A_{43} & A_{44} \end{bmatrix} \begin{bmatrix} \theta_1 \\ \theta_2 \\ \theta_3 \\ \theta_4 \end{bmatrix} = \begin{bmatrix} b_1 \\ b_2 \\ b_3 \\ b_4 \end{bmatrix} \qquad \begin{bmatrix} E_{11} & & E_{13} & E_{14} \\ E_{21} & E_{22} & & \\ & E_{32} & E_{33} & \\ & & E_{43} & E_{44} \end{bmatrix} \begin{bmatrix} \dot{m}_1 \\ \dot{m}_2 \\ \dot{m}_3 \\ \dot{m}_4 \end{bmatrix} = \begin{bmatrix} f_1 \\ f_2 \\ f_3 \\ f_4 \end{bmatrix}$$

a – Energy matrix *b – mass flow matrix*

Figure 4.2: Sub-matrices of energy and mass flow equations (Aasem, 1993)

In figure 4.2a, ***Y*** is represented by the sub-matrix components $\boldsymbol{A_{11}, A_{12}, A_{13}}$, etc., ***x*** by $\boldsymbol{\theta_1, \theta_2, \theta_3}$, etc. and ***Z*** by $\boldsymbol{b_1, b_2, b_3}$, etc. while in figure 4.2b, ***Y*** is represented by the sub-matrix components $\boldsymbol{E_{11}, E_{12}, E_{13}}$, etc., ***x*** by $\boldsymbol{m_1, m_2, m_3}$, etc. and ***Z*** by $\boldsymbol{f_1, f_2, f_3}$, etc.

These components (***A***, ***b***, ***E*** and ***f***) represent the properties (thermodynamic, structural and dimensional) of the plant component being modelled. ***A*** and ***E*** represent future time step matrix coefficients while ***b*** and ***f*** represent known terms and boundary conditions. They are determined for each plant component from their coefficient generators, which are compiled/written into their algorithms/codes.

Algorithms/codes for plant components contain equations and parameters that describe its thermo-physical properties, dimensional and structural characteristics, environment and other simulation parameters like simulation time-step, etc., Interrelationship between these properties are described by the plant's energy and mass flow equations, and they (properties) are utilised for determining essential quantities and parameters like thermal resistances, energy exchange and transfer, and so on, required for obtaining/generating the sub-matrix coefficients.

4.1.3 Formulation and Solution of the Plant Equation Matrix

After determining characteristics equation sets for all the plant components that make up the plant network, and developing their sub-matrices, formulation of the overall plant matrix for the network proceeds. It is worth mentioning that substantial parts of both the sub- and

overall matrices is empty, void, and containing zero coefficient matrix. The overall equation matrix for a plant network looks like figure 4.3.

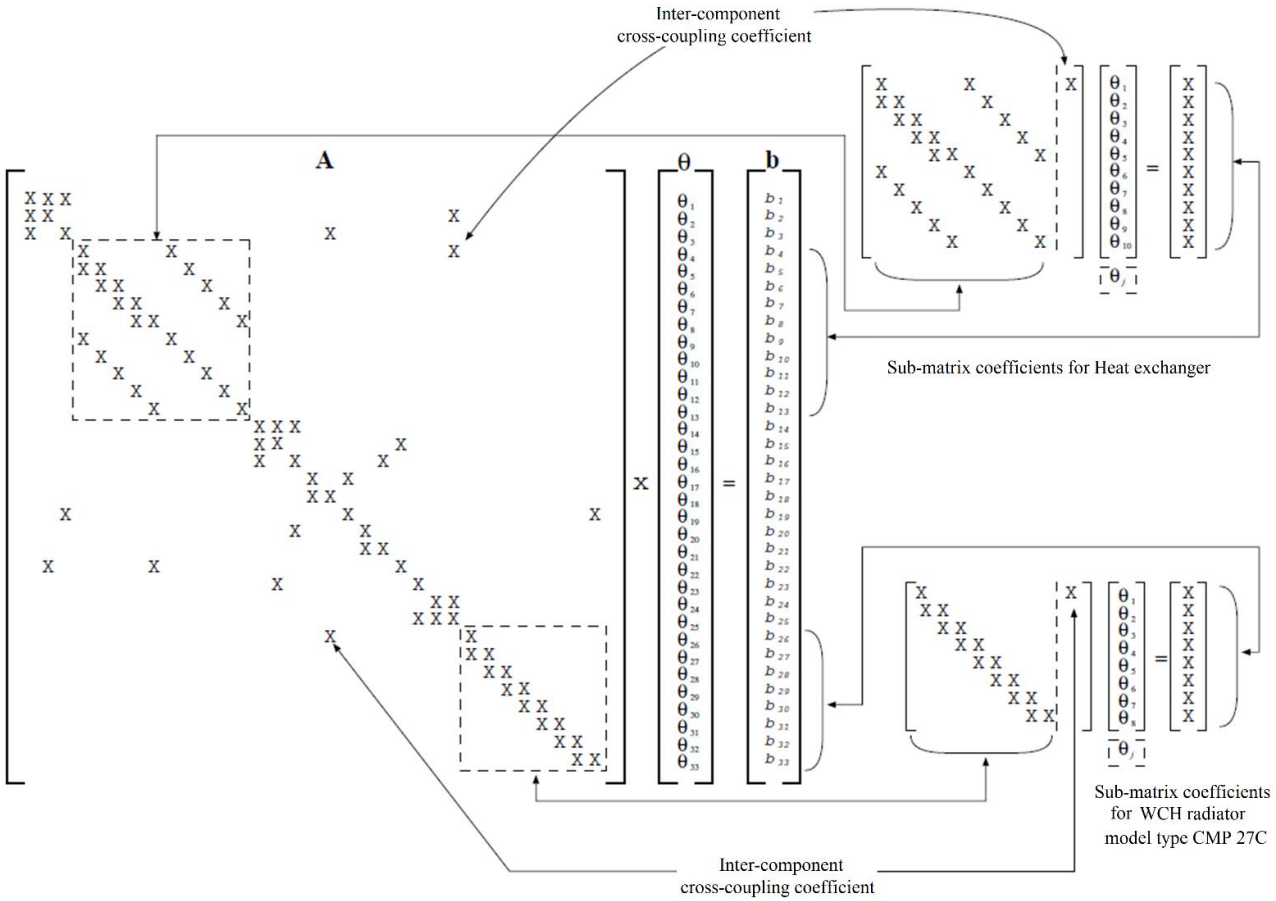

Figure 4.3: Plant network equation matrix (Aasem, 1993)

The size of sub-matrices is determined by number of coefficients for each plant component and the size of overall matrix is determined by the total number of all the plant components present in the plant network. Data used for building up the matrices and solving the plant's energy and mass balance equations are obtained from ESP-r's plant components database. The database contains specific information about all plant components that make up the software's plant repository. They serve as guides for retrieval of data relating to total number of non-zero coefficients present in each plant component's sub-matrix, number of inter-component/plant cross-coupling coefficients and location of the first coefficient within the sub-matrix elements.

After retrieval of required data, the matrix equation is constructed for the plant, after which the solver proceeds to solve the set of simultaneous equations. This is done by first decomposing the LHS matrix to its upper triangular component followed by processing of the non-zero element (or coefficients).

Processing of only the non-zero coefficients is an approach whereby advantage is taken of the sparse nature of the overall plant matrix, which helps to reduce processing time. This is because the matrix decomposition process results in generation of some new, additional, non-zero elements whose positions must be determined before proceeding to the next step (detailed explanation of the steps and procedure is given by Aasem (1993). And following conventional techniques, the number of equations to be solved, given an ***n*** by ***n*** matrix is in the magnitude of $\boldsymbol{n^3}$ (Jennings, (1985) in Aasem (1993)). This is also compounded by the fact that the plant modelling approach in ESP-r sometimes require solving for up to three state variables (first phase and second phase mass flows and, for air conditioning, fluid temperature and relative humidity), which could result in trebling the computational time per time-step. By processing only the non-zero elements/coefficients, both computational time and storage requirements are greatly reduced.

4.2 Component Deployment and Integration

The function of a PCM thermal store is storage of heat (residual, waste, excess) by taking advantage of the large amount of heat absorbed when the storage material/substance changes phase, either from solid to liquid or liquid to gas. The stored heat is released as it changes back to its original phase and can be utilised later, during periods of energy/heat scarcity or for prolonging/extending energy/heat availability. The storage systems discussed in this report is such a system and is proposed to function within (or in conjunction with) a thermal/heat delivery (HVAC) system. A simple HVAC system would consist of a heat

source, a working, or heat transfer, fluid, duct or channel for fluid flow, a heat exchanger for exchanging heat with space, or if air in direct injection into space, a distributor or diffuser, and a heat storage device. When joined or linked together, these components constitute a plant network. ESP-r plant database contains several plant models that are suitable representations of each of the listed components.

The thermal storage battery model is a shell that contains phase change material and has several tubes or pipes running through it lengthwise which carry the heat transfer fluid. While the fabric integrated thermal storage slab is a rectangular block of PCM with tubes interspersed within at intervals running from top to bottom. Both systems are modelled as a shell-and-tube heat exchanger (see chapter 3 for detailed model description).

4.2.1 Component Deployment

Deployment of plant models into ESP-r implies writing an ESP-r specific or identifiable source code/algorithm for the models, adding same to the software's database and updating the software's plant database file to contain information/data about the plant model. It is necessary to also edit some plant specific code compilation, execution and subroutine call up code files within the software's database and archives.

Plant source codes/algorithms in ESP-r follow a particular pattern and can be divided into two parts or sections. One part serves as the plant's internal processor and is employed for solving internal equations and processing internal data, the outcome of which produces, or generates results that form parameters used for the other part. Examples of internal processes are discretisation, initialisation of variables, updating of state/phase, determination of thermal resistances/conductance, etc.

The second part of plant source code connects the plant to ESP-r and serves as the channel for retrieval of information/data that are required for building and processing of the plant's sub-matrix, and for other plant specific information/data that ESP-r uses for generating and

storing results for output and for representing the plant at the user interface. It also contains instructions for carrying out pre-simulation checks and for assigning information/data about plant component to appropriate variables/arrays. The plant component, in like manner, obtains information/data it requires for some of its internal processes, information like simulation time step, mass flow rate of working fluid, etc, from the programme.

Information exchange between the internal processor part of plant models source code and ESP-r. as well as the part that connects to it is accomplished through parameters/variables referred to as common variables. They are parameters that serve to unify data/information from the plant with those of the software. They are data stores (mostly array types) wherein data (variables) about all the components that make up a building model and associated plants (network), are stored in locations (array positions) that facilitate identification of each component. Each array size is determined by several factors that include number and type components that make up the building model (plants and zones), the component (plant or building) to be processed, number of plant connections, etc. The common variables identify all the variables/parameters that the machine uses for its analysis.

Some of the common variables are databases containing miscellaneous plant or zone data, while others are single variables that define or mark nodes for processing (iteration) or indicate position of plant withing a plant network, plant's node connection number(s), or properties of working fluids, like water temperature and flow rates. Some of the variables point directly to models (plant components), with one of their array elements identifying the plant component, while others point to nodes within or representing the plant, with an array element identifying the plant's node. A more detailed explanation of 'common' variables and description of some sample plant specific common variables is given in appendix A.

4.2.1.1 Coefficient Generator and Static

As discussed, plants' source codes are made up of two (2) parts, the internal processor and the part that connects to ESP-r. This second part of the plant source code/algorithm is again, made up of two separate subroutines, the coefficient generator and the 'static'. The 'static' subroutine serves as some sort of boundary definition programme, or code. It is initiated at the onset of simulation and checks parameter values chosen by user during building and plant network definition against the minimum and maximum values defined for each of the parameters in the plant component's data contained in the plant database file/archive. It also performs the task of checking that the plant's setup data conforms to rules set within the 'static' subroutine and checks for correctness in choice/specification of nodes connection numbers for the plant, the type of working fluid and the number of input variables from the plant. The subroutine contains the necessary common variable and plant model code specific local variables. It can either be written as a separate file or as one of the subroutines in the file containing the coefficient generator subroutine.

The coefficient generator subroutine, as the name implies, is the subroutine that generates/produces outputs from the plant component which serve as coefficients that are utilised for building and solving the plant's equation sub-matrix. It is the plant component's execution programme/code and contains its numerical model, the energy and mass balance equations. It also contains the necessary common variables and plant model code specific local variables.

Outputs from the coefficient generator are designated ***COUT(1)***, ***COUT(2)*** and ***COUT(3)*** and represent the self-coupling (or future time dependent) coefficients, the cross-coupling (future time independent) coefficient and present-time coefficient, respectively, of the matrix equations. This designation is the same for the different state variables, which have their own designations. Further explanation is given in section 4.2.2.3, under Model output.

In most cases, the coefficient generator subroutine contains the plant's internal processor, i.e., both written in one single programme or subroutine. This is the case with most of the plant components in ESP-r. Sometimes also, the coefficient generator is written as a separate programmes/subroutine, separate from the internal processor code subroutine, but it will have a command to call for the internal processor source code.

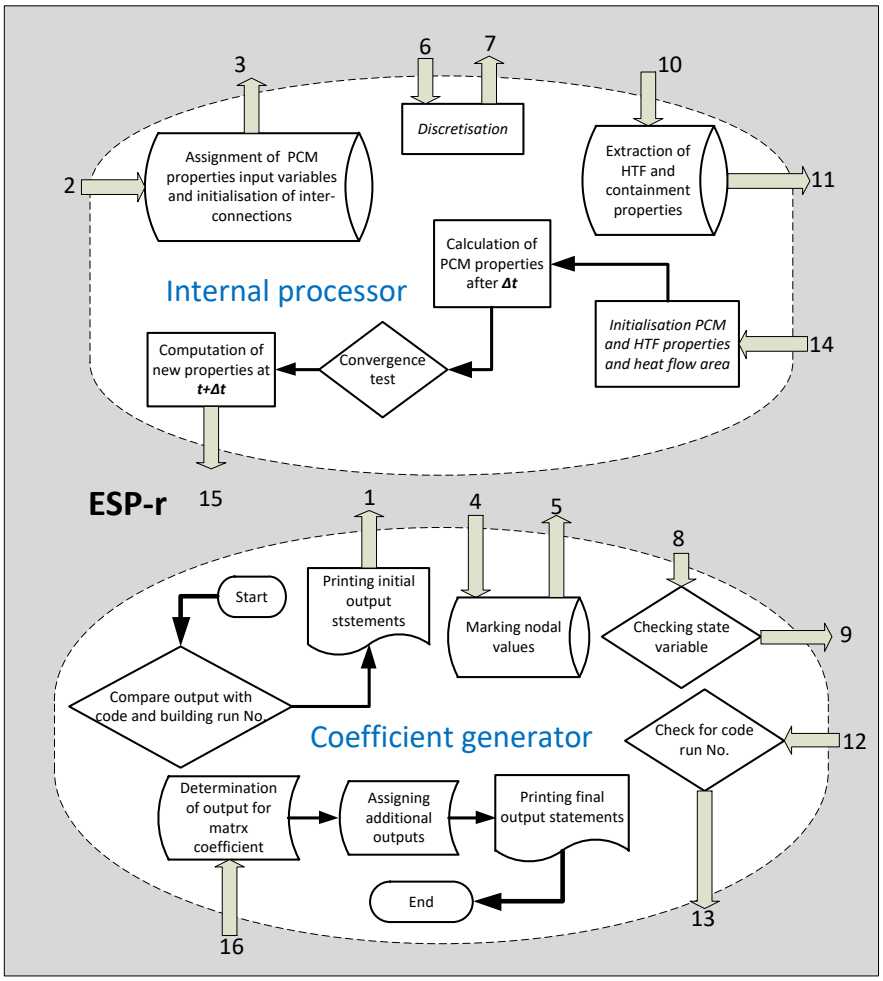

Figure 4.4: Depiction of PCM heat storage battery model's source code showing inter-relationship and information flow between internal processor and coefficient generator.

The coefficient generator subroutine for the PCM thermal stores and their internal processors are written in one (1) single programme or subroutine (each).

Figures 4.4 and 4.5 are depictions of both plant models' source codes, showing interaction and information exchange between the internal processor and the coefficient generator. The exchanges are indicated with numbers in the order they occur, number 1 being the first and

16 the last. All information input and output are from and to ESP-r through the common variables. The numbers in the figures indicate sequence of data/information flow (exchange). Execution of the models begins and ends within the coefficient generator.

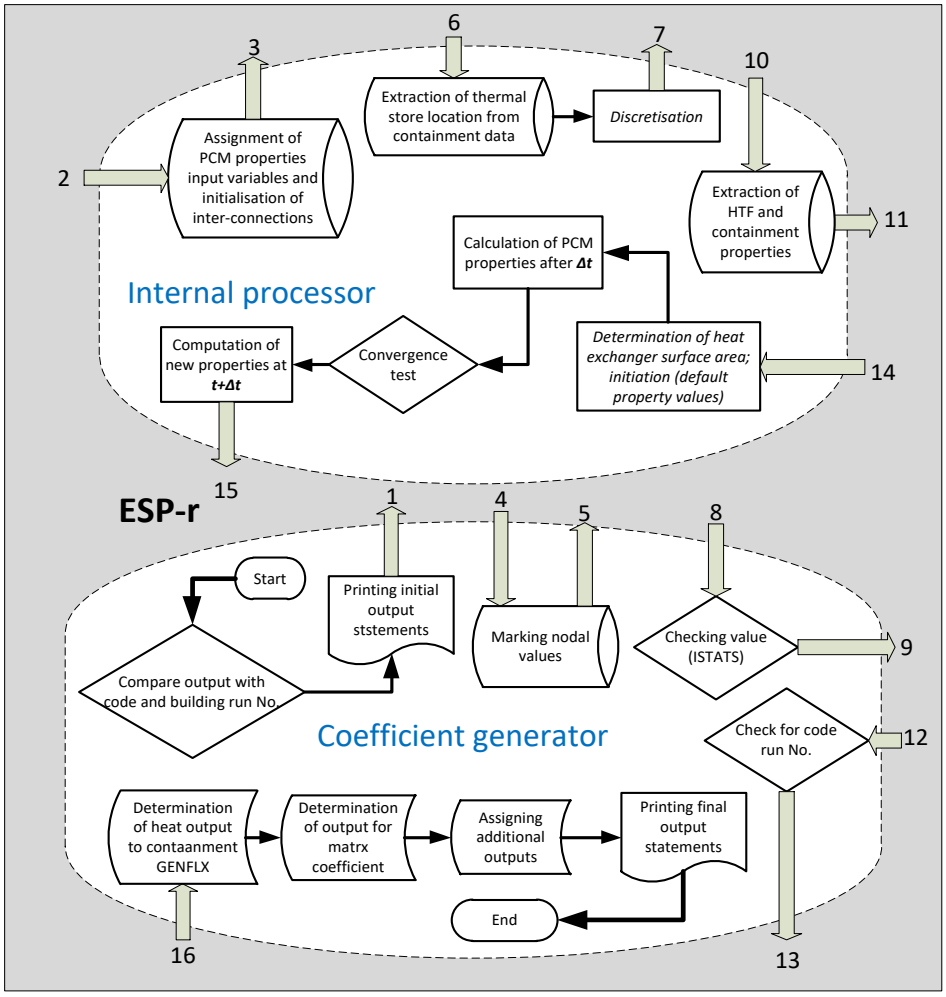

Figure 4.5: Depiction of active fabric integrated PCM thermal storage slab model's source code showing inter-relationship and information flow between internal processor and coefficient generator.

4.2.1.2 Plant Database File/Archive

As discussed, new plant component deployment requires updating ESP-r's plant database file to contain information/data about the plant model. The database contains information about all its plant components, information that are required for developing and processing plant sub-matrix, as well as execution of the plant's source codes and for representing them at the user interface.

Format and arrangement of data/information in the database follows a strict pattern that facilitates retrieval of data and information. This information includes the plant component's description, its nodal scheme description, number and data contents of thermo-physical properties and input variables/parameters for plant components, designated as ADATA and BDATA, number and content of conditional input variable, denoted CDATA, number of additional output items and variables from plant, and mass flow data for plant component. All the constituents of plant's data in ESP-r's plant database file/archive mentioned above are described in appendix B.

One other constituent of the plant data in ESP-r plant database is the plant database code. Every plant in ESP-r is assigned a plant database code which is a number that serves as the plant's address or identification tag. Assigning plant database codes is a way of indexing plant components in ESP-r, and the number identifies the plant component, enabling the programme to target it for processing during simulation.

4.2.1.3 Installation and Compilation Files

After registering information/data about the plants in plant database file, it is necessary to edit plant specific local compilation and execution script code/files within ESP-r, as well as the plant matrix set up and the components static set up code files.

The local installation and compilation script code/files facilitate building of object code files for plant components, and installation and compilation of the new plant models' source codes along with other existing plants models' source codes during the programme installation/compilation.

The plant matrix set up code is responsible for enabling the ESP-r to identify the new component(s) and process it/them during simulation and/or program execution. It is also responsible for calling up component coefficient generators and for determining appropriate

equation generators for all plant components. The component static set up code is responsible for calling up plant component 'static' code/subroutine.

After assigning plant database codes to each of the PCM thermal store models, their plant database data was developed. These were entered into the plant database file/archive. The relevant plant specific local compilation and execution script code/files were also edited to contain the plant models' source codes/algorithms file names, as were the plant matrix set up code file and the plant component static set up code file to include the plants' coefficient generator subroutine and 'static' subroutine names and arguments (respectively). Afterwards, the programme was re-compiled.

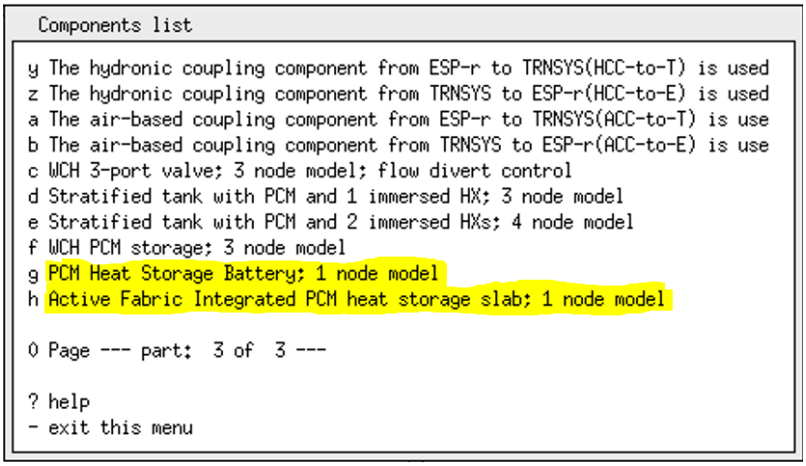

Figure 4.6: Snapshot of ESP-r plant component list

After compilation, the two (2) plant components are featured among other plant components and are listed in the 'Solar and Others' plant type/category. Figure 4.6 is snapshot of the third page of ESP-r's plant components list, from the network definition and component type page of the user interface. The highlighted items on the list are the PCM thermal storage systems. The heat storage battery is listed as 'PCM Heat Storage Battery: 1 node model' (item 'g') while the fabric integrated thermal storage slab is listed as 'Active Fabric Integrated PCM heat storage slab; 1 node model' (item 'h').

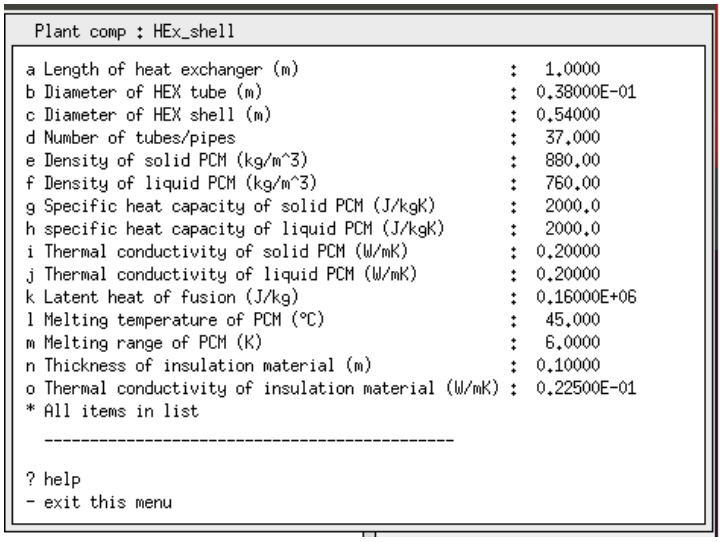

Figure 4.7: Display synopsis for PCM heat storage battery

Figures 4.7 and 4.8 are snapshots of plant display synopses for the heat storage battery (tagged Hex_shell) and the fabric integrated PCM thermal storage slab (tagged wall_hex_A), respectively, showing dimensional and thermo-physical properties of each component in a plant network.

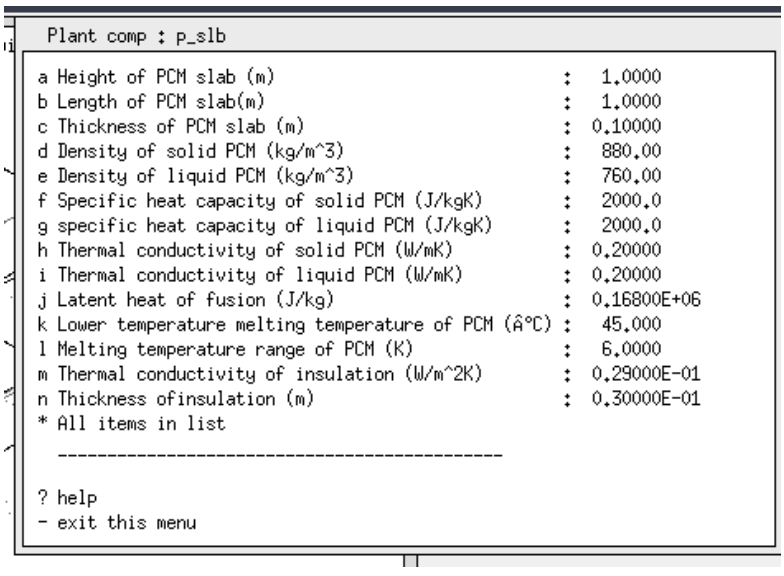

Figure 4.8: Display synopsis for PCM wall slab

The component codes allow user to select or indicate physical characteristics of the thermal stores and properties of the phase change material.

For the heat storage battery, the first three (3) items on the list represent dimensional characteristics of the battery. Modelled as a shell-and-tubes heat exchanger, 'Length of heat exchanger' indicates the length of the cylinder that is the shell containing phase change material; 'Diameter of Hex tubes' indicates diameter of the heat transfer flow tube(s)/channel; and 'Diameter of Hex shell' indicates diameter of the cylindrical shell.

The fourth item specifies the number of tubes in the shell. This number enable determination of the amount of PCM in shell. The fifth to the thirteenth item relate to properties of the phase change material. 'Density of solid PCM' and 'Density of liquid PCM' are self-explanatory as are 'Specific heat capacity of solid PCM' and 'Specific heat capacity of liquid PCM'; and 'Thermal conductivity of solid PCM' and 'Thermal conductivity of liquid PCM'. Latent heat of fusion refers to the energy absorbed when PCM changes phase from solid to liquid (or released when it changes phase from liquid to solid); Melting temperature is the lowest temperature at which the PCM begins to change phase and Melting range is the temperature interval over which the phase change occurs. The last two items represent properties of insulation material. Both are also self-explanatory.

Similarly, for the active fabric integrated thermal store, the first three (3) items on the list represent physical characteristics of the thermal store. 'Height of PCM slab' indicates height of the cuboid shaped PCM slab while 'Length of PCM slab' indicates length of the slab and 'Thickness of PCM slab' indicates thickness/depth of the slab. The next nine items relate to properties of the phase change material and are similar to the description given for the PCM heat storage battery. The last two items similarly represent properties of insulation material.

4.2.2 Component integration

The numerical models developed herein are thermal stores which employ phase change materials as heat storage media. Both models follow a similar pattern and method for sourcing input parameters from and generating outputs for ESP-r.

The source codes outline solution/determination of energy transformations experienced by both the heat transfer fluid and the phase change material upon excitation of its node by nodes to which they are connected, or linked, within a plant network during simulation and program execution.

Since the two models developed are similar in terms of their processes, types of equations processed and methods, and the general category of information/data obtained from ESP-r, the integration process is discussed in a generic manner for both models together. There are, nonetheless, some differences between them relating to some of the data extracted from the programme as inputs and how each interact with the system, with the fabric integrated thermal store generating an additional output that relate to its being fabric integrated. This is discussed subsequently.

4.2.2.1 Model Code Execution

Building (and plant) simulation processes in ESP-r begin with execution of the static code/program/subroutine. Functions of this code has been discussed in the section 4.2.1. It is necessary to execute the 'static' code first because the checks it performs determine whether associated plant codes execution can proceed using values selected by user during building model set up or not. After completion of the checks to satisfaction based on conditions and constraints for associated plant components, simulation proceeds with execution of the building and plant components' codes.

Execution of the thermal stores' code entails executing each component's coefficient generator to obtain state variable coefficients for the necessary sub-matrix equation. As explained in 4.1.1, only the first phase and second phase mass flow state variables are relevant to the PCM thermal stores. Nevertheless, the second phase mass flow state variable is accounted for in the source codes and assigned a self-coupling (future time dependent) coefficient of 1. The hydrogen flow state variable is irrelevant and excluded from the source codes.

The models' codes execution begins with checks and comparisons of number of outputs from code with number time it has been executed and number of times the building has been simulated. Results of the checks inform the plant source codes of what code specific property values to utilise for program initiation, whether initial default values or saved values from previous simulation/execution. This is followed by assigning of parameters specified by used for thermo-physical properties of the plant and parameters representing the plant component's node, extracted from ESP-r's common variable block to relevant variables. These serve as input parameters for the source code/algorithm.

After determination of the input parameters, the code proceeds to divide the PCM block into grids employing equations 3.23 and 3.24 (radial discretisation for the heat storage battery) after determining size of grid. Grid size determination is based on findings of the sensitivity analysis (tests and results discussed in chapter 5) and is written into the source codes. Axial discretisation and size of radial cells, and discretisation of the fabric integrated heat store, is accomplished by dividing heat exchanger length, depth of annulus, breadth and height, by the respective grid size determination factors.

A second check is done to ascertain which sub-matrix equation is being solved at the main plant matrix level and informs the source code which state variable coefficients to generate

for output or mark for processing during execution. Determination of the appropriate state variables has been discussed as being dependent on the type of state equations employed for determining property changes of the plant component, which for the present models, are energy and first phase mass flow. Therefore, the coefficient generator is written to process energy and mass balance equations and generate state variable coefficients for temperature and mass flow.

Upon determining the state variable coefficients to be generated, the code proceeds with extraction of information about the component's environment, its containment, and data relating to the type of fluid to which its node is connected – temperature and mass flow rate, and the percentage of fluid flowing into component from the programme via the common variables. Included in the data extracted from the programme are the implicit/explicit weighing factor for iteration time step updating and the simulation time step/interval. This is followed by a third check for the number of times the code has been executed before the current process.

Afterwards, all PCM properties are initialised. This initialisation is governed by result of the check for number of times code has been execution and determines whether to utilise saved values of PCM properties (from previous executions) or set all to default initial values. Default initial values assume PCM is in solid phase and at temperature of surrounding.

This is followed by determination of heat exchange surface areas for each cell using equations 3.21 and 3.22 and 3.25 for the thermal storage battery and equations 3.64 to 3.66 for the fabric integrated thermal store, then the heat transfer coefficient of the heat transfer fluid and thermal resistances/conductance for the PCM block are determined. The processes described above are depicted in Figure 4.9.

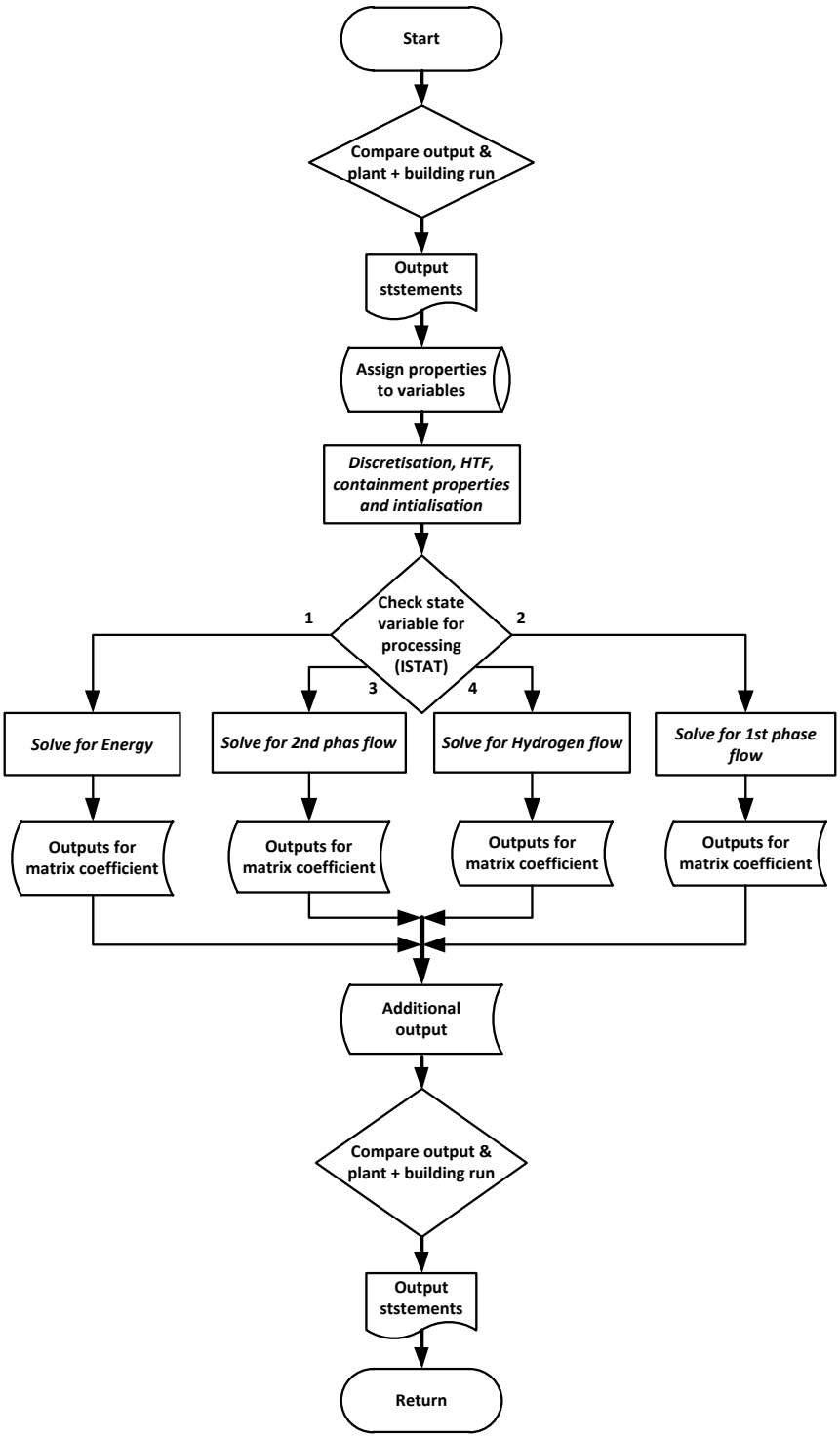

Figure 4.9: Generic plant code execution flow chart excluding solution of energy equation.

4.2.2.2 The Iterative Solution

All the parameters, PCM and HTF properties, condition of plant environment as well as variables and parameters determined above form the inputs and governing parameters/factors for the iterative process. This is the process of repeatedly processing the energy equation to

solve for future time variables, PCM temperatures, phase, liquid fraction, thermal conductance (or resistance) and energy level (enthalpy), given the initial values until a convergence criterion is satisfied (details in chapters 3 and 5).

The iterative process entails solving equations 3.24 to 3.29 and 3.59 to 3.65, which represents energy (and associated properties) change (and transformations) for the heat transfer fluid and PCM using the parameters obtained in the previous processes. These parameters serve as initial, or present time values/parameters (at tine ***t***) for the iteration.

As stated in the chapter 3, the Gauss-Seidel iterative scheme was employed for iterating the numerical solution and determining properties of the system at expiration of simulation (or code execution) time step/interval, denoted in codes as ***Δt***. The time step interval is an ESP-r specified parameter, one of the parameters obtained via the common variable block/data (see appendix A).

The iterative process begins by establishing a convergence criterion that compares difference between initial temperature, at time ***t***, of the PCM and its new temperature, after time (***t + Δt),*** to10^{-7} (Hosseini, Rahimi, & Bahrampoury, 2014) and setting up a solution loop that stops upon its satisfaction. The energy equations representing energy, and heat flow, are solved for each PCM cell at end of iteration time interval, ***Δt***, after which new set of thermo-physical properties are determined for the PCM. Convergence test is carried out at the end of the processes, which are either repeated, if criterion is not satisfied, or stopped (the loop ends) so that the algorithm proceeds to the next steps if convergence criterion is satisfied. Figure 4.10 is a diagrammatic representation of the model's solution process starting from after determination of which state variable to be calculated or is being processed. In the diagram, the state variable determined is assumed to be energy, that is ISTATS is equal to 1 (see Figure 4.9).

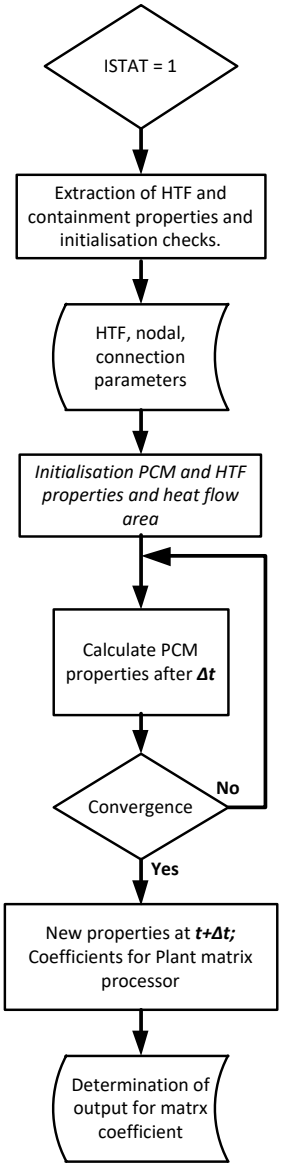

Figure 4.10: Model code execution flow chart after determining for which state variable to calculate value of ISTATS.

4.2.2.3 Model Output

Upon convergence, the code proceeds to determine new thermal properties for the PCM, which represent properties after elapsed time, ($t + \Delta t$), These new properties are utilised to generate outputs from the models. As discussed earlier, the state variable to be processed by the plant matrix processor is determined from the state variable checks and informs the choice of state variable for which solutions are obtained during source code execution. This in turn, informs the choice of output state variables.

The state variables output from the plant models' source codes are employed for building each plant model's sub-matrix equation sets and for inclusion in the overall plant network matrix equation. They (outputs) are designated ***COUT(1)***, ***COUT(2)*** and ***COUT(3)***. As explained earlier, they represent the self-coupling (or future time dependent) coefficients, the cross-coupling (future time independent) coefficient and present-time coefficient, respectively, of the matrix equations. The designations are the same regardless of which state variables are requested by the matrix processor.

The models also generate outputs relating to the amount of heat absorbed and released by the phase change materials from and into the heat transfer fluid. These are outputted into the system's plant results database as additional outputs via common variables.

4.2.2.4 The thermal storage Battery

The thermal storage battery model, as discussed in chapter 3, is modelled as a shell-and-tubes heat exchanger, with the PCM contained in the shell serving as the second heat transfer fluid. The model design is not rigid and could take up any shape or characteristics desired with a few adjustments to some of the equation sets and expressions. The shell in this case was modelled as cylinder using radial symmetry and discretisation. Therefore, adjustments would be necessary for conformity to the chosen shape or configuration.

The source code is written in a way that information about characteristic dimensions is specified by user during model set up. They are, in this design, for a cylindrical shell and tubes heat exchanger. List of these information is given in figure 4.7 and described in section 4.2.1.3. The plant model requires to be contained and can be contained within a zone.

4.2.2.5 The Fabric Integrated Thermal Store

The fabric integrated thermal storage slab was modelled as a rectangular block of PCM with water tubes interspersed at intervals within it (details in chapter 3). It is designed to be

inserted into the building fabrics, within walls, floors or ceilings in specified zones of the building model, which informs the type of containment (that is environment) the user can select or chose during model set up. One of the checks performed by the static code/subroutine ensures that the thermal store is placed in a solid structure/material.

The information about characteristic dimensions, specified by user during model set up, are those of a rectangular block and only the length and breadth can be specified. The list of parameters is depicted in Figure 4.8 with description in section 4.1.2.3. The size of the thermal storage slab cannot, however, exceed the dimensions of the surface, or material wherein it is contained. Thickness of the slab is specified within the code as dependent on the containment material's thickness and although it is insulated, properties of the insulation material has been written into the codes as with the thickness. So, component data displayed for editing at program interface does not include insulation material properties.

Temperature data about the thermal store's surrounding, utilised for the simulation, are those of the containment material. These values are utilised for code/program initiation regardless of the results of checks conducted at onset of code execution (section 4.2.2.1). The output parameters are similar to the ones discussed in section 4.2.2.3.

4.3 Summary

The deployment and integration of the thermal store models into ESP-r has been discussed. Some explanation and description of the plant matrix processor was done, highlighting the process for developing sub-matrix and overall matrix equation sets for a plant network within ESP-r. The procedure for deploying new plant models into the programme was also enumerated, followed by details of the plant models' source code's integration and execution during system processing/simulation.

The chapter concludes with a brief discussion of differences between the two (2) models with regards to structural characteristics, and communication with ESP-r about input and output variables and parameters.

The proceeding chapter will focus on discussing the procedures and results of validation and other verification processes carried out for the models.

Chapter 5

MODEL VERIFICATION AND VALIDATION, AND SENSITIVITY ANALYSIS

5.0 Introduction

This chapter discusses methods, procedures and results of determination of validity, functionality and sensitivity tests of the source codes employed for the model. Validation was carried out by comparing results from running simulations of the model with results reported in publications while it was verified by comparing results from manual computation/calculation from model equations with results from running model with the ESP-r simulation machine. Its sensitivity to changes in values of some parameters (constant) utilised in writing the source code, like grid size and convergence criteria, was carried out by altering their values and assessing impact on model performance and output.

5.1 Verification and Validation of Numerical Model

Validation and verification are integral parts of model development processes as they are means by which concerns about accuracy of the results the model produces are addressed. According to Sergent (2013), model verification implies "ensuring that the computer program of the…model and its implementation are correct" while model validation is the "substantiation that a model, within its domain of applicability, possesses a satisfactory range of accuracy consistent with [its] intended application" (Sergent, 2013). Department of

Defence (1998) (in Cook & Skinner (2005)) also define validation as "the process of determining the degree to which a model or simulation is an accurate representation of the real world from the perspective of [their] intended use, and verification as the "process of determining that a model or simulation implementation accurately represents the developer's conceptual description and specification". Thus, a model is valid if it can be established that it is accurate within the 'acceptable range of accuracy' that is required for its intended purpose (Sergent R. G., 2013) and verified if it is established that it 'has been developed using sound and established software engineering techniques' (Cook & Skinner, 2005).

Validation and verification are important to numerical models because they are representations of actual systems and processes, and are developed using equations and expressions that predict, in most cases, ideal and perfect situations and conditions that may not exist in nature, or that change and vary at rates hard or impossible to predict. In the context of model development, the concept can be divided into four processes or stages, conceptual model validation, computerized model verification, operational validation and data validity.

5.1.1 Model Verification and Validation Processes/Stages

Conceptual model validation involves establishing that the theories and assumptions that form the basis for a model are correct and the model reasonably represents the problem entity for the intended purpose (Sergent, 2009).

Verification of the computerized model entails assuring that the conceptual model is correctly programmed by a computer and properly implemented.

Operational validation determines that outputs from the model falls within a satisfactory range of accuracy acceptable for its intended purpose.

Data validity implies ensuring adequacy and correctness of all data required for developing, evaluating, assessing, and experimenting with, or on, the model.

5.2 Model Verification Methods

Model verification entails determining correctness and accuracy of the computer program and its implementations. Basically, testing to ensure that the model does what it is designed to do, for example, determine changes in temperatures and enthalpies of a substance as it absorbs or releases energy. Therefore, verification implies testing to certify that the underlying theories, equations and assumptions are accurate to within acceptable limits and that the algorithm (computer program) is properly written and structured.

This can be done by applying one of two approaches, or methods, static or dynamic testing (Fairley (1976) in Sargent (2014). Static testing involves empirical assessment and analysis of the computer program by structured walkthroughs, correctness proofs, and program structure and properties examination (Sergent, 2009) while dynamic testing entails executing the computer program under various conditions to determine whether the computer program and its implementations are correct (Sergent R. G., 2013).

Dynamic testing employs several methods/approaches, some of which are beyond the scope of this work or not intended for the type of model developed. The methods/approaches that are applicable here are discussed below.

Debugging – Test conducted on models' codes/algorithms to check for the presence of bugs. It involves writing, or including, command lines/statements in the models' codes instructing print out or production of outputs for some of the parameters/variables computed during execution of the codes at certain points within the algorithm, or stages during execution, other than the final output. These statements have no role/function in the code other than to check

its behaviour. The outputs can later be examined for correctness and accuracy, to within expected limits.

Tracing – Similar to debugging, in that it is also used to check for bugs in models' codes. It requires the use of tracing and debugging tools, programs, that through increased visibility, analysis, and testing, analyses code/programs for presence of bugs. Examples of these are forcheck, gdb debugger, TotalView for HPC, Froglogic Squish, Sentry, etc. Most are available for a price while only a handful are free. Forcheck and the gdb debugger were employed for analysing the present models' source codes.

Consistency Testing – Involves running simulation of the code being tested to check whether results produced by the model for a set of input parameters are similar to results produced for another set of input parameters whose effect on the system are similar to the former. Although a negative outcome from this test does not always suggest modelling errors, they provide opportunities for either better understanding of the model, if the outcome can be explained, or the need for further investigation and analysis.

5.3 Model Verification Tests and Results

Both static and dynamic verification tests were carried out for the models' codes. While results of every verification test cannot be feasibly reported in this writeup, like results of the static tests and some of the dynamic tests, the ones that can be reported are discussed below. All errors identified during initial static tests, debugging and tracing tests were corrected and the models were tested again and verified by re-running simulations. Subsequently it can be reported that the codes and their implementation are correct and accurate for the intended purpose. The reports below refer to dynamic tests.

5.3.1 Consistency test

Consistency test for the models was done by running one of the codes under null conditions. This entails equalising all the temperatures values for the PCM cells, surrounding and HTF inlet so that both external (input) and internal (initial) conditions are equal and there is no heat input or withdrawal from the PCM during simulation. The results of PCM temperatures and HTF outlet temperatures are plotted against simulation time. Two (2) tests were conducted, one (1) for a temperature below phase change temperature (PCM solid) and the other for a temperature above the phase change temperature (PCM liquid). Properties of the PCM were set in accordance with its phase during each test.

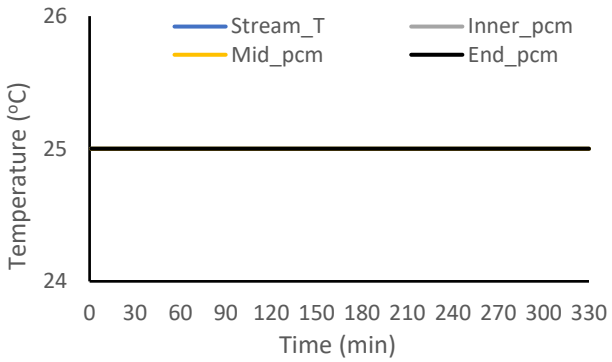

Figure 5.1: Temperature profiles for null test - T = 25°C

Figures 5.1 and 5.2 are plots of simulation results from the models for temperatures 25°C (PCM is solid) and 75°C (PCM is liquid), respectively. The profiles show average heat transfer fluid stream temperature (stream_T) and temperatures of the PCM block divided into three (3) sections designated Inner_pcm, Mid_pcm and End_pcm, representing PCM innermost section (closest to heat transfer fluid), middle section and section farthest from the heat transfer fluid respectively. As can be seen from the figures, all temperature values remain relatively unchanged throughout the test.

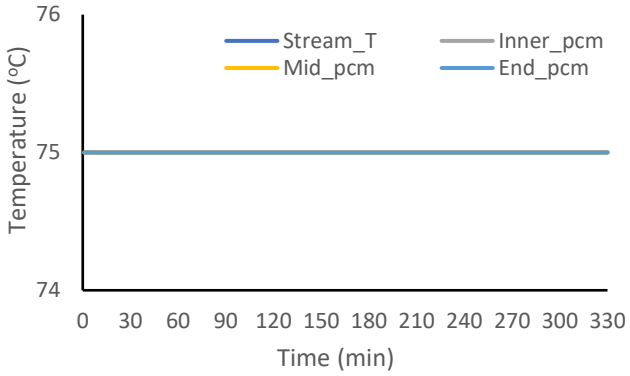

Figure 5.2: Temperature profiles for null test 2 - T = 75°C

Another consistency test was done by running the models with different types of PCM and under charging and discharging conditions. Water was used as heat transfer fluid circulated at mass flow rate was 0.0167 kg/m^3. Total simulation time was 350 min with charging during the first 170 minutes and discharging during the remaining 180 minutes. Table 5.1 contains properties of the phase change materials and heat transfer fluid used for the tests. The two (2) PCM used were paraffin wax and paraffin_53 whose properties were obtained from Himran, Suwono, & Mansoori (1994) and Inaba & Tu (1997) respectively. Each was charged by setting HTF inlet temperature to a temperature 27K above its higher phase change temperature and discharged by setting HTF inlet temperature to a temperature 28K below the lower phase change temperature while maintaining surrounding temperatures at the discharge temperature.

Table 5.1: Properties of PCMs and HTF used for consistency tests.

	Properties		
	Parffin_53	Paraffin wax	HTF
Melting temp (°C)	53	43-56	-
Specific Latent heat of fusion(J/kg)	164000	266000	-
Specific heat capacity (sol) (J/kgK)	2130	2950	-
Specific heat capacity (liq) (J/kgK)	2620	2510	4187
Thermal conductivity (sol) (W/mK)	0.28	0.24	-
Thermal conductivity (liq) (W/mK)	0.19	0.24	0.58
Density - Sol (kg/m3)	978	818	-
Density - Liq (kg/m3)	795	760	1000

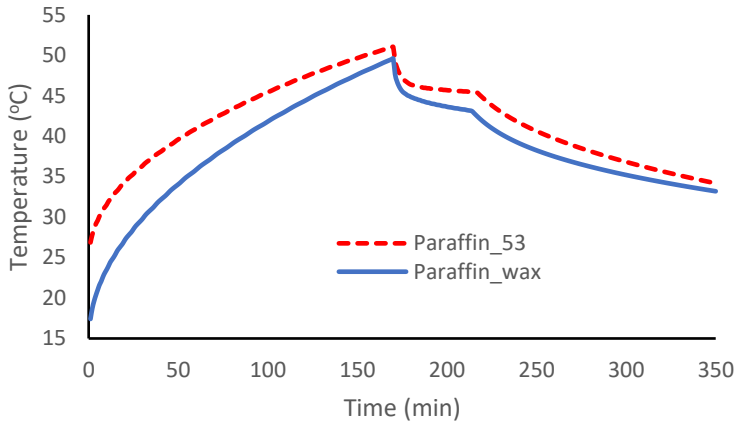

Figure 5.3: PCM temperature profiles – consistency test results

Figure 5.3 is the plot of PCM temperature plotted against time. Both plots show similar profiles. This is despite the differences between the PCM properties, one of which changes phase at a single temperature. The implication being that the results produced by the model for both set of input parameters (PCM properties and charging and discharging temperatures) are similar, showing consistency of the model.

5.3.2 Dynamic Test – ESP-r vs Computational Analysis

A further dynamic test was done by implementing the models in the ESP-r building energy simulation system, being the system for which they are designed, and running simulations of building models with the thermal stores in the plant networks and comparing simulation result with results from executing model codes outside of the software.

The building model employed for ESP-r simulation testing was a training model of two rooms linked by a corridor called ‘cellular_hires’ (Figure 5.4), obtained from the software’s database. It was developed with a plant network containing an air source heat pump, two (2) domestic hot water radiators and the PCM Thermal storage battery.

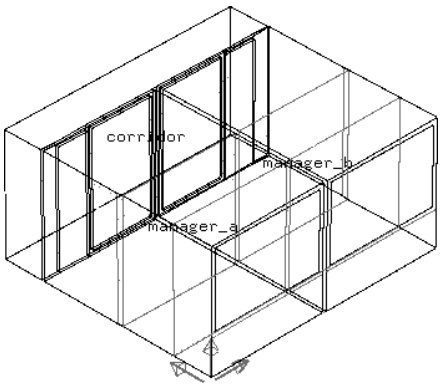

Figure 5.4: ESP-r test building model – 'cellular_hires' (ESP-r database)

Plant control strategy for the air source heat pump to operate freely was applied and simulation was run over a one-day period. The free running/operation setting for the heat pump was adopted to obtain a series of heat input into network over various periods of the day as the pump switches on and off, and to observe and assess charging and discharging of the PCM thermal store.

Since interaction of the models with ESP-r is via heat transfer fluid (models produce coefficients utilised by the engine to determine temperature of models' water node), results of PCM thermal store's nodal temperature (that is water stream temperature at thermal store node) extracted from the simulation results were compared with HTF stream temperature determined computationally from model energy equations and correlations. Computational determination was done by developing a computer algorithm for processing the energy equations and generating outputs of the heat transfer fluid temperatures and executing using the same water (HTF) inlet temperatures, mass flow rate and simulation time interval utilised for simulating the building model in ESP-r.

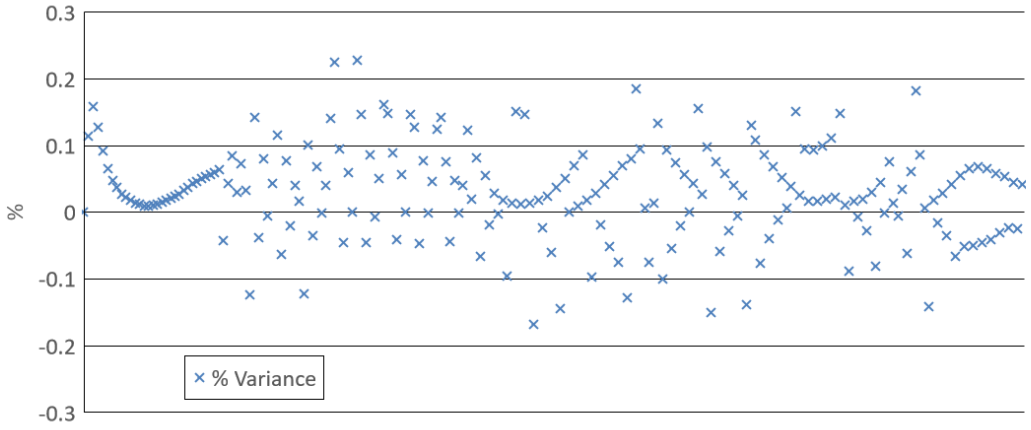

Figure 5.5: Percentage variance of HTF stream temperatures determined computationally from water node temperatures obtained from ESP-r simulation

Figure 5.5 is a plot of percentage variance of HTF stream temperature determined computationally and water node temperature obtained from ESP-r simulation of building model containing thermal store. It is an indication of how much computationally determined HTF stream temperatures varies from thermal store water node temperatures obtained from ESP-r simulation results. A percentage variance of zero indicates that the temperature values are equal, positive values indicate that computationally determined temperatures are higher than those from ESP-r while negative values indicate the reverse.

As shown in the diagram, percentage variance values are greater than zero at beginning of simulation and for a length of time afterwards indicating that HTF temperatures obtained from computational results were higher than those obtained from ESP-r simulation. It is unclear why this is the case. The figure also shows distribution of the percentage variance above and below the zero line, with more above the line, for the rest of the simulation/testing period. Maximum percentage variance was 0. 269% while the minimum percentage variance was -0.175%. This result is consistent with expectations because simulation in the software (ESP-r) involves processing of many other components' codes, the building, its zones, components and associated plants alongside the thermal store model in contrast to the

computational analysis involving an isolated and individual code. Closeness of the temperature plots/result, as shown by the very small percentage variance, indicates close agreement between the results and sufficiently demonstrates and verifies accuracy of the formulae and equations employed for the models.

5.4 Model Validation

As mentioned earlier, model validation implies testing to ascertain that a model is, within its domain of applicability, accurate in its representation of actual systems. There are several methods or techniques employed for validating numerical models, some of which are not applicable for present models type or require data that could not be accessed. One that is applicable and feasible is comparison with/to other validated model(s). This method entails comparing various results of the model to results of other (similar) numerical or analytical models, or physical models/systems that have been previously validated. This technique is applied for validating the PCM thermal stores and discussed below.

5.4.1 Validation Test and Results

Results from running simulation of the numerical codes for the shell-and-tube PCM heat store was compared with results reported by Hosseini et al. (2012), Hosseini, Rahimi, & Bahrampoury (2014) and Seddegh, Wang, & Henderson (2016) for a double pipe heat exchanger containing PCM in the annulus. The shell-and-tube PCM heat store was developed with the same thermo-physical properties for both the PCM and heat transfer fluid, heat transfer fluid flow properties and physical characteristics of the heat exchanger as those reported in the reference materials. The analysis was also carried out within the same time frame, following the order and timing for charging and discharging of the systems.

5.4.1.1 Reference Systems and Material Description

Hosseini et al. (2012) and Hosseini, Rahimi, & Bahrampoury (2014) reported on development and testing/analysis of both numerical and experimental models of a double pipe heat exchanger with PCM in the annulus. The physical model is a 1m long horizontal cylinder, the shell, which contains the PCM, with inner and outer diameters 85 mm and 87.5 mm, respectively. It has an inner copper tube, 22 mm in diameter, through which water flows to exchange heat with the PCM. The central copper tube is connected at different times during the experimentation to two water flow loops, hot water flow loop for charging and cold water flow loop for discharging. The entire system was insulated with 60 mm thick glass wool and RT50 paraffin was the PCM employed for the study. Properties of RT50 and heat transfer fluid, water, are listed in table 5.2.

Table 5.1: Properties of PCM and HTF obtained from Hosseini et al (2014)

	Properties	
	PCM	HTF
Melting temp (^oC)	45-51	-
Specific Latent heat of fusion(J/kg)	168000	-
Specific heat capacity (sol)(J/kgK)	2000	-
Specific heat capacity (J/kgK)	2000	4187
Thermal conductivity (sol)(W/mK)	0.2	-
Thermal conductivity (liq) (W/mK)	0.2	0.58
Density - Sol (kg/m3)	780	-
Density - Liq (kg/m3)	780	1000

They charged the system by connecting to the hot water flow loop maintained at 70 °C and flowing at 0.0167 kg/s for 150 min and discharged by switching to the cold water flow loop, which was maintained at 25 °C, flowing at same flow rate for 180 min. They repeated the experiment for HTF inlet temperatures of 75 °C and 80 °C, at same flow rate and lengths of time, and at the same discharge temperature, flow rate and elapsed time. Surrounding temperatures were maintained at the cold water loop temperature of 25°C.

The numerical model they reported was set up with similar dimensions, employing the same PCM and simulated under the same HTF charging and discharging conditions as the experimental model for comparison. They also conducted charging only and discharging only tests and for both experimental and numerical models by charging the PCM for 150 minutes with inlet water temperatures 70, 75 and 80 °C and discharging for 180 minutes from initial temperatures of 70, 75 and 80 °C, and did comparisons of PCM temperature profiles from both tests.

The models reported by Seddegh, Wang, & Henderson (2016) are similar to that described above with the same physical dimensions and they used the same phase change material, RT50, and heat transfer fluid, water, for their assessments. They also circulated the heat transfer fluid at the same flow rate of 0.0167 kg/s. They, however, charged their system by circulating hot water at constant temperature of 85°C through the inner tube for 330 min while maintaining surrounding temperature at 20°C. Their numerical model was similarly set up with the same dimensions and physical characteristics as their experimental model, and they used the same PCM and ran simulations under the same HTF conditions.

5.4.1.2 Result Discussion – Comparison with Results Reported by Hosseini et al, 2012 and Hosseini, Rahimi, & Bahrampoury (2014)

The shell-and-tubes PCM thermal store model was set up with same dimensional properties/characteristics as the experimental model in both reference materials. Applying the same PCM properties, simulations were also run under the same conditions and HTF flow properties as reported in each report. Effective PCM temperature was plotted against time for continuous PCM charging and discharging test and charging and discharging only tests. Results were afterwards compared with plots of numerical and experimental tests reported by the authors.

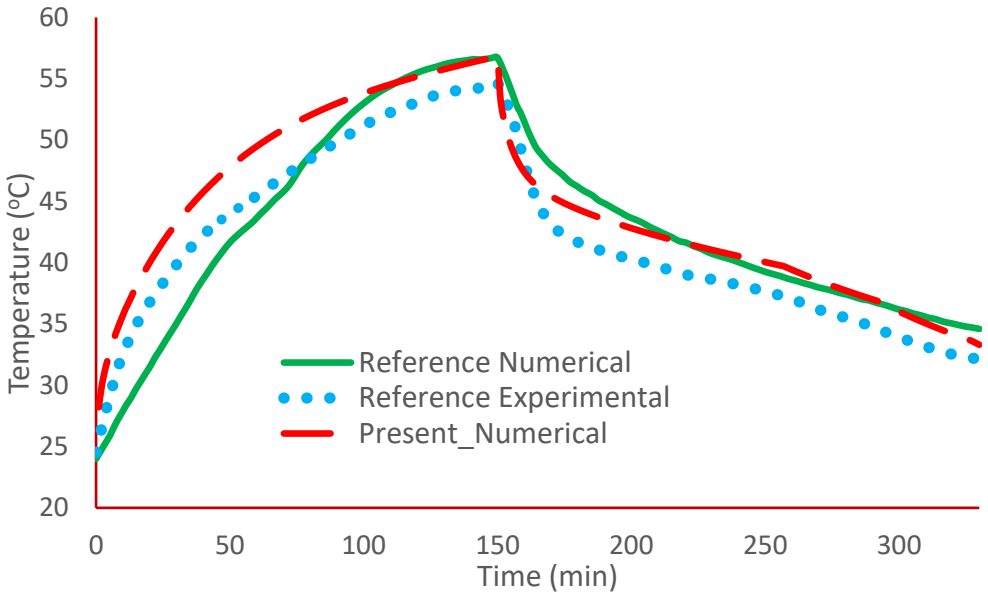

Figure 5.6: Average PCM temperature for present model compared with results from Hosseini et al. (2012) and Hosseini, Rahimi, & Bahrampoury (2014)

Figure 5.6 to 5.8 are plots of average PCM temperatures plotted against time from results of present study for the continuous charging and discharging tests, and the charging only and discharging only tests alongside similar plots of temperature profiles for continuous charging and discharging, experimental and numerical analysis, and the charging only and discharging only tests, numerical, reported by Hosseini et al. 2012 and Hosseini, Rahimi, & Bahrampoury (2014).

Figure 5.6 (continuous charging and discharging tests) shows close resemblance and agreement between temperature profiles of present study and reference material. The three temperature profiles have similar pattern and layout. Profile for present study (model) show a closer resemblance to temperature profiles of experimental model from reference material during the early part of the discharging process. The graphs are reflective of the temperature profile of a phase change material that is heated from a temperature below its phase change

temperature to one well above it and that is releasing heat when cooled from a temperature above its phase change temperature to one below it.

The few differences between plots of present study and those of reference material can be attributed to the different assumptions made in formulating and developing the numerical models (these have already been discussed in chapter 3). Also, according to the authors, "overall average temperature [for the experimental test] … is calculated using sixteen thermocouples" positioned at various locations within the PCM block. They gave no indication as to the method adopted for determining same for the numerical test. Average temperatures for the present study were obtained by summing up all cell temperatures and averaging over the entire block.

It is obvious from Figure 5.6 that neither present study nor reference numerical study has 100% agreement with experimental results (from reference). Differences between results of the present numerical study (and those of reference numerical), though small and within acceptable limits, are attributable to several factors. These include instrumental and random errors, measurement and human errors, in relation to experiments, and a combination of factors like mesh/grid size, convergence process and model assumptions that have impact on results from numerical model. While concerted efforts were made to tailor present numerical models along those of the reference material, not enough information was provided with regards to the experimental model to inform assumptions for the modelling.

For the charging only tests reported by Hosseini et al. (2012) and Hosseini, Rahimi, & Bahrampoury (2014), heat transfer fluid inlet temperature was set to charging temperatures 70 °C and repeated for 75 and 80 °C HTF inlet temperatures, with initial PCM temperature of 25 °C and simulations were run for the model for 150 min charging time. Discharging tests was done by setting heat HTF inlet temperature to 25 °C while PCM initial temperature was

set to 70 °C and repeated for 75 and 80 °C and simulated for 180 min discharge time. HTF mass flow rate for both tests was 0.0167 kg/s.

The average PCM temperatures from results of the tests were plotted against time and compared with similar plots from reference material. They are show in figures 5.7 and 5.8.

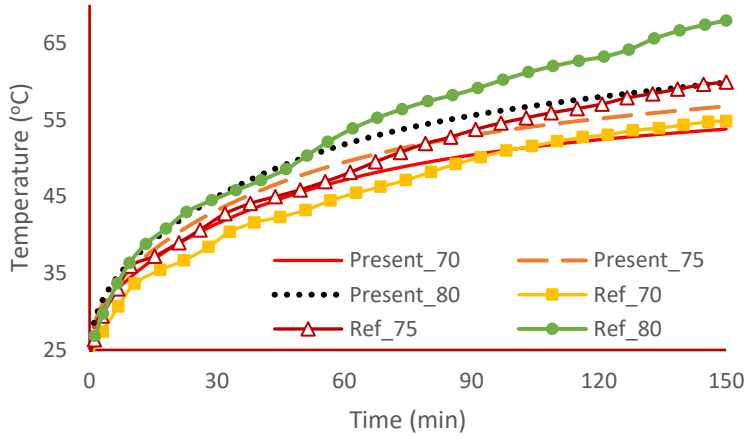

Figure 5.7: Comparison of reference (Hosseini et al., 2012; Hosseini, Rahimi, & Bahrampoury, 2014) and present model PCM temperature profile - charging only

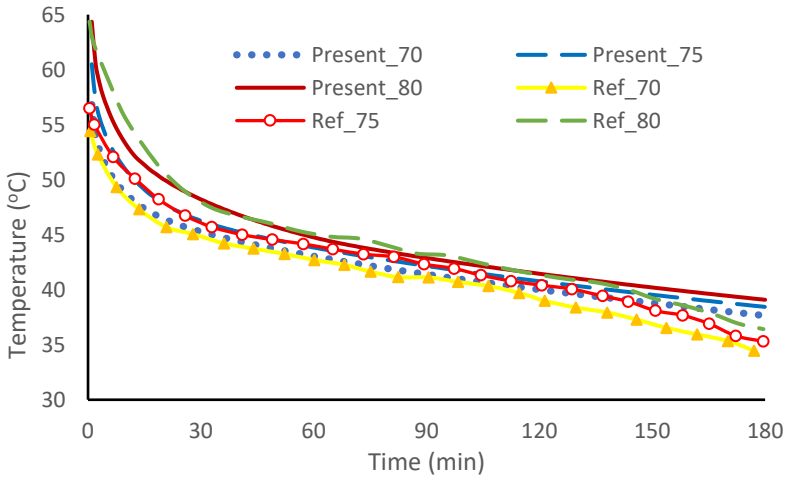

Figure 5.8: Comparison of reference (Hosseini et al., 2012; Hosseini, Rahimi, & Bahrampoury, 2014) and present model PCM temperature profile - discharging only.

The figures show closeness between plots of present study and those of reference material, indicating close agreement between the results and models.

5.4.1.3 Result Discussion – Comparison with Results Reported by Seddegh et al., (2016)

Charging tests reported by Seddegh et al., (2016) was duplicated in present model by setting heat transfer fluid inlet temperature and mass flow rate to 85 °C and 0.0167 kg/s,

respectively, initial PCM temperature to 20 °C and running simulations for 330 min (charging time). Average PCM temperatures from results were similarly plotted against time and compared with similar plots from reference material and show in figures 5.9.

As shown in the figure, the plot of temperature profile from results of present study has similar profile as those from the reference material, showing an almost perfect alignment at the second half of the process. This is an indication of close agreement between the results and models.

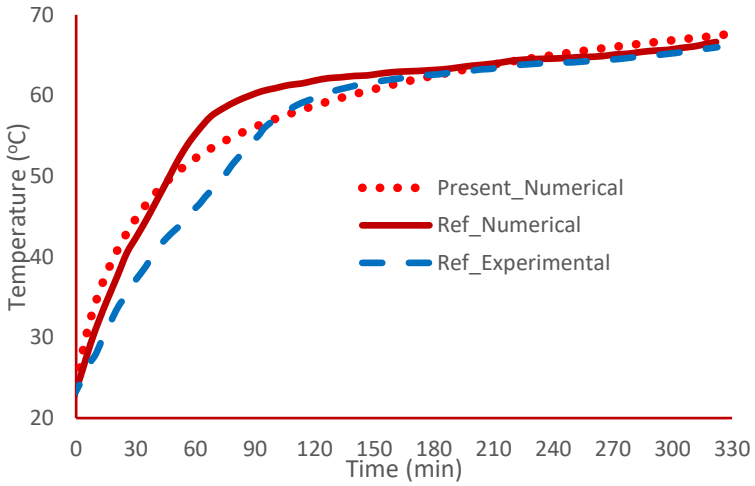

Figure 5.9: Comparison of reference (Seddegh et al., 2016) and present model PCM temperature profile - charging only.

Agreement between present numerical, as well as results of reference numerical study, and reference experimental results, as shown in Figure 5.9, is equally less than 100%. Design of the numerical model for testing was based on information provided by the authors and they were followed with adherence.

5.5 Sensitivity Analysis

Sensitivity analysis is a means by which effect of different values of an independent variable on a dependent variable can be assessed under specific set of assumptions. Another way to

put it would be to say that sensitivity analyses study how various sources of uncertainty in a mathematical model contribute to the model's overall uncertainty (Investopedia, 2020). It is an important tool in model building and result communication as it gives essential insights into the model's behaviour, its structure and response to changes in inputs (Borgonovo & Plischke, 2016; Confalonieri et al., 2010), thereby providing information regarding its stability, robustness and performance. Sensitivity analysis is employed to quantify the importance of each of the model's parameters (inputs) on system.

Since all inputs for the present models represent structural and thermo-physical properties of the system, there is an expectation that changes in their values should produce changes in system output, or performance. There are, however, other parameters that also exert some influence on the result outputs and system performance but not in the same way as the properties. Their influence (if any) would be indirect, relating to the simulation process, and running and execution of the models' codes, and in turn, accuracy of result outputs. Such parameters include simulation time, time step, number of iteration steps (or loops), discrete cell (or grid) size and iteration convergence criterion. These are typically constants and have fixed values at beginning of simulations.

Appropriate choices of these parameters are necessary for obtaining accurate results within a reasonable computational time frame (Boettinger & Banerjee, 2015). In order to understand what influence these parameters may have on system performance and form a basis for the choice and determination of their values, and to test robustness and stability of the source codes and algorithms, sensitivity analyses were carried out for the models against variations, or alterations in the values and magnitude of some of these parameters. This was accomplished by running series of simulations of the models while altering the values of the parameters and comparing results of heat transfer fluid stream temperatures and time taken for each code/program to execute.

As described and explained in chapters 3 and 4, the model codes are made up of two parts. One part, the main code, simulates the entire PCM heat storage system and links the model to the ESP-r platform while the second part, a sub-code withing the main code, simulates PCM melting process and response to heat input and output to and from it. Virtually all of the inputs for the main code are derived from ESP-r, which also determines/controls parameter values for the number of iterations, total simulation time and iteration time interval/step. These parameters cannot be specified within model codes. Subsequently, only parameters relating to the sub-code are analysed for sensitivity of the codes to changes. These are the discrete cell, or grid, sizes and convergence criterion.

To assess impact of these parameters on model output/performance each model was simulated, and results are afterwards plotted against the various values chosen for each parameter. PCM and heat transfer fluid properties in table 5.2 were employed for the simulations. Heat transfer fluid inlet for charging and discharging were 80 °C and 25 °C, respectively. Simulations were run for 30 and 15 min, charging and discharging times, respectively, and results recorded for HTF outlet stream temperatures and program execution time.

5.5.1 Discrete cell size

Discrete cell is the representative volume of the model wherein local equilibrium is (assumed to be) achieved at a time scale comparatively shorter than computational time step. The value of a field quantity within each cell is assumed to be representative of the average over the model. The size of the cell for the shell-and-tube PCM heat exchanger was determined by dividing the heat exchanger by whole numbers, grid factors, along the radial (radius) and axial (length) axes to obtain cells with dimensions $\boldsymbol{d_r}$ and $\boldsymbol{d_a}$ for the shell-and-tubes heat exchanger while the PCM wall slab was divided along its height, length and thickness, that is, the x-, y- and z- axes, to obtain cell dimensions $\boldsymbol{d_x}$, $\boldsymbol{d_y}$ and $\boldsymbol{d_z}$.

5.5.1.1 The Shell-and-Tubes Thermal Store

Assessment of the PCM shell-and-tubes heat/thermal store model's sensitivity to cell/grid size was conducted by running simulations for thermal store with two different inner tube and shell diameters. One had inner tube and shell diameters of 0.0254m and 0.5m, respectively while inner and shell diameters of the other system were 0.022 and 0.185m respectively. Both were 1m long.

Radial grid sizes were varied by dividing thickness of annulus by different grid factors between 2 and 20 to obtain radial cell dimensions, $\boldsymbol{d_r}$, between 0.003m and 0.03m and axial grid sizes were varied by dividing the exchanger length by axial grid factors between 10 and 100 to obtain axial cell dimensions, $\boldsymbol{d_a}$, between 0.01 and 0.1m. These produced cells/grids ranging from 20 to 2000.

Simulations of the models were run with HTF charging and discharging temperatures of 80 °C and 25 °C respectively. Total run time was 30 minutes with charging done in the first half, 15 minutes, and discharging in the second 15 minutes. Results of HTF outlet temperature and time taken for computer to execute the code, execution time, was recorded for analysis.

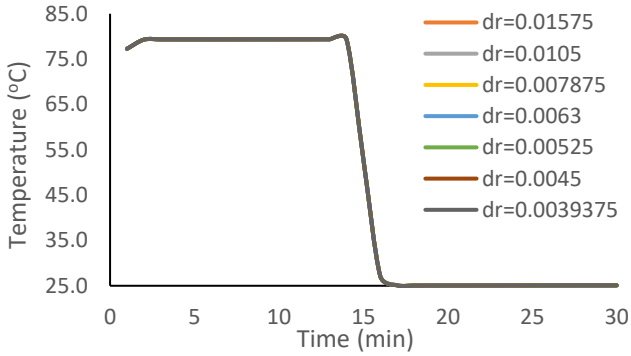

Figure 5.10: HTF exit temperature for different d_r - Heat storage battery.

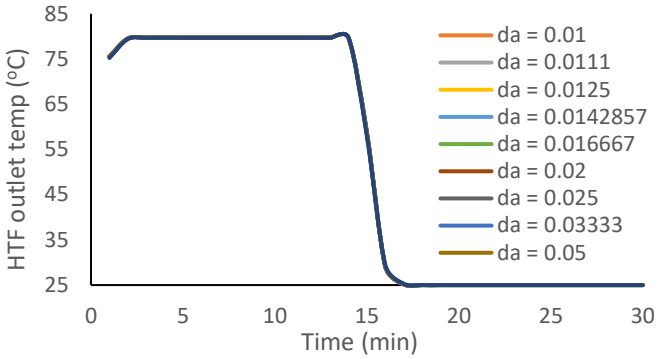

Figure 5.11: HTF exit temperature for different d_a - Heat storage battery.

Results show that the model output is unaffected by changes in size of the grid, i.e., lengths of $\boldsymbol{d_r}$ or $\boldsymbol{d_a}$ (Figures 5.10 and 5.11). This agrees with Abolghasemi, Keshavarz, & Mehrabian (2012) and Benmoussa, Benzaoui, & Benmoussa (2017). The only impact of reducing the grids is how long it take to run the model, simulation time. The finer the grid, the longer the program execution time (Figures 5.12 and 5.13). The implication of these is that size of the grid does not impact performance of model in any way and the choice is based on expenditure of computational time.

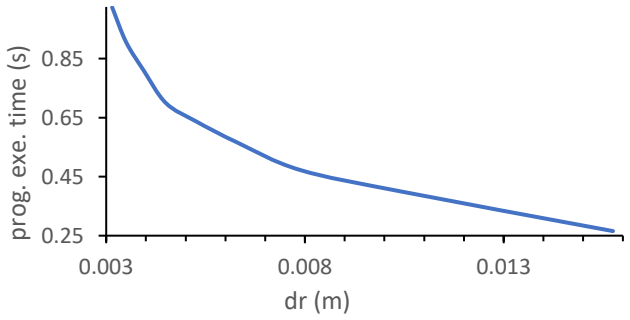

Figure 5.12: Plots of program execution time against dr – Heat storage battery.

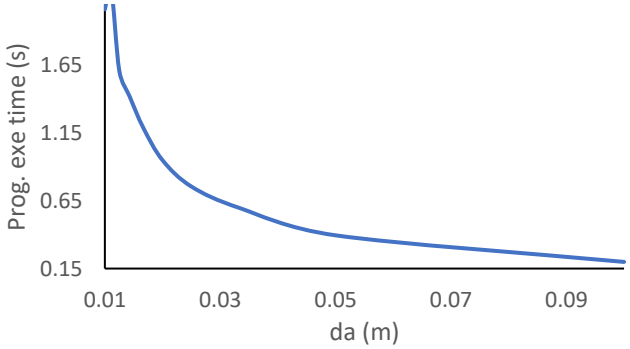

Figure 5.13: Plots of program execution time against da – Heat storage battery.

It was also observed during the tests that small number of cells/grids results in PCM temperature plot profile that assume a ‘staircase’ shape rather than a smooth curve as shown in Figure 5.14. Reason for this phenomenon was explained by Alexiades & Solomon (1993) who suggested 80 as minimum cell/grid number to obtain a smooth PCM temperature plot profile. However, smooth temperature profile was achieved with number of cells/grids above 125 (see figures 5.15a and b).

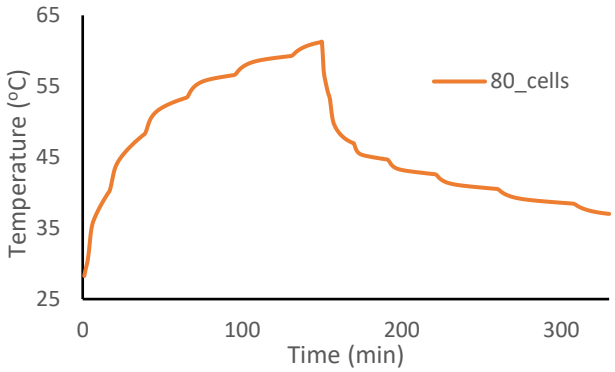

Figure 5.14: Plot PCM temperature against time for small number of cells/grids showing 'staircase' profile

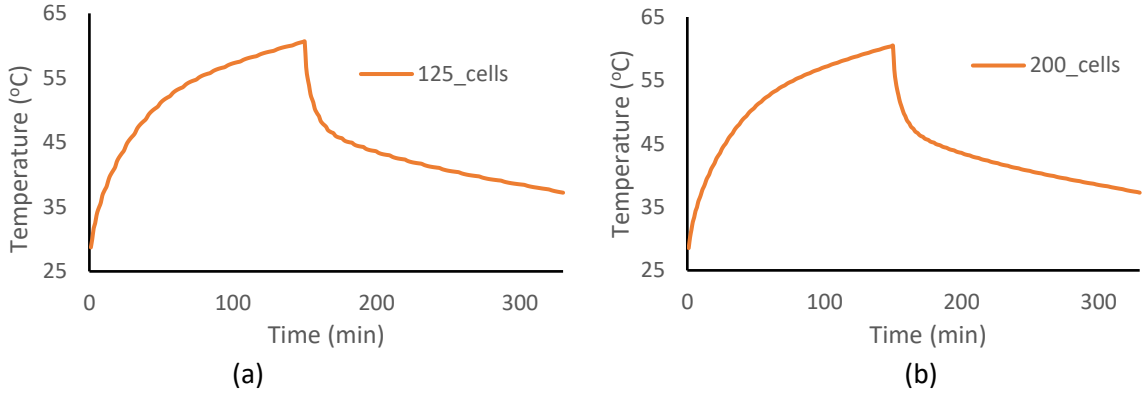

Figure 5.15: Plot PCM temperature against time showing progression from 'staircase' to ‘smooth’ profile.

It has been shown that the cell number (or size) has no impact on output, or performance of model. The smaller cell number, and bigger cell size only has impact on the smoothness, or otherwise, of the plot/diagram of the results.

5.5.1.2 The Fabric Integrated PCM Thermal Store

Similarly, the PCM wall thermal store was assessed for its model's sensitivity to cell/grid size by running simulations of slabs with a thickness of 0.075m, length 0.5m and height 1.0m. The slab was divided by grid factors between 10 and 60; 6 and 20; and 2 and 7 along the x-, y- and z- axes respectively, to obtain ***dx***, ***dy*** and ***dz*** between 0.0167 and 0.1; 0.0045 and 0.016; and 0.01 and 0.04 respectively, and cell/grid number between 60 and 840.

Simulations of were similarly run with HTF charging and discharging temperatures of 80 °C and 25 °C, respectively for total run time of 30 minutes, split between charging and discharging times. System was charged during the first 15 minutes and results of HTF outlet temperature and program execution time was recorded for analysis.

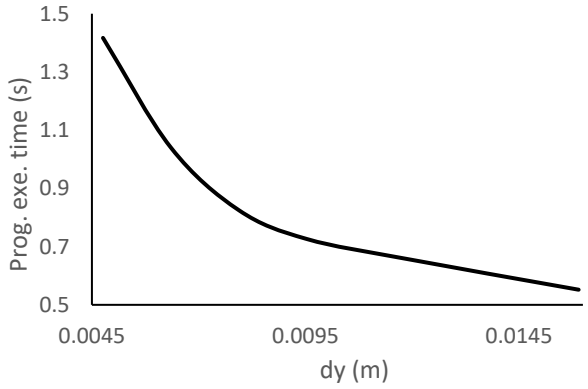

Figure 5.16: Plot of program execution time against dy – PCM wall slab

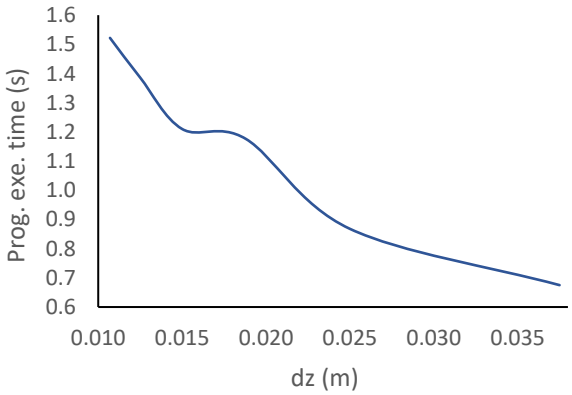

Figure 5.17: Plot of program execution time against dz – PCM wall slab

Like findings from analysis of the shall-and-tube heat store model, reducing grids only led to increasing simulation time. Results also show that changes in sizes of ***dy*** and ***dz*** have very little, negligible, impact on model output, as depicted in figures 5.16 and 5.17 which are profiles of program execution times plotted against grid lengths ***dy*** and ***dz***. Figure 5.18 shows simulation time remaining relatively constant between ***dz*** equal to 0.015 and 0.02 m.

It was observed, however, that the model shows significant sensitivity to changes in grid size along the **x**-axis, ***dx*** (figure 5.18). As shown in the figure, the profiles coalesce as ***dx*** is reduced below 0.033m. This suggests that reducing ***dx*** below 0.033m does very little to refine the results.

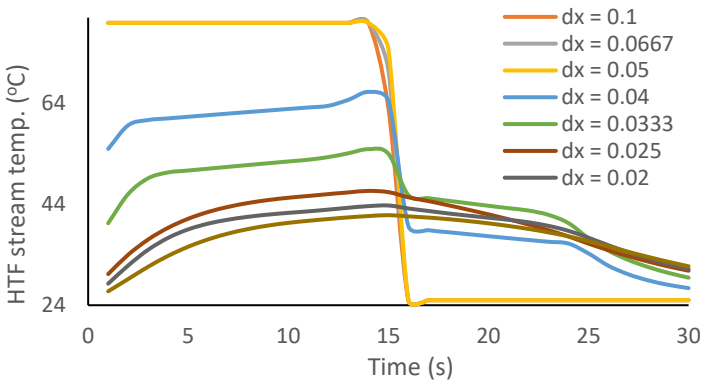

Figure 5.18: HTF exit temperature for different dx – Fabric integrated PCM slab,

5.5.2 Convergence Criterion

Convergence criterion is the condition set/used to establish and verify convergence of a sequence of iterations. While the criterion is unsatisfied iterative process is repeated continually and only stops upon its satisfaction. It is important when developing numerical algorithms for solving non-linear equations employing either the explicit or implicit time integration schemes to have criterion for terminating processes/iteration loops (Lindfield & Penny, 2019) and an optimum value is needed to be set/determined in order to obtain accurate solutions in a reasonable time (Boettinger & Banerjee, 2015).

As discussed in chapter 3, the Gauss-Seidel iterative method was employed for solving the energy balance equation for PCM melting and determination of PCM properties at time (***t***+1). The method employs a process of repeated iteration until convergence criterion is satisfied. This implies solving equation 3.113 (chapter 3) until maximum absolute value of difference between the PCM temperatures before and after elapsed time is less than a constant (tolerance). Summarily, a sensitivity analysis of the model was carried out to assess effect of changes in this constant on outputs and obtain an optimum value. This was done by analysing simulation time and result output with respect to the criteria.

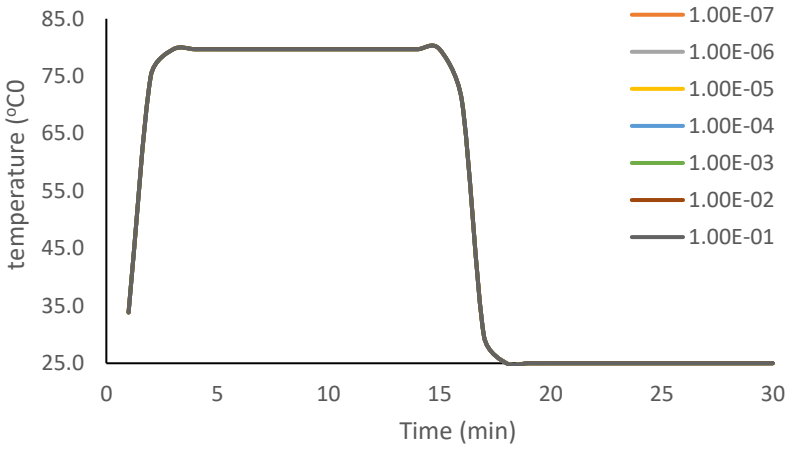

Figure 5.19: HTF exit temperature for different convergence criteria

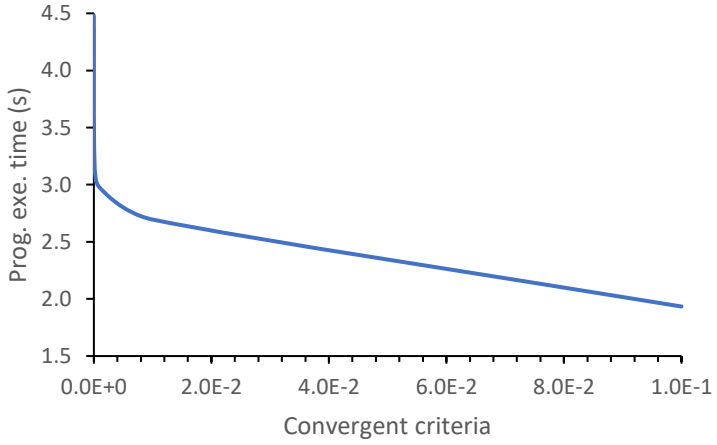

Figure 5.20: Simulation time against convergence criteria

Figure 5. 19 is plot of HTF exit temperature profile over simulation time while figure 5.20 is plot of program execution time against convergence criteria. The former shows no impact by convergence criteria on output while the latter shows that any criterion below 0.001 results in unnecessary consumption of computational power.

5.5.3 Discrete End cell/node Interaction – Fabric Integrated Thermal Store

A further assessment was carried out for the wall PCM slab on account of the simplification method adopted for the model (chapter 3). This relates to the PCM-tube-PCM sandwich that was adopted for simplifying the model. Only one such sandwich, as representation of the slab, was modelled with number of tubes employed as scaling factor withing the model code.

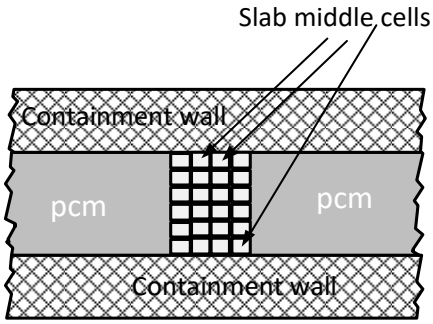

Figure 5.21: Representation of PCM slab middle cell interaction

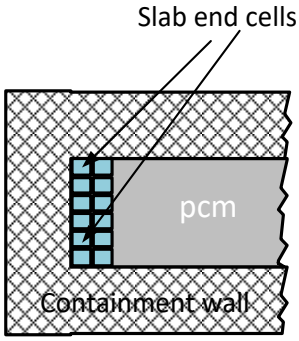

Figure 5.22: Representation of PCM slab end cells interaction

The implication being that condition of PCMs at either ends of the slab were subject to different conditions and interaction in comparison to PCMs at middle of slab. Discrete end cells for sandwich, PCM-tube-PCM, at middle of slab have interactions with other PCM cells

on all sides (except for cells at each face, which interact with containment wall) while discrete end cells for sandwich at either ends of slab have interactions similar to those at the middle except on one side, the side farthest from HTF tube (Figures 5.21 and 5.22), where interaction is with containment material.

Purpose of this analysis is to assess impact, if any, of this disparity/difference on results from the model. This was accomplished by developing two variants of the model codes, with each variant modelled with discrete end cells to have the two types of interactions, and installing into ESP-r. Two plant networks each comprising a heat pump, two domestic radiators and water pipes for connection, were developed for the ESP-r training building models described in section 5.4.2 and shown in Figure 5.6. Each plant network was fitted with each one variant of the PCM wall thermal store model and simulations were run for the building model separately with each of the thermal store model variant.

Results of nodal temperatures and containment surface temperatures for both model variants were obtained from simulation results, plotted against time for comparison. These are shown in Figures 5.23 – 5.25.

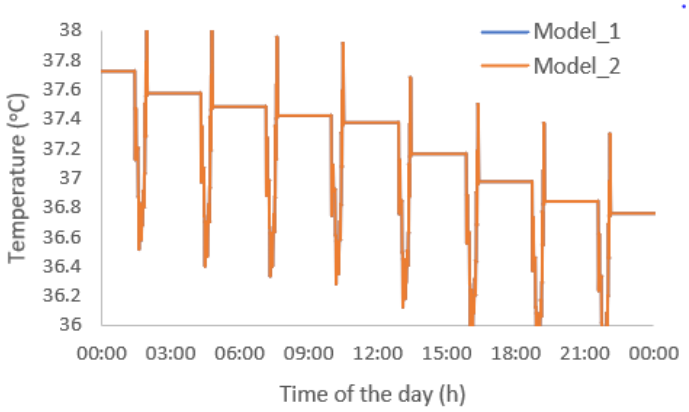

Figure 5.23: Comparison of nodal temperatures

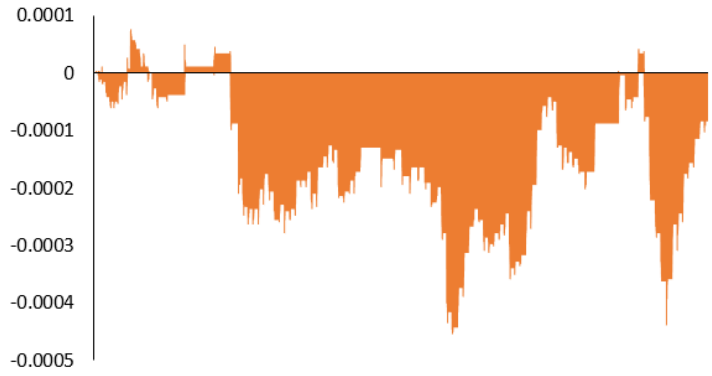

Figure 5.24: Nodal temperature difference between model 1 and model 2

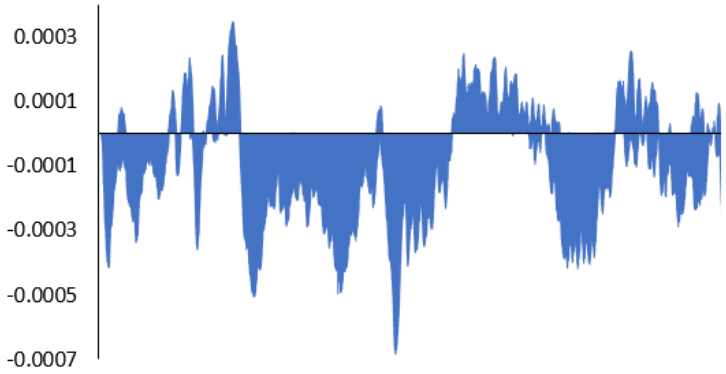

Figure 5.25: Containment surface temperature difference between model 1 and model 2

As shown in the figures, impact of the difference end cells (node) interactions on nodal temperature or temperature of containment surface is very small, quite negligible. This is expected given that total size of the end cells/nodes is very small in comparison to overall size of the thermal store.

5.6 Summary

In this chapter, the methods and procedures for verifying and validating the PCM thermal store models, as well as the results of the processes have been discussed. The models were verified using structured walk throughs, debugging and consistency tests while validation was accomplished by comparing results from simulating them with results reported of models of similar phase change thermal storage systems in journals. These reports discussed tests of

both experimental and numerical models and the comparisons show very close agreement between them and the PCM thermal store models. The models were also assessed for sensitivity to changes/variations in values of some of the parameters that represent constant inputs in the numerical codes, as well as for possible impacts the choice of model configuration (for the PCM wall thermal store only) would have on the performance.

The tests and analysis show that the models' computer programs and their implementation are correct and that they possess satisfactory range of accuracies that are consistent with their intended applications.

The next chapter will focus on case study tests to assess the potential application of the models vis-à-vis the assessment of energy saving potentials of deploying phase change material based thermal storage systems in domestic space and water heating applications.

Chapter 6

CASE STUDIES WITH BUILDING MODELS

6.0 Introduction

This chapter focuses on demonstration of the thermal store models. It describes study methodology and approaches for deploying and testing the models with an aim to highlight possible areas of application as well as assessment of effectiveness of deploying such systems for domestic heating (and cooling) applications such as shifting heating system operations from peak to off peak energy demand period and for reducing system's energy consumption, energy cost and CO_2 emissions.

As part of push towards achieving its goal of 80% reduction in CO_2 emissions by year 2050, the UK's government has placed emphasis on electrification of its energy systems (Department of Energy and Climate Change, 2010; Wilson, et al., 2013), focussing attention on electric vehicles and replacement of gas driven technologies with heat pumps for space and water heating (Quiggin & Buswell, 2016; Protopapadaki & Saelens, 2017).

With deployment of heat pumps in individual homes regarded as one of the primary objectives to achieving this aim (Critoph & Metcalf, 2019), there are potential problems associated with deployment of large number of heat pumps on the electrical grid (Love, et al., 2017; Arnold, 2016) that will ultimately require mitigation. These include black out occasioned by excessive demand peaks and the inability of the system to effectively achieve instantaneous supply-demand balancing (Quiggin & Buswell, 2016), network instability and a host of other problems related to low voltage distribution and supply (Navarro & Ochoa,

2014), some of which includes network current surge, equipment damage, electrocution and fire outbreaks (Moldovan, Damian, & Georgescu, 2017).

One of the ways to address these problems is employing energy storage, which can help with managing loads, flattening load profiles and smoothening out energy demand peaks and fluctuations (Münster & Lund, 2007). These results are achievable if operation of the heat pumps is manipulated to shift their running/operation periods/time away from peak energy demand periods to off-peak energy demand periods (Muruganantham et al., 2010).

Assessment and analysis of this load shifting potential, as well as cost and energy saving benefits, using the PCM based thermal energy storage systems, which employs the PCM thermal storage models developed herein, with heat pump powered heating systems forms the basis for the case studies described below. Details of tests and analysis of the results from two case studies will be discussed.

Case study 1 assesses performance of the thermal storage battery and the fabric integrated thermal store models and investigates their application as latent heat energy storage systems employed for back shifting heat pump operation (and energy consumption) away from peak to off-peak energy demand periods. The heat storage battery and the fabric integrated thermal store were deployed with heat pump powered water and space heating systems for assessment and comparison with heating systems employing no thermal storage. The heat storage battery was deployed for storing and delivering heat to the heat transfer fluid (water) employed for supplying heat to both domestic water heating and space heating systems while the fabric integrated thermal store was deployed within walls and floors and employed for space heating only.

Case study 2 conducts a comparative analysis of performance between systems employing latent heat thermal energy storage systems and heating systems employing sensible heat

thermal energy storage systems. The thermal storage battery was compared to a water-based sensible heat storage system using conventional hot water storage tank (system) for space and water heating while the fabric integrated thermal store was compared to active walls and floor integrated sensible heating systems using thermal mass construction materials.

The analyses were carried out using a pre-developed ESP-r archetype model of a 2-storey semidetached building employing an air source heat pump-based water and space water heating system. The same building model was employed for both case studies but with different plant network/systems for each case study and heating systems. Details of the building and plant systems are given in following sections.

Different plant networks representing the different types of heating systems were applied to the building model. All the plant networks contain an air source heat pump, domestic hot water tank, connecting pipes, flow dividers and converging valves and flow control valves. Individual zones domestic hot water radiator sizes were determined based on the sizes and volume of the zones, with radiator in the living room, tagged ‘liv’ zone, which is the largest zone, being the largest.

One plant network was equipped with the heat storage battery to depict water and space heating system with latent heat thermal storage, another was fitted with a conventional buffer (hot water storage) tank to represent the same type of heating system but with sensible heat thermal storage. The third plant network was fitted with a set of the fabric integrated thermal stores, installed within the walls, to represent space heating system with active wall integrated latent heat storage while the fourth network was fitted with a set of the fabric integrated thermal stores, installed within floors, to represent space heating system with active floor integrated latent heat storage system. The fifth plant network contained no heat storage system and served as a control.

The fabric integrated thermal store model is equally useful for assessing sensible heat fabric integrated thermal stores. All that is required is to substitute properties of sensible heat materials for the PCM properties. So, the same plant network, and components, employed for the latent heat system were used for the sensible heat systems after substituting the PCM properties.

The simulations were run using weather data for Glasgow, longitude and latitude 55.9^{o}N and 4.1^{o}W, respectively, in year 2017 and during the three winter months of December, January and February. The heating systems were evaluated for impact on heat pump performance with regards to effectiveness in meeting water and space heating requirements and energy consumed by the heat pump to supply the heating requirement, as well as total heat energy supplied to the zones and total energy cost for the heating, and CO_2 equivalents of the energy consumed by heat pump to provide heating for dwelling. The cost of electricity was determined from electricity pricing, tariffs, obtained from Bulb Energy Limited (2020) while CO_2 emissions were estimated using conversion factors from Department for Business, Energy & Industrial Strategy (2020).

6.1 System Description

6.1.1 Building Model

6.1.1.1 Model Description

The building model is a single-story semi-detached house, reflective of UK housing stock. This type of building houses about 32% of the UK's population (Atkin, 2017) and makes up 23% of households in Scotland, according to 2011 national census (National Records of Scotland, 2018). The building contains two identical houses that are mirror images of each other. Each house is made up of two floors with two hallways (one on each floor) connected

by a stairway. The bedrooms and bathroom(s) (at least one of each) are located on the top (or first) floor while the living room and kitchen are located on the ground floor.

The model used is a pre-developed ESP-r architype model with nine separate spaces/enclosures, referred to as zones, obtained from ESP-r archives/database. The zones are the two bedrooms, one living room, one bathroom, one kitchen, one equipment room, the roof and the two hallways, upper and lower hallways, (the upper hallway includes the stairway). It has a total floor area of 130.395m^2 spread over three levels, the ground and upper floors, and the roof space. A sketch of the building model is shown in figure 6.1 while a description of the sizes of individual zones is given in table 6.1.

Table 6.2: Size description of individual zones

Zone	tag	Floor area (m2)	Volume (m3)
Bathroom	bath	5.25	13.1
Bedroom_1	bed1	17.625	45.5
Bedroom_2	bed2	14.01	35.2
Equipment	equip	3.3	7.28
Hallway	hall1	12.57	12.7
Kitchen	kit	5.25	13.1
Living room	liv	27.36	68.4
Roof	roof	42.5	51
Upper hallway	up_hall	2.53	18.2

The model bears a close resemblance to actual architectural representation of a real building and adequately replicates its thermodynamic behaviours. It comprises detailed representation of the building's geometry, fabric/construction materials, and air leakage characteristics. It also entails component-based heating system and control strategy representation as well as details of occupants and equipment heat gains, and hot water draw profiles.

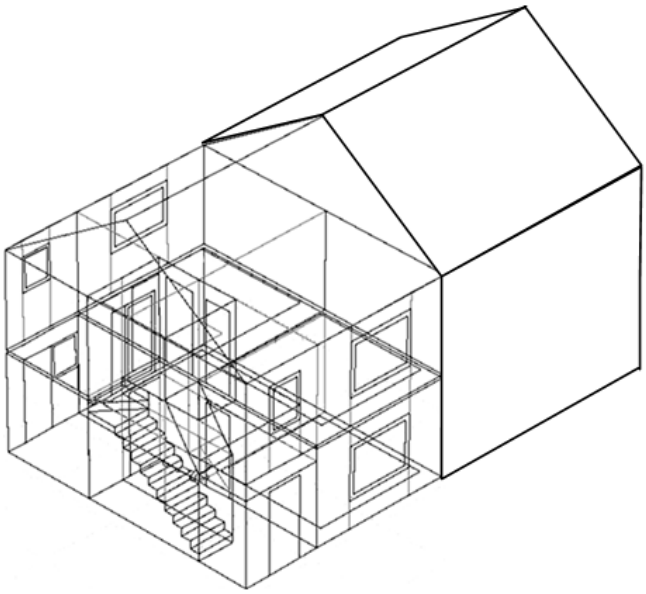

Figure 6.1: Sketch of a semi-detached house/building. The ESP-r model represents one half of the building.

6.1.1.2 Building Construction and Properties

According to Hong et al. (2011, 2013) a thermally efficient building is necessary for the amount of thermal storage required to shift operations of a heat pump from peak to off-peak energy demand period to be practical. Subsequently, the construction components chosen from the ESP-r construction database for all external walls of the building model were code compliant wall assumed for Scotland SBEM equivalent construction component. It is an eight-layer composite wall with combined U-value less than 0.17 W/m^{2}K. This is the maximum U-values for building insulation envelopes for Scotland, given in the 2019 building standards technical handbook for domestic buildings published by Local Government and Communities Directorate (2019). Component for the floors is parquet slab-on-grade floor over concrete slab with XPS insulation. It is a nine-layer composite with combined U-value of 0.17 W/m^{2}K. In order to meet the Scottish standard U-value of 0.15 W/m^{2}K (Local Government and Communities Directorate, 2019), thickness of one of the layers of XPS

insulation was increased from 1m to 1.50m. The roof is a ten-layer passive house low slope roof with cellulose fibre insulation and service void.

6.1.2 Occupancy

6.1.2.1 General Occupancy for Dwelling

The building model is assumed to be occupied by a family of three, comprising two adults (parents) and one teenage child. Although this number of occupants is slightly higher than the national average household size of 2.3 persons estimate from the 2011 UK Census (Office for National Statistics, 2011), estimates from Office for National Statistics - Labour Force Survey (2019), indicates that households occupied by a couple and one dependent child make up the largest proportion, about 43.68%, of households occupied by families with dependent children in the UK. They are the third largest category of households (with regards to number of occupants), after households with single and two occupants, for the year 2019. Also, teenage children make up 35% of children in households in Scotland (figure 6.2) (National Records of Scotland, 2015).

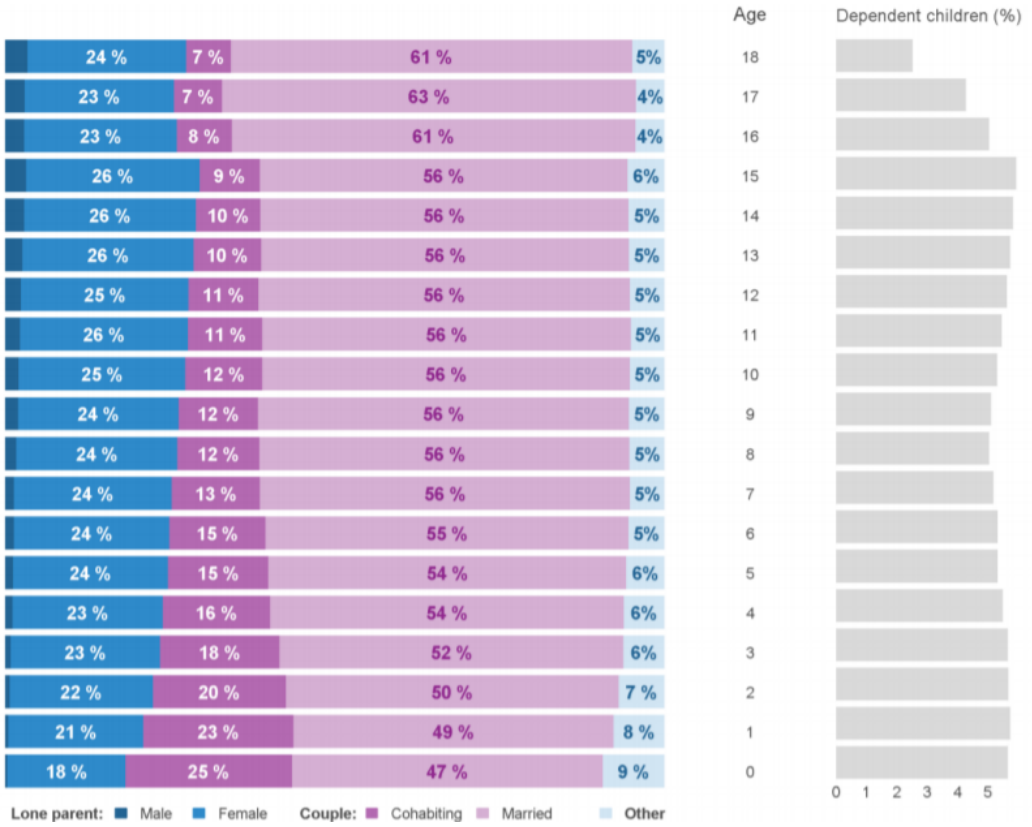

Figure 6.2: Household composition for dependent children by age, Scotland, 2011 (National Records of Scotland, 2015)

The dwelling is assumed to be occupied between 12:00 am – 8:00 am and between 4:00 pm – 12:00 am on weekdays, and between 12:00 am – 10:00 am and between 4:00 – 12:00 am on weekends and holidays.

This assumption differs from findings reported in the Time Use Survey, UK (Gershuny & Sullivan, 2017) for weekdays, wherein periods of absence from homes were determined as being between 09:00 am – 5:00 pm for weekdays, but is the same as the occupancy scenario proposed by Yao & Steemers (2005) for households with three occupants who work full time. There is, however, agreement with the Time Use Survey occupancy figures for weekends occupancy.

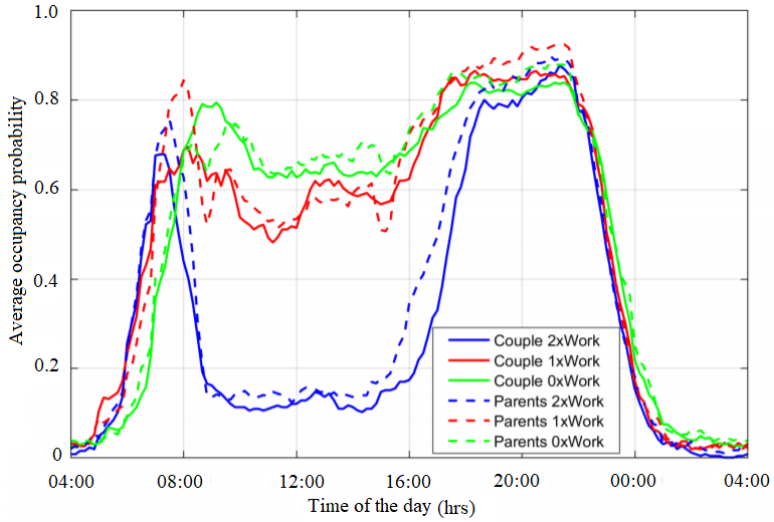

Figure 6.3: Average occupancy for couples and parents by employment status (Gershuny & Sullivan, 2017)

The adopted scenario assumes that the adult occupants work full time, between 9:00 am and 5:00 pm, on weekdays and would have been out of the house at least an hour before 09:00 am and most likely not return until at least an hour after 5:00 pm. This is in agreement with the proposed occupancy scenario by Yao & Steemers (2005) which correlates with the average occupancy probability data from the Time Use Survey (Gershuny & Sullivan, 2017) for couples and parents by employment status (Figure 6.3). There is low occupancy probability around 8.00am and 5.00pm, when both couples and, both parents are working (blue solid and dashed lines of Figure 6.3).

Their teenage child, being of school age, is also most likely to leave the home at about the same time on weekday mornings but return around 4:00 pm, except during holidays, which tallies with the periods of absence from the house in scenario suggested by Yao & Steemers (2005). Pictorial depiction of the general occupancy scenario employed for the research and that of the UK Time Use Survey are shown in Figure 6.4. Active occupancy is represented by yellow colour, beige represents dormant (sleeping) occupancy while red represents absence from the dwelling.

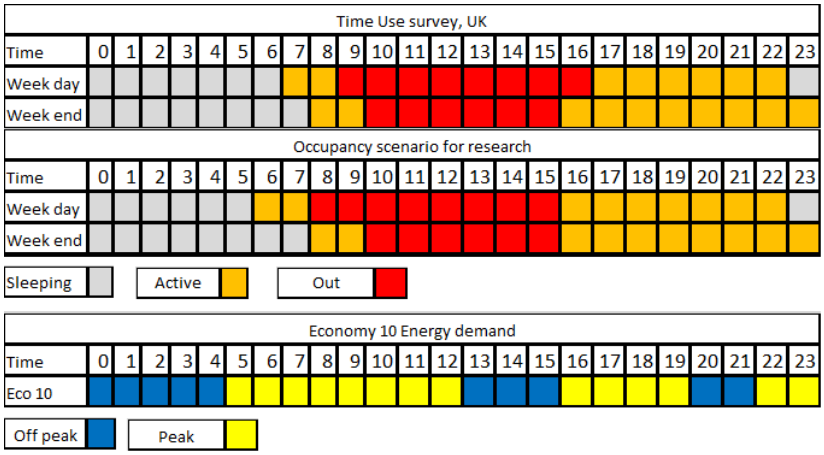

Figure 6.4 Occupation (general) and Off-peak energy demand period

Active occupancy for weekends is the same as in the Time Use Survey, between 12 am and 8 am in the mornings but different for weekdays mornings as the time is moved forward by one hour to obtain the same two hours active occupancy period before the occupants leave the dwelling, that is 12am – 7am for the Time Use Survey but 12am – 6am for present (research) scenario. The evening times are the same for both scenarios, 11pm – 12am.

6.1.2.2 Zonal Occupancy

Occupancy scenarios were developed for individual zones during the occupied periods and utilised for setting individual zone/plant control and heating strategies for all the zones.

Bedrooms

While the UK Time Use Survey data gives indication of how much time people spend indoors and away from homes, it says nothing about which rooms of the house time is spent. And there is very little report on how time is spent in specific rooms within dwellings save the work of Khajehzadeh & Vale (2015) who discussed the results of a survey of households in New Zealand to determine length time people spend in each of the rooms of their houses. Because their sample size was very small, they admitted that "the findings are mostly indicative". Nevertheless, they reported 8.5hrs as average time spent by respondents in bedrooms. This falls within the recommended sleep time of 7 – 10 hours for adults (Mayo Foundation for Medical Education and Research (MFMER), 2020) and teenagers (Bruck,

2006). Coupled with the time of presence in the home from the UK Time Use Survey and the adopted scenario of 14 hours, this suggests that the largest proportion of time spent indoors are spent in bedrooms and probably for sleeping. Subsequently, occupancy scenarios for the two bedrooms, bed1 and bed2 zones, for weekdays, were based on a combination of the findings reported by Khajehzadeh & Vale (2015) and personal experience and family dynamics.

The 'bed2' zone/room is assumed to be the teenage child's room and assumed occupied during periods they are present in the dwelling except for short periods in the mornings, late afternoons and evenings, possibly to get meals from the kitchen or spend time with the rest of the family in the living room. 'Bed1' is assumed occupied when at least one of the parents is present, which, again based on personal experience, is during the night, mornings and immediately after return from work (5.00pm and 6.00pm) and late in the evenings between 9.00pm to 11pm (Figure 6.5).

Living Room and Kitchen

Reports on time spent in living rooms and kitchen is also scares. The report by Khajehzadeh & Vale (2015) was vague on the subject, combining both rooms into a category. But Lloyds Bank (2013) reported 3.8 hrs as average time spent in living rooms and 1.6 hrs as average time spent in kitchens. The idea of combining the two rooms into a category as done by Khajehzadeh & Vale (2015) and personal experience suggest that there are overlaps between time spent in each of the two rooms. Therefore, the same occupancy was adopted for both zones for all day types. The profile was derived from the BREDEM heating regime (version 8) for living rooms (Building Research Establishment (BRE), 2014) with slight adjustment due to disparities between the duration and times of the heating regime and time of absence from dwelling given in the UK Time Use Survey (Gershuny & Sullivan, 2017) for weekends as well as the adopted scenario for weekdays. The BREDEM heating regime assumes that the

living room is heated for 9 hours on weekdays, between 7am and 9am and between 4pm and 11pm, and for 16 hours on weekends, between 7am and 11pm (continuous) (Anderson, et al., 2010). This agrees with time of absence from dwelling given in the UK Time Use Survey (Gershuny & Sullivan, 2017) for weekdays but contradicts the weekend timings of absence from dwelling given as 9am – 4pm. Subsequently, morning occupancy for both rooms/zones are assumed to be one (1) hour on weekday, between 7.00am and 8.00am, two (2) hours on weekends and holidays, between 8.00am and 10.00am while evening occupancy are between 4pm and 11pm for weekdays, weekends and holidays.

Bath and Hallways

Due to inability to predict what times and period the bath and two (2) hallways are occupied without the use of occupancy models which is not available for this work, zero occupation was assumed for them. Nevertheless, radiator settings and heating control for the three (3) zones were set to supply heating when the dwelling is occupied, which is when at least one on the occupants is indoors. Figure 6.5 is a pictorial depiction of individual zone occupancy scenarios.

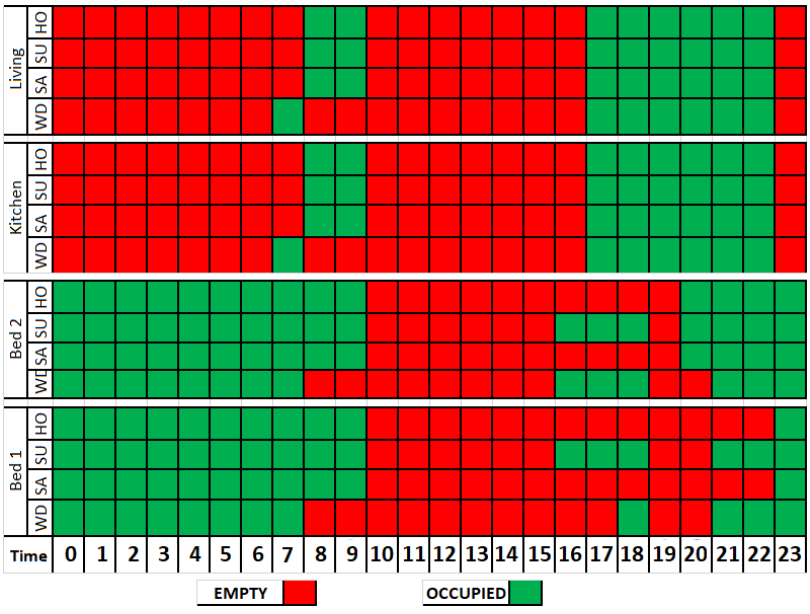

Figure 6.5: Occupancy scenarios for the bedrooms, kitchen and living room - WD, SA, SU and HD stand for weekdays, Saturdays, Sundays and holidays respectively

6.1.3 Plant Network/Heating System

6.1.3.1 Plant Networks

Figures 6.6, 6.7 and 6.8 are representations of the three basic types of plant networks (heating systems) adopted for the case studies. They show the primary components and connections with the radiator assemblies. Figure 6.6 is the plant network for heating system containing the PCM thermal stores, while Figure 6.7 is the plant network for heating system containing buffer/hot water storage tank (sensible heat thermal storage) and Figure 6.8 is plant network for heating system with no thermal storage, employed as control.

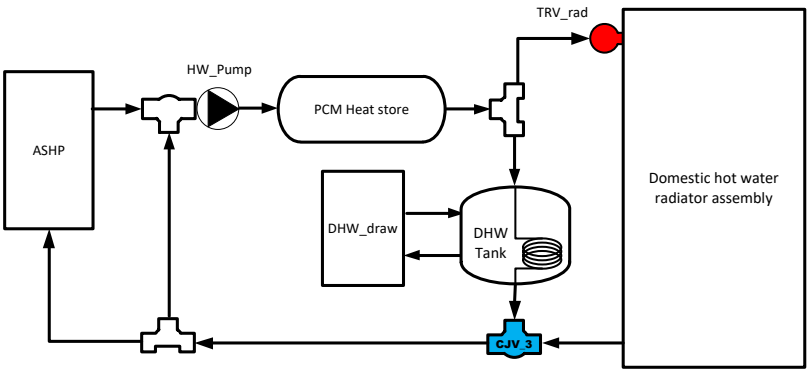

Figure 6.6: Plant network (with PCM thermal store)

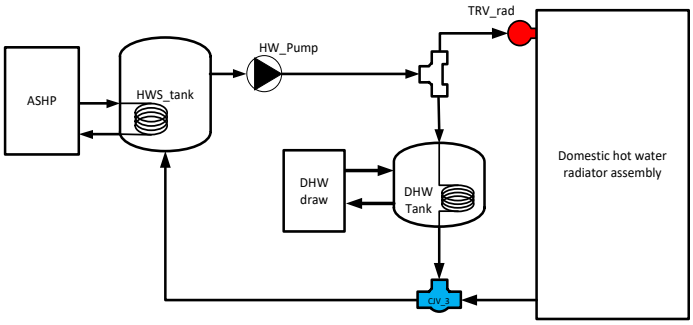

Figure 6.7: Plant network (with buffer/hot water storage tank)

The fabric integrated thermal stores are installed (embedded into walls and floors) in designated zones. The details of the installations in walls (surfaces) and rooms (zones), are given in relevant sections, and plant network diagram (4 PCM slabs) is shown in Figure 6.19.

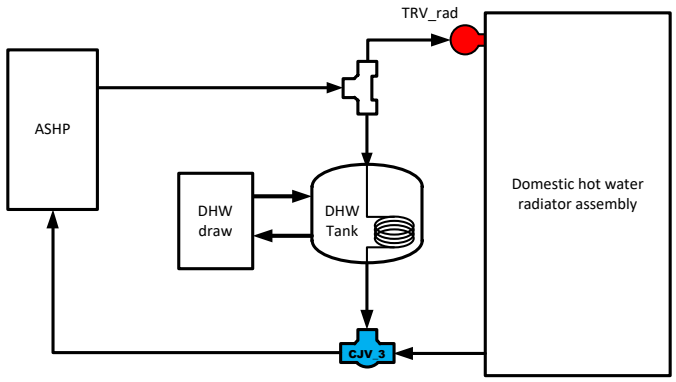

Figure 6.8: Plant network with no thermal storage (control)

A circulation pump is installed in all plant networks with thermal stores for the purpose of circulating hot water through the system when the heat pump is off. It is placed immediately after the heat pump.

The basic primary components, present in all plant networks, are the air source heat pump, the domestic hot water tank, hot water radiators and a stochastic plant representation of hot water usage/draw. These are discussed in more details below. All components are linked/connected by ESP-r models of water pipe, flow diverging and converging valves and flow control valves.

6.1.3.2 Air Source Heat Pump

Heating requirements for the dwelling is provided by an air source heat pump, denoted ASHP in the Figures. The ESP-r model of air source heat pump is described in Kelly, Tuohy, & Hawkes (2014). Following recommendation of a 1kW heating requirement for every 10m^2 of floor area by BoilerGuide Limited (2020), a heat pump with nominal thermal output of 9.0 kW was selected for the tests for total floor area of 87.895m^2. Its average coefficient of performance is 2.8.

6.1.3.3 Domestic Hot Water Tank

The domestic hot water tank is employed for supplying hot water usage for the dwelling. This is “a common setup in the UK” ((Kelly, Tuohy, & Hawkes, 2014) for heating systems

supplied by heat pumps. It is heated indirectly by the heat pump through an internal water heating coil by heat pump, and from which hot water is drawn for domestic use. The domestic hot water tank is represented in ESP-r by a stratified tank model described by Padovan & Manzan (2013). It has a capacity of 300 litres, being approximate size for a household of 3 – 5 persons (Sarbu & Sebarchievici, 2017).

6.1.3.4 Hot Water Draw

Hot water draw from the domestic hot water tank over time is determined via a hot water draw model in ESP-r based on the work of Jordan & Vajen (2005) which was included in all the plant networks. Table 6.1 list parameters assumed for the hot water draw (plant) model. Daily hot water draw was put at 100 litres. Although this value is a little less than the estimate given by Energy Savings Trust (2013) for the UK and higher than the 30 litres per person per day suggested by Sarbu & Sebarchievici (2017), it agrees with Kelly, Tuohy, & Hawkes (2014).

Table 6.3: Parameters employed for domestic hot water draw calculations.

Main draw configurations

Nominal daily hot water draw (l)	100
Seasonal variation of hot water draw (%)	10
Phase shift of seasonal variation (W/K)	28
Number of holiday periods	3

Fraction of draw at specific times

Draw period start time (hr)	00:00	06:00	09:00	16:00	23:00
Fraction of daily draw taken in period (%)	10	50	5	30	5

Specification for draw types

	Basin	Appliances	Bath	Shower
Fraction of daily draw for this type (%)	14	36	10	40
Draw volume flow rate (l/min)	1	6	12	8
Flow rate standard deviation (l/min)	2	2	1.67E-02	5.00E-02
Nominal duration (min)	1	1	10	5
Draw weekday probability modifier (-)	1	1	0.7	1
Draw weekend probability modifier (-)	1	1	1.4	1

6.1.3.5 Hot Water Radiators

Seven domestic hot water radiators are installed, one in each zone except the equipment and roof zones and provide heating to the dwelling from heating system. The two node models of domestic hot water radiator in ESP-r were employed for the radiators. Each is fitted with flow control valves, also ESP-r plant models, which regulate flow of hot water through them in response to temperature of the zones/rooms.

6.1.4 Zone and Plant Control

6.1.4.1 Air Source Heat Pump Control

Operation of the air source heat pump is controlled by a thermostatic control switch that switches it off or on in response to the temperature of water in the PCM thermal storage battery for plants networks/heating systems with same thermal store. The switch responds to temperature of the living room, zone 'liv', for all other plant networks/heating systems. Following assumptions in BREDEM for heating demand room dry bulb temperature of 21^{o}C (Building Research Establishment (BRE), 2014; Shipworth, et al., 2010) and the observation by Huebner, et al.(2013) of a heating demand temperature of 20.58^{o}C and average room temperature of 19.52^{o}C, an upper and lower zone/room temperature setting of 22.5^{o}C and 19.5^{o}C, respectively, similar to the suggestion of Kelly, Tuohy, & Hawkes (2014), was adopted. So, the heat pump is switched off when zone temperatures rise above the upper setting and switched on when they fall below the lower setting.

For plant network/heating system containing the thermal storage battery, the upper and lower melting temperatures of the phase change material, that is 51^{o}C and 45^{o}C, respectively, was used as the upper and lower limit for setting the thermostatic control switch.

6.1.4.2 Domestic Hot Water Tank Temperature Control

Water flow through the radiator assembly for all types of plant network/heating system was controlled by one thermostatic flow control valve (labelled 'TRV_rad' in Figures 6.6 – 6.8). It was set to maintain temperature of water in the domestic hot water tank between 43^{o}C and 45^{o}C, and to give it priority over the radiator assembly, following methodology described by Kelly, Tuohy, & Hawkes (2014). This is a general control strategy for all test models that ensures that maintaining temperature of water in the domestic hot water tank between this range (on/off control with dead band of 10^{o}C) is prioritised. This was accomplished by setting 'TRV_rad', to shut off flow to the radiators when water temperature in the hot water tank falls below the lower limit so that 100% of flow is diverted to the hot water tank.

6.1.4.3 Domestic Radiator Control (Zone Temperature Control)

Hot water flow into each of the seven domestic hot water radiators, and heat delivery to the zones, was controlled/regulated by individual valve components that mimic the action of thermostatic radiator valves/water flow control valves to maintain zone temperatures between upper and lower zone temperature setting established earlier at 22.5^{o}C and 19.5^{o}C.

6.1.4.4 Circulation Pump Control

The circulation pump's operation is also controlled by a thermostatic control switch that was set to allow operation only during the occupied periods, and in response to dry bulb temperature of 'bed2' zone, switching it on and off when temperatures go outside the19.5^{o}C and 22.5^{o}C range.

6.1.5 Simulation Period, Model Location and Weather

Simulation year was set for 2017 using generic UK weather data obtained from ESP-r climate file database and location of the building was set as Glasgow, UK (55.9N and 4.1W).

All simulations were run during the winter months of December, January and February, which contain the coldest period of the simulation year. This is spread over a 3 day period, starting from 3:00 pm on the 7th through to 2:00 pm on the 9th of January, with minimum and maximum ambient temperatures of -6.4^{o}C and 2.2^{o}C, respectively (Figures 6.9 and 6.10).

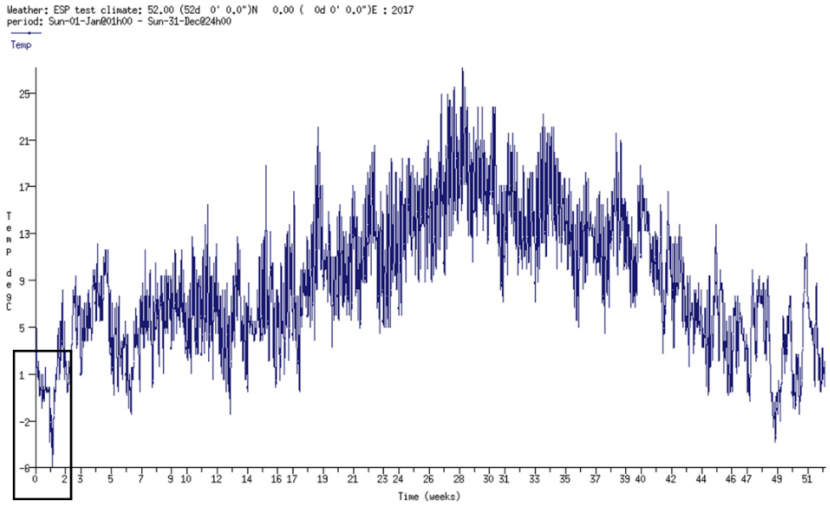

Figure 6.9: Weather graph for simulation year

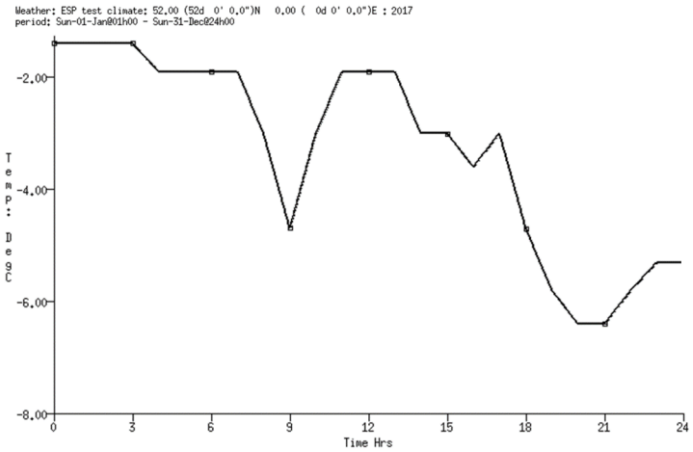

Figure 6.10: Weather graph showing boxed portion of figure 6.9.

6.2 Case Study 1 – Application for Shifting Heating Energy Demand from Peak to Off-Peak energy Demand Period.

The PCM heat storage battery stores heat using phase change material as heat storage medium. It was proposed as an analysis tool for assessing effectiveness of employing such

systems for shifting heating energy demand away from the peak demand period to the off-peak demand period, as well as energy cost and CO_2 emission reduction. Subsequently, a series of tests were carried out to examine this effectiveness (or lack thereof), as well as demonstrate the benefits of incorporating the models into the ESP-r software for the purpose of analysing performance of buildings that deploy PCM based thermal energy storage systems.

In order to assess and investigate the performance and application for energy load shifting, the types of heating systems described in section 6.1.3.1 were simulated using the building model described in section 6.1.1, that is, a semidetached house with nine zones and whose plant network contains the main/common components, an air source heat pump, domestic hot water tank, seven domestic hot water radiators, connecting pipes, hot water circulation pump, flow dividers and converging valves and flow control valves.

All heating systems with thermal storage were set to operate only during the off-peak energy demand period for the economy 10 energy tariff while system with no thermal storage was set to operate only when there is heating demand from/by the zones of the building, which are only during the occupied periods. The heating system with no thermal storage was afterwards set to operate only during the off-peak energy demand period of the economy 10 energy tariff for a second simulation to establish a baseline duration for heating requirement for the dwelling and to determine size of heat/thermal energy storage material requirement.

Simulation results were analysed for performance assessment by determining and comparing energy consumption and cost, as well as CO_2 emissions for each type of heating system.

6.2.1 PCM Heat Storage Battery

6.2.1.1 Strategy for determining size of PCM storage/Base Case.

To estimate size of thermal storage required to augment the heating system for it to adequately meet both hot water and space heating demands of the dwelling, building was simulated with the base case plant network (no thermal storage). The general plant and zone control strategies described in 6.1.4 were employed and the heat pump was set to operate during the occupied periods. The heat pump supplies heat on demand for the dwelling and the simulation was run over the winter months of December. January and February to capture the winter period. This was tagged test 1.

The maximum heating demand for the dwelling was obtained from simulation results and extrapolated over a day to determine maximum daily energy required to supply heating to the dwelling. This was employed to determine the mass, and volume, of thermal storage required to augment the ASHP.

PCM properties in table 6.3, obtained from Rubitherm Technologies GmbH (2018), were used for the simulations. The material was chosen because its lower phase change temperature, 45^{o}C, is equal to the upper temperature limit for water in the domestic hot water tank. This was to ensure the thermal storage can deliver heat to water in the domestic hot water tank. Volume of PCM employed for the latent heat thermal storage was estimated as 3.135 m^3. It was contained in the shell of a shell-and-tubes heat exchanger 2.0 m tall with 1.55 m inner shell diameter, containing 631 tubes of 0.0254 m diameter through which heat transfer fluid flows.

Table 6.4: Properties of PCM used for analysis.

Property description	Values
Melting temp range (^{o}C)	45-51
Specific Latent heat of fusion(J/kg)	168000
Specific heat capacity (sol)(J/kgK)	2000
Specific heat capacity (J/kgK)	2000
Thermal conductivity (sol)(W/mK)	0.2

Thermal conductivity (liq) (W/mK)	0.2
Density - Sol (kg/m3)	880
Density - Liq (kg/m3)	760

6.2.1.2 Simulation of Model with PCM thermal Storage Battery

The amount (mass) of PCM was determined from tests 1 above and the plant network was reconstituted to include the PCM heat storage battery (i.e., take the form of network type in figure 6.6). After setting the thermal store with specified dimensions and using properties of PCM listed in Table 6.3, simulations were run for the building model over the same winter months as for the previous test. This was tagged test 2.

The general control strategy for the domestic hot water radiators' flow control valves (section 6.1.3.5) was adopted for the test, and the ASHP operations were restricted to the off-peak energy demand periods for economy 10 tariff with control strategy set to power on and off in response to temperature of the living room, zone 'liv'.

The operation of the circulation pump was also restricted to the occupied periods only, being able to work when the ASHP is in the off mode. This ensures that heat could be drawn from the thermal store, to utilise stored heat at any time during the occupied periods. It was set to respond to temperature in the living room, zone 'liv', powering on when zone temperature falls below 19.5^{o}C and off when it rises above 22.5^{o}C.

Zone temperatures and air source heat pump energy data from simulation results were utilised to determine possible energy cost and mass of CO_2 equivalent of emissions and compared with results from tests 1 for assessment.

6.2.1.3 Results and Discussion

Table 6.4 is a summary analysis of plant results from tests 1 and 2, for heating system with no thermal storage and heating systems with PCM thermal storage battery, respectively. The table shows average monthly energy cost, monthly energy consumption and CO_2 equivalent

of emission, as well as total operating time for the heat pumps in both systems during each of the three simulation months.

Table 6.5: Plant Result analysis and System comparison (PCM thermal store vs base case) – Monthly averages.

	Ave. daily run time (min)	Ave. daily Energy use (kWh)	Monthly energy cost (£)	Ave. daily emission (kg of CO_2 Equiv.)
	No thermal storage			
Dec	307.23	8.39	50.67	1.96
Jan	320.73	8.75	53.27	2.04
Feb	292.89	8.03	44.46	1.87
	With pcm battery			
Dec	247.73	6.74	26.71	1.57
Jan	255.52	6.95	27.51	1.62
Feb	241.91	6.60	23.67	1.54

To supply heating requirement of the dwelling, heat pump in heating system with no thermal storage, operated only during the occupied periods (i.e., no load shifting, test 1), has a minimum daily average operating time of 292.89 minutes, consuming a minimum average of 8.03 kWh of energy daily. This amounted to minimum monthly energy cost of £44.46 and 1.878kg of CO_2 equivalent minimum daily emission of. For the system with thermal storage, operated only during the off-peak energy demand period for economy 10 energy tariff (test 2), the minimum monthly daily average heat pump operating time was estimated as 241.91 mins, consuming energy at minimum daily average of 6.60 kWh, which is equates to 1.54 kg of CO_2 equivalent minimum daily average emission, and an estimated monthly minimum energy cost of £23.67.

Table 6.6: Result Analysis and Summary findings (pcm thermal store and base case)

	Mean zone temp (°C)	Max Heat Load (kW)	Total heating delivered (kWh)	Ave hot water temp (°C)
Test 1 (no thermal store)				
Dec	19.25	4.8566	505.52	50.31
Jan	19.21	4.738	525.57	49.89
Feb	19.37	4.4609	377.47	49.13
Test 2 (with PCM heat storage battery)				
Dec	19.24	6.1646	504.04	49.45
Jan	19.20	6.143	525.03	49.12
Feb	19.34	5.5508	376.36	48.56

Summary of results for zone temperatures, maximum heating load, total heat delivered to meet heating requirements and average domestic hot water temperature for each month of the simulation period, are listed in Table 6.5. As shown in the table, maximum heating load (i.e., heating energy demand on heat pump) is higher for system with thermal storage relative to system with no thermal storage (base case) for each of the simulation month. This is due to the thermal store which represents additional demand on the heat pump. Also obvious from the table are the relative closeness of the mean/average monthly zone and hot water temperatures, and heating energy delivered to supply required heating for the dwelling by the two heating systems. The closeness of the mean/average monthly zone dry bulb temperature, hot water temperatures and heating energy delivered to supply required heating for the dwelling give indications that the system with thermal store, despite the increased peak heating load has capability to measure up to system with no thermal storage.

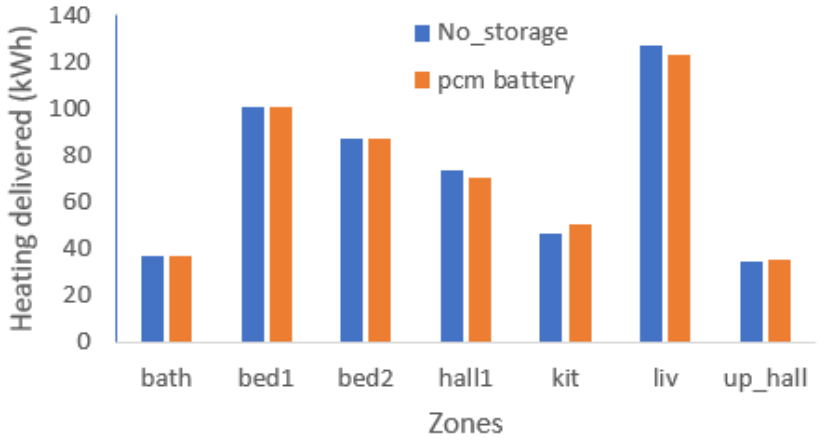

Figure 6.11: Comparison of heat delivered to meet zonal energy demand – December

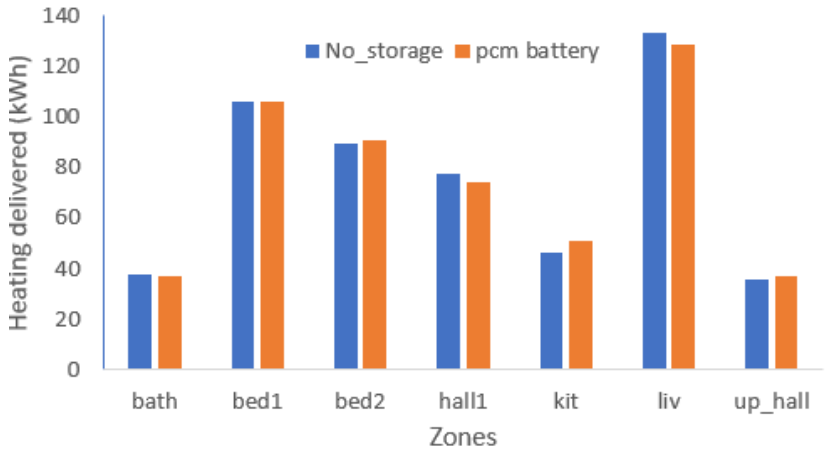

Figure 6.12: Comparison of heat delivered to meet zonal energy demand – January

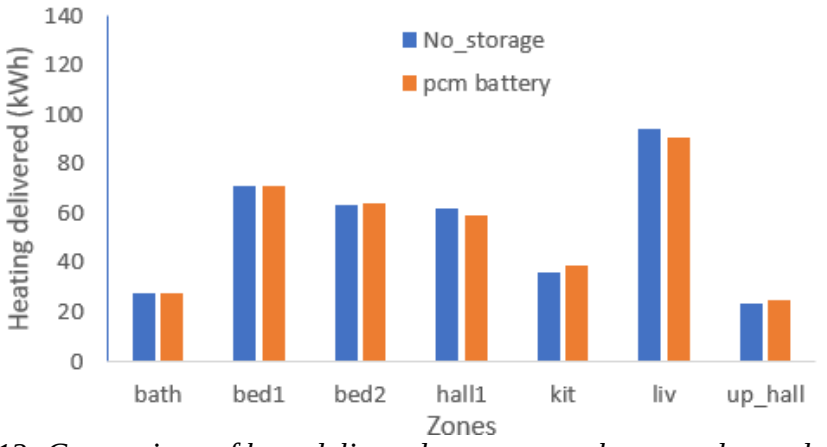

Figure 6.13: Comparison of heat delivered to meet zonal energy demand – February.

Comparison between the systems is displayed in Figures 6.11 to 6.16, which were plotted from simulation results. Figures 6.11 to 6.13 are comparison of heating supplied by the heating systems to each of the zones in response to heating requirement/demand in the zone

for each of the simulation month. Heat delivery to the zones by system with PCM battery is slightly lower than that supplied by base case system, particularly to the living room, zone 'liv'. The effect of the lower heat delivery is shown to be significant for all the zones as percentages of total simulation time zone dry bulb temperatures were maintained above the 19.5°C mark, depicted in Figures 6.14 to 6.16, are lower in comparison with the base case (no thermal storage) system. Nevertheless, average zone temperatures for the dwelling in all the three simulation months are less than 19.5°C for both system (Table 6.5), and about 2% below for systems with thermal storage.

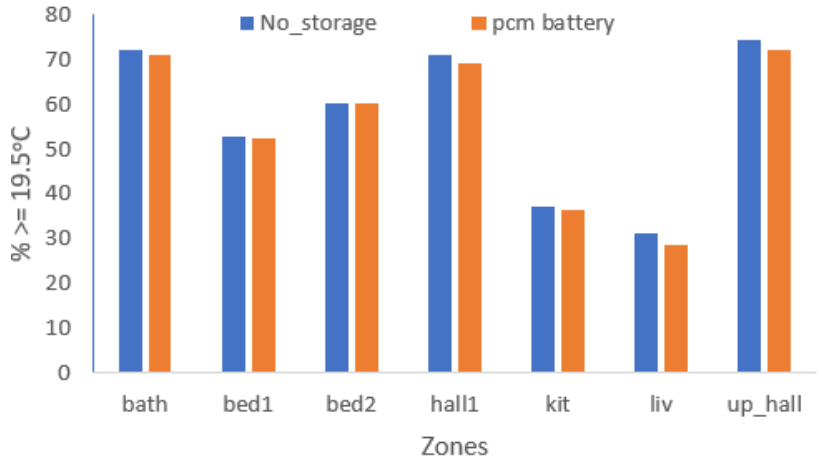

Figure 6.14: % of period zone temp >= 19-5°C – December.

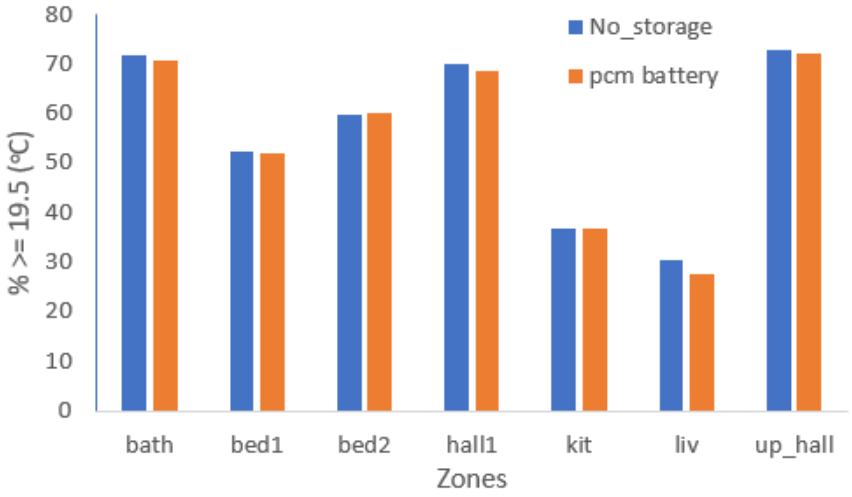

Figure 6.15: % of period zone temp >=19-5°C – January.

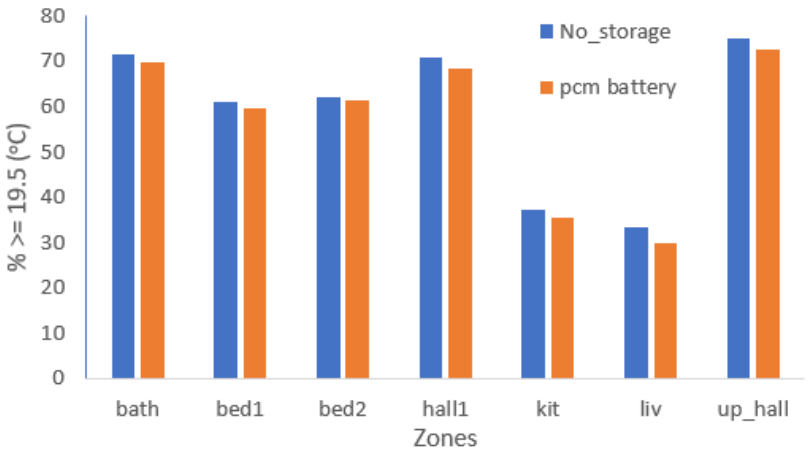

Figure 6.16: % of period zone temp >=19-5°C – February.

As explained in section 6.1.4.3, heating delivery to zones was controlled/regulated by individual valves to maintain zone temperatures between desired range. Also, individual zone/plant control valves setting were based on occupancy scenarios (section 6.1.2). So, the lower heat delivery to the living room, as shown in Figures 6.11 – 6.13, is due to the shorter occupancy for the zone (see Figure 6.5) in comparison to the bedrooms. Nevertheless, despite the higher peak heating load, the heating system with thermal storage was able to maintain temperatures of zones very close, comparatively, to system with no thermal storage, and doing so while operating only during the 10-hour off-peak energy demand period of the economy 10 energy tariff.

Further assessment of operation and performance of the heat pump for the two heating systems was done by looking at a snapshot of the performance data for the coldest week of the simulation period, that is, 3rd to 9th January. The data examined were temperature of water in domestic hot water tank, dry bulb temperature of the living room, zone 'liv', and number of minutes the zone temperatures fell below the 19.5°C mark (unmet minutes), as well as percentage of total heating demand period this constitutes, based on the occupancy scenario adopted for the zone (section 6.1.2.2). These are shown in Figures 6.17 and 6.18 and Table 6.6. The living room was chosen for reference because it has the highest heating energy

requirement, as shown in Figures 6.11 – 6.13, while the domestic hot water tank chosen because the heating systems' operations were geared toward provision of hot water for the dwelling, thus prioritizing maintenance of water temperature in domestic hot water tank at desired levels.

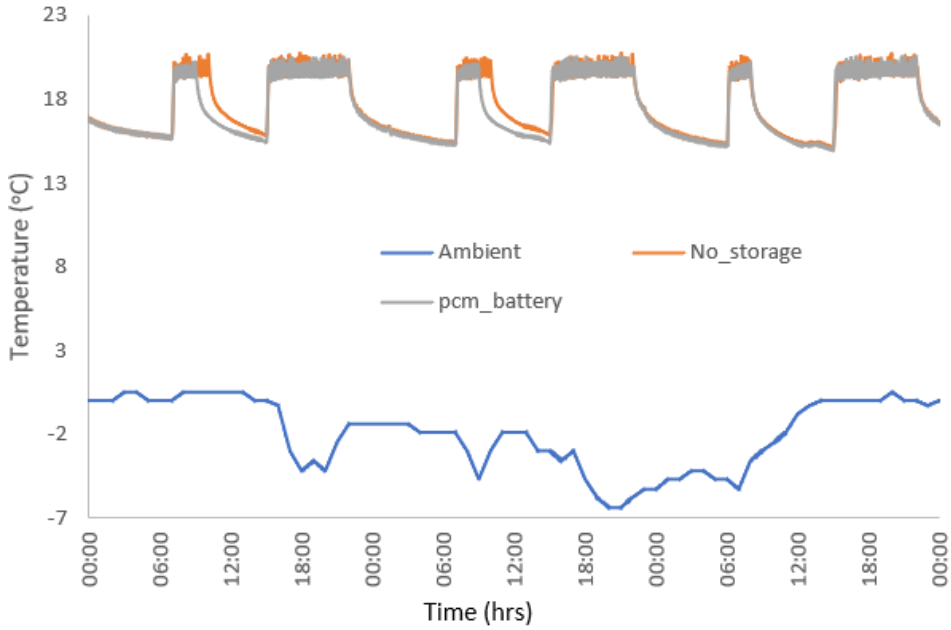

Figure 6.17: Heating system comparison – Living room dry bulb temperature – PCM battery vs base case

Figure 6,17 shows plot of dry bulb temperature of the living room, zone 'liv', for both heating systems over the coldest three (3) days of the simulation period (7th to 9th Jan), along with plot of ambient dry bulb temperature during the same period. As can be seen from the figure, the zone temperature plots are almost identical but for the shorter clusters at beginning of days 7 and 8 for system with PCM battery. This shows that although the results show system (with PCM battery) not measuring up to the base case system with regards to percentage of simulation period zone temperatures were above required range, as depicted in Figures 6.14 to 6.16, this does not indicate diminished ability to provide heating for the dwelling as temperatures were maintained above 19.5^{o}C during most of the required, occupied, periods (for the living room). Unmet minutes, when zone temperature was below

19.5°C (shown in Table 6.6), for system with thermal storage was 1119 minutes, which is equal to 32.16% of the heating demand period for system with thermal storage, although less than 887 minutes and 25.49% of the heating demand period for system with no thermal storage.

Table 6.7: Unmet minutes for living room zone (PCM battery vs base case).

	No storage	Pcm battery
Time < 19.5 (min)	887.00	1119.00
% of occupied period	25.49	32.16

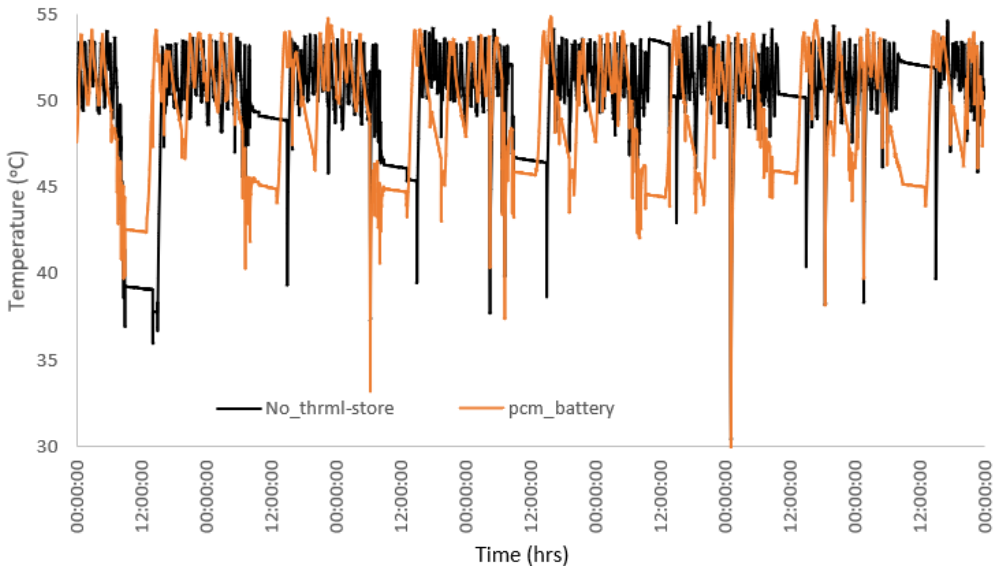

Figure 6.18: Heating systems comparison – Domestic hot water temperature during coldest 3 days of simulation period (7 – 9, Jan).

The difference in performance is also shown in Figure 6.18, which is plot of domestic hot water temperatures against time of the day for both heating systems. The system with thermal storage is clearly not as effective in maintaining temperature of domestic hot water within desired range, with temperature falling below the 43°C lower limit several times more compared to the base case system. These are however, for very short durations after the heat stored in PCM is depleted. According to Table 6.5, the heating system was able to maintain a minimum average domestic hot water temperature of 48.56°C all through the simulation period, which were the coldest periods of the year.

As revealed by Figures 6.11 – 6.18 and Tables 6.4 and 6.5, the heating system with thermal storage, whose operation is shifted to the off-peak energy demand period, is capable of meeting zones heating requirements comparatively to heating system with no thermal storage, operated during both peak and off-peak energy demand periods without back shifting. This demonstrates the effectiveness, or ability, of the thermal store to aid load shifting of heating systems operation, with possibilities for running the system entirely during the off-peak energy demand period, as well as savings on energy cost and reduction in greenhouse gas emissions.

It is obvious that the lower energy cost for system with thermal storage is attributable to its limited operation time, being constrained to operate within a ten hour period, 12:00 – 5:00 am; 1:00 pm – 4:00 pm and 8:00 pm – 10 pm, aided by the PCM thermal storage battery. Outside these times/periods, the heat pump is off and heating demand is supplied from the heat stored in the thermal store. This also explains the lower performance with regards to percentage of time zone temperatures are maintained above 19.5^{o}C in comparison to heating system whose operation was not restricted to the off-peak energy demand period (system with no thermal storage and no load shifting).

6.2.2 The Fabric Integrated PCM Thermal Storage Slab

Most applications for heating or cooling in buildings wherein PCMs are employed for thermal storage, they are used as passive systems. Reports detailing performance analysis and application PCM in passive systems include, among others, the works of Kasaeian et al. (2017), Cui et al. (2017), Frigione, Lettieri, & Sarcinella (2019) and Berardi & Soudian (2018).There are also evidence showing PCM applications in active thermal storage systems,

but mostly with under floor heating (Kalnæs & Jelle, 2015; Whiffen & Riffat, 2013; Ansuini, Roberto, Giretti, & Lemma, 2011) but very little on application in building walls.

The analysis discussed below is aimed at assessing performance of the fabric integrated heat storage model in application with building wall integrated heating system to determine effectiveness in load shifting applications. Like the analysis of system with the heat storage battery (test 2), the system performance will be assessed in terms of energy required to supply the heating demand of the dwelling, cost of the energy and energy equivalent amount of CO_2 emissions, comparing with heating system with no thermal storage (tests 1).

6.2.2.1 Plant Network Development and Building Model Simulation

The plant network of the building model employed for test 2, shown in Figure 6.6, was reconstituted and the PCM thermal storage battery was replaced with four fabric integrated thermal storage slabs for the wall installation and two for the floor installation. Four slabs were used because of limitations on the size of a single unit which must fit within wall construction while two were used for the floors because ground floor construction allowed more room for larger sized slabs.

So, for the wall installation, one slab each was installed in one wall within each of the bedrooms and two within walls in the living room (network depiction shown in Figure 6.19). The two slabs for the floor installation were installed within the floor of the living room.

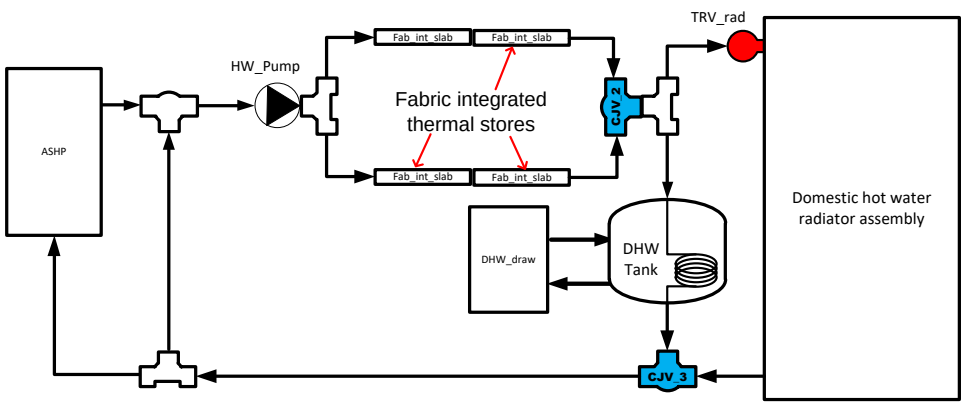

Figure 6.19: Plant network showing fabric integrated thermal store connections.

Each of the thermal storage slabs installed within walls was 3 m by 2 m by 0.1m, length, height and depth, respectively and are insulated by 0.03m. The slabs used for floor installation were each 3 m by 2.5 m by 0.15m, length, height and depth, respectively and are insulated by 0.08m of fibreglass wool insulation. Properties of PCM employed are those in Table 6.3. Reason for the PCM choice has been discussed.

Plant control strategy adopted for the simulations also restricted operations of the heat pump to the off-peak energy demand periods for economy 10 energy tariff, and its thermostatic control switch was set to power on in respond to temperatures of PCM in the thermal store. Operation of the circulation pump was also restricted to the occupied periods only in response to temperature in the living room, zone 'liv', between the same temperature range, and the general control for the domestic hot water radiators, which were set to maintain zone temperatures between 19.5^{o}C and 22.5^{o}C, was applied.

Simulations were run over the same three winter months for both types/versions of heating system and results were examined and analysed for zone temperatures, heating delivered and plant energy consumption, energy cost and mass of CO_2 equivalent, and compared with results from test 1 and 2. The analysis for wall installation was tagged test 3 and floor installation analysis was tagged test 4.

6.2.2.2 Results and Discussion

Summary analysis of the heating systems' performance, obtained from simulation results, tests 3 and test 4, are listed in table 6.7. Test 3 was simulation of heating system with PCM thermal storage in walls while test 4 was simulation of heating system with PCM thermal storage in floors. The table shows heat pump operating time, average energy consumption, energy cost and CO_2 equivalent of emission during each of the three (3) simulation months.

Table 6.8: Plant Result analysis and Systems comparison (PCM slabs) – Monthly averages.

	Ave. daily run time (min)	Ave. daily Energy use (kWh)	Monthly energy cost (£)	Ave. daily emission (kg of CO_2 Equiv.)
	With pcm in walls			
Dec	332.37	8.94	35.31	2.08
Jan	311.11	8.37	33.09	1.95
Feb	295.88	8.01	28.73	1.87
	With pcm in floors			
Dec	275.26	7.49	29.66	1.75
Jan	262.15	7.14	28.27	1.66
Feb	252.84	6.89	24.75	1.61

The heat pump for heating system with thermal store in walls was operational for a minimum daily average of 295.88 minutes, slightly higher than the 292.89 minutes for the base case system (Table 6.4), and minimum average daily consumption was 8.01 kWh, which is, however, slightly lower than 8.03 kWh for the base case system (Table 6.4). The mass of CO_2 equivalent emission is equal to that of the base case system, 1.87kg. These amounts to minimum monthly energy cost of £28.73, lower than £44.46 for the base case system.

For the system with PCM thermal storage in floors, minimum monthly daily average heat pump operating time was estimated as 252.84 mins, minimum daily average energy consumption of of 6.89 kWh, which equates to 1.61 kg of CO_2 equivalent minimum average daily emissions and an estimated minimum monthly energy cost of £24.75. This, in comparison with 292.89 min. operating time, 8.03 kWh minimum daily energy consumption, 1.87 kg of CO_2 equivalent emission and £44.46 monthly energy cost for the base case system, show considerable reduction in energy cost and emission.

The lower cost of energy for these systems relative to the base case system is also due to the constrained operating period of ten (10) hours for the heat pumps (12:00 and 5:00 am; 1:00 pm and 4:00p pm, and 8:00 pm and 10 pm), and the lower cost of energy during these periods, as observed with system with PCM battery.

Additional findings from the tests are given in Table 6.8, which contains summary results of mean/average zone dry bulb temperatures, maximum heating load, total heat delivered to meet heating requirements of dwelling and average domestic hot water temperature for each of the simulation months.

Table 6.9: Result analysis and *Summary findings (PCM slabs).*

	Mean zone temp (°C)	Max Heat Load (kW)	Total heating delivered (kWh)	Ave hot water temp (°C)
Test 3 (with wall PCM slabs)				
Dec	19.2	5.4768	502.33	50.32
Jan	19.17	5.3463	524.36	50.44
Feb	19.31	4.7666	375.2	49.81
Test 4 (with floor PCM slabs)				
Dec	19.21	5.8456	502.72	50.05
Jan	19.17	5.3865	524.03	50.72
Feb	19.32	5.5124	375.52	50.07

Compared with summary results from test 1 (the base case) in Table 6.5, Table 6.8 shows a slightly lower heat delivery by both systems to meet heating demand by dwelling. This explains the lower average zonal temperatures relative to the base case. Also, the thermal storages introduced additional heating load on both systems, as depicted by the peak heating loads being higher than for the base case system.

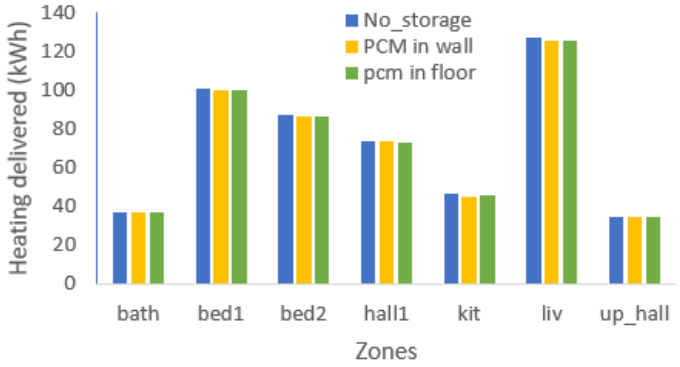

Figure 6.20: Heat delivered to meet zone heating requirement (December)

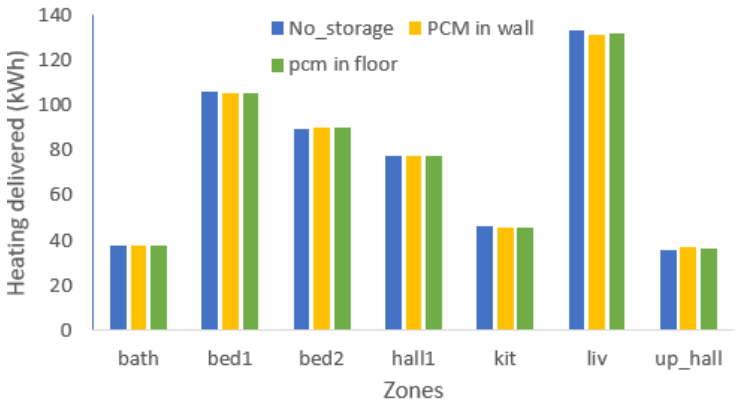

Figure 6.21: Heat delivered to meet zone heating requirement (January)

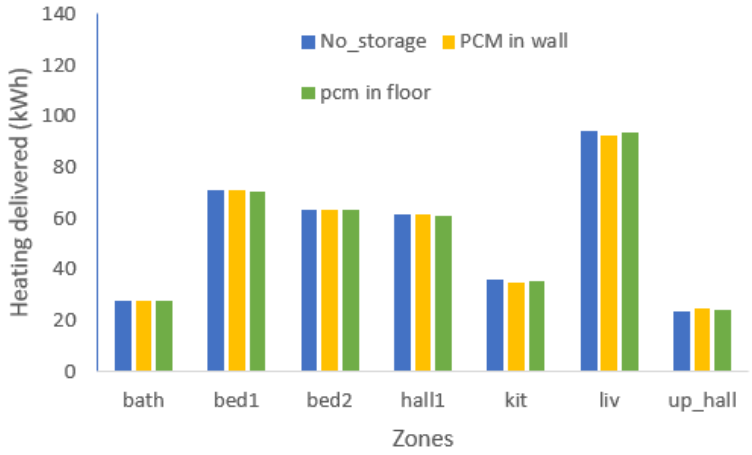

Figure 6.22: Heat delivered to meet zone heating requirement (February)

Further comparison between the two systems (thermal storage in walls and floors) and the base case (no thermal storage) system is done with Figures 6.20 to 6.22, which are plots of energy delivered to each zone and Figures 6.23 to 6.25, which are plots of percentage of time zone dry bulb temperatures were maintained above 19.5^{o}C over each of the simulation months.

While the figures show small differences between the systems (with thermal storage) and the base case system (no thermal storage), they, nevertheless show how close the two heating systems came to meeting heating demands of individual zones in comparison with the base case system, notwithstanding the lower values for mean/average zone temperatures, lower total heat delivery and higher peak heating loads, relative to the base case system, as shown in table 6.8.

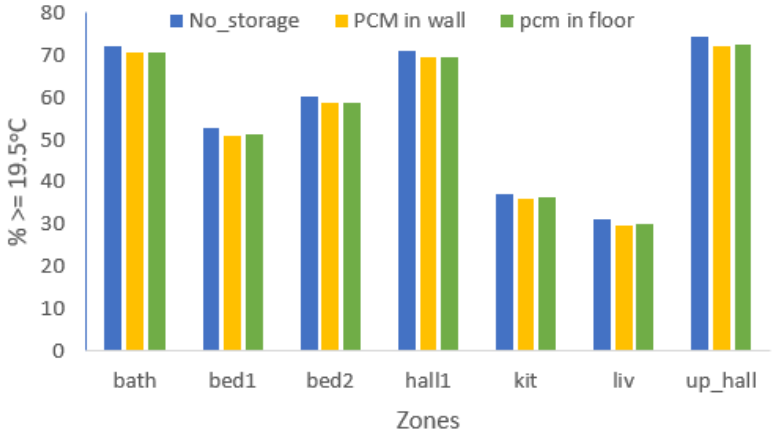

Figure 6.23: % of time zone temp >19-5°C (December)

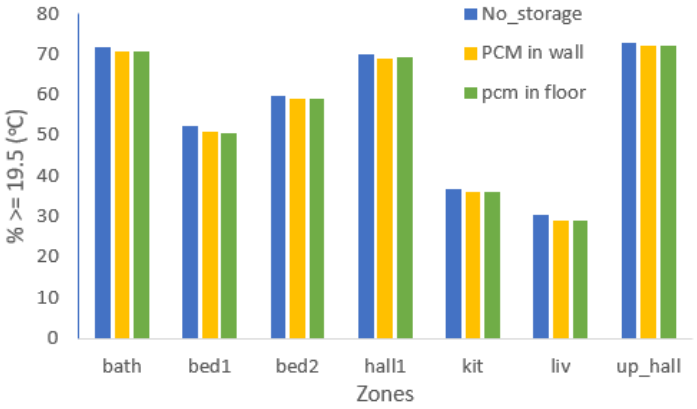

Figure 6.24: % of time zone temp >19-5°C (January)

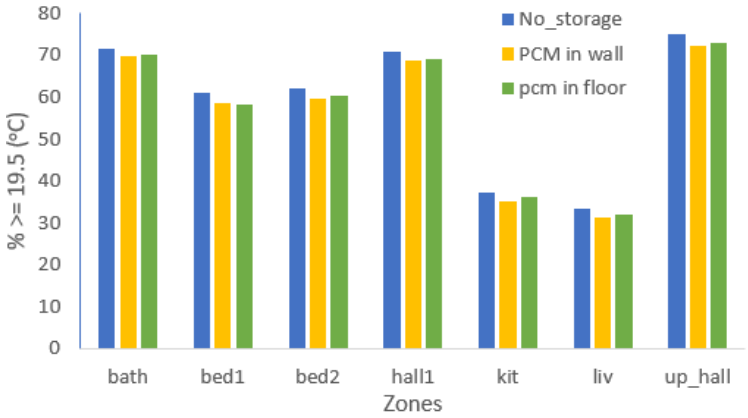

Figure 6.25: % of time zone temp >19-5°C (February)

This is indication that the systems with the thermal storage within building fabric, wherein heat pump was operated only during the off-peak energy demand periods, are capable of maintaining zone temperatures within desired levels for reasonable proportion of the time when compared to system with no thermal storage.

Comparative performance of the two heating systems relative to the base case systems is further emphasised with Figures 6.26 and 6.27, and Table 6.9, which represent a snapshot of performance data from simulation results for the coldest week of the simulation year, 3rd to 9th January. Figures 6.26 and 6.27 are plots of dry bulb temperatures of the living room, zone 'liv', and ambient temperatures, during the coldest three (3) days, 7th – 9th Jan, only and temperatures of water in domestic hot water tank respectively while Table 6.9 lists number of minutes the zone temperatures were below 19.5°C mark and the percentage of heating demand period they constituted. Both figures contain similar plots from the base case heating system.

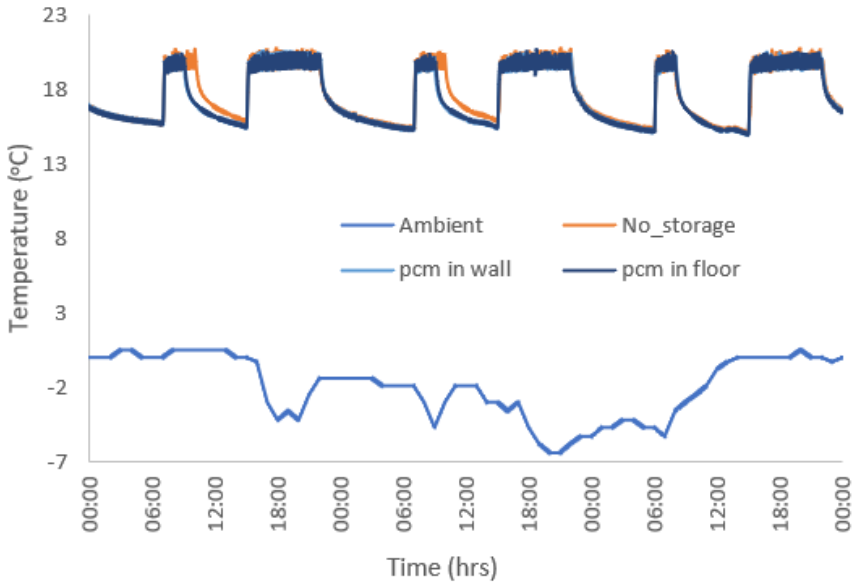

Figure 6.26: Heating system comparison – Living room dry bulb temperature – PCM slabs

The plot shows that zone temperatures are clearly above 19.5°C during most of the occupied periods for the zone, showing ability of the heating systems, which were operated during the off-peak energy demand period, to maintain desirable conditions within the dwelling. Total unmet minutes for both systems (Table 6.9) are 1060 min, thermal storage in walls, and 1046 min, thermal storage in floors, which make up 30.46% and 30.06% of heating demand

periods, PCM in walls and PCM in floors respectively. This contrasts with 887 min unmet minutes that make up 25.49% of heating demand period (table 6.6).

Table 6.10: Unmet minutes for the living room *(PCM slabs).*

	pcm in wall	pcm in floor
Time < 19.5 (min)	1060.00	1046.00
% of occupied period	30.46	30.06

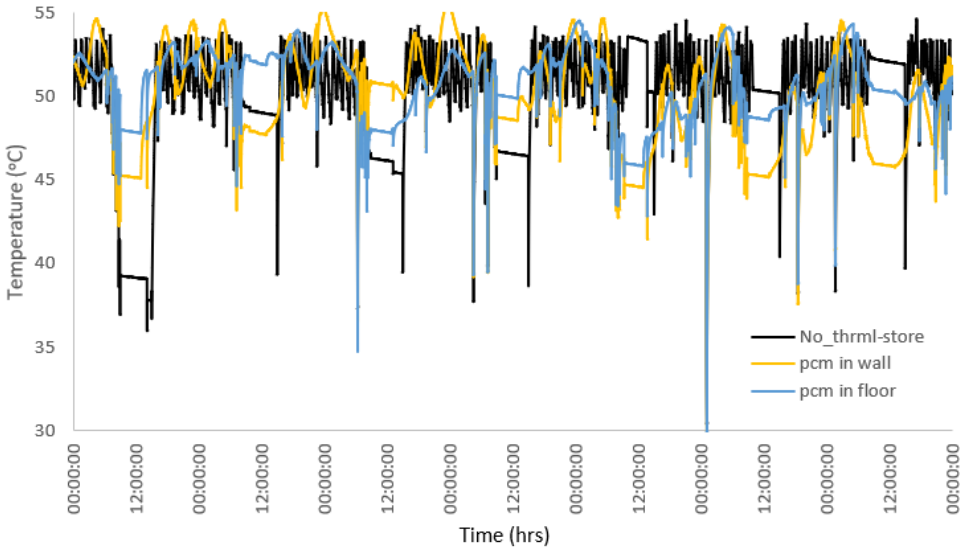

Figure 6.27: Heating systems comparison – Domestic hot water temperature profile.

Profile of the domestic hot water temperatures (Figure 6.27) show occasional momentary drops in temperatures below the 43^{o}C lower limit for the heating systems with thermal storage. Nevertheless, hot water at temperatures above the desired level was available for most of the occupied periods for the dwelling. This further establishes that the heating systems can provide sufficient heating for the dwelling while operating only during the off-peak energy demand period. It shows that application of the thermal storage (PCM) was effective in shifting energy consumption away from the peak energy demand period to the off-peak demand period with little compromise to heat delivery, zone temperatures maintenance withing desired limit and hot water availability at desired temperatures. There is also the added advantage of lowering energy cost and greenhouse gas emissions.

6.3 Case Study 2 – Comparison with Sensible Heat Thermal Storage Systems

The PCM thermal storage systems employ PCM, a latent heat thermal storage material, for storing heat. One of the motivations for research into PCMs and other latent heat thermal energy storage systems is the possibility of employing them as substitute, or replacements for sensible heat thermal systems due, in large, to their higher thermal storage capacities or density over relatively small temperature ranges, allowing storage of more heat/energy per unit mass and volume. This implies smaller, lighter and more compact storage systems. Several authors have undertaken and reported on comparative analysis between systems employing latent heat thermal storage systems and sensible heat thermal storage systems (Foudhil et al., 2012; Wang, Faghri, & Bergman, 2012) with a consensus that in spite of some challenges with properties of some phase change materials, systems employing them still show considerable improved performance.

Here, a comparison between the two (2) PCM thermal storage systems and comparable sensible heat storage systems was undertaken. The PCM heat storage battery was compared to conventional hot water storage system (buffer tank) while the fabric integrated thermal storage slab was compared to active thermal mass heat storage system with similar installation.

Simulation of the sensible heating systems was accomplished using the same building model described in section 6.1.1. and reconstituting the plant networks to replace the latent heat thermal storage plants (systems) with comparative sensible heat storage plant (systems). That is, the PCM heat storage battery was replaced by hot water storage tank and the fabric integrated PCM thermal storage slabs were replaced by thermal masses. The results obtained from simulation of these models were analysed for energy consumed to provide heating for

the dwelling, energy cost and equivalent mass of CO_2 emission, and compared to results obtained from earlier simulations of the latent heat thermal storage systems, tests 2, 3 and 4 (section 6.2).

While the analysis conducted here does not attempt to re-prove or validate a proven fact about performance of latent heat storage systems over sensible heat storage systems, it serves as a means of further validating the thermal storage models, showing conformity of their results with established findings and demonstrating their usefulness for the intended purpose.

6.3.1 Hot Water Tank Storage Tank sizing

A hot water storage tank, represented by a similar stratified tank model as the domestic hot water tank reported by Padovan & Manzan (2013), and similarly heated indirectly by the heat pump through an internal heating coil at its bottom, is employed for the study. Sizing of the tank was accomplished by estimating the volume of water that can store amount energy required to supply maximum heating energy demand by the dwelling (Table 6.4) obtained from test 1. This was estimated as 7.0 m^3 to be contained in a water storage tank 2.75 and 1.8 m in diameter

6.3.1.1 Simulation of Model with Hot Water Storage Tank

The general control for the domestic hot water radiators, maintaining zone temperatures between 19.5^{o}C and 22.5^{o}C, was again applied and the ASHP operations was restricted to the off-peak energy demand periods for economy 10 tariff, with its thermostat is set to respond to temperature in zone ‘liv’, so that it is powered on when value is below 19.5^{o}C and off when it rises above 22.5^{o}C. Operation of the circulation pump was restricted to the occupied periods also in response to temperature in zone ‘liv’ between 19.5^{o}C and 22.5^{o}C. Simulations were run for the model over the same winter months, December, January and February (tagged test 5), and results were examined and analysed for zone temperatures, energy delivered and plant

energy consumption and energy cost and CO_2 emission, and compared to results from test 2, heating system with PCM heat storage battery.

6.3.1.2 Results and Discussion

Analysis of plant results from simulation and comparison between the heating systems, deploying latent heat thermal storage (PCM thermal storage battery) and system deploying sensible heat thermal storage (hot water storage tank), is shown in Table 6.10. The table contains average monthly energy cost, monthly energy consumption, CO_2 equivalent of emission and total operating time for the heat pumps in both systems during each of the three simulation months determined from simulation results.

Table 6.11: Plant Result analysis and System comparison (PCM vs HWS) – Monthly averages

	Ave daily run time (min)	Ave. daily Energy use (kWh)	Monthly energy cost (£)	Ave daily emission (kg of CO_2 Equiv.)
	With pcm battery			
Dec	247.73	6.74	26.71	1.57
Jan	255.52	6.95	27.51	1.62
Feb	241.91	6.60	23.67	1.54
	With HWS			
Dec	252.03	6.82	27.02	1.59
Jan	264.84	7.15	28.33	1.67
Feb	243.11	6.62	23.73	1.54

From the table, the heating system employing sensible heat thermal storage (water) is seen to have a slightly higher average daily minimum operating time, 243.11 min, consumes a little more energy, at minimum average of 6.62 kWh per day, is a bit more expensive to run, with minimum average monthly energy cost of £23.73. This is in comparison to system employing latent heat thermal storage (PCM) which operates at minimum average of 241.91 min per day, consumes energy at minimum average of 6.60 kWh/day and cost a minimum average of

£23.67 monthly to run. Both however, produce the same quantity of emission,1.54 kg of CO_2 equivalent.

Table 6.12: Result Analysis and Summary findings from test 5

	Mean zone temp (°C)	Max Heat Load (kW)	Total heating delivered (kWh)	Ave hot water temp. (°C)
Dec	19.18	5.508	500.37	47.2
Jan	19.13	5.4114	522.18	46.96
Feb	19.32	4.9312	375.08	46.92

Further summary and analysis of simulation results for model with hot water storage tank as thermal store only, is listed in Table 6.11. Comparisons between the two systems and the base case system are shown in Figures 6.28 to 6.33.

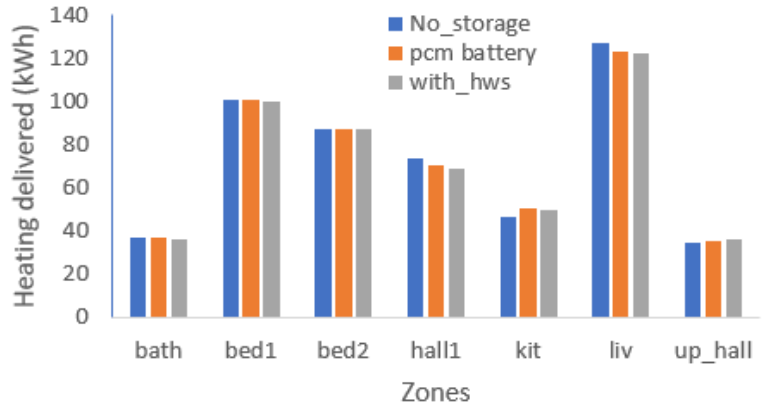

Figure 6.28: Comparison of heat delivered to meet zonal energy demand – December.

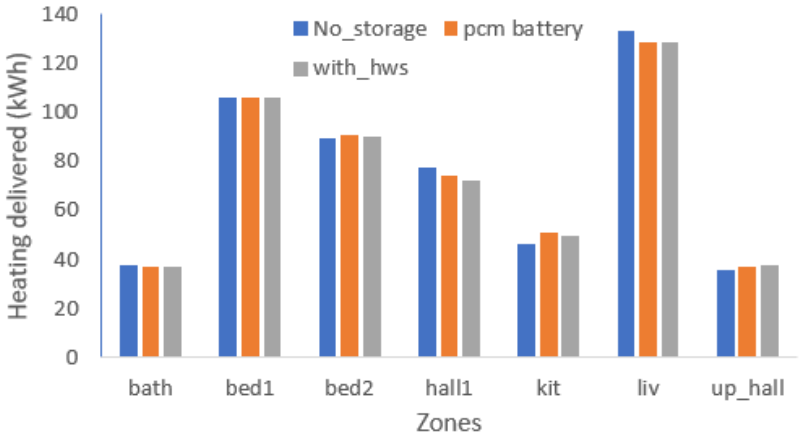

Figure 6.29: Comparison of heat delivered to meet zonal energy demand – January.

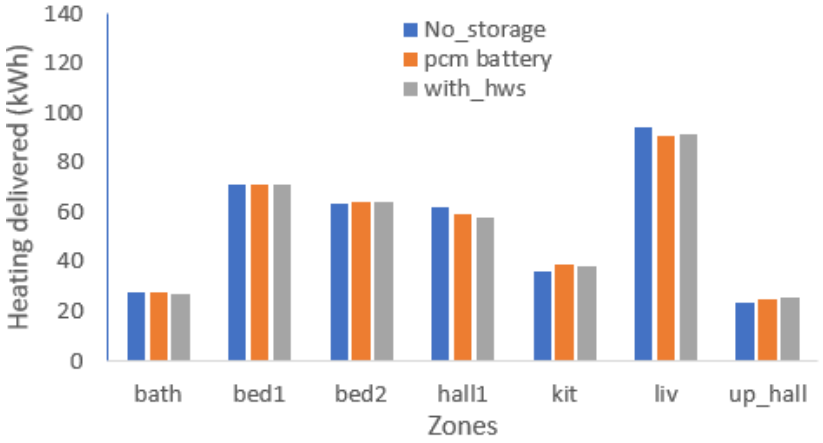

Figure 6.30: Comparison of heat delivered to meet zonal energy demand – February.

Figures 6.28 – 6.30 compare energy supplied by each system to meet heating requirement of each zone of the dwelling while Figures 6.31 – 6.33 compare percentages of simulation period zone dry bulb temperatures were maintained at and above 19.5°C. They show relative balance in performance between both systems with thermal storage, with each outperforming the other in equal number of zones. Both systems also performed comparatively well, overall, compared with the base case heating system (no thermal storage).

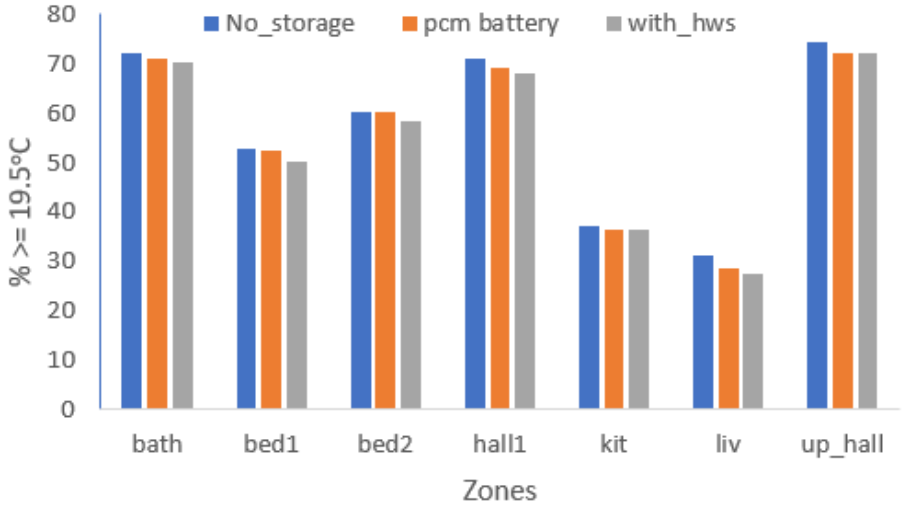

Figure 6.31: % of period zone temp >= 19-5°C – December.

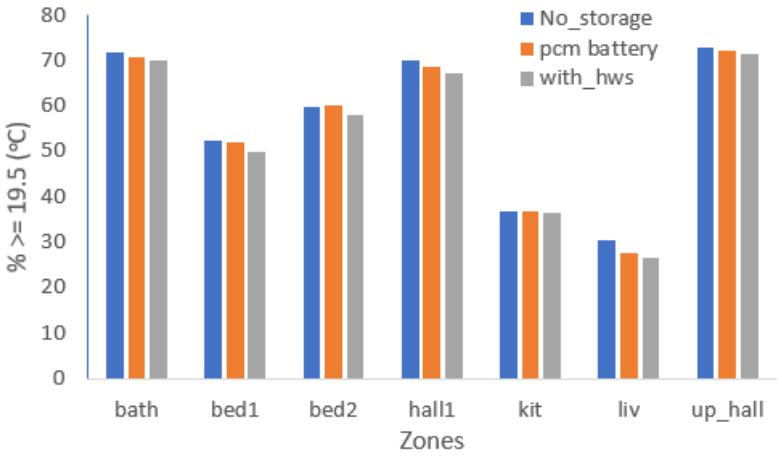

Figure 6.32: % of period zone temp >= 19-5^{o}C – January.

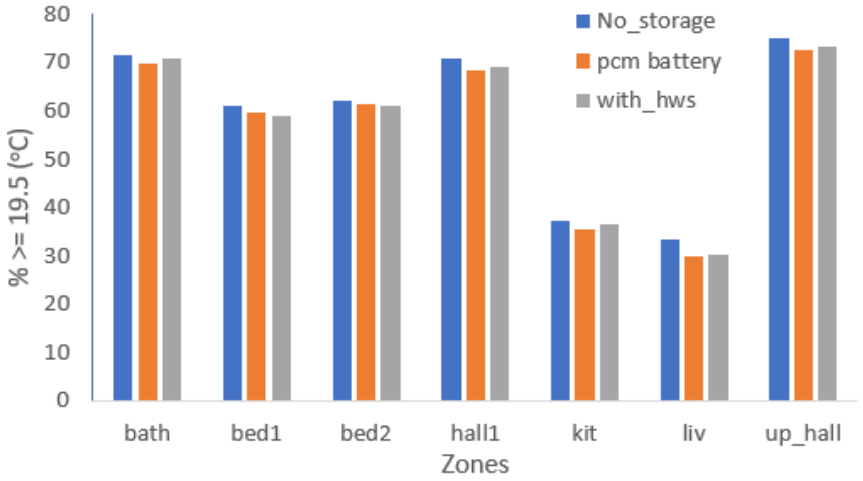

Figure 6.33: % of period zone temp >= 19-5^{o}C – February.

Comparative performance of the heating systems is further demonstrated in Figures 6.31 to 6.33. Dry bulb temperatures of zones were maintained above 19.5^{o}C for almost equal percentages of the time for all the zones and simulation months for both systems, except for the month of February when systems employing hot water as thermal store performed slightly better than system with PCM battery, almost at par with that of the base case system for most of the zones. This is, however, not indicative of the system's superior performance in comparison with system employing PCM battery, as demonstrated earlier with Table 6.110 and will be further demonstrated below.

Further analysis of plant results too focus on the week with lowest ambient temperatures during the simulation period, week beginning from 3rd to 9th of January, that is Figures 6.34 and 6.35, plots of dry bulb temperatures of the living room (7th – 9th) and temperature of water in domestic hot water tank, show very close performance, as the zone temperature profiles, for systems with thermal storage, of Figure 6.34 are clearly indistinguishable except for the evening of day 8. The visible dip in profile for system with hot water storage tank show its lower performance. Nevertheless, both systems still fall short of performance of the base case system.

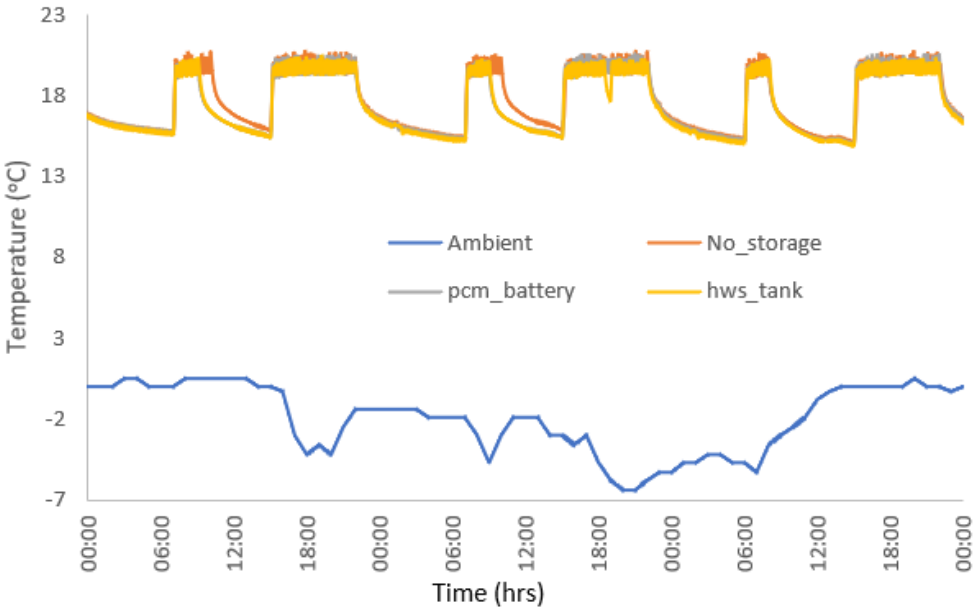

Figure 6.34: Heating system comparison – Living room dry bulb temperature – PCM battery vs HWS tank

Table 6.13: Unmet minutes for living room zone (PCM battery vs HWS tank).

	Pcm battery	HWS tank
Time < 19.5 (min)	1225.00	1237.00
% of occupied period	35.20	35.55

Unmet minutes for system with PCM battery was 1225 min, lower than unmet minutes for system with HWS tank, 1237 min, both of which equate to 35.2% and 35.55% of the heating demand period for system with thermal storage and system with HWS tank respectively.

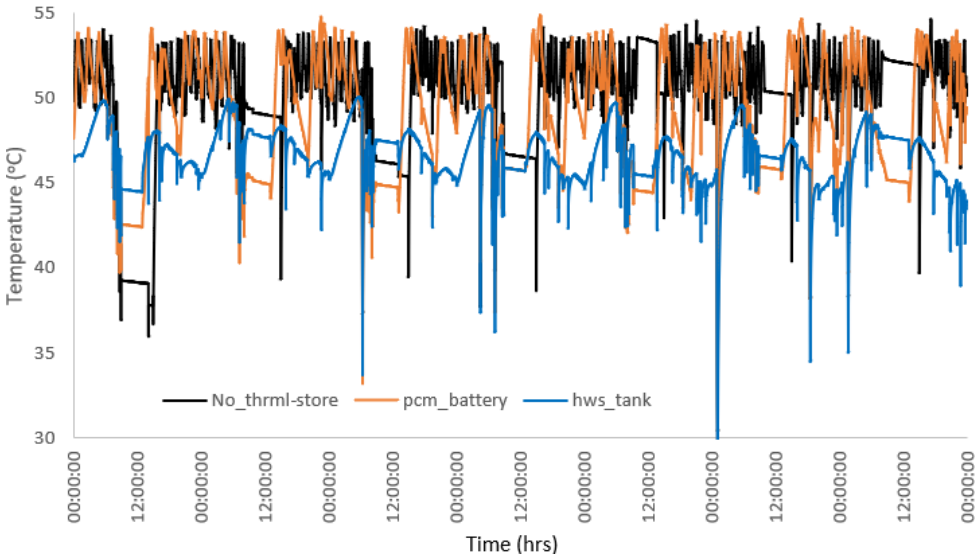

Figure 35: Heating system comparison – PCM battery vs HWS tank.

Figure 6.35 show the heating system with PCM battery as being also more effective at providing hot water in comparison with the hot water storage tank system. Both systems were, nevertheless, effective in maintaining hot water temperatures above the 43.5^{o}C levels for most of the occupied periods.

Overall, the system employing water as thermal, sensible, store show a lower performance in comparison with system employing PCM, latent, thermal storage. The superior performance of system with PCM battery can be appreciated more when the difference in size and bulk of both systems is taken into consideration. Water used for sensible heat thermal storage (estimated from maximum heating load estimate for base case system) was contained in a tank with height of 2.75 and diameter 1.8 m while the PCM employed for the latent heat thermal storage is contained in a tank 2 m in height and 1.55 m shell diameter. These results, and the distinct difference in the size of the hot water tank relative to size of the PCM battery, agree with established findings and conclusions (common knowledge) regarding comparison between heating systems employing hot water storage tanks for heat storage and heating systems employing phase change materials for heat storage.

6.3.2 Fabric Integrated Thermal Mass Storage Systems

As at the time of concluding this research work, there are no active building wall integrated sensible heat storage systems in ESP-r. Subsequently, the fabric integrated PCM thermal storage slab model was employed for simulating thermal mass system integrated into walls and floors after substituting the properties of PCM (in the plant) with those of a construction material used for building walls and floors, obtained from ESP-r construction material database.

The same property values were used for both solid and liquid material, and values chosen for the specific latent heat of fusion and melting (phase change) temperature used are fictitious, and very high, to ensure that the materials remain in the solid phase throughout the simulations. Thus, energy supplied through the air source heat pump would never be enough to raise temperature and heat energy content of the material beyond the level required for phase change. This way, heat energy can only be stored as sensible heat.

Table 6.14: Properties of construction material used as thermal mass.

Property description	Values	
	Wall	Floor
Melting temp range (^{o}C)	1000	1000
Specific Latent heat of fusion(J/kg)	$1x10^{10}$	$1x10^{10}$
Specific heat capacity (J/kgK)	2930	840
Thermal conductivity (W/mK)	0.19	0.41
Density (kg/m3)	700	1200

The material employed as thermal mass for wall integrated system is a single component wall construction material tagged ‘mass_part’ in ESP-r database while the material employed for floor installation is a concrete slab, one of the components of the slab-on-grade floor over concrete slab with XPS insulation used for floor construction of the building model (section 6.1.1.2). Thermal properties of the materials are listed in table 6.13.

6.3.2.1 Simulation of Model with Thermal Mass Heat Storage in Walls

The same building model, and plant network, employed for test 4 (section 6.2.2) was used for simulating building model with active wall integrated thermal mass heating system after editing properties of the PCM thermal storage slabs to reflect properties of the construction material listed under 'Wall' in table 6.6. The size and location of the components in each of the zones (rooms) remain the same (section 6.2.2) and the same plant control strategy was adopted, that is, ASHP operating during the off-peak energy demand periods for economy 10 tariff and powering on and off in response to temperature in the living room, zone 'liv' between 19.5^{o}C and 22.5^{o}C. The circulation pump operation was also restricted to the occupied periods and the general control strategy for the domestic hot water radiators' flow control valves was adopted. The simulation, tagged test 6, was run over the same winter week, 3rd – 9th January and the result were examined and analysed for zone temperatures, energy delivered and plant energy consumption, energy cost and CO_2 emission.

6.3.2.2 Results and Discussion

Table 6.15 Plant Result analysis and System comparison (PCM vs thermal mass - walls) – Monthly averages

	Ave daily run time (min)	Ave. daily Energy use (kWh)	Monthly energy cost (p)	Ave daily emission (kg of CO_2 Equiv.)
	with pcm in walls			
Dec	332.37	8.94	35.31	2.08
Jan	311.11	8.37	33.09	1.95
Feb	295.88	8.01	28.73	1.87
	with thermal mass in walls			
Dec	303.79	8.16	32.27	1.90
Jan	311.34	8.38	33.14	1.95
Feb	321.41	8.69	31.13	2.03

Plant results analysis and comparison of the heating systems, latent and sensible heat fabric integrated thermal storage in walls, is shown in Table 6.14. It lists estimates of average monthly energy cost, monthly energy consumption, CO_2 equivalent of emission and total

operating time for the heat pumps in both systems during each of the three simulation months determined from simulation results.

For system with latent heat (PCM) thermal storage, minimum average heat pump running time was estimated from simulation results as 295.88 min/day compared to 321.41 min/day for system with sensible heat (thermal mass) thermal storage. Minimum average daily energy consumption was estimated at 8.01 kWh and 8.16 kWh for system with latent heat thermal storage and system with sensible heat thermal storage, respectively while minimum cost of running both systems and minimum CO_2 equivalent emissions are £28.73 and 1.87 kg of CO_2 equivalent, respectively, for system with latent heat thermal storage, and £31.13 and 1.90 kg of CO_2 equivalent, respectively, for system with sensible heat thermal storage.

List of key findings from simulation results for only system with sensible heat thermal storage (thermal mass) in walls is given in Table 6.15.

Table 6.16: Result analysis and Summary findings (thermal mass in walls)

	Mean zone temp (^oC)	Max Heat Load (kW)	Total heating delivered (kWh)	Ave hot water temp (^oC)
Dec	19.20	5.0206	501.99	50.35
Jan	19.16	5.1414	523.88	50.45
Feb	19.30	4.8814	374.77	49.95

Compared with summary results from test 3, for heating system with fabric integrated PCM thermal store in walls (latent heat storage) in Table 6.8, heating load/demand and heat delivery to meet heating demand for dwelling appear relatively equal for both systems, as well as the average domestic hot water temperatures.

A comparing total energy delivered to each zone over each simulation month and percentage of time zone temperatures were maintained above 19.5^oC for both systems, Figures 6.36 to 6.41, also show almost equal performances, and close to that of the base case system.

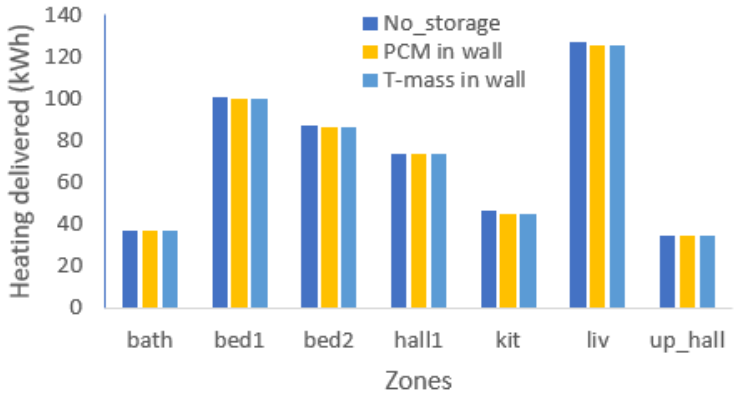

Figure 6.36: Comparison of heat delivered to meet zonal energy demand – December.

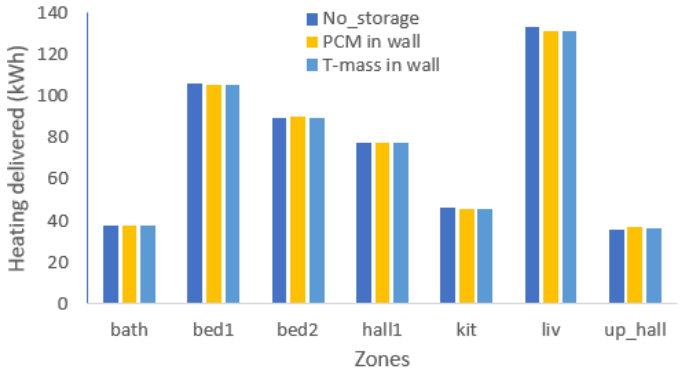

Figure 6.37: Comparison of heat delivered to meet zonal energy demand – January.

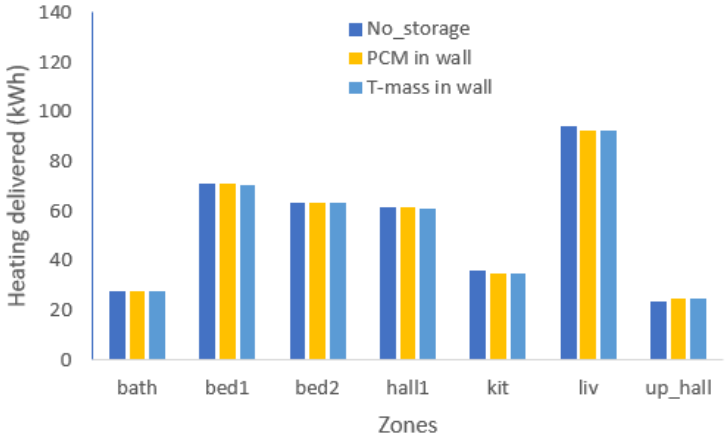

Figure 6.38: Comparison of heat delivered to meet zonal energy demand – February.

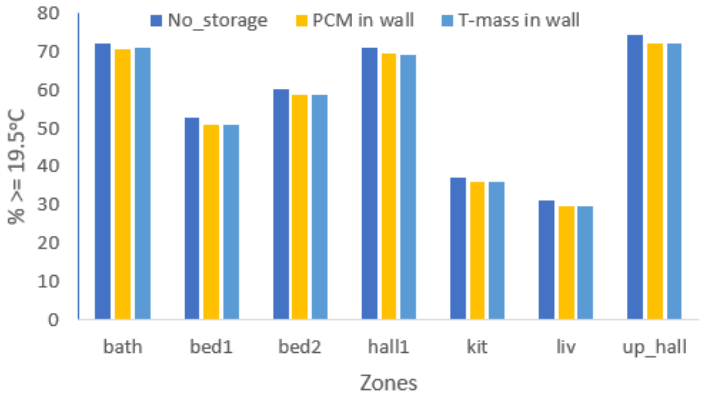

Figure 6.39: % of period zone temp >= 19-5°C – December.

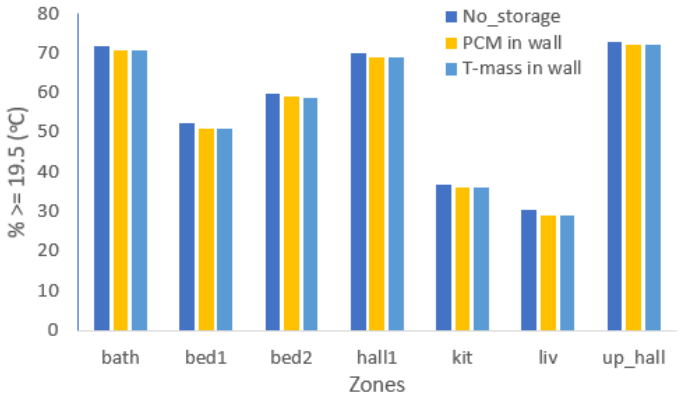

Figure 6.40: % of period zone temp >= 19-5°C – January.

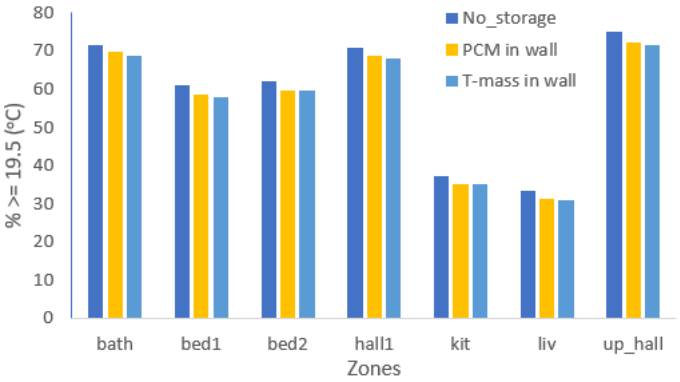

Figure 6.41: % of period zone temp >= 19-5°C – February.

Analysing performance data during week with lowest ambient temperatures of the simulation period, week beginning from 3rd to 9th of January, using plots of dry bulb temperature profiles of the living room, zone 'liv' (for only the tree coldest days, 7th – 9th) and temperature of water in domestic hot water tank (Figures 6.42 and 6.43), the very closeness in performance of the systems is further revealed. The zone temperature profiles for the two system with thermal storage indistinguishable from each other and also bear close

resemblance to zonal temperature profile from the base case systems. This shows effectiveness of both systems in maintaining zone temperatures within desired levels.

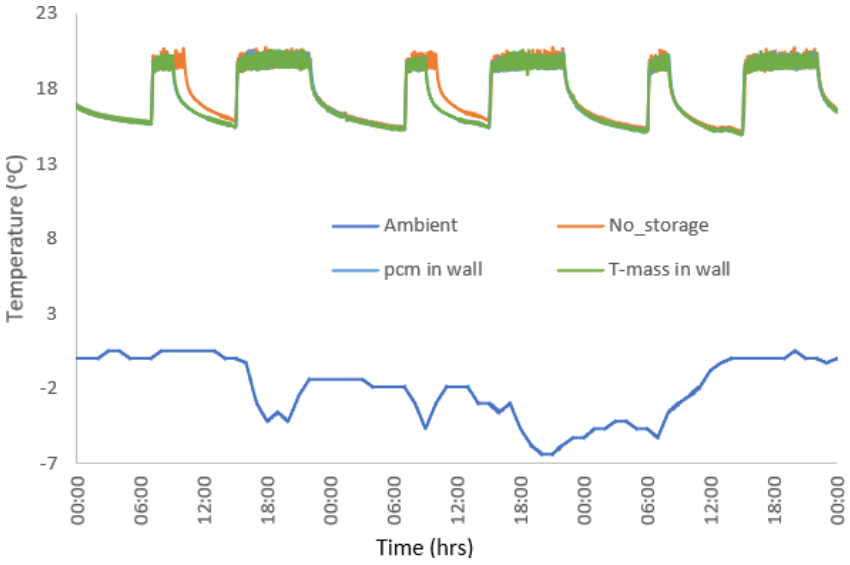

Figure 6.42: Heating system comparison – Living room dry bulb temperature – Latent vs sensible heat thermal store

The difference between the systems is however revealed in the number of minutes temperatures of the living room zone fell below the 19.5^{o}C mark listed, unmet minutes, in Table 6.16. This was estimated at 1060 min for system with latent heat thermal storage and 1045 min for system with sensible heat thermal storage, equivalent to 30.46% and 30.03% for latent heat systems and sensible heat systems respectively.

Table 6.17: Unmet minutes for the living room *(PCM slabs).*

	pcm in wall	T-mass in wall
Time < 19.5 (min)	1060.00	1045.00
% of occupied period	30.46	30.03

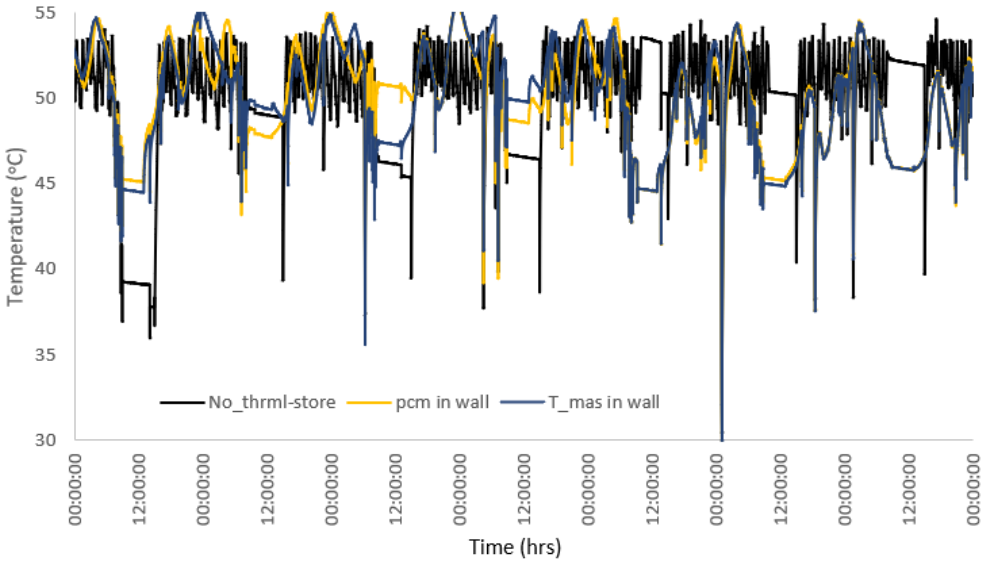

Figure 6.43: Heating system comparison – Domestic hot water temperature.

Despite the higher number of unmet minutes, the system deploying latent heat thermal storage displays a slightly greater effectiveness in maintaining hot water temperatures at desired range at certain periods compared with system deploying sensible heat thermal storage, as shown in Figure 6.43. Both systems were equally able to maintain the temperatures above the 43.5°C levels for the most part of the occupied periods.

6.3.2.3 Simulation of Model with Thermal Mass Heat Storage in Floors

Simulation of model with underfloor thermal mass heating system was similarly done using the building model and associated plant network used for test 7 (section 6.2.2) after editing the properties of PCM thermal storage slabs to reflect the properties of the construction material listed under 'Floor' in table 6.10.

Also, the size and location of the thermal stores in each of the zones (rooms) were not changed and the same plant control strategy for the ASHP, the circulation pump and the hot water radiators was adopted. The simulations, tagged test 7, were also run over the same winter months of December, January and February, and the result were examined and analysed for zone temperatures, energy delivered and plant energy consumption energy cost and CO_2 emission.

6.3.2.4 Result and Discussion

Summary analysis of plant results from simulation of the two heating systems with fabric integrated thermal storage in floors (latent heat and sensible heat thermal storage) is shown in Table 6.17. The table contains estimates from heat pump performance data for average monthly energy cost, monthly energy consumption, CO_2 equivalent of emission and total operating time for the heat pumps in both systems during the simulation months.

Table 6.18: Plant Result analysis and System comparison (PCM vs thermal mass - floors) – Monthly averages

	Ave daily run time (min)	Ave. daily Energy use (kWh)	Monthly energy cost (£)	Ave daily emission (g of CO_2 Equiv.)
	with PCM in floors			
Dec	275.26	7.49	29.66	1.75
Jan	262.15	7.14	28.27	1.66
Feb	252.84	6.89	24.75	1.61
	with thermal mass in floors			
Dec	290.05	7.87	31.13	1.83
Jan	278.79	7.57	29.95	1.76
Feb	293.80	7.98	28.62	1.86

Minimum average heat pump running time estimate for system with latent heat (PCM) storage was 252.84 min/day compared to 278.79 min/day for system with sensible heat (thermal mass) storage while minimum average daily energy consumption was estimated at 6.89 kWh and 7.57 kWh, system with latent heat storage and system with sensible heat storage, respectively. The estimates for minimum energy cost and CO_2 equivalent emissions were £24.75 and 1.61 kg, respectively, for system with latent heat storage, and £28.62 and 1.76 kg, respectively, for system with sensible heat storage.

Key findings from simulation of model with thermal mass heat storage only are listed in table 6.18. Comparing with results for system with latent heat storage (system with PCM in floor) listed in Table 6.8, performances of the systems are also comparatively equal.

Table 6.19: Result analysis and Summary findings (thermal mass in floors)

	Mean zone temp (°C)	Max Heat Load (kW)	Total heating delivered (kWh)	Ave hot water temp. (°C)
Dec	19.2	5.3817	502.03	50.64
Jan	19.16	5.4352	523.96	50.52
Feb	19.31	5.5713	374.97	50.01

The close performance is also depicted in Figures 6.44 and 6.49, which are plots of energy delivered to each zone and percentage of time zone temperatures were maintained above 19.5°C over each of the simulation month (along with similar plots from the base case system).

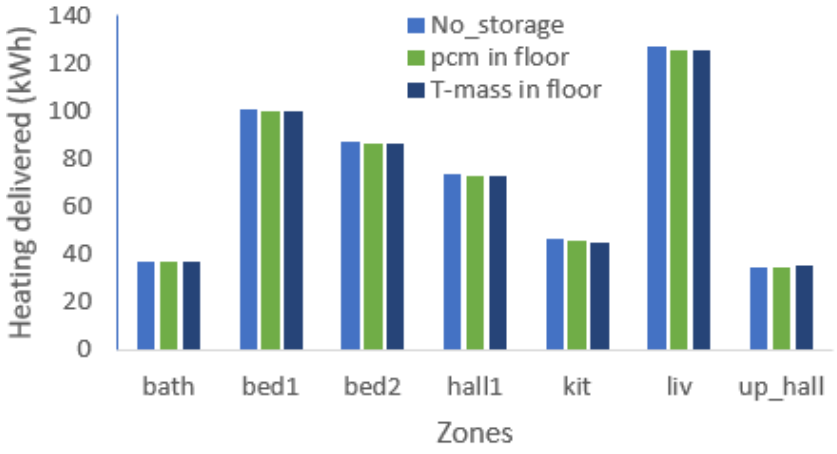

Figure 6.44: Comparison of heat delivered to meet zonal energy demand – December

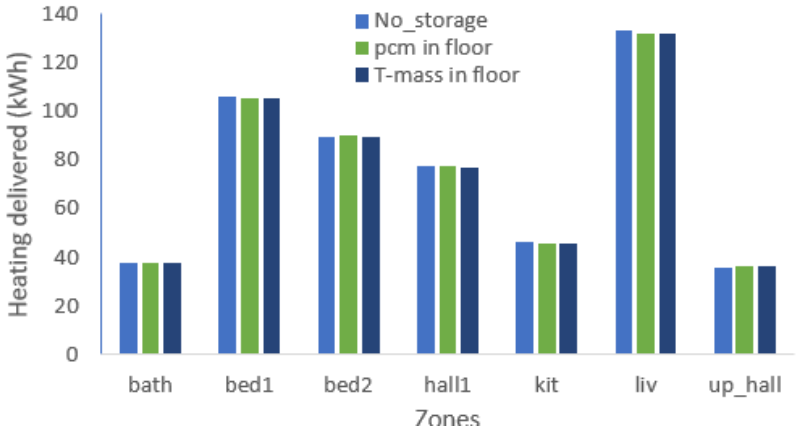

Figure 6.45: Comparison of heat delivered to meet zonal energy demand – January

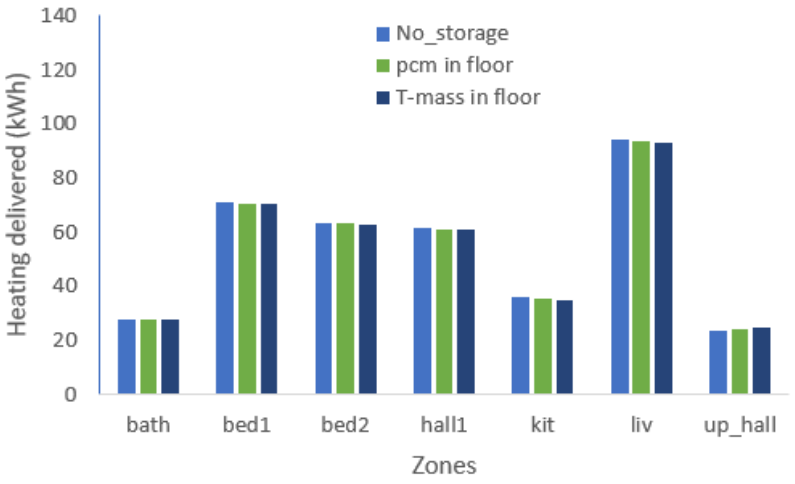

Figure 6.46: Comparison of heat delivered to meet zonal energy demand – February

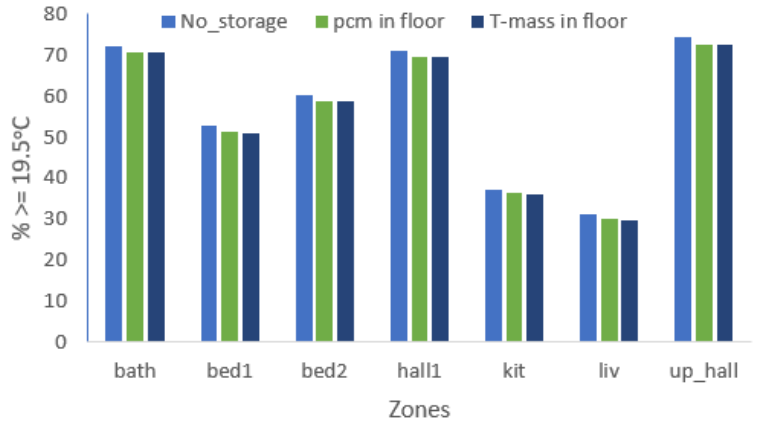

Figure 6.47: % of period zone temp >= 19-5°C – December.

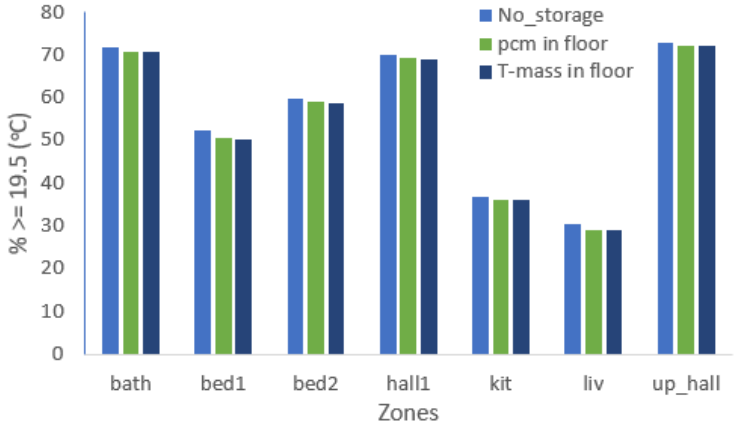

Figure 6.48: % of period zone temp >= 19-5°C – January.

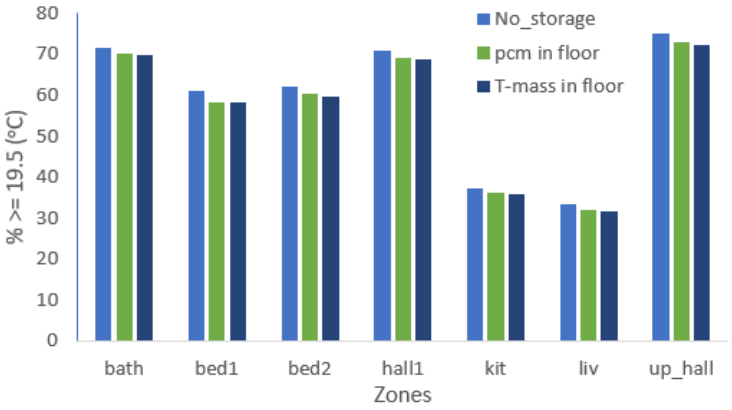

Figure 6.49: % of period zone temp >= 19-5°C – February.

The figures show the very close performances by the two systems (with thermal storage in floors) for both heating delivery and percentage of time zone dry bulb temperatures were maintained at and above 19.5°C.

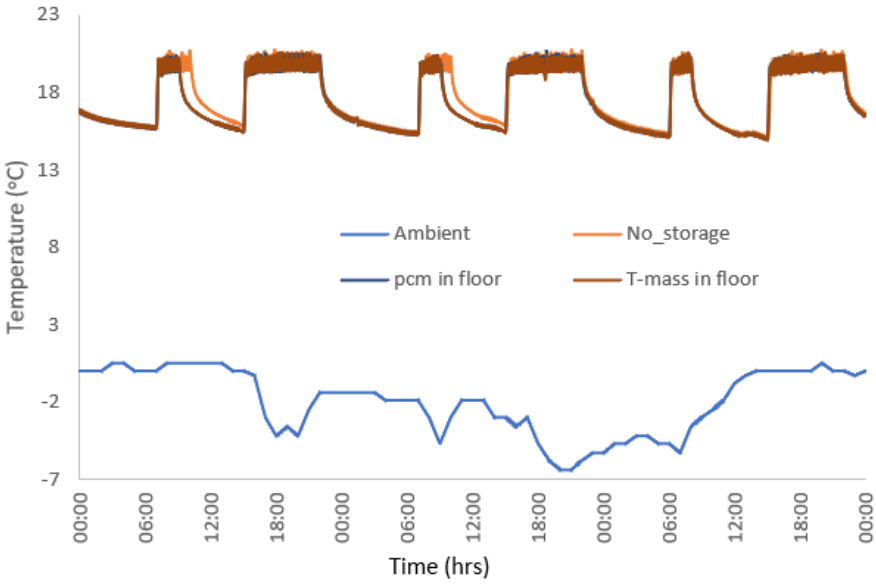

Figure 6.50: Heating system comparison – Living room dry bulb temperature. – latent heat vs sensible heat thermal store in floors.

As with analysis of previous heating systems, further performance comparisons was also done by analysing simulation data for dry bulb temperature of the living room (tree coldest days, 7th – 9th only) temperatures of water in domestic hot water tank and number of minutes the zone temperatures were below 19.5°C during the week with lowest ambient temperatures of the simulation, 3rd to 9th of January, as well as what percentage of heating demand period

they equate to. Plots of the data, along with similar plots from base case system, are shown in Figures 6.50 and 6.51 while the unmet minutes and percentages are listed in table 6.19.

Figure 6.50 also show the closeness of performance of the heating systems, with very little difference between the temperature profiles, unlike with temperature profile from the base case system. They also demonstrate high effectiveness in maintaining zone temperatures within desired levels comparative to the base case system.

Table 6.20: Unmet minutes for the living room (PCM slabs).

	pcm in floor	T-mass in floor
Time < 19.5 (min)	1046.00	1050.00
% of occupied period	30.06	30.17

The difference in performance, although small, is apparent in Table 6.19. Here, the unmet minutes for both systems are estimated at 1046 min and 1050 min, latent heat system and sensible heat system respectively. The percentages of heating demand period these constitute are 30.06% and 30.17% for latent heat systems and sensible heat system, respectively.

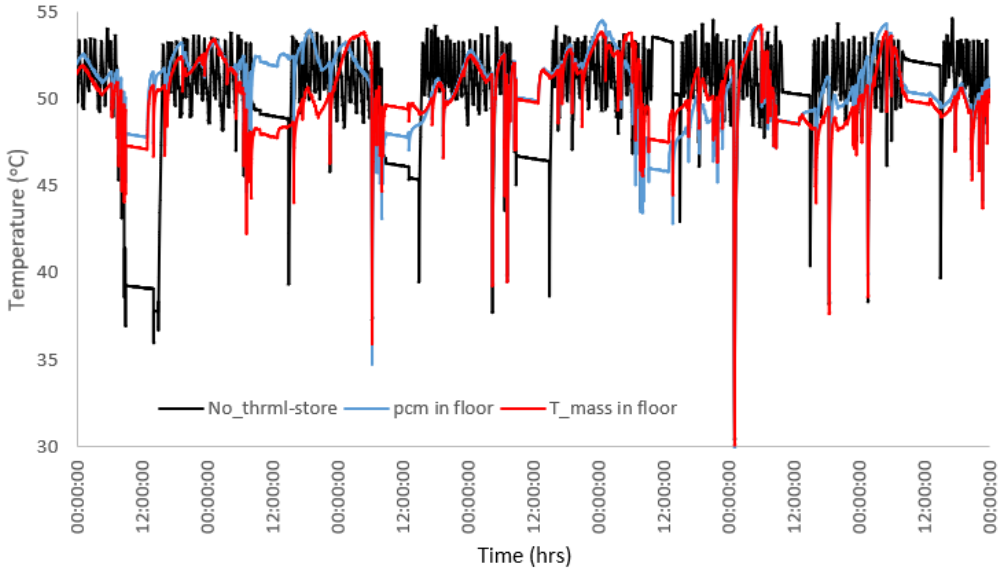

Figure 6.51: Heating system comparison – Domestic hot water temperature.

The difference between their performance is again revealed in profile of temperatures of water in domestic hot water tank shown in Figure 6.51. While both systems were able to keep hot water temperatures above the 43.5^{o}C levels for virtually all the occupied periods, as shown in Figure 6.51, the heating system with sensible heat thermal storage show greater performance. Also, both systems' performances fall short of performance of the base case system.

6.4 Summary

The thermal store models were employed assessing and analysing load shifting potential, cost and energy saving benefits of using the PCM based thermal energy storage systems after their successful installation and implementation into ESP-r. Procedures and methodologies for the test were discussed in details with discussions of the results and findings throughout the chapter. The chapter also discussed potential application of the PCM thermal store for CO_2 emission reduction, as well as a comparative analysis of the PCM thermal storage battery with conventional hot water storage (buffer) tank heating system and the fabric integrated PCM thermal store with similar fabric integrated thermal mass heat storage system.

Observations from comparison test show consistency with established findings regarding application of PCM heat storage systems and comparisons between them and sensible heat thermal storage systems. As stated earlier, the primary objective of the tests and case studies was not to re-prove or re-validate proven fact about performance of latent heat storage systems, their application in energy load shifting or advantages over sensible heat storage systems. Rather the objective is to further validate the thermal storage models and show that results obtained, as well as conclusions reached, from deploying them in building energy

simulation systems such as ESP-r, conform to established findings from similar systems, and to demonstrate their usefulness for the intended purpose.

The proceeding chapter will chronicle and summarise the various observations and determinations from all the previous chanters. It will also make attempts at suggestions for further and additional work/research resulting from the one just undertaken.

Chapter 7

CONCLUSIONS AND RECOMMENDATIONS FOR FUTURE RESEARCH

7.0 Introduction

This chapter discusses what was done and accomplished through the research considering the stated aim and objectives. Attempt is made at brief review of the research process with highlights of the summary of discussions from different chapters, as well as findings from case studies, highlighting usefulness and benefits of deploying phase change materials for thermal energy storage in domestic applications. It also discusses the main contributions and the benefits for building energy analysis and predictions and proffers some suggestion for further work.

7.1 Research Justification

The stated aim of the research is the development of models of active PCM based heat/thermal energy storage plant systems for integration/incorporation into ESP-r building energy modelling system This was proposed to be accomplished through the following objectives:

1. Development of numerical models of a heat/thermal storage battery and an active building fabric integrated heat/thermal store for implementation in ESP-r using PCM as heat storage medium.

2. verification and validation of the developed models
3. integration/implementation of the models in(to) ESP-r's plant system/database, and
4. demonstration of the models with case studies and assessing for possible areas of application and effectiveness in building energy management with regards to energy cost and CO_2 emission and system volume reduction and carrying out comparative analysis of the plant systems with conventional sensible heat thermal energy storage systems employed in similar manner and for similar purpose.

The work was predicated on review of modelling and representation methods for phase change material in ESP-r, as well as review of the types of PCM based building and plant systems in its arsenal. The review was discussed in chapter 2, beginning with an appraisal of the software's functionality regarding problem definition, processing, analysis and solution. The methods and approaches employed for modelling phase change materials were examined and discussed based on a categorisation of the existing PCM systems as active and passive systems and/or as building fabric integrated and non-fabric integrated systems (plants). The review also examined and discussed the modelling methods/approaches with a view to highlighting shortcomings and inadequacies of the existing methods/approaches.

Inadequacies of the apparent heat capacity method employed for modelling the passive fabric integrated PCM system in the software with regards to accurate determination of thermal properties during phase change were noted as being due to the non-linear nature of specific heat capacities of substances during change of phase, as well as the cumbersome requirements for mitigating errors due to this non-linearity, which have propensity for producing more errors. It was also emphasised that the method's reliance on the assumption (or expectation) that specific heat capacities of PCMs are different for different phases (liquid, solid, etc) is faulty for many organic PCMs.

The analysis also indicated that while the enthalpy method was employed for modelling an add on active PCM code/model for existing hot water storage tank model in the software, this is a tool used for determining temperature of PCMs embedded (or inserted) within the tank when required during processing of the tank's code. Although combined with the hot water storage tank model the tool is useful for assessing thermal storage, it cannot be employed for assessing PCMs alone and for making comparisons with hot water storage systems due to impact/influence of water contained in the storage tank. This reduces the software's ability to be employed for building assessments and analysis of under scenarios that include deployment of PCM based heat/thermal stores.

7.2 Methodology

7.2.1 Numerical Model

In line with stated objectives, mathematical/numerical models of two (2) PCM based thermal storage plant systems were developed. One was a thermal storage battery composed of a shell containing PCM, through which rows of tubes/pipes run lengthwise and the second a building fabric integrated thermal storage slab made up of alternating columns of rectangular PCM blocks and water tubes/pipes. The models and the modelling method and procedure were discussed in chapter 3, beginning with analysis of heat conduction through phase change materials. The energy conservation equations were formulated for discrete volumes of material and employed for developing enthalpy formulae which was used for modelling the energy change and phase transformations experienced by the PCM due to heat input and extraction.

It has been established that expressions of the enthalpy formula are valid for both the liquid and solid phases of the material. So, use of the method for modelling the PCM in the fabric integrated thermal store is an improvement over the method employed for modelling existing

fabric integrated PCM in ESP-r which employs the apparent heat capacity method. As emphasised in chapters 1 and 2, the apparent heat capacity method relies on variations of specific heat capacity of materials with temperature. This is a non-linear relationship that is not easy to determine during phase change, particularly for substances that changes phase over a single, or fixed, temperature, and requires the introduction of a fictitious melting temperature range for the PCM (AL-Saadi & Zhai, 2013; Madad, Mouhib, & Mouhsen, 2018). The method also presupposes that the substance would have different heat capacities for each of the phases, which is not always the case with the paraffins whose solid phase specific heat capacity is the same for the liquid phase.

Also, the existing fabric integrated thermal store in ESP-r is passive and functions, in combination with traditional building materials, to increase thermal capacity of constructions (Heim & Clarke, 2004). Passive systems do not require a dedicated/specific heat transfer or delivery system to deliver or extract heat energy into/from them. They passively absorb or reject heat on account of temperature difference between them and their surroundings. Their effectiveness is dependent on difference between their temperatures and that of their surrounding and movement of air around them.

Given detailed description of each physical model, the discretised energy equations and expressions employed for representing and describing the energy change and phase transformation processes, and interaction between the heat transfer fluid and PCM, were solved using a numerical algorithm that employs the Gauss-Seidel iterative scheme.

7.2.2 Model Verification and Validation

Having developed models of the thermal storage plant components, their numerical codes were subjected to verification and validation tests to assess robustness and correctness of the computer programs and their implementation, and to ascertain that their range of accuracies are satisfactory and consistent with intended applications. Discussed in chapter 5, the

methods and procedures include structured walk throughs, debugging and consistency tests, for verification, while they were validated by comparing results from simulating/executing their codes with results reported by Hosseini et al., (2012), Hosseini, Rahimi, & Bahrampoury (2014) and Seddegh, Wang, & Henderson (2016) for models of similar thermal storage systems using the same phase change material.

The models were also subjected to sensitivity analysis, looking at impact of changes/variations in values of some parameter constants within the numerical codes, as well choice of model configuration (for the fabric integrated PCM thermal store only) on the performance of the systems. Impact of choice of model configuration, as well as some of the consistency tests, were done after models were installed into ESP-r.

7.2.3 Model Integration into ESP-r

After verification and validation, the models' numerical source codes were integrated, i.e., registered, into ESP-r's plant database. The procedure entails writing the source codes with parameters and variables whose names and/or codes are recognisable by the software, as well as building up plant data for each of the plant models for the software's plant database. Implementation is complete when all necessary codes and subroutines within ESP-r are edited to contain links and call up instructions for the PCM thermal storage plant models, as well as compilations instructions for the plant models followed by re-installation of the software. Verification tests after installation showed proper integration and implementation of the PCM thermal store models.

7.2.4 Model Demonstration

Each of the models were subsequently deployed within plant networks for a building model which was simulated and assessed for impact of the thermal storage plants on energy performance, cost saving and CO_2 emission reduction of heat pump space and water heating systems. Also, their application for demand side manipulation of the heating system was

assessed, as well as a comparison with similar thermal storage systems that employ- sensible heat thermal storage materials.

According to Critoph & Metcalf (2019), heat pumps are expected to play a pivotal role in the UK government's energy systems effort to achieving its goal of 80% reduction in CO2 emissions by year 2050, which is centred around electrification of the nation's energy system (Department of Energy and Climate Change, 2010; Wilson, et al., 2013). With potential problems associated with deployment of large number of heat pumps on the electrical grid (Love, et al., 2017; Arnold, 2016), storage of energy, waste or supplemental, is seen as viable mitigant, capable of helping with load management, load profiles flattening and smoothening out of energy demand peaks and fluctuations (Münster & Lund, 2007). These are achievable by effectively manipulating heat pumps operation to shift away from peak energy demand periods to off-peak energy demand periods (Muruganantham et al,, 2010).

7.2.4.1 Case study 1 – Back shifting heat pump operations.

Application of PCM thermal storage for shifting heat pump operation away from the peak energy demand period to the off-peak energy demand period was investigated by comparing results from simulating a building model equipped with two types of heating systems and two different heat pump operation settings. One of the heating systems had no thermal storage and the heat pump was operated to supply heating to dwelling on demand, working during both the peak and off-peak energy demand periods, while the other had thermal storage and the heat pump was operated only during the off-peak energy demand period of the economy 10 energy tariff.

The fabric integrated thermal store model was deployed in two different configurations of heating systems with thermal storage. It was installed in walls in one configuration and

installed in floors in the second configuration. Together with the thermal storage battery, three types of thermal storage systems were studied and analysed.

The results show reductions in both energy cost and emissions as heating systems with the PCM thermal storage performed suitable well, comparative to heating system with no thermal storage, and effect shifting of heat pump operating away from peak to the off-peak energy demand period. Although results show slightly lower average zone dry bub temperatures and higher number of unmet heating minutes in comparison with no thermal storage system, all the systems with PCM thermal storage were able to maintain individual zone temperatures within desired levels during the occupied periods and keep hot water temperatures above desired levels for most of the occupied periods.

7.2.4.2 Case study 2 – Comparison with sensible heat thermal storage systems.

In this case study, comparisons were made between thermal storage systems employing latent heat thermal storage materials and sensible heat thermal storage materials. The heating systems were operated only during the off-peak energy demand periods of the economy 10 energy tariff with a view to assessing comparative effectiveness of the types of thermal storage in effecting heating systems operation shift away from the peak energy demand periods. The thermal storage battery was compared with conventional hot water storage tank while the fabric integrated thermal stores were compared with fabric integrated thermal storage systems that employ thermal mass such as concrete for thermal storage.

Results from the study show that, although performances were close in terms of maintaining zonal dry bulb temperatures and temperatures of hot water within desired levels, and unmet heating minutes, systems deploying PCM (latent heat systems) were cheaper to run and produced the least amount of emission when compared to systems employing sensible heat material as thermal storage.

7.3 Contributions

7.3.1 Improved Capability for PCM Simulation

One of the objectives of the demonstration process was stated as showing comparability of the thermal storage models with existing similar systems. These systems are not contained in ESP-r's plant system and cannot be deployed when employing the software for building energy simulation and analysis. These factors were emphasised in chapter 1 and discussed as part of the observations from analysing the building modelling tool in chapter 2. The software does not have, as at time of writing up this thesis, a dedicated PCM thermal energy storage plant system with capabilities for substituting conventional hot water storage tank systems in the software.

The developed systems have capacities for applications in modelling and representing some the physical systems advertised as available for deployment for both domestic and industrial applications and are germane to efforts and research into ways of reducing energy demand and consumption, as well as CO_2 emissions, from buildings. Additionally, the models represent improvements on the present PCM modelling methods employed in EnergyPlus. As explained in chapters 1 and 2, the method requires loading an enthalpy-temperature (h-T) curve or data for the PCM before commencement or continuous successive inputting of the enthalpy and corresponding temperature values into the program during execution. Whereas the modelling method adopted in this work eliminates these requirements.

7.3.2 Novelty of the Active Fabric Integrated PCM Thermal Storage Slab

Also, the existing building fabric integrated PCM model in the ESP-r is the passive type. The concept of active fabric integrated PCM heat storage system, like that reported by (Kong, Wang, Li, Yuan, & Yao, 2020), although gradually gaining attraction, is still relatively new.

This type of system has applications in both direct and indirect space heating, as well as in water heating. The model is novel and has not been implemented in ESP-r or any building energy analysis software package.

The model can also be employed to analyse non-PCM based active fabric integrated thermal storage systems like underfloor heating system that employ concrete, or other high density thermal mass substances as thermal storage materials. By simply replacing properties of the PCM in the model with those of the chosen thermal mass substance, an active fabric integrated sensible heating thermal mass plant model can be made available for deployment in building model for assessment.

7.3.3 Conclusions from Case Studies

The case studies were able to demonstrate and show ability and effectiveness of employing the thermal store models for assessing performance of thermal storage system and for employing such for energy and load shifting applications.

Results from case study 1 show that heating systems employing PCM thermal storage can be effectively operated during the off-peak energy demand periods with little or no compromise to heat supply and provision of hot water to meet demand of dwellings, leading to reductions in energy cost and emissions, while results from case study 2 show the superior performance of latent heat thermal energy storage systems over sensible heat systems in terms of effectiveness and reduction in size.

7.4 Recommendations

7.4.1 Comparison with Actual Systems

The models were validated by making comparisons with reported work and showed very good agreement. However, the advantage and benefits of employing experimental data for possible tweaking and adjusting the final model were not taken. This was due, primarily, to

lack of funds to procure necessary equipment and material for experimentation. A more pointed experimental validation for a multi-tube PCM thermal store, such as the thermal storage battery and for a PCM thermal storage slab would help to establish the models' validity or identify areas that require modifications.

7.4.2 Considerations of other PCM characteristics and phenomenon

The effect of liquid flow within the PCM block, driven by buoyancy effect, was neglected while developing energy equations for the PCM models. While the effect is small for narrow PCM channels/containers, it is none the less present and the models could be improved by factoring the phenomenon. Also, some PCM undergo some processes like phase segregation as well as hysteresis and nucleation, which were also not considered. The models could be modified to take some of these factors into consideration as it would widen their application for a variety of phase change materials and enable them to better capture energy changes if the PCMs experience the phenomena.

8.0 References.

Aasem, E. O. (1993). *Practical Simulation of Buildings and Air-Conditioning Systems in the Transient Domain.* University of Strathclyde, Glasgow. Glasgow: ESRU, University of Strathclyde, Glasgow.

Abanda, F. H., & Byers, L. (2016). An Investigation of the Impact of Building Orientation on Energy Consumption in a Domestic Building using Emerging BIM (Building Information Modelling). *Energy, 97*, 517-527.

Abolghasemi, M., Keshavarz, A., & Mehrabian, M. A. (2012). Thermodynamic Analysis of a Thermal Storage Unit under the Influence of Nano-Particles added to the Phase Change Material and/or the Working Fluid. *Heat and Mass Transfer, 48*(11), 1961–1970. doi:10.1007/s00231-012-1039-1

Akeiber, H., Nejat, P., Majid, M. Z., Wahid, M. A., Jomehzadeh, F., Famileh, I. Z., . . . Zaki, S. A. (2016). A Review on Phase Change Material(PCM) for Sustainable Passive Cooling in Building Envelope. *Renewable and Sustainable Energy Reviews, 60*, 1470–1497.

Alawadhi, E. M., & Alqallaf, H. J. (2011). Building Roof with Conical Holes Containing PCM to Reduce the Cooling Load: Numerical Study. *Energy Conversion and Management, 52*(8-9), 2958–2964. doi:doi:10.1016/j.enconman.2011.04.004

Albertí, J., Raigosa, J., Raugei, M., Assiego, R., Ribas-Tur, J., Garrido-Soriano, N., . . . Fullana-i-Palmer, P. (2019). Life Cycle Assessment of a Solar Thermal System in Spain, Eco-Design Alternatives and Derived Climate Change Scenarios at Spanish and Chinese National Levels. *Sustainable Cities and Society*, *101467*, 101467.

Alexiades, V., & Solomon, A. D. (1993). *Mathematical Modeling of Melting and Freezing Processes.* Washington, DC: Hemisphere Publishing Corporation.

Almeida, F., Zhang, D., Fung, A. S., & Leong, W. H. (2010). Investigation of Multilayered Phase-Change-Material Modeling in ESP-R. *International High Performance Buildings Conference, July 12-15, 2010*, (pp. 3470; 1-8). West Lafayette.

Al-Mosawi, A. L. (2011). *Thermal Energy Storage for Building-Integrated Photovoltaic Components.* University of Strathclyde, G;asgow, Mechanical and Aerospace Engineering. Glasgow: ESRU.

Al-Saadi, S. N., & Zhai, J. (2013). Modeling Phase Change Materials Embedded in Building Enclosure: A Review. *Renewable and Sustainable Energy Reviews, 21*, 659-673.

AL-Saadi, S. N., & Zhai, J. (2013). Modeling Phase Change Materials Embedded in Building Enclosure: A Review. *Renewable and Sustainable Energy Reviews, 21*, 659-673.

Anderson, B. R., Chapman, P. F., Cutland, N. G., Dickson, C. M., Doran, S. M., Henderson, G., . . . Shorrock, L. D. (2010). *BREDEM-8: Model Description, 2001 Update.* London: Building Research Establishment.

Ansuini, R., R. L., Giretti, A., & Lemma, M. (2011). Radiant floors integrated with PCM for indoor temperature control. *Energy and Buildings, 43*, 3019-3026. doi:doi:10.1016/j.enbuild.2011.07.018

Arnold, M. P. (2016). *Integration of Residential Distributed Generators and Heat Pumps into the Low Voltage Grid from a Voltage Level Perspective.* Technichal University of Dortmund. Dortmund: Faculty of Electrical Engineering and Information Technology. Retrieved from https://core.ac.uk/download/pdf/46917314.pdf

Arteconi, A., Hewitt, N., & Polonara, F. (2012). State of the art of thermal storage for demand-side management. *Applied Energy, 93*, 371–389.

Atkin, J. (2017, August 11). *What type of housing do people live in?* Retrieved October 01, 2019, from Mortgage Finance Gazette: https://www.mortgagefinancegazette.com/market-news/housing/type-housing-people-live-11-08-2017/

Aydin, E., & Brounen, D. (2019). The Impact of Policy on Residential Energy Consumption. *Energy, 169*, 115-129.

Badescu, V. (2003). Model of a Thermal Energy Storage Device integrated into a Solar Assisted Heat Pump System for Space Heating. *Energy Conversion and Management, 40*(10), 1589-1604.

Barreneche, C., Navarro, L., De-Gracia, A., Fernández, A. I., & Cabeza, L. F. (2016). In Situ Thermal and Acoustic Performance and Environmental Impact of the Introduction of a Shape-Stabilized PCM Layer for Building Applications. *Renewable Energy, 85,, 85*, 281–286.

Barzin, R., Chen, J. J., Young, B. R., & Farid, M. M. (2015). Application of PCM Underfloor Heating in Combination with PCM Wallboards for Space Heating using Price Based Control System. *Applied Energy, 148,, 148*, 39–48.

Beausoleil-Morrison, I., Ferguson, A., Griffith, B., Kelly, N., MarÈchal, F., & Weber, A. (2007). Specifications for Modelling Fuel Cell and Combustion-Based Residential Cogeneration Devices within Whole-Building Simulation Programs. *A Report of Subtask B of FC+COGEN-SIM'. The Simulation of Building-Integrated Fuel Cell and Other Cogeneration Systems*, 111. (I. Beausoleil-Morrison, & N. Kelly, Eds.) Her Majesty the Queen in Right of Canada. Retrieved from https://strathprints.strath.ac.uk/6704/6/strathprints006704.pdf

Belmonte, J. F., Eguía, P., Molina, A. E., Almendros-Ibáñez, J. A., & Salgado, R. (2016). A Simplified Method for Modeling the Thermal Performance of Storage Tanks Containing PCMs. *Applied Thermal Engineering, 95*, 394–410.

Benmoussa, F., Benzaoui, A., & Benmoussa, H. (2017). Thermal Behavior of Latent Thermal Energy Storage Unit using Two Phase Change Materials: Effects of HTF Inlet Temperature. *Case Studies in Thermal Engineering, 10*, 475-483. Retrieved from https://doi.org/10.1016/j.csite.2017.10.010

Berardi, U., & Soudian, S. (2018). Benefits of latent thermal energy storage in the retrofit of Canadian high-rise residential buildings. *Building Simulation, 11*, 709–723. doi:https://doi.org/10.1007/s12273-018-0436-x

Bianco, L., Vigna, I., & Serra, V. (2017). Energy Assessment of a Novel Dynamic PCMs Based Solar Shading: Results from an Experimental Campaign. *Energy and Buildings, 150*, 608–624.

Boettinger, W. J., & Banerjee, D. K. (2015). Solidification. In Laughlin, & K. Hono (Eds.), *Physical Metallurgy* (5 ed., Vol. 1, pp. 639-850). London, Unuted Kingdom: Elsevier.

BoilerGuide Limited. (2020, Jan 04). *Get Free Quotes.* Retrieved from What Size Heat Pump Do I Need?: https://www.boilerguide.co.uk/articles/size-heat-pump-need#:~:text=Heat%20pumps%20vary%20in%20size,pump's%20output%20needs%20to%20be.

Borgonovo, E., & Plischke, E. (2016). Sensitivity Analysis: A Review of Recent Advances. *European Journal of Operational Research, 248*, 869–887.

Bruck, D. (2006). *Teenage Sleep: Understanding and Helping the Sleep of 12 - 20 Year Olds (E-Book).* Melbourne: Wellness Promotion Unit, Victoria University, Melbourne, Australia. Retrieved from http://vuir.vu.edu.au/467/1/teenagesleep.pdf

Brundtland Commission. (1987). *Our Common Future.* (V. Hauff, Ed.) London: Oxford University Press.

Building Research Establishment (BRE). (2014). *The Government's Standard Assessment Procedure for Energy Rating of Dwellings.* Watford: Building Research Establishment (BRE). Retrieved Aug 11, 2020, from Standard Assessment Procedure (SAP2012): https://www.bre.co.uk/filelibrary/SAP/2012/SAP-2012_9-92.pdf

Bulb Energy Limited. (2020, March 12). *Smart Tariff Electricity Rates during British Summer Time.* Retrieved from Our Smart Tariff can Save You Money: https://bulb.co.uk/smart/

Cabeza, L. F., Ibanez, M., Sole, C., Roca, J., & Nogues, M. (2006). Experimentation with a Water Tank Including a PCM Module. *Solar Energy Materials & Solar Cells, 90*, 1273–1282.

Caggiano, A., Mankel, C., & Koenders, E. (2019). Reviewing Theoretical and Numerical Models for PCM-Embedded Cementitious Composites. *Buildings, 9*(3), 1-26.

Canbazoğlu, S., Şahinaslan, A., Ekmekyapar, A., Aksoya, Ý. G., & Akarsu, F. (2005). Enhancement Of Solar Thermal Energy Storage Performance using Sodium Thiosulphate Pentahydrate of a Conventional Solar Water-Heating System. *Energy and Buildings, 37*(3), 235–242.

Castell, A., & Solé, C. (2015). Design of Latent Heat Storage Systems Using Phase Change Materials (PCMs). In L. F. Cabeza, & L. F. Cabeza (Ed.), *Advances in Thermal Energy Storage Systems - Methods and Applications* (pp. 285-305). London: Woodhead Publishing. doi:https://doi.org/10.1533/9781782420965.2.285

Castell, A., Martorell, I., Medrano, M., Pérez, G., & Cabeza, L. (2010). Experimental Study of Using PCM in Brick Constructive Solutions for Passive Cooling. *Energy and Buildings, 42*(4), 534–540.

Chaabane, M., Mhiri, H., & Bournot, P. (2014). Thermal Performance of an Integrated Collector Storage Solar Water Heater (ICSSWH) with Phase Change Materials (PCM). *Energy Conversion and Management, 78*, 897–903.

Chhugani, B., Klinker, F., Weinlaeder, H., & Reim, M. (2017). Energetic Performance of Two Different PCM Wallboards and their Regeneration Behavior in Office Rooms. *Energy Procedia, Volume, 122*, 625-630.

Chinese, D., Santin, M., & Saro, O. (2017). Water-energy and GHG nexus assessment of alternative heat recovery options in industry: A case study on electric steelmaking in Europe. *Energy, 141*, 2670-2687.

Chou, H. M., Chen, C. R., & Nguyen, V. L. (2013). A New Design of Metal-Sheet Cool Roof using PCM. *Energy and Buildings, 57*, 42–50. doi:doi:10.1016/j.enbuild.2012.10.030

Chwieduk, D. A. (2017). Towards Modern Options of Energy Conservation In Buildings. *Renewable Energy, 101*, 1194-1202.

Civan, F., & Sliepcevich, C. M. (1984). Efficient Numerical Solution for Enthalpy Formulation of Conduction Heat Transfer with Phase Change. *International Journal of Heat and Mass Transfer, 27*(8), 1424-1427.

Clarke, J. A. (2001). *Energy simulation in building design.* Ocford: Butterworth-Heinemann.

Comini, G., Del-Giudice, S., & Saro, O. (1990). A Conservative Algorithm for Multi-dimensional Conduction Phase Change. *International Journal for Numerical Methods in Engineering, 30*(4), 697–709.

Commission to the European Parliament and The Council. (2014). *Energy Efficiency and its Contribution to Energy Security and the 2030 Framework for Climate and Energy Policy.* Brussels: European Commission. Retrieved March 21, 2017, from

https://ec.europa.eu/energy/sites/ener/files/documents/2014_eec_communication_adopted_0.pdf

Confalonieri, R., Bellocchi, G., Bregaglio, S., Donatelli, M., & Acutis, M. (2010). Comparison of Sensitivity Analysis Techniques: A Case Study with the Rice Model WARM. *Ecological Modelling, 221*, 1897–1906.

Cook, D. A., & Skinner, J. M. (2005). How to Perform Credible Verification,Validation, and Accreditation for Modeling and Simulation. *Systems and Software Technology Comference, 18 April 2005* (pp. 20-24). Salt Lake City: CROSSTALK, The Journal of Defense Software Engineering. Retrieved 04 02, 2020, from https://pdfs.semanticscholar.org/c76f/f966a1c00696c39bd476a6e657f7a24f7468.pdf

Corrado, V., & Fabrizio, E. (2019). Chapter 5 - Steady-State and Dynamic Codes, Critical Review, Advantages and Disadvantages, Accuracy, and Reliability. In V. Corrado, & E. Fabrizio (Eds.), *Handbook of Energy Efficiency in Buildings - A Life Cycle Approach* (pp. 263-294). Oxford: Butterworth-Heinemann. doi:https://doi.org/10.1016/B978-0-12-812817-6.00011-5

Crawley, B. D., Hand, W. J., Kummert, M., & Griffith, T. B. (2008). Contrasting the Capabilities of Building Energy Performance Simulation Programs. *Building and Environment, 43*(4), 661–673.

Crawley, D. B., Lawrie, L. K., Pedersen, C. O., Winkelmann, F. C., Witte, M. J., Strand, R. K., . . . Griffith, B. T. (2004). Energyplus: New, Capable and Linked. *Journal of Architectural and Planning Research, 21*(14), 292-302.

Critoph, R. E., & Metcalf, S. J. (2019). *UK Summary Report on IEA Heat Pump Technology Collaboration Programme (TCP)Annex 43: Thermally Driven Heat Pumps.* London: Department for Business, Energy and Industrial Strategy. Retrieved 02 12, 2021, from https://assets.publishing.service.gov.uk/government/uploads/system/uploads/attachment_data/file/862625/Summary_report_on_IEA_Heat_Pump_Annex_43__1_.pdf

Croda International Plc. (2020, 02 24). *Domestic & Commercial Heating & Hot Water Systems*. Retrieved from Croda: https://www.crodatherm.com/en-gb/products-and-applications/crodatherm-wax/heat-storage-and-recovery/domestic-and-commercial-heating-and-hot-water-systems

Croda International Plc. (2020, Sept. 12). *Our Products & Markets*. Retrieved from Products & Markets: https://www.croda.com/en-gb/products-and-markets

Cui, Y., Xie, J., Liu, J., Wang, J., & Chen, S. (2017). A review on phase change material application in building. *Advances in Mechanical Engineering, 9*(6), 1-15. doi:https://doi.org/10.1177/1687814017700828

David, D., Kuznik, F., & Roux, J.-J. (2011). Numerical Study of the Influence of the Convective Heat Transfer on the Dynamical Behaviour of a Phase Change Material

Wall. *Applied Thermal Engineering*, 3117-3124. doi:doi:10.1016/j.applthermaleng.2011.04.001

De Gracia, A., Oró, E., Farid, M. M., & Cabeza, L. F. (2011). Thermal Analysis of Including Phase Change Material in a Domestic Hot Water Cylinder. *Applied Thermal Engineering, 31*, 3938-3945.

De-Gracia, A., Navarro, L., Castell, A., Boer, D., & Cabeza, L. F. (2014). Life Cycle Assessment of a Ventilated Facade with Pcm in its Air Chamber. *Solar Energy, 104*, 115–123.

De-Gracia, A., Navarro, L., Castell, A., Ruiz-Pardo, Á., Alvárez, S., & Cabeza, L. F. (2013). Experimental Study of a Ventilated Facade with PCM During Winter Period. *Energy and Buildings, 58*, 324-332. doi:https://doi.org/10.1016/j.enbuild.2012.10.026

Delcroix, B., Kummert, M., & Daoud, A. (2017). Development and Numerical Validation of a New Model for Walls with Phase Change Materials Implemented in TRNSYS. *Journal of Building Performance Simulation, 10*(4), 422-437.

Department for Business, Energy & Industrial Strategy. (2020, July 17). *The conversion factors are for use by UK and international organisations to report on 2020 greenhouse gas emissions.* Retrieved from Greenhouse gas reporting: conversion factors 2020: https://www.gov.uk/government/publications/greenhouse-gas-reporting-conversion-factors-2020

Department for Business, Energy and Industrial Strategy. (2019). *Energy Consumption in the UK (ECUK) 1970 to 2018.* London: Department for Business, Energy and Industrial Strategy. Retrieved 06 25, 2019, from https://www.gov.uk/government/statistics/energy-consumption-in-the-uk

Department for Business, Energy and Industrial Strategy, UK. (2020). *Final UK greenhouse gas emissions national statistics.* Retrieved April 21, 2020, from https://assets.publishing.service.gov.uk/government/uploads/system/uploads/attachment_data/file/862887/2018_Final_greenhouse_gas_emissions_statistical_release.pdf

Department of Defence. (1998). *DoD Modelling and Simulation Glossary.* Washington: Department of Defense. Retrieved 04 02, 2020, from www.dmso.mil/public/resources/glossary

Department of Energy and Climate Change. (2010). *2050 Pathways Analysis, July 2010.* London: Department of Energy and Climate Change, UK Government. Retrieved Dec 15, 2016, from https://assets.publishing.service.gov.uk/government/uploads/system/uploads/attachment_data/file/68816/216-2050-pathways-analysis-report.pdf

DesignBuilder Software Ltd. (2021). *EnergyPlus Simulation*. Retrieved July 01, 2021, from DesignBuilder:

https://designbuilder.co.uk/simulation#:~:text=DesignBuilder%20is%20the%20most%20established,renewables%2C%20HVAC%20and%20financial%20analysis.

Devaux, P., & Farid, M. M. (2017). Benefits of PCM Underfloor Heating with PCM Wallboards for Space Heating in Winter. *Applied Energy, 191*, 593–602.

Dong, L., Wang, Y., Scipioni, A., Park, H.-S., & Ren, J. (2018). Recent Progress on Innovative Urban Infrastructures System towards Sustainable Resource Management. *Resources, Conservation and Recycling, 128*, 355-359.

Dréau, J. L., & Heiselberg, P. (2016). Energy Flexibility of Residential Buildings using Short Term Heat Storage in the Thermal Mass. *Energy, 111*, 991-1002.

Dutil, Y., Rousse, D. R., Salah, N. B., Lassue, S., & Zalewski, L. (2011). A Review on Phase-Change Materials: Mathematical Modeling and Simulations. *Renewable and Sustainable Energy Reviews, 15*(1), 112–130.

Elarga, H., Fantucci, S., Serra, V., Zecchin, R., & Benini, E. (2017). Experimental and Numerical Analyses on Thermal Performance of Different Typologies of PCMs Integrated in the Roof Space. *Energy and Buildings, 150*, 546–557.

Ellerbrok, C. (2014). Potentials of Demand Side Management using Heat Pumps with Building Mass as a Thermal Storage. *Energy Procedia, 46+*, 214 – 219.

El-Omari, K., Le-Guer, Y., & Bruel, P. (2016). Analysis of Micro-Dispersed PCM-Composite Boards Behavior in a Building's Wall for Different Seasons. *Journal of Building Engineering, 7*, 361–371.

Energy Information Administration. (2019). *World total energy consumption by region and fuel.* Retrieved Feb 25, 2020, from International Energy Outlook 2019: https://www.eia.gov/outlooks/aeo/data/browser/?src=-f1#/?id=2-IEO2019&region=0-0&cases=Reference&start=2010&end=2021&f=A&linechart=~~Reference-d080819.79-2-IEO2019&ctype=linechart&chartindexed=0&sourcekey=0

Energy Savings Trust. (2013). *At Home with Water.* London: Energy Savings Trust. Retrieved March 2018, 12, from https://energysavingtrust.org.uk/sites/default/files/reports/AtHomewithWater%287%29.pdf

Energy Technologies Area. (2013, July 13). *Simergy: A Free, Comprehensive Graphical User Interface for Energy Modeling with EnergyPlus.* Retrieved from Energy Technologies Area/Berkeley Lab: https://eta.lbl.gov/news/article/56613/simergy-a-free-comprehensive-gr

Entrop, A., Halman, J., Dewulf, G., & Reinders, A. (2016). Assessing the Implementation Potential of PCMs: The Situation for Residential Buildings in the Netherlands. *Energy Procedia, 96*, 17–32.

ESRU. (2016, December 12). *ESP-r: Computing Platforms, Compilers and Code.* Retrieved from ESP-r: Computing Platforms, Compilers and Code: http://www.esru.strath.ac.uk/Programs/ESP-r_capabilities/platform_capabilities.html

European Commission. (2020). *Energy data — 2020 edition.* Retrieved Jan 21, 2020, from Eurostat - Products Statistical Books: https://ec.europa.eu/eurostat/documents/3217494/11099022/KS-HB-20-001-EN-N.pdf/bf891880-1e3e-b4ba-0061-19810ebf2c64

European Commission. (2020(a)). *2020 climate & energy package*. Retrieved May 12, 2020, from Climate strategies & targets: https://ec.europa.eu/clima/policies/strategies/2020_en

European Environment Agency. (2020). *Trends and projections in Europe 2020 - Tracking progress towards Europe's climate and energy targets.* Luxembourg: European Environment Agency. doi:doi:10.2800/830157

European Parliament and the Council of the European Union (EUROPA). (2010, May 19). *Directive 2010/31/EU on the Energy Performance of Buildings.* Retrieved from Build Up - The European Portal for Energy Efficiency in Buildings: https://www.buildup.eu/en/practices/publications/directive-201031eu-energy-performance-buildings-recast-19-may-2010

Eurostat. (2020, June 25). *Energy Consumption in Households*. Retrieved from Eurostat - Statistics Explained: https://ec.europa.eu/eurostat/statistics-explained/index.php/Energy_consumption_in_households

Faghri, A., & Zhang, Y. (2006). *Transport Phenomena in Multiphase Systems.* London: Academic Press.

Fairley, R. E. (1976). Dynamic Testing of Simulation Software. *1976 Summer Computer Simulation Conference* (pp. 40 - 46). Washington, DC: Simulation Councils, La Jolla, California.

Fang, X., Fan, L.-W., Ding, Q., Yao, X.-L., Wu, Y.-Y., Hou, J.-F., . . . Hu, Y.-C. (2014). Thermal Energy Storage Performance of Paraffin-Based Composite Phase Change Materials Filled with Hexagonal Boron Nitride Nanosheets. *Energy Conversion and Management, 80*, 103-109.

Fang, Y., & Medina, M. (2009). Proposed Modifications for Models of Heat Transfer Problems Involving Partially Melted Phase Change Processes. *Journal of ASTM International, 6*(9), 1-20.

Faraj, K., Khaled, M., Faraj, J., Hachem, F., & Castelain, C. (2020). Phase Change Material Thermal Energy Storage Systems for Cooling Applications in Buildings: A Review. *Renewable and Sustainable Energy Reviews, 119*, 109579.

Farid, M. M., Khudhair, A. M., Razack, S. A., & Al-Hallaj, S. (2004). A review on phase change energy storage: materials and applications. *Journal of Energy Conversion and Management, 45*(9-10), 1597–1615.

Feng, S., Shi, M., Li, Y., & Lu, T. J. (2015). Pore-Scale and Volume-Averaged Numerical Simulations of Melting Phase Change Heat Transfer in Finned Metal Foam. *International Journal of Heat and Mass Transfer, 90*, 838–847.

Ferreira, V. J., López-Sabirón, A. M., Royo, P., Aranda-Usón, A., & GermánFerreira. (2015). Integration of environmental indicators in the optimization of industrial energy management using phase change materials. *Energy Conversion and Management, 104*, 67-77.

Feustel, H. E. (1995). *Simplified Numerical Description of Latent Storage Characteristics for Phase Change Wallboard, Indoor Environment Program, Energy And Environment Division.* University of California. California: U.S. Department of Energy, Office of Scientific and Technical Information. doi:doi:10.2172/70723

Figueiredo, A., Vicente, R., Lapa, J., Cardoso, C., Rodrigues, F., & Kämp, J. (2017). Indoor Thermal Comfort Assessment using Different Constructive Solutions Incorporating PCM. *Applied Energy, 208*, 1208–1221.

Fokaides, P. A., Kylili, A., & Kalogirou, S. A. (2015). Phase Change Materials (PCMs) Integrated into Transparent Building Elements: A Review. *Materials for Renewable and Sustainable Energy, 4*(6), 1-13. doi:https://doi.org/10.1007/s40243-015-0047-8

Foudhil, W., Dhifaoui, B., Jabrallah, S. B., Dutil, Y., & Rousse, D. R. (2012). Numerical Simulation of Thermal Storage by Latent and Sensible Heat in a Porous Vertical Channel: Performance Analysis and Comparison. *Numerical Heat Transfer, Part A: Applications, 62*(12), 948-972. doi:https://doi.org/10.1080/10407782.2012.715982

Frazzica, A., Manzan, M., Sapienza, A., Freni, A., Toniato, G., & Restuccia, G. (2016). Experimental Testing of a Hybrid Sensible-Latent Heat Storage System for Domestic Hot Water Applications. *Applied Energy, 183*, 1157–1167.

Frigione, M., Lettieri, M., & Sarcinella, A. (2019). Phase Change Materials for Energy Efficiency in Buildings and Their Use in Mortars. *MAterials, 12*(8), 1260. doi:doi: 10.3390/ma12081260

Gai, L., Varbanov, P. S., Walmsley, T. G., & Klemes, J. J. (2019). Process Integration Using a Joule Cycle Heat Pump. *Chemical Engineering Transactions, 76*, 415-420.

Gassenfeit, B., & Brüggemann, D. (2014). Monolithic Masonry with PCM for Thermal Management. *Energy Procedia, 48*, 1355-1364.

Gershuny, J. I., & Sullivan, O. (2017, Jan 16). *United Kingdom Time Use Survey, 2014-2015.* doi:http://doi.org/10.5255/UKDA-SN-8128-1

Goia, F., Bianco, L., Cascone, Y., Perino, M., & Serra, V. (2014). Experimental Analysis of an Advanced Dynamic Glazing Prototype Integrating PCM and Thermotropic Layers. *Energy Procedia, 48,, 48*, 1272–1281.

Goia, F., Zinzi, M., Carnielo, E., & Serra, V. (2015). Spectral and Angular Solar Properties of a PCM-Filled Double Glazing Unit. *Energy and Buildings, 87,, 87*, 302–312.

Gounni, A., & El-Alami, M. (2017). The Optimal Allocation of the PCM within a Composite Wall for Surface Temperature and Heat Flux Reduction: An experimental Approach. *Applied Thermal Engineering, 127*, 1488–1494.

Guarino, F., Dermardiros, V., Chen, Y., Rao, J., Athienitis, A., Cellura, M., & Mistretta, M. (2015). PCM Thermal Energy Storage in Buildings: Experimental Study and Applications. *Energy Procedia, 70*, 219 – 228.

Guichard, S., Miranville, F., Bigot, D., & Boyer, H. (2014). A Thermal Model for Phase Change Materials in a Building Roof for a Tropical and Humid Climate: Model Description and Elements of Validation. *Energy and Buildings, 70*, 71-80.

Halford, C. K., & Boehm, R. F. (2007). Modeling of Phase Change Material Peak Load Shifting. *Energy and Buildings, 30*(3), 298–305.

Hasan, M. I., Basher, H. O., & Shdhan, A. O. (2018). Experimental Investigation of Phase Change Materials for Insulation of Residential Buildings. *Sustainable Cities and Society, 36*, 42–58.

Hashemi, H. T., & Sliepcevich, C. M. (1967). A Numerical Method for Solving Two-Dimensional Problems of Heat Conduction with Change of Phase. *Chemical Engineering Progress Symposium Series, 63*, 34–41.

HeatVentors Kft. (2020). *The revolution of storing thermal energy*. Retrieved 02 24, 2020, from Heat Tank: https://www.heatventors.com/?gclid=Cj0KCQiAzZL-BRDnARIsAPCJs73qW44qfS7m_2NmaiPtr20NrHJIzTzyF5fmSpQ3r4P8-z7Nn-FjnXwaAmD1EALw_wcB

Heier, J., Bales, C., & Martin, V. (2015). Combining Thermal Energy Storage with Buildings - A Review. *Renewable and Sustainable Energy Review, 42*, 1305-1325.

Heim, D., & Clarke, J. A. (2004). Numerical Modelling and Thermal Simulation of PCM–Gypsum Composites with ESP-r. *Energy and Buildings, 36*(8), 795–805.

Hensen, J. L. (1991). On the Thermal Interaction of Building Structure and Heating and Ventilating System. *PhD Thesis*. Eindhoven: Eindhoven University of Technology.

Himran, S., Suwono, A., & Mansoori, A. (1994). Characterization of Alkanes and Paraffin Waxes for Application as Phase Change Energy Storage Medium. *Energy Sources, 16*(1), 117-128. doi:10.1080/00908319408909065

Holden, E., Linnerud, K., & Banister, D. (2014). Sustainable development: Our Common Future revisited. *Global Environmental Change, 26*, 130-139.

Hong, J., Kelly, N. J., Richardson, I., & Thomson, M. (2013). Assessing Heat Pumps as Flexible Load. *Proceedings of Institute of Mechanical Engineering Part A: Journal of Power and Energy*, *227*(1), 30-42.

Hong, J., Kelly, N. J., Thomson, M., & Richardson, I. (2011). The Influence of Thermal Storage on Microgeneration Flexibility. *The 2nd Int. Conf. in Microgeneration Technologies* (pp. 4-6). Glsagow: University of Strathclyde, Glasgow.

Hosseini, M. J., Rahimi, M., & Bahrampoury, R. (2014). Experimental and Computational Evolution of a Shell and Tube Heat Exchanger as a PCM Thermal Storage System. *International Communications in Heat and Mass Transfer*, *50*, 128–136.

Hosseini, M. J., Ranjbar, A. A., Sedighi, K., & Rahimi, M. (2012). A Combined Experimental and Computational Study on the Melting Behavior of a medium Temperature Phase Change Storage Material inside Shell and Tube Heat Exchanger. *International Communications in Heat and Mass Transfer*(39), 1416-1424.

Hu, Y., Guo, R., Heiselberg, P. K., & Johra, H. (2020). Modeling PCM Phase Change Temperature and Hysteresis in Ventilation Cooling and Heating Applications. *Energies*, *13*(23), 6455. Retrieved from https://doi.org/10.3390/en13236455

Huebner, G. M., McMichael, M., Shipworth, D., Shipworth, M., Durand-Daubin, M., & Summerfield, A. (2013). Heating Patterns in English Homes: Comparing Results from a National Survey against Common Model Assumptions. *Building and Environment*, *70*, 298 - 305. doi:http://dx.doi.org/10.1016/j.buildenv.2013.08.028

Hurtado, L. A., Rhodes, J. D., Nguyen, P. H., Kamphuis, I. G., & Webber, M. E. (2017). Quantifying Demand Flexibility based on Structural Thermal Storage and Comfort Management of Non-Residential Buildings: A Comparison between Hot and Cold Climate Zones. *Applied Energy*, *195*, 1047–1054.

Inaba, H., & Tu, P. (1997). Evaluation of Thermophysical Characteristics on Shape-Stabilized Paraffin as a Solid-Liquid Phase Change Material. *Heat and Mass Transfer, 32*(4), 307-312. doi:10.1007/s002310050126

International Energy Agency. (2020(a), June). *Tracking Buildings 2020*. Retrieved from IEA Tracking Report - June 2020: https://www.iea.org/reports/tracking-buildings-2020

International Energy Agency. (2020(b)). *Buildings - A Source of Enormous Untapped Efficiency Potential*. Retrieved from IEA: https://www.iea.org/topics/buildings

Investopedia. (2020, 01 13). *Sensitivity Analysis*. Retrieved from Investopedia: https://www.investopedia.com/terms/s/sensitivityanalysis.asp

Izquierdo-Barrientos, M. A., Belmonte, J. F., Rodríguez-Sánchez, D., Molina, A. E., & Almendros-Ibáñez, J. A. (2012). A Numerical Study of External Building Walls Containing Phase Change Materials (PCM). *Applied Thermal Engineering, 47*, 73-85.

Jamil, H., Alam, M., Sanjayan, J., & Wilson, J. (2016). Investigation of PCM as Retrofitting Option to Enhance Occupantthermal Comfort in a Modern Residential Building. *Energy and Buildings, 133*, 217–229.

Jennings, A. (1985). *Matrix Computation for Engineers and Scientists.* New York: John Wiley & Sons.

Jensen, S. (1993). *Validation of Building Energy Simulation Programs, Part I & II, Reasearch Report PASSYS Subgroup Model Validation and Development.* Brussels: EUR 15115 EN, TIL, CEC.

Jeon, J., Jeong, S. G., Lee, J. H., Seo, J., & Kim, S. (2012). High Thermal Performance Composite PCMs Loading xGnP for Application to Building using Radiant Floor Heating System. *Solar Energy Materials and Solar Cells, 101,, 101*, 51–56.

Jin, X., Medina, M. A., & Zhang, X. (2013). On the Importance of the Location of PCMs in Building Walls for Enhanced Thermal Performance. *Applied Energy, 106*, 72–78.

Jordan, U., & Vajen, K. (2005). DHWCALC: Program to Generate Domestic Hot Water Draws with Statistical Means for User Defined Conditions. *ISES Solar World Congress.* Orlando.

Kalnæs, S. E., & Jelle, B. P. (2015). Phase change materials and products for building applications: A state-of-the-art review and future research opportunities. *Energy and Buildings*(94), 150–176. doi:doi: 10.1016/j.enbuild.2015.02.023

Kamali, S. (2014). Review of free cooling system using phase change material for building. *Energy and Buildings*(80), 131-136. doi:doi: 10.1016/j.enbuild.2014.05.021

Kant, K., Shukla, A., & Sharma, A. (2017). Heat Transfer Studies of Building Brick Containing Phase Change Materials. *Solar Energy, 155*, 1233–1242.

Karaipekli, A., & Sarı, A. (2016). Development and Thermal Performance of Pumice/Organic PCM/Gypsum Composite Plasters for Thermal Energy Storage in Buildings. *Solar Energy Materials & Solar Cells, 149*, 19–28.

Kasaeian, A., Bahrami, L., Pourfayaz, F., Khodabandeh, E., & Yan, W.-M. (2017). Experimental studies on the applications of PCMs and nano-PCMs in buildings: A critical review. *Energy and Building, 154*, 96–112. doi:http://dx.doi.org/10.1016/j.enbuild.2017.08.037

Kelly, N. J. (1998). Towards a Design Environment for Building Integrated Energy Systems: The Integration Of Electrical Power Flow Modelling with Building Simulation. *PhD Thesis*. Glasgow: ESRU, University of Strathclyde.

Kelly, N. J., Tuohy, P. G., & Hawkes, A. D. (2014). Performance Assessment of Tariff-Based Air Source Heat Pump Load Shifting in a UK Detached Dwelling Featuring Phase Change-Enhanced Buffering. *Applied Thermal Engineering, 71*(2), 809-820.

Kendrick, C., & Walliman, N. (2007). Removing Unwanted Heat in Lightweight Buildings using Phase Change Materials in Building Components: Simulation Modelling for PCM Plasterboard. *Architectural Science Review, 50*(3), 265-273.

Kensby, J., Trüschel, A., & Dalenbäck, J.-O. (2015). Potential of Residential Buildings as Thermal Energy Storage in District Heating Systems – Results from a Pilot Test. *Applied Energy, 137*, 773-781.

Khadiran, T., Hussein, M. Z., Zainal, Z., & Rusli, R. (2015). Encapsulation Techniques for Organic Phase Change Materials as Thermal Energy Storage Medium: A Review. *Solar Energy Materials and Solar Cells, 143*, 78-98.

Khajehzadeh, I., & Vale, B. (2015). How do people use large houses? In R. H. Crawford, & A. Stephan (Ed.), *49th International Conference of the Architectural Science Association, 2-4 December 2015* (pp. 153–162). Melbourne: Architectural Science Association; The University of Melbourne. Retrieved from http://anzasca.net/wp-content/uploads/2015/12/ASA_2015_Proceedings.pdf

Kim, M., Kim, M. S., & Chung, J. D. (2004). ransient Thermal Behavior of a Water Heater System Driven by a Heat Pump. *International Journal of Refrigeration, 27*(4), 415-421.

Kong, X., Lu, S., Li, Y., Huang, J., & Liu, S. (2014). Numerical Study On The Thermal Performance of Building Wall and Roof Incorporating Phase Change Material Panel for Passive Cooling Application. *Energy and Buildings, 81*, 404-415.

Kong, X., Wang, L., Li, H., Yuan, G., & Yao, C. (2020). Experimental Study on a Novel Hybrid System of Active Composite PCM Wall and Solar Thermal System for Clean Heating Supply in Winter. *Solar Energy, 195*, 259-270.

Kośny, J. (2015). Short History of PCM Applications in Building Envelopes. In J. Kośny, & B. Derby (Ed.), *PCM-Enhanced Building Components - An Application of Phase Change Materials in Building Envelopes and Internal Structures* (pp. 21-59). New York: Springer International Publishing . doi:https://doi.org/10.1007/978-3-319-14286-9_2

Kozak, Y., Rozenfeld, T., & Ziskind, G. (2014). Close-contact Melting in Vertical Annular Enclosures with a Non-isothermal Base: Theoretical Modeling and Application to Therma Storage. *International Journal of Heat and Mass Transfer*(72), 114–127.

Kuczyński, T., & Staszczuk, A. (2020). Experimental Study of the Influence of Thermal Mass on Thermal Comfort and Cooling Energy Demand in Residential Buildings. *Energy, Article in press*, 116984.

Kumar, G. S., Nagarajan, D., Chidambaram, L., Kumaresan, V., Ding, Y., & Velraj, R. (2016). Role of PCM Addition on Stratification Behaviour in a Thermal Storage Tank - An Experimental Study. *Energy, 115*(Part 1), 1168-1178.

Kuravi, S., Trahan, J., Rahman, M. M., Goswami, D., & Stefanakos, E. K. (2010). Analysis of Transient Heat Transfer in a Thermal Energy Storage Module. *ASME 2010 International Mechanical Engineering Congress & Exposition, November 12-18, 2010.* Vancouver, British Columbia, Canada: American Society of Mechanical Engineers.

Kusama, Y., & Ishidoya, Y. (2017). Thermal Effects of a Novel Phase Change Material (PCM) Plaster under Different Insulation and Heating Scenarios. *Energy and Buildings, 141*, 226-237.

Kuznik, F., Virgone, J., & Johannes, K. (2011). In-Situ Study of Thermal Comfort Enhancement in a Renovated Building Equipped with Phase Change Material Wallboard. *Renewable Energy, 36*(5), 1458–1462.

Kylili, A., & Fokaides, P. A. (2017). Numerical Simulation of Phase Change Materials for Building Applications: A Review. *Advances in Building Energy Research, 11*(1), 1–25.

Labat, M., Virgone, J., David, D., & Kuznik, F. (2014). Experimental Assessment of a PCM to Air Heat Exchanger Storage System for Building Ventilation Application. *Applied Thermal Engineering, 66*, 375-382.

Lerner, S. E., Ishai, P. B., Agranat, A. J., & Feldman, Y. D. (2007). Percolation of Polar Nanoregions: A Dynamic Spproach to the Ferro-Electric Phase Transition. *Journal of Non-Crystalline Solids, 353*(47-51), 4422-4427. doi:DOI: 10.1016/j.jnoncrysol.2007.02.075

Lewis, R. W., & Ravindran, K. (2000). Finite Element Simulation of Metal Casting. *International Journal for Numerical Methods in Engineering, 47*(1-3), 29-59.

Li, D. H., Yang, L., & Lam, J. C. (2013). Zero Energy Buildings and Sustainable Development Implications – A Review. *Energy, 54*, 1–10.

Li, D., Zheng, Y., Liu, C., & Wu, G. (2015). Numerical Analysis on Thermal Performance of Roof Contained PCM of a Single Residential Building. *Energy Conversion and Management, 100*, 147–156.

Li, G., Koua, C., & Wang, H. (2019). Estimating City-Level Energy Consumption of Residential Buildings: A Lifecycle Dynamic Simulation Model. *Journal of Environmental Management, 240*, 451–462.

Lindfield, G., & Penny, J. (2019). *Numerical Methods Using MATLAB* (4 ed.). London: Academic Press.

Liu, Z., Li, W., Chen, Y., Luo, Y., & Zhang, L. (2019). Review of Energy Conservation Technologies for Fresh Air Supply in Zero Energy Buildings. *Applied Thermal Engineering, 148*, 544-556.

Lloyds Bank. (2013). *Britain at Home Report.* London: Lloyds Bank. Retrieved Dec 20, 2019, from https://www.lloydsbankinggroup.com/globalassets/documents/media/press-releases/lloyds-bank/2013/3009_home_report.pdf

Local Government and Communities Directorate. (2019, Jan 01). *Building Standards Technical Handbook 2019: Domestic.* Retrieved Oct 15, 2019, from Publication - Advice and Guidance: https://www.gov.scot/publications/building-standards-technical-handbook-2019-domestic/6-energy/6-2-building-insulation-envelope/

Long, L., Ye, H., Gao, Y., & Zou, R. (2014). Performance Demonstration And Evaluation of the Synergetic Application of Vanadium Dioxide Glazing and Phase Change Material in Passive Buildings. *Applied Energy, 136,, 136*, 89–97.

Love, J., Smith, A. Z., Watson, S., Oikonomou, E., Summerfield, A., Gleeson, C., . . . Lowe, R. (2017). The Addition of Heat Pump Electricity Load Profiles to GB Electricity Demand: Evidence From A Heat Pump Field Trial. *Applied Energy, 204*, 332-342.

Lu, S., Zhao, Y., Fang, K., Li, Y., & Sun, P. (2017). Establishment and Experimental Verification of TRNSYS Model for PCM Floor Coupled with Solar Water Heating System. *Energy and Buildings, 140*, 245–260.

Luburić, Z., Pandžić, H., Plavšić, T., Teklić, L., & Valentić, V. (2018). Role of energy storage in ensuring transmission system adequacy and security. *Energy, 156*, 229-239. doi:https://doi.org/10.1016/j.energy.2018.05.098

Madad, A., Mouhib, T., & Mouhsen, A. (2018). Phase Change Materials for Building Applications: A Thorough Review and New Perspectives. *Buildings, 8*(5), 63. doi:https://doi.org/10.3390/buildings8050063

Maivel, M., Ferrantelli, A., & Kurnitsk, J. (2018). Experimental Determination of Radiator, Underfloor and Air Heating Emission Losses due to Stratification and Operative Temperature Variations. *Energy and Buildings, 166*, 220-228.

Mankibi, M. E., Stathopoulos, N., Rezaï, N., & Zoubir, A. (2015). Optimization of an Air-PCM Heat Exchanger and Elaboration of Peak Power Reduction Strategies. *Energy and Buildings, 106*, 74–86.

Marin, P., Saffari, M., De-Gracia, A., Zhu, X., Farid, M. M., Cabeza, L. F., & Ushak, S. (2016). Energy Savings due to the use of PCM for Relocatable Lightweight Buildings Passive Heating and Cooling in Different Weather Conditions. *Energy and Buildings, 129*, 274–283.

Mayo Foundation for Medical Education and Research (MFMER). (2020, 08 12). *How many hours of sleep are enough for good health?* Retrieved from Healthy Lifestyle - Adult Health: https://www.mayoclinic.org/healthy-lifestyle/adult-health/expert-answers/how-many-hours-of-sleep-are-enough/faq-20057898

Mazo, J., Delgado, M., Marin, J. M., & Zalba, B. (2012). Modeling A Radiant Floor System with Phase Change Material (PCM) Integrated into a Building Simulation Tool: Analysis of a Case Study of a Floor Heating System Coupled to a Heat Pump. *Energy and Buildings, 47*, 458–466.

Mehling, H., & Cabeza, L. F. (2008). Chapter 9, Applications for heating and cooling in buildings. In H. Mehling, L. F. Cabeza, D. Mewes, & E. M. ed (Eds.), *Heat And Cold Storage with PCM: An Up To Date Introduction into Basics and Applications* (pp. 217-295). Berlin: Springer-Verlag Berlin.

Mehling, H., & Cabeza, L. F. (2008). *Heat and Cold Storage with PCM.* Berlin: Springer. doi:DOI 10.1007/978-3-540-68557-9

Mehrali, M., Latibari, S., Mehrali, M., Mahli, T. M., Sadeghinezhad, E., & Metselaar, H. S. (2014). Preparation of Nitrogen-Doped Graphene/Palmitic Acid Shape Stabilized Composite Phase Change Material with Remarkable Thermal Properties for Thermal Energy Storage. *Applied Energy, 135*, 339-349.

Meng, X., Yan, B., Gao, Y., Wang, J., Zhang, W., & Long, E. (2015). Factors affecting the In-Situ Measurement Accuracy of the Wall Heat Transfer Coefficient using the Heat Flow Meter Method. *Energy and Buildings, 86*, 754-765.

Mitchell, A. R. (1969). *Computational Methods in Partial Differential Equations (Introductory Mathematics for Scientists And Engineers).* New York: Wiley-Blackwell.

Moldovan, C., Damian, C., & Georgescu, O. (2017). Voltage Level Increase in Low Voltage Networks through Reactive Power Compensation Using Capacitors. *Procedia Engineering, 181*, 731-737. Retrieved from https://doi.org/10.1016/j.proeng.2017.02.459

Moreno, P., Castell, A., Solé, C., Zsembinszki, G., & Cabeza, L. F. (2014). PCM Thermal Energy Storage Tanks in Heat Pump System for Space Cooling. *Energy and Buildings, 82*, 399–405.

Morovat, N., Athienitis, A. K., Candanedoa, J. A., & Dermardiros, V. (2019). Simulation and Performance Analysis of an Active PCM Heat Exchanger intended for Building Operation Optimization. *Energy & Buildings, 199*, 47–61.

Münster, E., & Lund, H. (2007). Comparison of Electricity Balancing for Large Scale Integration of Renewable Energy in Six European Regions. In Z. Guzovic, N. Duic, & M. Ban (Ed.), *4th Dubrovnik Conference on Sustainable Development of Energy,*

Water and Environmental Systems. Dubrovnik: Forlag Uden Navn. Retrieved May 18, 2012, from http://desire.iwes.fraunhofer.de/files/dissemination/articles/03_Ebbe_&_Henrik_1_no_ppt.pdf

Muruganantham, K., Phelan, P., Horwath, P., Ludlam, D., & McDonald, T. (2010). Experimental Investigation of a Bio-Based Phase Change Material to Improve Building Energy Performance. *4th International Conference on Energy Sustainability. 1*, pp. 979-984. Phoenix, Arizona: ASME.

Najafian, A., Haghighat, F., & Moreau, A. (2015). Integration of Pcm in Domestic Hot Water Tanks: Optimization for Shifting Peak Demand. *Energy and Buildings*.

Narisada, K., & Schreuder, D. (2004). *Light Pollution Handbook.* Dordrecht: Springer Science & Business Media.

National Records of Scotland. (2015, Aug 27). *Household composition for specific groups of people in Scotland: Scotland's Census 2011.* Retrieved from Household composition for specific groups of people in Scotland: Scotland's Census 2011: https://www.scotlandscensus.gov.uk/documents/analytical_reports/HH%20report.pdf

National Records of Scotland. (2018, January 01). *Housing and Accommodation*. Retrieved October 01, 2019, from Scotland's Census - Shaping Our Future: https://www.scotlandscensus.gov.uk/housing-and-accommodation

Navarro, A., & Ochoa, L. N. (2014). *Deliverable 3.6 "What-if scenario impact studies based on real LV networks"*. Manchester: Electricity North West Limited (ENWL) - Low Voltage Network Solutions. doi:DOI: 10.13140/RG.2.1.1986.7600

Navarro, L., De-Gracia, A., Colclough, S., Browne, M., McCormack, S. J., Griffiths, P., & Cabeza, L. F. (2016). Thermal Energy Storage in Building Integrated Thermal Systems: A Review. Part 1. Active Storage Systems. *Renewable Energy, 88*, 526–547.

Nejat, P., Jomehzadeh, F., Taheri, M. M., Gohari, M., & Abd.Majidd, M. Z. (2015). A Global Review of Energy Consumption, CO2 Emissions and Policy in the Residential Sector (with an Overview of the Top Ten CO2 Emitting Countries). *Renewable and Sustainable Energy Reviews, 43*, 843-862.

Nkwetta, D. N., Vouillamoz, P.-E., Haghighat, F., El-Mankibi, M., Moreau, A., & Daoud, A. (2014). Impact of Phase Change Materials Types and Positioning on Hot Water Tank Thermal Performance: Using Measured Water Demand Profile. *Applied Thermal Engineering, 67*, 460-468.

Obitayo, O. A. (2011). *Simulation and Analysis of Phase Change Materials for Building Temperature Control.* University of Strathlyde. Glasgow: ASRU.

Odyssee-Mure. (2020). *Energy Consumption - Consumption by End-Use (EU).* Retrieved Jan 12, 2020, from SECTORAL PROFILE - HOUSEHOLDS: https://www.odyssee-

mure.eu/publications/efficiency-by-sector/households/declining-share-space-heating-eu.html

Office for National Statistics - Labour Force Survey (LFS). (2019, Nov 15). *Families and households.* Retrieved March 02, 2020, from Office for National Statistics: https://www.ons.gov.uk/file?uri=%2fpeoplepopulationandcommunity%2fbirthsdeathsandmarriages%2ffamilies%2fdatasets%2ffamiliesandhouseholdsfamiliesandhouseholds%2fcurrent/fandh2019final.xls

Office for National Statistics. (2011, March 12). *2011 Census*. Retrieved Dec. 12, 2017, from Population and household estimates for the United Kingdom: https://www.ons.gov.uk/peoplepopulationandcommunity/populationandmigration/populationestimates/bulletins/populationandhouseholdestimatesfortheunitedkingdom/2011-03-21#:~:text=The%20number%20of%20households%20in,census%20day%20was%2062.1%20million

Ogoh, W., & Groulx, D. (2012). Effects of The Number and Distribution of Fins on the Storage Characteristics of a Cylindrical Latent Heat Energy Storage System: A Numerical Study. *Heat and Mass Transfer, 48*(10), 1825–1835.

Oliver, A. (2012). Thermal Characterization of Gypsum Boards with PCM Included: Thermal Energy Storage in Buildings through Latent Heat. *Energy and Buildings, 48*, 1–7. doi:doi:10.1016/j.enbuild.2012.01.026

Ong, B. H., Walmsley, T. G., Atkins, M. J., & Walmsley, M. R. (2017). Total site mass, heat and power integration using process integration and process graph. *Journal of Cleaner Production, 167*, 32-43.

Ozdenefe, M., & Dewsbury, J. (2012). Dynamic Thermal Simulation of a PCM Lined Building with Energy Plus. In N. Altawell, K. Volkov, C. Matos, & P. F. De-Arroyabe (Ed.), *Recent Researches in Environmental and Geological Sciences, Energy, Environmental and Structural Engineering Series. 4*, pp. 359-364. Kos, Greece: WSEAS Press.

Özkan, D. B., & Onan, C. (2011). Optimization of Insulation Thickness for Different Glazing areas in Buildings for Various Climatic Regions in Turkey. *Applied Energy, 88*(4), 1331-1342.

Özkan, D. B., & Onan, C. (2011). Optimization of Insulation Thickness for Different Glazing Areas in Buildings for Various Climatic Regions in Turkey. *Applied Energy, 88*(4), 1331-1342.

Pablo-Romeroa, M. d., Pozo-Barajas, R., & Yñiguez, R. (2017). Global Changes in Residential Energy Consumption. *Energy Policy, 101*, 342–352.

Pacheco-Torgal, F. (2017). Introduction to Cost-Effective Energy-Efficient Building Retrofitting. In F. Pacheco-Torgal, F. Pacheco-Torgal, C.-G. Granqvist, B. P. Jelle, G. P. Vanoli, N. Bianco, & J. Kurnitski (Eds.), *Cost-Effective Energy Efficient Building Retrofitting* (pp. 1-20). Cambridge: Woodhead Publishing. Retrieved from https://doi.org/10.1016/B978-0-08-101128-7.00001-0

Padovan, R. (2014). *Analysis and Optimization of PCM Enhanced Storage Tanks for Solar Domestic Hot Water Systems.* University of Udine. Udine: University of Udine.

Padovan, R., & Manzan, M. (2013). Development of a Stratified Tank Storage Component for ESP-r with embedded Phase Change Material Modules. *Journal of Power and Energy - Proceedings of the Institution of Mechanical Engineers, Part A, 227*(1), 53-61. doi:DOI: 10.1177/0957650912454391

Pannier, M.-L., Schalbart, P., & Peuportier, B. (2018). Comprehensive Assessment of Sensitivity Analysis Methods for the Identification of Influential Factors in Building Life Cycle Assessment. *Journal of Cleaner Production, 190*, 466-480.

Passive House Institute (a). (2015). *Passive House Institute / About us.* Retrieved 01 21, 2019, from Passive House Institute: https://passivehouse.com/01_passivehouseinstitute/01_passivehouseinstitute.htm

Passive House Institute (b). (2015). *Passive House requirements.* Retrieved 01 21, 2019, from Passive House Institute: https://passivehouse.com/02_informations/02_passive-house-requirements/02_passive-house-requirements.htm

Peippo, K., Kauranen, P., & Lund, P. D. (1991). A mMulti Component PCM Wall Optimized for Passive Solar Heating. *Energy and Buildings, 17*(4), 259-270.

Pomianowski, M., Heiselberg, P., Jensen, R. L., Cheng, R., & Zhang, Y. (2014). A New Experimental Method to Determine Specific Heat Capacity of Inhomogeneous Concrete Material with Incorporated Micro-encapsulated-PCM. *Cement and Concrete Research, 55*, 22-34.

Protopapadaki, C., & Saelens, D. (2017). Heat Pump and PV Impact on Residential Low-Voltage Distribution Grids as a Function of Building and District Properties. *Applied Energy, 192*(15), 268-281. doi:https://doi.org/10.1016/j.apenergy.2016.11.103

Qian, D., Li, Y., Niu, F., & O'Neill, Z. (2019). Nationwide Savings Analysis of Energy Conservation Measures in Buildings. *Energy Conversion and Management, 188*, 1-18.

Qiu, Z., Ma, X., Li, P., Zhao, X., & Wright, A. (2017). Micro-Encapsulated Phase Change Material (MPCM) Slurries: Characterization and Building Applications. *Renewable and Sustainable Energy Reviews, 77*, 246–262. doi:https://doi.org/10.1016/j.rser.2017.04.001

Quiggin, D., & Buswell, R. (2016). The implications of Heat Electrification on National Electrical Supply-Demand Balance under Published 2050 Energy Scenarios. *Energy, 98*, 253-270. doi:https://doi.org/10.1016/j.energy.2015.11.060

Rahimpour, Z., Faccani, A., Azuatalam, D., Chapman, A., & Verbič, G. (2017). Using Thermal Inertia of Buildings with Phase Change Material for Demand Response. *Energy Procedia, 121*, 102-109. doi:https://doi.org/10.1016/j.egypro.2017.07.483

Real, A., García, V., Domenech, L., Renau, J., Montés, N., & Sánchez, F. (2014). Improvement of a Heat Pump Based HVAC System with PCM Thermal Storage for Cold Accumulation and Heat Dissipation. *Energy and Buildings, 83*, 108-116. doi:https://doi.org/10.1016/j.enbuild.2014.04.029

Reynders, G., Nuytten, T., & Saelens, D. (2013). Potential of Structural Thermal Mass for Demand-Side Management in Dwellings. *Building and Environment, 64*, 187-199.

Rozenfeld, T., Kozak, Y., Hayat, R., & Ziskind, G. (2015). Close-contact Melting in a Horizontal Cylindrical Enclosure with Longitudinal Plate Fins: Demonstration, Modeling and Application to Thermal Storage. *International Journal of Heat and Mass Transfer, 86*, 465–477.

Rubitherm Technologies GmbH. (2018, Nov. 12). *PCM RT-LINE*. Retrieved Nov. 12, 2019, from Datasheet - RT50: https://www.rubitherm.eu/media/products/datasheets/Techdata_-RT50_EN_06082018.PDF

Russell, M., & Surendran, P. (2001). Influence of Active Heat Sinks on Fabric Thermal Storage in Building Mass. *Applied Energy, 70*, 17–33.

Sadasivam, S., Zhang, D., & Fung, A. S. (2011). *An Iterative Enthalpy Method to Overcome the Limitations in ESP-r's PCM Solution Algorithm.* Montreal: ASHRAE Transactions.

Sadasivam, S., Zhang, D., Fung, A. S., & Almeida, F. (2011). An Iterative Enthalpy Method to Overcome the Limitations in ESP-r's PCM Solution Algorithm. *ASHRAE Transactions, 117*, 100-107.

Saffari, M., De-Gracia, A., Ushakc, S., & Cabeza, L. F. (2017). Passive Cooling of Buildings with Phase Change Materials using Whole-building Energy Simulation tools: A Review. *Renewable and Sustainable Energy Reviews, 80*, 1239–1255.

Şahan, N., Fois, M., & Paksoy, H. (2015). Improving tTermal Conductivity Phase Change Materials—A Study of Paraffin Nanomagnetite Composites. *Solar Energy Materials and Solar Cells, 137*, 61-67.

Sajjadian, S. M., Lewis, J., & Sharples, S. (2015). The Potential of Phase Change Materials to Reduce Domestic Coolingenergy Loads for Current and Future UK Climates. *Energy and Buildings, 93*, 83-89.

Samarskij, A. A., & Vabiščevič, P. N. (1995). *Computational Heat Transfer.* Chichester [u.a];: Wiley.

Samuel, D. G., Nagendra, S. M., & Maiya, M. P. (2013). Passive Alternatives To Mechanical Air Conditioning of Building: A Review. *Building and Environment, 66*, 54-64.

Sarbu, I., & Sebarchievici, C. (2017). *Solar Heating and Cooling Systems.* London: Academic Press.

Sargent, R. G. (2014). Verifying and Validating Simulation Models. In A. Tolk, S. Y. Diallo, I. O. Ryzhov, L. Yilmaz, S. Buckley, & J. A. Miller (Ed.), *2014 Winter Simulation Conference* (pp. 118 - 131). Savannah Georgia: Institute of Electrical and Electronics Engineers.

Šavija, B., & Schlangen, E. (2016). Use of Phase Change Materials (PCMs) to Mitigate Early Age Thermal Cracking in Concrete: Theoretical Considerations. *Construction and Building Materials, 126*, 332-344.

Schossig, P., Henning, H.-M., Gschwander, S., & Haussmann, T. (2005). Micro-Encapsulated Phase Change Materials Integrated into Construction Materials. *Solar Energy Materials and Solar Cells, 89*(2-3), 297–306.

Seddegh, S., Wang, X., & Henderson, A. D. (2016). A Comparative Study of Thermal Behaviour of a Horizontal and Vertical Shell-and-Tube Energy Storage Using Phase Change Materials. *Applied Thermal Engineering, 93*, 348–358.

Sergent, R. G. (2009). Verification and Validation of Simulation Models. In M. D. Rossetti, R. R. Hill, B. Johansson, A. Dunkin, & R. G. Ingalls (Ed.), *2009 Winter Simulation Conference* (pp. 162 - 176). Austin, Texas: Institute of Electrical and Electronics Engineers - IEEE.

Sergent, R. G. (2013). Verification and Validation of Simulation Models. *Journal of Simulation, 7*, 12–24.

Shatikian, V., Ziskind, G., & Letan, R. (2005). Numerical Investigation of a PCM-Based Heat Sink with Internal Fins. *International Journal of Heat and Mass Transfer, 48*(17), 3689–3706.

Shipworth, M., Firth, S. K., Gentry, M. I., Wright, A. J., Shipworth, D. T., & Lomas, K. J. (2010). Central Heating Thermostat Settings and Timing: Building Demographics. *Building Research & Information, 38*(1), 50-69.

Silva, T., Vicente, R., Amaral, C., & Figueiredo, A. (2016). Thermal Performance of a Window Shutter Containing PCM: Numerical Validation and Experimental Analysis. *Applied Energy, 179*, 64-84.

Singh, H., Muetze, A., & Eames, P. (2010). Factors Influencing the Uptake of Heat Pump Technology by the UK Domestic Sector. *Renewable Energy, 35*(4), 873-878.

Soares, N., Costa, J., Gaspar, A., & Santos, P. (2013). Review of passive PCM latent heat thermal energy storage systems towards buildings' energy efficiency:. *Energy and Buildings, 59*, 82–103. doi:doi: 10.1016/j.enbuild.2012.12.042

Soares, N., Gaspar, A. R., Santos, P., & Costa, J. J. (2016). Experimental Evaluation of the Heat Transfer Through Small PCM-Based Thermal Energy Storage Units for Building Applications. *Energy and Buildings, 116*, 18–34.

Souayfane, F., Fardoun, F., & Biwoleb, P.-H. (2016). Phase Change Materials (PCM) for Cooling Applications In Buildings: A Review. *Energy and Building*, *129*, 396-4313.

Srinivasan, P. S., & Ravikumar, M. (2014). Heat Transfer Analysis in PCM-Filled RCC Roof for Thermal Management. *Journal of Mechanical Science and Technology*, *28*(3), 1073–1078.

Statista. (2020, Jan 09). *Time spent cooking a weeknight meal in the UK 2019, by duration*. Retrieved from On average, how much time are you happy to spend cooking a weeknight meal?: https://www.statista.com/statistics/1085302/time-spent-cooking-weeknight-in-the-uk/#statisticContainer

Sunamp technology. (2020, 12 09). *Heating your home and water*. Retrieved from Sunamp: https://sunamp.com/residential/

Talmatsky, E., & Kribus, A. (2008). PCM storage for solar DHW: An unfulfilled promise? *82*(10), 861–869.

Tian, Y., & Zhao, C. (2013). A Review of Solar Collectors and Thermal Energy Storage in Solar Thermal Applications. *Applied Energy, 104*, 538–553.

Torres-Rivas, A., Pozo, C., Ewertowska, A., Boer, D., & Esteller, L. J. (2018). Systematic generation of insulation materials via DEA and Building modelling. In J. J. Anton Friedl (Ed.), *Computer Aided Chemical Engineering* (Vol. 43, pp. 457-462). Amsterdam: Elsevier B.V. doi:https://doi.org/10.1016/B978-0-444-64235-6.50082-6.

Turnpenny, J. R., Etheridge, D. W., & Reay, D. A. (2000). Novel Ventilation Cooling System for Reducing Air Conditioning in Buildings.: Part I: Testing and Theoretical Modelling. *Applied Thermal Engineering, 20*(11), 1019–1037.

Turnpenny, J. R., Etheridge, D. W., & Reay, D. A. (2001). Novel Ventilation System for Reducing Air Conditioning in Buildings. Part II: Testing of Prototype. *Applied Thermal Engineering , 21*(12), 1203–1217.

University of Illinois. (2021, March 30). *Input Output Refeerence.* Retrieved July 28, 2021, from EnergyPlus Documentation: https://energyplus.net/sites/all/modules/custom/nrel_custom/pdfs/pdfs_v9.5.0/InputOutputReference.pdf

Varga, Z., & Palotai, B. (2017). Comparison of low temperature waste heat recovery methods. *Energy,, 137*(C), 1286-1292.

Verbeke, S., & Audenaert, A. (2018). Thermal Inertia in Buildings: A Review of Impacts across Climate and Building Use. *Renewable and Sustainable Energy Reviews, 82*(3), 2300-2318.

Voller, V. R. (1996). An Overview of Numerical Methods for Solving Phase Change Problems. In W. J. Minkowycz, & E. M. Sparrow, *Advances In Numerical Heat Transfer, Volume 1* (Vol. 1, pp. 341-380). Washington DC: Taylor and Francis.

Wang, S., Faghri, A., & Bergman, T. L. (2012). A Comparison Study of Sensible and Latent Thermal Energy Storage Systems for Concentrating Solar Power Applications. *Numerical Heat Transfer, Part A: Applications, 61*(11), 860-871. doi:DOI: 10.1080/10407782.2012.672887

Watson, S. D., Lomas, K. J., & Buswell, R. A. (2019). Decarbonising Domestic Heating: What is the Peak GB Demand? *Energy Policy, 126*, 533-544.

Whiffen, T. R., & Riffat, S. B. (2013). A review of PCM technology for thermal energy storage in the built environment: Part I. *International Journal of Low-Carbon Technologies, 8*(3), 147–158. doi:https://doi.org/10.1093/ijlct/cts021

Wijesuriya, S., Brandt, M., & Tabares-Velasco, P. C. (2018). Parametric Analysis Of A Residential Building with Phase Change Material (PCM)-Enhanced Drywall, Precooling, and Variable Electric Rates in a Hot and Dry Climate. *Applied Energy, 222*, 497–514.

Wilson, I. A., Rennie, A. J., Ding, Y., Eames, P. C., Hall, P. J., & Kelly, N. J. (2013). Historical Daily Gas and Electrical Energy Flows through Great Britain's Transmission Networks and the Decarbonisation of Domestic Heat. *Energy Policy, 61*, 301-305. doi:https://doi.org/10.1016/j.enpol.2013.05.110

Yang, Y. K., Kang, I. S., Chung, M. H., Kim, S., & Park, J. C. (2017). Effect of PCM Cool Roof System on The Reduction in Urban Heat Island Phenomenon. *Building and Environment, 122*, 411-421.

Yao, R., & Steemers, K. (2005). A Method of Formulating Energy Load Profile for Domestic Buildings in the UK. *Energy and Buildings, 37*, 663–671.

Young, B. A., Falzone, G., Wei, Z., Sant, G., & Pilon, L. (2018). Reduced-Scale Experiments to Evaluate Performance of Composite Building Envelopes Containing Phase Change Materials. *Construction and Building Materials, 162*, 584-595.

Yuan, J., Farnham, C., Emura, K., & Alam, M. A. (2016). Proposal for Optimum Combination of Reflectivity and Insulation Thickness of Building Exterior Walls for Annual Thermal Load in Japan. *Building and Environment, 103*, 228-237.

Zastawna-Rumin, A., Kisilewicz, T., & Berardi, U. (2020). Novel Simulation Algorithm for Modeling the Hysteresis of Phase Change Materials. *Energies*, *13*(5), 1200. Retrieved from https://doi.org/10.3390/en13051200

Zeinelabdein, R., Omer, S., & Gana, G. (2018). Critical Review of Latent Heat Storage Systems for Free Cooling in Buildings. *Renewable and Sustainable Energy Reviews*, *82*, 2843–2868. Retrieved from http://dx.doi.org/10.1016/j.rser.2017.10.046

Zhou, Y., Zheng, S., Liu, Z., Wen, T., Ding, Z., Yan, J., & Zhang, G. (2020). Passive and Active Phase Change Materials Integrated Building Energy Systems with Advanced Machine-Learning Based Climate-Adaptive Designs, Intelligent Operations, Uncertainty-Based Analysis and Optimisations: A State-Of-The-Art Review. *Renewable and Sustainable Energy Reviews*, *130*, 109889. Retrieved from https://doi.org/10.1016/j.rser.2020.109889

Appendices

Appendix A – ESP-r Modules/Solvers and Description

Table A1: ESP-r Modules

Solver	Description
aco	Conducts acoustic assessment of the constituents of a building/model (occupants and furniture) and post-processing.
bps	The integrated (all domain) simulation engine. This is the module responsible for carrying out integrated simulation of the building model by running pre-defined assessment based on a specific model configuration file. It initialises the graphic user interface through which user can develop models, specify boundary conditions and initiate simulation. It is also responsible for coordinating all aspects of the simulation process, including inter-connection between other modules, and display of results. It does this by generating separate domain performance files based on number of domains implied by the model.
c2e	This module performs pressure coefficients estimation in the surrounding of a building.
cfg	*Surface adjacency is established by this module after a geometric scan of models.
clm	Weather display, analysis, and conversion tool. It performs climate and weather data processing, analysis and display, and enables user to create, modify and analyse climate data sets in a compatible manner. It is also used for weather file conversions and for exploring weather patterns, as well as identifying representative periods of seasons.
dbm	The database manager. Responsible for managing database items and creating ascii generic database which can be read and converted to binary database files.
dfs	A stand-alone CFD flow solver (module). It assesses whether a CFD domain can be solved and solves where static boundary conditions are applicable. It has facilities for reviewing domain gridding and for presenting results of assessment.
e2r	The radiance models manager, exporter, controller, and viewer. It is responsible for translating and controlling building/model radiance and visual assessment/processing, and for daylight and glare calculations.
ecnv	The model import and export facility. This is responsible for converting ESP-r data to other programming languages and vice versa.

eco	This performs life cycle and environmental impacts assessments of building models
grd	2D and 3D grid specification tool. It is responsible for applying multi-dimensional grids to building models. It creates control volumes and nodes for all elements and defines/controls points of intersection and connections between them. It is also responsible for graphical display of multi-dimensional gridding and connections.
ish	Shading and insolation pre-processor and display module. It performs predictions and viewing of direct and diffuse shading on opaque and transparent surfaces and insolation of internal surfaces. It deals with zones of arbitrary complexity within the limits of current ESP-r version for surfaces-per-zone, including those with explicit internal mass surfaces.
mfs	Stand-alone fluid mass flow modelling module that simulates fluid flow in buildings and plant configurations. This entails calculating fluid flow through branches and nodes in a network that represents a building or plant configuration. It uses iterative mass balance approach wherein the nodal pressures (of unknown pressure nodes) are adjusted until the mass residual of each internal node satisfies some criterion.
mld	Stand-alone micro-toxin display and reporting module. It analyses micro-toxins in models using temperature and humidity patterns and compares against database. It is also responsible for graphical display of results.
mrt	*Calculates surface to surface view factors and sensor view factors
net	*Creates icon-based network descriptions
pdb	Plant component template (database) management module. This maintains plant component description files, where data used by *esrubps* for plant operation/simulation are kept. It enables exploration of plant components details (nodal scheme and attributes) and conversion between the ASCII and binary representations.
prj	Project Manager: This is the module responsible for commissioning technical assessments and analysis of models, defining form and composition of zones and events within, defining environmental controls and setting up parameters for simulation assessment. It is also responsible for invoking the simulator (bps) and results extractor (res), as well as other modules, as required for model resolution improvements. It is equipped for checking models and displaying related images at beginning of or at specific points during simulation. It has capabilities for building multiple variants of a base case model.
pro	*Responsible for event profiles management.

res	Graphical results display and reporting module. Responsible for processing and developing results libraries and databases for presentation as specified by user. It initialises user terminal and user-specified results database and displays the main menu.
tdf	Responsible for temporal (short timestep data) files management.
vew	Hidden line and wireframe model display tool. It renders file as hidden line wireframe images.
* - *Copied from* (ESRU, 2016)	

Appendix B – ESP-r Common Variables Block

Common variables are parameters/variables that ESP-r uses for identifying or specifying properties, characteristics and nature of all the constituents/components of a building model earmarked for simulation. These range from thermophysical and flow properties, type of phase, dimensional properties/characteristics, inter-relationship between systems, type and nature/size of data, Connection or pointers to relevant components and parameters of modules are parameters represented by variables contained in the system's common block file/database. These 'common' variables are contained in a file named 'common_list'. They are mostly array type parameters/variables whose array size is determined by a number of factor like number and type components that make up the building model (plants and zones), the component to be processed, number of plant connections, etc. They identify all the variables/parameter that the machine uses for its analysis.

Some of the variables are databases containing miscellaneous plant or zone data while others are single variables that define or mark nodes for iteration or indicate node connection numbers, or properties of working fluids, like water temperature and flow rates. Some of the variables point directly to model components, with one of their array elements identifying the component, while others point to nodes within or representing components, with an array element identifying the component node.

Table A.1 contains some sample plant specific common variables. The array elements represented by numbers 1, 2 and 9 in the table indicate miscellaneous data contained in the database relating to components. They range from specific properties or state of working fluids to number of non-zero matrix coefficients associated with the component.

Table B1: Some common variables in ESP-r

Variable	**Description**
ICONDX(i, j, k)	Defines connection number for plant in a network
NPCDAT(i, 9)	Defines components' node numbers within plant network
ICSV(x, mpvar)	Indicates node flagged for iteration
CSVI(x, mpvar)	Present time variable for plant
CSVF(x, mpvar)	Future time variable for plant
PCNTMP(i)	Present time temperature of plant surrounding
PCNTMF(i)	Future time temperature of plant surrounding
CONVAR(y, 1)	Temperature of water entering plant component
CONVAR(y, 2)	Mass flow rate of water through plant component
PCONDR(y)	Fraction of mass flow through component
ADATA(i, 1)	Holds input variable data for component algorithm
i = ipcomp	'ipcomp' is the database identification, code or number of plant component
j = mnodec	'mnodec' is the number of nodes per plant component. It also denotes specific node number for the plant.
k = mpconc	'mpconc' is the maximum allowable connections to a plant node and specific node connection number
x = mpnode	Plant node identification number
y = mpcon	index of component's connection in plant network
mpvar	Number of state variables
1, 2 and 9 indicate what type, or nature, of data contained in those portions of the database. In the case of ADATA, the number represents a specific input variable number, the amount of which is unique to individual components.	

Appendix C – Components of Plant Database

As mentioned in the sections above, database codes, or numbers, are required for recognition and identification of models/components in the ESP-r machine. The numbers are part of database items stored in the machines database folder, 'ESP-rDatabases'. The database contains all the data and information that ESP-r utilises for analysing building performances. They include climate data, construction materials data, optics and plant components data, which holds information about every plant component. Information about component description, its nodal scheme description, number of ADATA, BDATA and CDATA items and variables, number of additional output items and variables and mass flow component data.

C1 – Component Description

Component Description contains information about what generic type component belongs, a brief description, the date it was inserted in the database, its type (single or multiple) and component code number.

C2 – Nodal Scheme

Nodal scheme description lists information about number of nodes in the component, the number of non-zero matrix elements and their matrix positions, node connections and variable type.

C3 – A-, B- and CDATA

ADATA and BDATA variables are thermo-physical properties of the component/model. There is a pre-set value for each property and a minimum and maximum value. The pre-set values are adjustable by user at interface, but the minimum and maximum values depict limits that user may not exceed. CDATA items/values serve as some base, or control, parameter that determine the component's function and operation. It is also adjustable at user interface.

C4 – Additional Outputs

These represent outputs from component other than its nodal temperature and flow properties that may be of interest in assessing its impact on the building performance analysis.

C5 – Mass Flow Component Data

These are information or data about the heat transfer fluid, like representative flow equation, type of fluid and dimensional properties of the fluid flow path/channel, and other flow properties.

Appendix D – Sample Temperature-Enthalpy data input for melting and solidifying curves in EnergyPlus

Table D1: Temperature-Enthalpy data (Zastawna-Rumin, Kisilewicz, & Berardi, 2020)

Material Property: Phase Change,
PCM plate, !- Name
-40, !- Temperature 1 {C}-temperature beyond phase change range
0, !- Enthalpy-m 1 {J/kg} – melting enthalpy
0, !- Enthalpy-s 1 {J/kg} – solidification enthalpy
23, !- Temperature 2 {C}
2005, !- Enthalpy-m 2 {J/kg}
3005, !- Enthalpy-s 2 {J/kg}
25, !- Temperature 3 {C}
6570, !- Enthalpy-m 3 {J/kg}
12714, !- Enthalpy-s 3 {J/kg}
27, !- Temperature 4 {C}-temperature within phase change range
12714, !- Enthalpy-m 4 {J/kg} – melting enthalpy
29200, !- Enthalpy-s 4 {J/kg} – solidification enthalpy
28, !- Temperature 5 {C}
25300, !- Enthalpy-m 5 {J/kg}
29300, !- Enthalpy-s 5 {J/kg}
29, !- Temperature 6 {C}

30000, !- Enthalpy-m 6 {J/kg}
30300, !- Enthalpy-s 6 {J/kg}
30, !- Temperature 7 {C}
33000, !- Enthalpy-m 7 {J/kg}
31300; !- Enthalpy-s 7 {J/kg}

Appendix E – ASHP Energy Consumption Profiles over Coldest week of Simulation

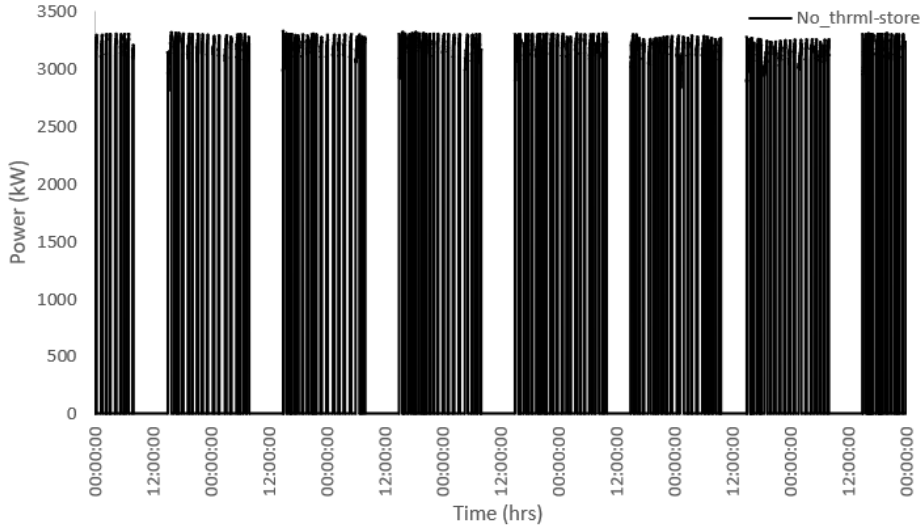

Figure E1: Heating system with no thermal storage

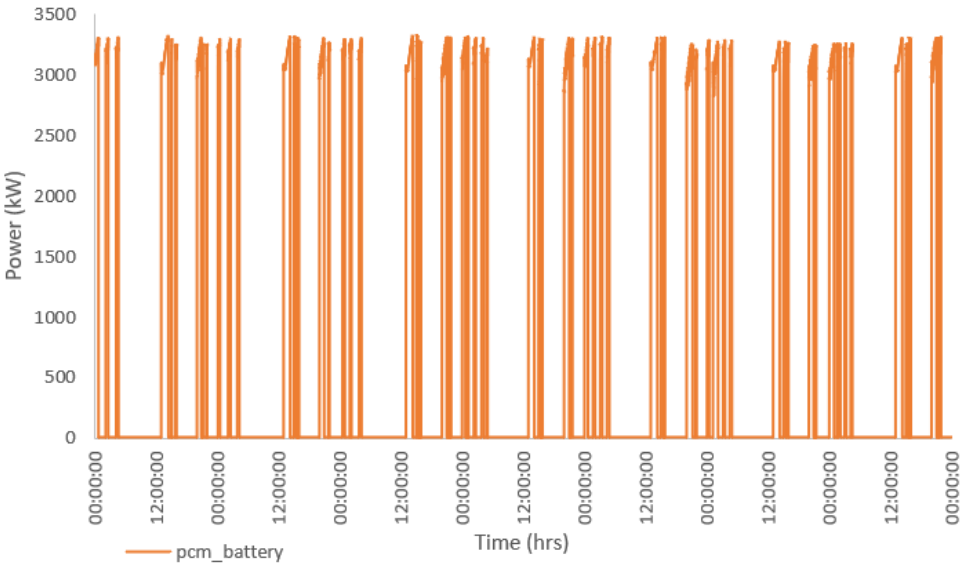

Figure E2: Heating system with PCM battery

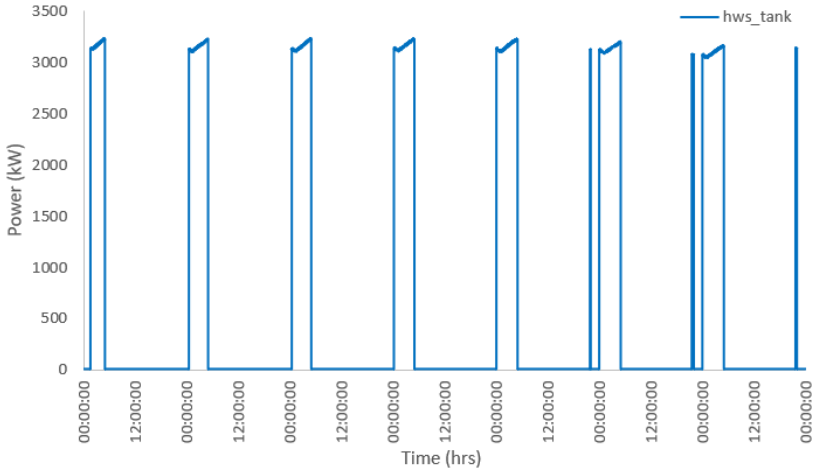

Figure E3: Heating system with hot water storage tank

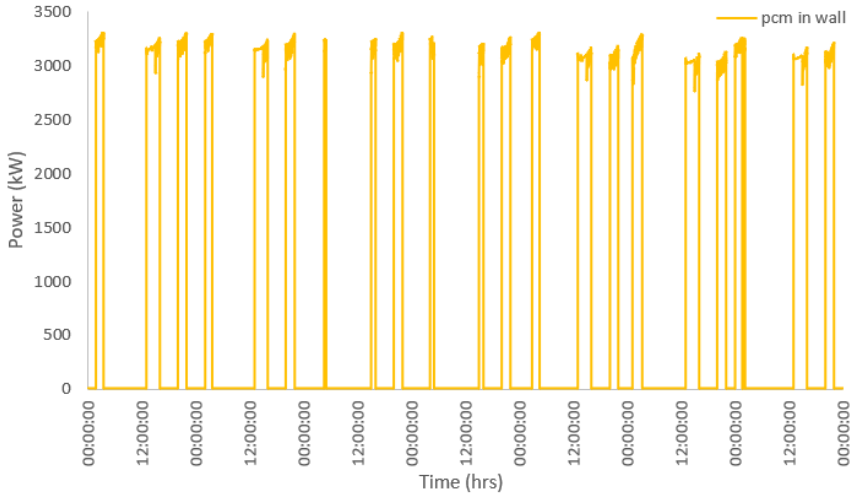

Figure E4: Heating system with PCM in walls

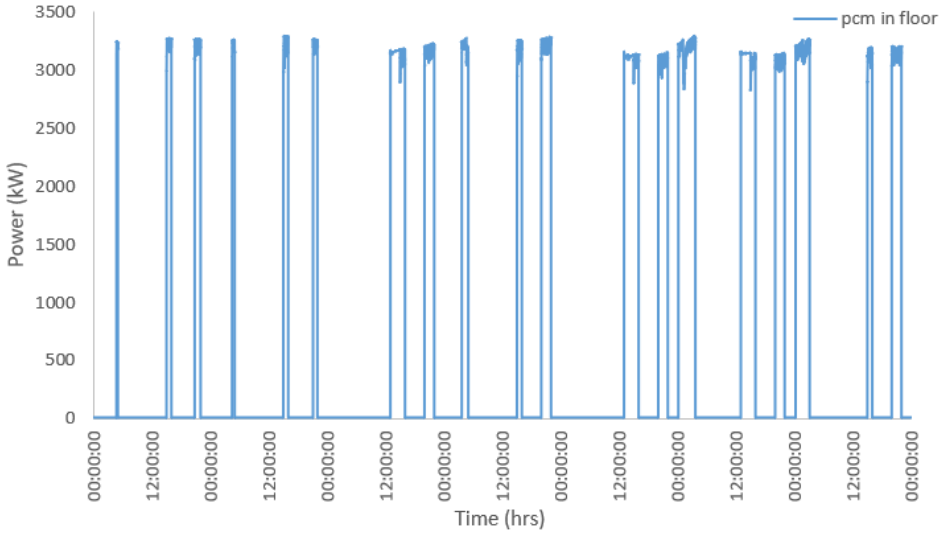

Figure E5: Heating system with PCM in floors

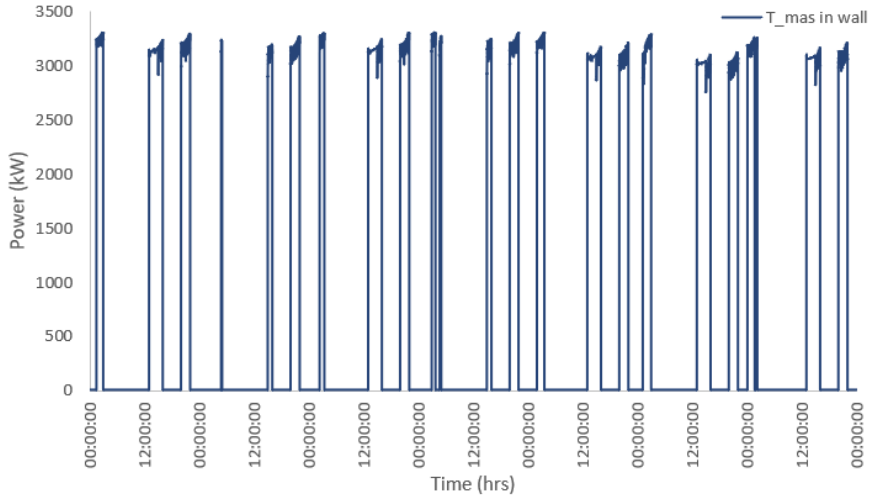

Figure E6: Heating system with thermal mass in walls

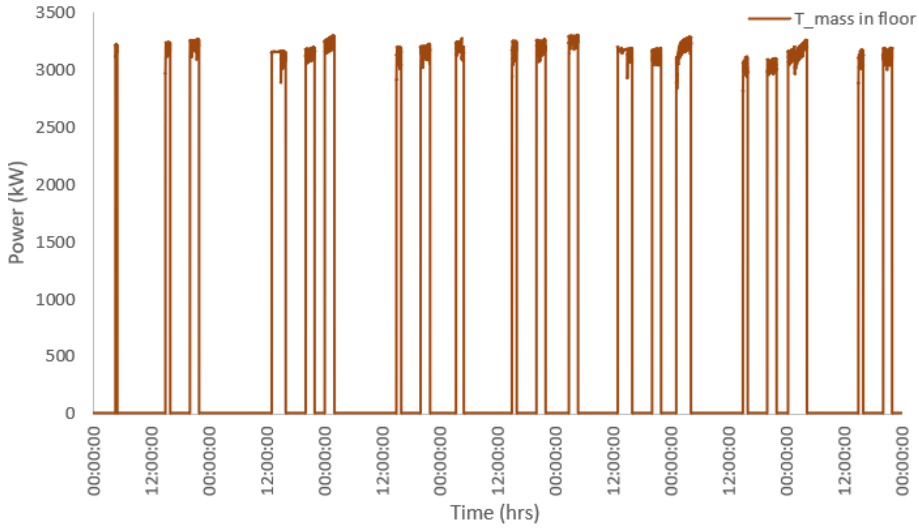

Figure E7: Heating system with thermal mass in floors